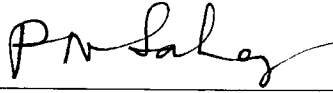


TESIS DEFENDIDA POR:

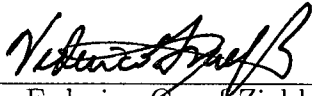
Selene Solorza Calderón

Y APROBADA POR EL SIGUIENTE COMITÉ



---

Dr. Pratap Narayan Sahay Sahay  
*Director de Tesis*



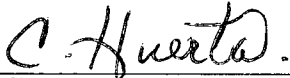
---

Dr. Federico Graef Ziehl  
*Miembro del Comité*



---

Dr. Cecilio Javier Rebollar Bustamantes  
*Miembro del Comité*



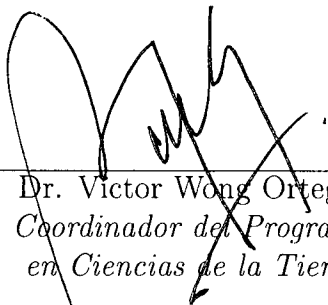
---

Dr. Carlos Isidoro Huerta López  
*Miembro del Comité*



---

Dr. Mauricio Reyes Rúaiz  
*Miembro del Comité*



---

Dr. Victor Wong Ortega  
*Coordinador del Programa  
en Ciencias de la Tierra*

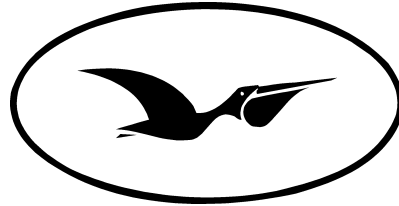


---

Dr. Raúl Ramón Castro Escamilla  
*Director de Estudios de  
Posgrado*

Ensenada, Baja California, México, 14 de septiembre de 2005.

CENTRO DE INVESTIGACIÓN CIENTÍFICA Y DE  
EDUCACIÓN SUPERIOR DE ENSENADA



PROGRAMA DE POSGRADO EN CIENCIAS  
EN CIENCIAS DE LA TIERRA

**Torsional and Extensional Waves in  
Fully-Saturated Porous Cylinders**

TESIS

que para cubrir parcialmente los requisitos necesarios para obtener el grado de  
DOCTOR EN CIENCIAS

**Presenta:**  
**SELENE SOLORZA CALDERÓN**

Ensenada, Baja California, México, 14 de septiembre de 2005.

**Resumen** de la tesis que presenta **Selene Solorza Calderón**, para cubrir parcialmente los requisitos necesarios para obtener del grado de **DOCTOR EN CIENCIAS en CIENCIAS DE LA TIERRA**. Ensenada, Baja California, México, 14 de septiembre de 2005.

## **Torsional and Extensional Waves in Fully-Saturated Porous Cylinders**

Aprobado por



---

Dr. Pratap Narayan Sahay Sahay  
Director de Tesis.

La técnica de barras resonantes se utiliza frecuentemente para determinar los módulos elásticos de un sólido. En esta metodología se trabaja con una muestra cilíndrica o rectangular de longitud finita a la cual se le excita un modo característico de onda, por ejemplo la torsional o la longitudinal, y se registra su frecuencia de resonancia.

Al utilizar esta metodología en las mediciones dinámicas de las constantes elásticas de un medio poroso (esto es, una matriz sólida saturada con un fluido viscoso) además de la velocidad de la onda también se observa atenuación. Por lo que los valores de la atenuación deben estar vinculados con las propiedades del fluido, es decir, con la porosidad, la viscosidad y la permeabilidad. Sin embargo, en la actualidad no existe una manera clara y precisa de vincular las propiedades del medio poroso con las observaciones hechas en el laboratorio para la velocidad y la atenuación de la onda.

De manera que para llevar a cabo este vínculo es necesario resolver los correspondientes problemas de valor a la frontera usando como marco de referencia la teoría poroelástica.

Es por eso que en esta tesis se estudian nuevamente los problemas de valor a la frontera para las ondas torsionales y extensionales obteniéndose fórmulas que vinculan la velocidad y la atenuación observadas con las propiedades del medio poroelástico de una manera clara y transparente. Con base en estas fórmulas se pueden diseñar un conjunto de experimentos de laboratorio que nos permiten interpretar apropiadamente los datos torsionales y extensionales.

**Palabras clave:** medio poroso, cilindros, ondas torsionales y ondas extensionales

**Abstract** of the thesis by **Selene Solorza Calderón**, presented as partial requirement in order to obtain the **Doctor Degree** in **EARTH SCIENCES**. Ensenada, Baja California, Mexico. September 14, 2005.

The resonance-bar technique is often used to determine the elastic moduli of a solid. In this methodology one works with a cylindrical or rectangle core of finite length which is excited into a characteristic mode of standing wave, such as torsional or longitudinal, and the resonance frequency is recorded.

When this methodology is used in the dynamic measurement of the elastic moduli of a porous material (i.e. a solid matrix saturated with viscous fluid), one also observes attenuation. Thus, the attenuation values must be linked to fluid properties, namely porosity, viscosity and permeability. However, a clear and transparent way to link the porous media properties with the laboratory velocity and attenuation data has not been realized yet .

In order to link the observed velocity and attenuation to the properties of the solid, fluid constituents and permeability one has to work-out appropriate boundary-value problems in the framework of the equations of motion for the poroelasticity approach.

In this thesis I have worked out the torsional and extensional boundary-value problems in a cylindrical geometric figure and developed formulas that link velocity and attenuation to solid and fluid constituent properties in a clear and transparent manner. Based upon this formulas a set of experiments can be design to interpreted torsional and longitudinal data properly.

**Key words:** porous medium, cylinder, torsional waves and extensional waves.

Para mi mamá y miemá.

# Agradecimientos

Mis más sinceros agradecimientos:

A mi director de tesis Dr. Pratap N. Sahay por el apoyo que siempre me ha brindado.

A los miembros del comité de tesis por su colaboración: Dr. Federico Graef, Dr. Carlos I. Huerta, Dr. Mauricio Reyes, pero en especial al Dr. Cecilio J. Rebollar por el apoyo que me brindó en todo momento.

Muchas gracias al Dr. Emitt Young por su valiosa colaboración.

Al Consejo Nacional de Ciencia y Tecnología, por su apoyo de manutención y colegiatura en el programa de posgrado del CICESE.

A la Universidad Autónoma de Baja California por la beca que me brindó para finalizar la tesis de doctorado.

A mis hermanas Sol y Lluvia que siempre han estado presentes en todo momento.

A mi tía Magdalena por sus acertados consejos.

A Gloria Rubí, Alvaro Alvarez, Juan Tapia y Nahara Ayala por su apoyo.

A mis grandes amigos: Aida Dueñas y Jorge Polanco; Beatriz Martín y Antonio González; Dulce Vargas, Idalmis (Ave) Fernández, Gema y Miguel, Ricardo Balderas, GRACIAS por su apoyo y por haber compartido conmigo tanto momentos de dicha, la chorcha inolvidable y también mis momentos en matlab.

# Synopsis (spanish)

La técnica de barras resonantes se usa frecuentemente para determinar el módulo de elasticidad de un sólido. En ésta metodología se excita un modo característico de una muestra cilíndrica o rectangular, por ejemplo el modo torsional o longitudinal, y se mide su frecuencia de resonancia. La frecuencia de resonancia para la vibración del modo torsional está vinculada con la rigidez del sólido. Para el modo longitudinal la frecuencia de resonancia está relacionada con el módulo de Young y la razón de Poisson.

Cuando este método se aplica a una muestra poroelástica (i.e. una matriz sólida saturada con un fluido viscoso), también se observa atenuación en el campo de onda. Este mecanismo de atenuación en un material poroso es debido a:

- 1) el movimiento del fluido con respecto a la matriz sólida, y
- 2) la viscosidad del fluido que satura al poro.

Es por eso que los valores medidos de la atenuación deben estar vinculados con las propiedades del fluido, la porosidad y la permeabilidad. Entonces para vincular las mediciones observadas de la velocidad y la atenuación de la onda con las propiedades del sólido y del fluido es necesario resolver los apropiados problemas de valor a la frontera usando la teoría de la poroelasticidad.

Desde 1952 varios investigadores han intentado resolver los problemas de valor a la

---

frontera asociados con las vibraciones torsional y longitudinal en el marco teórico de la poroelasticidad, sin embargo, aún no se logra vincular de manera clara y transparente las fórmulas para la velocidad y la atenuación observadas con las propiedades del medio poroso. En esta tesis, se resuelven los problemas de valor a la frontera para las ondas torsional y longitudinal para encontrar las fórmulas que vinculan la velocidad y la atenuación de la onda con las propiedades del medio poroso de una manera clara y transparente. Entonces, estas fórmulas se pueden usar para interpretar apropiadamente los datos que se originan de las mediciones de los experimentos de barras resonantes al excitar los modos torsional y longitudinal.

Los modos torsional y longitudinal son problemas que se reducen a movimientos bidimensionales. Para el caso elástico la naturaleza del movimiento de la onda longitudinal es en ambas direcciones, tanto en la radial como en la axial, por lo que hay que considerar dos desplazamientos (los cuales son independientes del azimut) que generan tanto movimiento compresional como de cizalla, los cuales están acoplados y se propagan a la misma velocidad. Para un cilindro poroso este modo de vibración se vuelve muy complicado porque los movimientos en la dirección radial y axial existen tanto para el sólido como para el fluido, por lo que hay que considerar cuatro desplazamientos. Para evitar que el problema de valor a la frontera del modo longitudinal se vuelva matemáticamente intratable, debido al acoplamiento entre los movimientos compresional y de cizalla tanto del sólido como del fluido viajando en la misma dirección y con la misma velocidad, solamente se considera como caso de estudio las vibraciones extensionales; que son un caso especial de las oscilaciones longitudinales en cilindros porosos. En la vibración extensional el movimiento axial es de naturaleza compresional, esto es, la dirección de propagación es a lo largo de la dirección axial, y la naturaleza del movimiento radial es prácticamente de cizalla, debido a que ésta es ejecutada perpendicularmente



---

a la dirección de propagación.

Cuando la onda extensional se propaga en un medio poroso saturado completamente con un fluido, se genera un pico de atenuación alrededor de la frecuencia crítica de Biot, conocido como el pico de atenuación de Biot, debido a la disipación de la energía generada por el movimiento relativo del fluido con respecto a la matriz sólida. La disipación de la energía varía dependiendo de la frecuencia. De acuerdo a la literatura ampliamente aceptada sobre este tema, a bajas frecuencias el proceso dominante en la atenuación es la viscosidad del fluido, por lo que el movimiento del fluido está en fase con la matriz porosa, esto ocasiona que la disipación de la energía sea mínima. Esta disipación de la energía alcanza su máximo cuando el efecto de la viscosidad del fluido en la superficie del poro es comparable con el tamaño del poro. Conforme incrementa la frecuencia el acoplamiento debido a la viscosidad del fluido se vuelve débil ocasionando un mínimo movimiento relativo entre el sólido y el fluido, así que la disipación de la energía es muy poca. Para el caso de un cilindro con condiciones de superficie de esfuerzos libres y poro abierto, además del pico de atenuación de Biot se presenta un pico de atenuación adicional. En este caso la condición de presión cero en la superficie exterior del cilindro ocasiona una disipación en la presión del fluido dentro del cilindro, si la mitad del periodo del tiempo de la onda es mayor que el tiempo requerido para que la presión del fluido se disipe sobre el radio del cilindro.

La naturaleza de la vibración de una onda torsional para el caso elástico es idéntica al movimiento de cizalla. En un medio poroso, la teoría de Biot ignora el rol del movimiento de cizalla del fluido ocasionando que el movimiento torsional sea igual al movimiento de cizalla del medio sólido, lo cual es válido sólo para frecuencias por debajo de la frecuencia crítica de Biot. La teoría modificada de Biot incorpora de manera

---

natural el movimiento de cizalla del fluido en la vibración torsional generando movimiento torsional para la región de frecuencias por arriba de la frecuencia crítica de Biot.

El problema de propagación de una onda longitudinal en un medio sólido (no poroso), elástico, isotrópico y homogéneo fue estudiado por Pochhammer (1876). En esa época, el problema de valor a la frontera para las ondas longitudinales era muy complicado debido a la naturaleza trascendental de las funciones involucradas en el mismo. Pochhammer desarrolló una forma rudimentaria de descomposición de la solución en vectores armónicos (en coordenadas cilíndricas) y los utilizó en el sistema acoplado de ecuaciones diferenciales parciales para desacoplarlas, obteniendo un conjunto de ecuaciones de onda escalares. De este modo pudo deducir la forma general de la solución válida para el dominio infinito. Posteriormente, utilizando condiciones de frontera de esfuerzos libres en la superficie radial del cilindro obtuvo la relación de dispersión para la onda longitudinal y realizó un análisis detallado de la misma. La ecuación de dispersión resultante (llamada ecuación de Pochhammer) es una ecuación trascendental la cual sugiere que las ondas P y S, que están desacopladas para un medio infinito, ahora están acopladas debido a las condiciones de frontera.

Chree (1889) mostró como aproximar la ecuación de dispersión, que es una ecuación trascendental, a una ecuación algebraica para los modos extensionales de orden bajo, donde el movimiento compresional de la partícula se realiza a lo largo de la dirección axial y el movimiento de cizalla de la partícula se realiza a lo largo de la dirección radial (ambos propagándose con la misma velocidad), y la longitud de la onda es ordenes de magnitud mayor que el radio del cilindro. Al resolver la ecuación algebraica resultante Chree obtuvo que la velocidad de este modo es controlada básicamente por el módulo de Young, el cual es modificado mínimamente por el cuadrado del radio del cilindro y

la razón de Poisson.

El análisis numérico de la ecuación trascendental obtenida por Pochhammer es muy complicado, por lo que fue hasta setenta años después cuando las computadoras emergieron que se pudo llevar a cabo. Bancroft (1941), replanteó la ecuación de Pochhammer de una manera apropiada para mostrar analíticamente que cuando la longitud de la onda axial es muy pequeña comparada con el radio del cilindro la velocidad de la onda extensional es igual a la velocidad de la onda de Rayleigh. Además presentó un análisis numérico del desplazamiento de la onda extensional a través del cilindro mostrando como el movimiento de la onda se confina en la superficie del cilindro conforme la longitud de onda axial se vuelve infinitesimal, originando de esta manera que la velocidad de la onda extensional sea igual a la velocidad de la onda de Rayleigh.

Davies (1948) corroboró todos los resultados obtenidos por Bancroft sobre el estudio que hizo de la ecuación de Pochhammer. Además, presentó una serie de experimentos de laboratorio para comparar la teoría de Pochhammer con los resultados experimentales obteniendo concordancias aceptables entre ambos.

Siguiendo el trabajo de Davis, el problema de valor a la frontera para las ondas extensionales propagándose en cilindros poros, circulares, homogéneos, isotrópicos y completamente saturados con un fluido fue estudiado por primera vez por Gardner (1962) utilizando como marco de referencia la teoría de Biot.

En un cilindro poroso el movimiento relativo entre el sólido y el fluido en la superficie del cilindro determina las condiciones de frontera del problema a considerar. Cuando el poro esta completamente saturado con un fluido y se puede mover libremente hacia

---

adentro y hacia afuera de la superficie se le llama frontera de poro abierto; cuando el fluido y el sólido se mueven al unísono a través de la superficie del cilindro de tal manera que no se permite que el fluido se mueva hacia adentro y hacia afuera de la superficie se le llama frontera de poro cerrado.

Gardner estudió solamente el problema de valor a la frontera de esfuerzos libres y poro abierto, utilizando como marco de referencia a la teoría de Biot. En las relaciones constitutivas de Biot se ignora la contribución de la viscosidad del fluido ocasionando que esta teoría tenga dos grados de libertad menos de los esperados. Estos dos grados de libertad están asociados con la onda S lenta, la cual es de carácter no propagativo en dicha teoría. Esto genera que en lugar de tener un determinante de cuatro por cuatro igual a cero para de allí determinar la relación de dispersión para el modo extensional se tiene un determinante de tres por tres.

Desde los fundamentos de la teoría de Biot la existencia de la onda S lenta se ignora y solamente se toman en consideración las ondas P rápida, P lenta y S rápida, pues si se tomara en consideración la onda S lenta (que es de carácter no propagativo), tendríamos una singularidad en la teoría. Entonces en esta teoría se ignora la contribución de la onda S lenta en el proceso de las ondas extensionales debido a que no se toma en consideración la contribución de la viscosidad del fluido en las relaciones constitutivas.

La relación de dispersión resultante para la onda extensional es una ecuación trascendental debido a la naturaleza trascendental de las funciones involucradas. Gardner usó una aproximación ad hoc para transformar en funciones algebraicas las funciones trascendentales y así obtener una ecuación de dispersión puramente algebraica, la cual es matemáticamente soluble.

Bajo la consideración de que la longitud de la onda es órdenes de magnitud mayor que el radio del cilindro Gardner obtuvo fórmulas para la velocidad de fase y la atenuación en la región de bajas frecuencias, esta región se encuentra por debajo de la frecuencia crítica de Biot. Dichas fórmulas están vinculadas con las constantes elásticas de la teoría de Biot. Se puede mostrar que la fórmula que obtuvo Gardner para el primer modo de la onda extensional implica que la velocidad de fase está controlada por el módulo de Young de la matriz porosa sin fluido y la densidad de masa total. La atenuación, por su parte, está controlada por la frecuencia, la viscosidad del fluido, la permeabilidad y el cuadrado del radio del cilindro.

Gardner también estudio la relación de dispersión para la región de frecuencias por arriba de la frecuencia crítica de Biot usando como hipótesis que la permeabilidad es dependiente de la frecuencia y trató de obtener las fórmulas para la velocidad de fase y la atenuación. Sin embargo también utilizó como hipótesis que la longitud de la onda axial es órdenes de magnitud mayor que el radio del cilindro, condición que sólo es válida para frecuencias por debajo de la frecuencia crítica de Biot. Además, Gardner no pudo establecer la relación entre la velocidad de fase y la atenuación con las propiedades del cilindro poroso en la región de frecuencias por arriba de la frecuencia crítica de Biot.

Berriman (1983) también estudió el problema de valor a la frontera de vibraciones extensionales de cilindros porosos sujetos a fronteras de esfuerzos libres y poro abierto. Tomó el límite de bajas frecuencias, esto es, la región en la cual la longitud de la onda axial es órdenes de magnitud mayor que el radio del cilindro y reprodujo las fórmulas obtenidas por Gardner.

Para frecuencias ultrasónicas no es válida la suposición de que la longitud de onda axial es órdenes de magnitud mayor que el radio del cilindro, así que se mantiene la naturaleza trascendental de la ecuación de dispersión asociada a las ondas extensionales, por lo que la solución analítica del problema se vuelve complicada y solamente es posible estudiarla numéricamente para este rango de frecuencias, esto es la región de frecuencias mucho mayores que la frecuencia crítica de Biot.

Berryman mostró numéricamente que para frecuencias ultrasónicas el valor de la velocidad de fase tiende al valor de la velocidad de la onda de Rayleigh. Sin embargo, no pudo desarrollar la relación existente entre la velocidad de fase y la atenuación con las propiedades del cilindro poroso.

Berryman también resolvió el problema de valor a la frontera de poro cerrado para el caso extensional. Además, presentó la solución numérica para la relación de dispersión de este problema para las frecuencias ultrasónicas. Él mostró numéricamente que para frecuencias ultrasónicas la velocidad de fase tiende a la velocidad de la onda de Rayleigh. Sin embargo, nuevamente no pudo desarrollar la relación existente entre la velocidad de fase y la atenuación con las propiedades del cilindro poroso.

White (1986) presentó un claro análisis acerca del pico de atenuación que aparece a frecuencias menores que la frecuencia crítica de Biot y lo llevo a cabo utilizando las fórmulas obtenidas por Gardner. El análisis se restringió estrictamente a bajas frecuencias puesto que la solución, para el problema de valor a la frontera del caso de poro abierto, describe aceptablemente las mediciones observadas en el laboratorio para esta región de frecuencias.

En dicho análisis White encontró numéricamente que la frecuencia de relajación, debida al efecto de la superficie del cilindro, es directamente proporcional a la permeabilidad y es inversamente proporcional a la viscosidad del fluido y al cuadrado del radio del cilindro. La magnitud del pico de atenuación cambia dependiendo del valor del módulo de rigidez de la matriz porosa y del modulo de cizalla. Así, la superficie del cilindro no afecta la magnitud del pico de atenuación, pero cambia la frecuencia a la cual éste aparece. Ésto sólo lo mostró numéricamente y no llevó a cabo ningún análisis analítico.

Dunn (1986) solamente presentó un desarrollo matemático sistemático para los problemas de valor a la frontera para las ondas extensionales en cilindros porosos, homogéneos, isotrópicos y completamente saturados con un fluido viscoso sujetos a condiciones de frontera de poro abierto y poro cerrado. En el caso de poro abierto presentó soluciones numéricas, sin embargo para el caso cerrado no presento ni la solución numérica ni tampoco la analítica. Además, tampoco presentó la relación existente entre la velocidad de fase y la atenuación con las propiedades del cilindro poroso, para ninguno de los problemas de valor a la frontera que analizó.

Mörig y Burkhardt (1989), usando cilindros con las mismas propiedades en la matriz porosa y el fluido, y cambiando solamente el radio del cilindro midió la atenuación de las ondas extensionales. En la región por debajo de la frecuencia crítica de Biot los datos obtenidos concuerdan aceptablemente con la teoría desarrollada por Gardner para las ondas extensionales. Sin embargo, para altas frecuencias encontraron mecanismos adicionales para la atenuación, los cuales no son considerados en la teoría de Gardner.

Jonson y colaboradores (1995) también estudiaron la teoría desarrollada por Gardner y llegaron a la conclusión de que la ecuación obtenida por Gardner para bajas frecuencias

no es aplicable a todo el rango de bajas frecuencias. Mostraron bajo qué circunstancias las aproximaciones hechas por Gardner en las ecuaciones trascendentales involucradas son apropiadas por lo que la fórmula de aproximación de Gardner sólo es válida para el rango de frecuencias en el que estas aproximaciones son válidas.

El único análisis que se tiene para las ondas torsionales en cilindros finitos, porosos, isotrópicos, homogéneos y completamente saturados con un fluido viscoso fue presentado por Dunn en 1986. Este análisis está basado en la teoría poroelástica de Biot, por lo que Dunn llegó a la conclusión de que la velocidad de la onda torsional es la misma que la velocidad de la onda de cizalla para un medio infinito.

Los análisis realizados anteriormente para las ondas torsionales y extensionales están orientados a la predicción de las propiedades de cilindros porosos.

Basándose en la teoría poroelástica de Biot, Gardner, Johnson y colaboradores obtuvieron fórmulas que vinculan las propiedades del cilindro poroso con las mediciones observadas en el laboratorio para la velocidad de fase y la atenuación de la onda extensional, válidas sólo para bajas frecuencias. A su vez Dunn obtuvo las fórmulas que vinculan las propiedades del cilindro poroso con las mediciones observadas en el laboratorio para la velocidad de fase y la atenuación de la onda torsional, solamente para la región de bajas frecuencias.

Sin embargo, las metodologías desarrolladas por Gardner, Johnson y colaboradores, y Dunn no son claras y los resultados presentados no describen de forma explícita el vínculo que se está buscando entre las propiedades del cilindro poroso y las observaciones realizadas en el laboratorio. Además, de que para altas frecuencias dichas fórmulas



para las ondas torsionales y extensionales no se han obtenido aún.

En esta tesis desarrollaré el análisis analítico y numérico para los problemas de valor a la frontera para las ondas torsionales y extensionales para cilindros porosos, isotrópicos, homogéneos y saturados completamente con un fluido viscoso. En este trabajo se presenta una metodología sistemática y clara de como se vinculan las propiedades del medio poroso con las observaciones de la velocidad de fase y la atenuación de los modos de vibración torsional y extensional. De esta manera se tiene una idea clara de como deducir las propiedades del cilindro mediante las observaciones hechas en el laboratorio. Más aún, en este trabajo no sólo se presentan las fórmulas para bajas frecuencias, sino que también se obtienen las fórmulas para la región de altas frecuencias.

Las fórmulas obtenidas en esta tesis para las vibraciones torsionales y extensionales reproducen los resultados obtenidos por Dunn y Gardner para la región de bajas frecuencias. Además, para la región de altas frecuencias se obtienen expresiones claras que las vinculan con las propiedades del cilindro poroso, caso que no se tenía con las teorías desarrolladas previamente a este trabajo.

Por lo que basándose en este trabajo se pueden diseñar un conjunto de experimentos de laboratorio tanto para las vibraciones torsionales como para las extensionales y así determinar por ejemplo la permeabilidad o la tortuosidad en un cilindro poroso.

La teoría de la propagación de ondas en medios porosos fue introducida a mediados del siglo pasado por Biot (1956; 1962). En esta formulación, el cambio en la porosidad durante la deformación no aparece explícitamente en las relaciones constitutivas. Esto excluye la dependencia de la razón de deformación del fluido en el tensor de esfuerzos,

de otra manera esto generaría que la energía potencial no se conserva, lo cual contradice la suposición sobre la que esta teoría está asentada, de que la energía potencial se conserva. Esto origina que no se tome en consideración la atenuación debida a la viscosidad del fluido que satura al poro. Además, ocasiona matemáticamente que esta teoría sea inconsistente pues solamente se tienen cuatro grados de libertad en lugar de los seis que se esperarían.

Recientemente, mediante el promediado volumétrico de las ecuaciones dinámicas descritas a escala del poro, se ha desarrollado sobre bases firmes una teoría poroelástica (la Cruz and Spanos (1985; 1989); de la Cruz et al. (1993); Hickey et al. (1995); Sahay (1996) and Sahay et al. (2001)), donde el cambio en la porosidad durante la deformación esta explícitamente presente en las relaciones constitutivas. Las relaciones constitutivas de esta teoría poroelástica incorporan de manera natural el proceso de atenuación debida a la viscosidad del fluido que satura al poro, además del ya conocido proceso de disipación Darciano.

Por lo tanto, esta teoría se puede considerar como la teoría de Biot corregida para el proceso de relajación de la viscosidad del fluido que satura al poro, de aquí en adelante a esta teoría la llamaremos teoría de Biot modificada. Cabe remarcar que este proceso de relajación origina una dependencia de la atenuación con el número de onda, mientras que la disipación Darciana es independiente del mismo. Para una muestra porosa saturada con un fluido muy viscoso, tal como petróleo crudo o chapopote, este proceso de relajación es importante. Además, al incorporar este proceso en las relaciones constitutivas el marco teórico es matemáticamente consistente pues ya se tienen seis grados de libertad, caso que no se tenía en la teoría de Biot.

Esta tesis esta dividida en 7 capítulos. A continuación se describe brevemente el contenido de cada capítulo.

En el capítulo 2, se lleva a cabo un análisis de la teoría desarrollada por Biot. En este capítulo se muestra que la razón de deformación del fluido no se considera en el tensor de esfuerzos del fluido ocasionando que la teoría de Biot pierda dos grados de libertad y en consecuencia sea matemáticamente inconsistente. Además, la ausencia de la razón de deformación del fluido en el tensor de esfuerzos del fluido ocasiona que no se tome en consideración la atenuación debida a la viscosidad del fluido que satura al poro, mecanismo que es importante para muestras porosas saturadas con fluidos altamente viscosos. Posteriormente se presenta la teoría de Biot corregida para la viscosidad del fluido que satura al poro, a la que hemos llamado teoría de Biot modificada. Utilizando la técnica de promediado volumétrico la razón de la deformación del fluido y el cambio en la porosidad se incorporan de una manera natural y transparente en las relaciones constitutivas originando que la teoría modificada de Biot sea matemáticamente consistente, puesto que se incorporaron los dos grados de libertad que la teoría de Biot no consideraba. Enseguida se derivan las ecuaciones de movimiento utilizando como marco de referencia a la teoría de Biot modificada, y representando al vector de desplazamiento en términos de los desplazamientos del sólido y el fluido.

Tradicionalmente el análisis de las vibraciones torsionales y extensionales para cilindros porosos se lleva a cabo en términos de los desplazamientos del sólido y el fluido, sin embargo las variables naturales a considerar son el desplazamiento del centro de masa y el relativo, las cuales no son muy utilizadas aún.

El desplazamiento del centro de masa y el relativo son las variables naturales del pro-

---

blema puesto que en la realidad los geófonos registran el desplazamiento del centro de masa, el cual está asociado con el movimiento en fase del sólido y el fluido, es decir registran el movimiento al unísono de estas dos componentes. El desplazamiento relativo cuantifica el flujo del fluido, puesto que representa al movimiento relativo entre el fluido y la matriz porosa. Mientras que el desplazamiento relativo no se detecta directamente, su efecto es medible mediante la atenuación que presenta el desplazamiento del centro de masa. Debido a estas razones las ecuaciones de movimiento se reescriben en términos del desplazamiento del centro de masa y el relativo. Estas variables son las que se utilizan en el planteamiento de los problemas de valor a la frontera para las oscilaciones torsionales y extensionales.

En el capítulo 3 se plantean los problemas de valor a la frontera para las ondas torsionales y extensionales para cilindros porosos, isotrópicos, homogéneos saturados con un fluido, en el marco de la teoría poroelástica de Biot modificada. Las ecuaciones de movimiento están en coordenadas cilíndricas, las cuales son las coordenadas naturales del sistema para las vibraciones torsionales y extensionales de cilindros porosos. Los problemas correspondientes son bidimensionales, por lo que se muestran los problemas de valor a la frontera bidimensionalmente.

En el capítulo 4 se presenta la solución del problema de valor a la frontera asociado con las oscilaciones torsionales de cilindros finitos, porosos, isotrópicos, homogéneos saturados con un fluido, planteado en el marco de la teoría poroelástica de Biot modificada. Utilizando la teoría de perturbación de valores característicos, en el problema en consideración, se obtienen las expresiones para la frecuencia de resonancia y de atenuación temporal. Estas expresiones están vinculadas de una manera clara y transparente con las propiedades del cilindro poroso.

En este capítulo primeramente se presenta la solución general del problema de valor a la fronteras para las oscilaciones torsionales utilizando la técnica de funciones características. Las expresiones analíticas para la frecuencia de resonancia y de atenuación temporal obtenidas de esta manera son algebraicamente complicadas para mostrar la dependencia de las propiedades del cilindro de una manera clara y sencilla. Es por eso que estas expresiones se trabajan desde el punto de vista de la teoría de perturbación de valores característicos buscando que las propiedades del cilindro poroso esten vinculadas de una manera transparente y sencilla.

Entonces, para obtener la solución al problema de valor a la frontera de las oscilaciones torsionales de cilindros finitos porosos mediante la teoría de perturbación se selecciona una transformación de manera que la parte diagonal del operador transformado se pueda considerar como el operador sin perturbar y que la parte restante del operador se pueda considerar como la parte perturbada, con la característica de que los valores de la frecuencia de resonancia y de atenuación temporal contenidas en el operador sin perturbar se aproximen a los valores exactos de la frecuencia de resonancia y de atenuación temporal del problema original. Puesto que el operador sin perturbar es diagonal las fórmulas de la frecuencia de resonancia y de atenuación temporal se obtienen inmediatamente del mismo.

En la última sección de este capítulo se presenta un resumen de las fórmulas importantes obtenidas para el modo torsional.

El capítulo 5 presenta el hecho de que la excitación del modo torsional en un cilindro poroso es una técnica robusta para la medición dinámica de la rigidez de los materiales.

En esta técnica se excita el modo torsional en una muestra cilíndrica de longitud finita y se registra su frecuencia de resonancia y la atenuación temporal.

Utilizando los resultados del análisis realizado para el problema de valor a la frontera asociado con el modo de vibración torsional de un cilindro finito, isotrópico, homogéneo y completamente saturado con un fluido viscoso resuelto en el marco de referencia de la teoría de Biot modificada (capítulo 4) se pueden diseñar un conjunto de experimentos de laboratorio para el caso de vibraciones torsionales y así poder determinar las propiedades del cilindro poroso.

En el problema de oscilaciones torsionales están involucrados siete parámetros. Cuatro de los siete son propiedades constitutivas, las cuales son: las densidades de masa del sólido y el fluido, viscosidad del fluido y porosidad. Estos cuatro parámetros se pueden obtener fácilmente utilizando procedimientos ya conocidos. Puesto que estos cuatro parámetros son conocidos, se presentan los procedimientos usados para determinar los tres parámetros macroscópicos restantes: el módulo de cizalla de la matriz porosa, la permeabilidad y la tortuosidad, utilizando vibraciones torsionales.

En el capítulo 6 se presenta la solución a los problemas de valores a la frontera de ondas extensionales para un cilindro poroso, isotrópico, homogéneo saturado completamente con un fluido viscoso sujeto a condiciones de frontera de poro abierto y poro cerrado usando como marco de referencia a la teoría poroelástica de Biot modificada. En este capítulo se desarrollan las expresiones para la velocidad de fase y la atenuación extensional, en las cuales la dependencia con las propiedades del cilindro poroso son transparentes, para ambos casos de condiciones de fronteras, es decir para el poro abierto y el poro cerrado.

La solución general para las vibraciones extensionales de cilindros porosos se obtienen sólo numéricamente, para las condiciones de frontera de poro abierto y poro cerrado, debido a que la ecuación de dispersión para el problema de valor a la frontera de poro abierto es una ecuación de cuarto orden y para el caso de poro cerrado es de tercer orden, las cuales al resolverlas analíticamente no muestran de manera clara la dependencia de las propiedades del cilindro para la onda extensional en ambos casos. Como el objetivo es mostrar la naturaleza de cómo se propaga una onda extensional en un cilindro poroso el análisis numérico de la solución de estas ecuaciones de dispersión es más que suficiente.

Aunque para el problema de poro abierto existen cuatro raíces, que representan a los cuatro procesos existentes para este caso, solamente uno de ellos representa a la onda extensional y los otros tres se pueden considerar como procesos disipativos. Estas raíces son números complejos en los cuales la parte real está relacionada con la velocidad y la razón de la parte imaginaria con la parte real representa la atenuación de la onda que se está propagando en el cilindro.

Al realizar la gráfica de la onda extensional se observa que tanto la velocidad de fase como la atenuación tienen tendencias sencillas (tendencia lineal por regiones de frecuencias), por lo que se puede deducir que la dependencia de la velocidad de fase y la atenuación con las propiedades del cilindro poroso debe ser simple.

Así que utilizando argumentos físicos la ecuación de dispersión para las ondas extensionales que es de orden cuatro se puede reducir a una ecuación cuadrática de tal manera que la raíz que contiene la información de la onda extensional que se propaga en el cilindro esté contenida en esta nueva ecuación de dispersión. Resolver analíticamente

un polinomio de orden dos es una tarea sencilla, por lo que ya contamos con una expresión analítica para la velocidad de fase y la atenuación de la onda extensional que esta vinculada de una manera clara y transparente con las propiedades del cilindro poroso.

La expresión obtenida de la ecuación de dispersión simplificada muestra cómo la atenuación esta controlada por la permeabilidad, la viscosidad del fluido y el radio del cilindro, y cómo el valor de la velocidad de fase incrementa del valor del módulo de Young para una matriz sin fluido al valor del módulos de Young pero ya con la matriz saturada con el fluido. Es decir, aquí tenemos una muestra clara de cómo el fluido afecta la velocidad de fase dependiendo en la región de frecuencias en la que se está realizando la medición.

Para el problema de valor a la frontera de ondas extensionales que se propagan en cilindros porosos sujetos a condiciones de frontera de poro abierto se ha desarrollado una metodología clara y consistente, la cual se usará ahora utilizando condiciones de frontera de poro cerrado. Para este caso se obtiene una ecuación de dispersión de tercer orden, la cual se puede resolver mediante un procedimiento estandar. La expresión de la velocidad de fase y la atenuación extensional encontradas mediante este procedimiento no muestra de manera clara y transparente su dependencia con las propiedades del cilindro poroso. Al resolver numéricamente esta ecuación de dispersión de tercer orden y graficar sus soluciones se obtiene que para altas frecuencias, la región de frecuencias por arriba de la frecuencia crítica de Biot, las gráficas de estos tres procesos muestran inestabilidades numéricas, por lo que el análisis del caso de poro cerrado sólo se limita a la region de bajas frecuencias, es decir frecuencias por debajo de la frecuencia crítica de Biot.



Como la ecuación de dispersión para el problema de poro cerrado es de tercer orden entonces existen tres raíces, que representan las ondas existentes en este caso, pero solamente una de ellas es la onda extensional que se propaga a través del cilindro poroso y las otras dos son ondas de difusión. Al resolver numéricamente esta ecuación de dispersión y graficar sus soluciones se obtiene que para el rango de bajas frecuencias, que es el rango de interés, la velocidad de fase y la atenuación para la onda extensional posee una tendencia sencilla, por lo que es lógico suponer que la dependencia con las propiedades del cilindro poroso deben de ser sencillas. Es por eso que bajo argumentos físicos la ecuación de dispersión se reduce de orden tres a una ecuación de segundo orden, en la cual está contenida la información de la onda extensional. Así que al resolver esta ecuación cuadrática ya se tiene una expresión analítica para la velocidad de fase y la atenuación de la onda extensional en la cual la dependencia con las propiedades del cilindro poroso emergen automática y claramente.

El análisis de la ecuación de dispersión simplificada muestra cómo la atenuación es controlada por la permeabilidad y la viscosidad del fluido y que la velocidad de fase es regida por el módulo de Young correspondiente a la matriz saturada con un fluido.

En la última sección de este capítulo se presenta un resumen de las fórmulas importantes obtenidas para el modo extensional.

En el capítulo 7 se presentan las conclusiones de esta tesis:

En el marco de la teoría poroelástica de Biot modificada se llevó a cabo un análisis completo para la vibración de ondas torsionales y extensionales de cilindros porosos completamente saturados con un fluido viscoso.

En el caso torsional, se mostró que los procesos propios que constituyen la ecuación de onda son el proceso rápido (una onda propagándose en el cilindro) y otra onda disipativa. El primer proceso es el que se observa en el experimento de las barras resonantes al excitar el modo torsional.

Para estudiar apropiadamente el problema de valor a la frontera de las ondas torsionales se desarrolló una metodología sistemática y clara, mediante la cual se obtuvieron expresiones para la frecuencia de resonancia y de atenuación que están vinculadas de manera automática y clara con las propiedades del cilindro poroso.

En el caso extensional, se mostró la solución del problema de valor a la frontera sujeto a condiciones de frontera de poro abierto y poro cerrado. En el problema de poro abierto se obtuvo una onda que se propaga a través del cilindro poroso, la onda extensional, y tres ondas disipativas. En el problema de poro cerrado se obtuvo una onda que se propaga a través del cilindro, la onda extensional, y dos ondas disipativas. En esta tesis se mostró cómo para el caso de condición de frontera de poro abierto la atenuación es controlada por el radio del cilindro, la permeabilidad y la viscosidad del fluido y que la velocidad de fase esta gobernada para muy bajas frecuencias por el módulo de Young de la matriz sin fluido y para bajas frecuencias por el módulo de Young de la matriz saturada con el fluido viscoso. En el caso de condición de frontera de poro cerrado la velocidad de fase esta controlada por el módulo de Young de la matriz saturada con el fluido viscoso y la atenuación esta gobernada por la permeabilidad y la viscosidad del fluido.

Con base en estos resultados se pueden diseñar un conjunto de experimentos de la-

boratorio para determinar algunas de las propiedades del cilindro poroso como son la permeabilidad, la tortuosidad, el módulo de cizalla de la matriz porosa, entre otros.

# Contents

	Page
<b>Synopsis (spanish)</b>	<b>i</b>
<b>Contents</b>	<b>xxii</b>
<b>List of Figures</b>	<b>xxiv</b>
<b>List of Tables</b>	<b>xxxiv</b>
<b>Tables of Notation</b>	<b>xxxvi</b>
<b>I Introduction</b>	<b>1</b>
I.1 Introduction .....	1
I.2 Previous work .....	4
I.3 Objective of the thesis .....	9
I.4 Framework .....	11
I.5 Outline of thesis .....	12
<b>II Poroelasticity Framework: An overview</b>	<b>17</b>
II.1 Biot theory .....	19
II.2 Modified Biot theory .....	22
II.2.1 General form of constitutive relation by volume average approach	22
II.2.2 Reduction of the general form to Biot constitutive relations corrected for pore-fluid viscous relaxation .....	24
II.3 Modified Biot theory in terms of the centre-of-mass and internal fields	26
II.3.1 Dynamical variables .....	26
II.3.2 Extended dynamical variables framework .....	29
<b>III Formulation of Boundary Value Problems for Torsional and Longitudinal Standing Waves</b>	
III.1 Governing equations in cylindrical coordinates .....	33
III.2 Torsional problem .....	34
III.3 Longitudinal problem .....	35
<b>IV Standing Torsional Waves in Porous Cylinder</b>	<b>38</b>
IV.1 General solution of the problem .....	39
IV.1.1 Eigenfunction expansion .....	39
IV.1.2 Reduction to a coupled ordinary differential equation system .....	40
IV.1.3 Eigenfrequency .....	41
IV.1.4 Some numerical results .....	43
IV.2 The eigenvalue perturbation approach .....	49

	Page
IV.2.1 The framework .....	51
IV.2.2 The dimensionless parameter $\Upsilon$ .....	52
IV.2.3 Regime I: $\Upsilon < 1$ (inertia dominated regime) .....	53
IV.2.4 Regime II: $\Upsilon > 1$ (viscosity dominated regime) .....	76
IV.2.5 Comparison with the previous work .....	91
IV.3 Summary .....	97
<b>V Frame Shear Modulus, Permeability and Tortuosity Factor by Torsional Resonance Experiments</b> .....	<b>99</b>
V.1 Direct measurement of frame shear modulus by air saturated sample .....	99
V.2 Measurement of permeability .....	100
V.2.1 High permeability rocks .....	101
V.2.2 Low permeability rocks .....	102
V.3 Measurement of tortuosity factor .....	103
<b>VI Extensional Waves in Porous Cylinder</b> .....	<b>104</b>
VI.1 Governing equations .....	105
VI.2 Decoupling .....	106
VI.3 Elemental solutions for decoupled potentials .....	109
VI.4 Expressions of displacements and stresses .....	110
VI.5 Dispersion relation for longitudinal mode for open-pore stress-free boundary condition .....	112
VI.6 The $\Theta$ function .....	120
VI.7 Simplification of $\Theta$ 's functions .....	121
VI.8 The dispersion relation for extensional mode for open-pore stress-free boundary condition .....	123
VI.9 Numerical solution .....	126
VI.10 The complex extensional expression in terms of material properties .....	137
VI.10.1 Regime I: $\omega \ll \Omega$ .....	141
VI.10.2 Regime II: $\Omega \ll \omega$ .....	152
VI.11 Dispersion relation for longitudinal mode for closed-pore stress-free boundary condition .....	157
VI.12 The dispersion relation for extensional mode for closed-pore stress-free boundary condition .....	163
VI.13 Numerical solution .....	166
VI.14 The complex closed-pore extensional expression in terms of material Properties .....	168
VI.15 Comparison with the previous work .....	184
VI.16 Summary .....	190
<b>VII Conclusions</b> .....	<b>193</b>

---

	Page
<b>Bibliography</b>	<b>196</b>
<b>Appendix</b>	
<b>A Notation</b>	<b>199</b>
<b>B Data</b>	<b>201</b>
<b>C Dry-Frame Frequency</b>	<b>202</b>
<b>D Eigenvalue Perturbation Computations</b>	<b>204</b>
<b>E Complex Fast- and Slow- P Wave Velocities</b>	<b>209</b>
E.1 Region below Biot critical frequency: $\omega \ll \Omega$ .....	210
E.2 Region above Biot critical frequency: $\Omega \ll \omega$ .....	212
<b>F Complex Fast- and Slow- S Wave Velocities</b>	<b>214</b>
F.1 Region below Biot critical frequency: $\omega \ll \Omega$ .....	215
F.2 Region above Biot critical frequency: $\Omega \ll \omega$ .....	216

# List of Figures

Figure	Page
<p>1 The plot of torsional resonance frequency, <math>\Re\omega_1(1,1)</math>, the blue curve and temporal attenuation frequency, <math>\Im\omega_1(1,1)</math>, the red curve versus fluid viscosity associated with the fast process corresponding to the first harmonics in radial and axial directions, eq (90). Both curves are scaled by the resonance frequency of the dry-frame, <math>\omega_0(1,1)</math>, and its corresponding equation is given in 421. For clarity the crossover viscosities A, B and C, whose explicit representations are given later in section IV.2.4.4, are also marked.</p>	45
<p>2 Gráfica de la frecuencia de resonancia torsional en azul, <math>\Re\omega_1(1,1)</math>, y de la frecuencia de atenuación temporal en rojo, <math>\Im\omega_1(1,1)</math>, contra la viscosidad del fluido correspondiente al proceso rápido asociado con los primeros armónicos en las direcciones radial y axial, ec (90). Ambas curvas están escaladas con la frecuencia de resonancia asociada a la matriz porosa sin fluido, <math>\omega_0(1,1)</math>, cuya correspondiente ecuación es 421. Por claridad también se muestran las viscosidades de frontera A, B y C, cuyas expresiones están dadas en la sección 4.2.4.4.</p>	46
<p>3 The plot of temporal attenuation frequency, <math>\Im\omega_3(1,1)</math>, versus fluid shear viscosity for the slow process corresponding to the first harmonics in radial and axial directions, eq (92). In this process the real part of the eigenfrequency is zero, therefore it is not plotted.</p>	47
<p>4 Gráfica de la frecuencia de atenuación temporal, <math>\Im\omega_3(1,1)</math>, contra la viscosidad del fluido correspondiente al proceso lento asociado con los primeros armónicos en las direcciones radial y axial, ec (92). En este proceso la parte real de las frecuencias características son cero, por lo que no se muestran.</p>	48
<p>5 For the regime I (<math>\Upsilon &lt; 1</math>) the comparison of exact (eq 90), zero<sup>th</sup>-order (eq 108), and second-order (eq 436) corrected values of the torsional resonance and temporal attenuation frequencies associated with the fast process. The exact resonance, <math>\frac{\Re\omega_1(1,1)}{\omega_0(1,1)}</math>, and temporal attenuation, <math>\frac{\Im\omega_1(1,1)}{\omega_0(1,1)}</math>, frequencies are presented as blue and red curves, respectively. On the respective exact curves, the zero<sup>th</sup>-order resonance and temporal attenuation frequencies are superimposed as dashed-black lines, and the dashed-green curves are their second-order corrected values.</p>	57

Figure	Page
6	58
<p>Región I (<math>\Upsilon &lt; 1</math>): comparación de los valores exactos (ec 90), de orden cero (ec 108), y segundo orden (ec 436) de las frecuencias de resonancia y atenuación temporal torsional correspondientes al proceso rápido. Las curvas exactas de la frecuencia de resonancia, <math>\frac{\Re\omega_1(1,1)}{\omega_0(1,1)}</math>, y la atenuación temporal, <math>\frac{\Im\omega_1(1,1)}{\omega_0(1,1)}</math>, se muestran en azul y rojo, respectivamente. Sobre las respectivas curvas exactas se superimponen las curvas de las frecuencias de resonancia y la atenuación temporal de orden cero en líneas punteadas negras, y las curvas de segundo orden están representadas por líneas punteadas verdes.</p>	
7	60
<p>In the regime I (<math>\Upsilon &lt; 1</math>) the % deviation from the exact values of the zero<sup>th</sup>-order resonance frequency associated with the fast process. The deviation curves are monotone functions. On the plots the upper bounds of viscosity (or <math>\Upsilon</math>) correspond to the deviation being 1%.</p>	
8	61
<p>Región I (<math>\Upsilon &lt; 1</math>): desviación porcentual de los valores de orden cero con respecto a los valores exactos de la frecuencia de resonancia asociados con el proceso rápido. La curva de la desviación porcentual muestra una tendencia monótona creciente. En la gráfica el límite superior de la viscosidad (o <math>\Upsilon</math>) corresponde a la desviación porcentual del 1%.</p>	
9	62
<p>In the regime I (<math>\Upsilon &lt; 1</math>) the % deviation from the exact values of the zero<sup>th</sup>-order temporal attenuation frequency associated with the fast process. The deviation curves are monotone functions. On the plots the upper bounds of viscosity (or <math>\Upsilon</math>) correspond to the deviation being 1%.</p>	
10	63
<p>Región I (<math>\Upsilon &lt; 1</math>): desviación porcentual de los valores de orden cero con respecto a los valores exactos de la frecuencia de atenuación temporal asociados con el proceso rápido. La curva de la desviación porcentual muestra una tendencia monótona creciente. En la gráfica el límite superior de la viscosidad (o <math>\Upsilon</math>) corresponde a la desviación porcentual del 1%.</p>	
11	64
<p>In the regime I (<math>\Upsilon &lt; 1</math>) the % deviation from the exact values of the second-order corrected resonance frequency associated with the fast process. The deviation curves are monotone functions. On the plots the upper bounds of viscosity (or <math>\Upsilon</math>) correspond to the deviation being 1%.</p>	



Figure		Page
12	Región I ( $\Upsilon < 1$ ): desviación porcentual de los valores de segundo orden con respecto a los valores exactos de la frecuencia de resonancia asociados con el proceso rápido. La curva de la desviación porcentual muestra una tendencia monótona creciente. En la gráfica el límite superior de la viscosidad (o $\Upsilon$ ) corresponde a la desviación porcentual del 1%.	65
13	In the regime I ( $\Upsilon < 1$ ) the % deviation from the exact values of the second-order corrected temporal attenuation frequency associated with the fast process. The deviation curves are monotone functions. On the plots the upper bounds of viscosity (or $\Upsilon$ ) correspond to the deviation being 1%.	66
14	Región I ( $\Upsilon < 1$ ): desviación porcentual de los valores de segundo orden con respecto a los valores exactos de la frecuencia de atenuación temporal asociados con el proceso rápido. La curva de la desviación porcentual muestra una tendencia monótona creciente. En la gráfica el límite superior de la viscosidad (o $\Upsilon$ ) corresponde a la desviación porcentual del 1%.	67
15	In the regime I ( $\Upsilon < 1$ ) the comparison of exact (eq 90) and approximate expression of the torsional resonance (eq 113) and temporal attenuation (eq 114) frequencies associated with the fast process. The exact resonance, $\frac{\Re\omega_1(1,1)}{\omega_0(1,1)}$ , and temporal attenuation, $\frac{\Im\omega_1(1,1)}{\omega_0(1,1)}$ , frequencies are presented as blue and red curves, respectively. On the respective exact curves, the approximate resonance and temporal attenuation frequencies are superimposed as dashed-black lines.	69
16	Región I ( $\Upsilon < 1$ ): comparación de los valores exactos (ec 90), y de las fórmulas de aproximación para la frecuencia de resonancia (ec 113), y la frecuencia de atenuación temporal (ec 114) correspondientes al proceso rápido. Las curvas exactas de la frecuencia de resonancia, $\frac{\Re\omega_1(1,1)}{\omega_0(1,1)}$ , y la atenuación temporal, $\frac{\Im\omega_1(1,1)}{\omega_0(1,1)}$ , se muestran en azul y rojo, respectivamente. Sobre las respectivas curvas exactas se superimponen las curvas de las fórmulas aproximadas para las frecuencias de resonancia y atenuación temporal en líneas punteadas negras.	70

Figure		Page
17	For the regime I ( $\Upsilon < 1$ ) the comparison of the exact (eq 92) and the zero <sup>th</sup> -order (eq 115) values of the temporal attenuation frequency associated with the slow process, $\Im\omega_3(1,1)$ . The exact temporal attenuation frequency is presented as red curve, on the exact curve the zero <sup>th</sup> -order values are superimposed as dashed-black line.	72
18	Región I ( $\Upsilon < 1$ ): comparación de los valores exactos (ec 92) y de orden cero (ec 115) de la frecuencia de atenuación temporal torsional correspondientes al proceso lento, $\Im\omega_3(1,1)$ . La curva exacta de la atenuación temporal se muestra en rojo y sobre la respectiva curva exacta se superimpone la curva de la atenuación temporal de orden cero en líneas punteadas negras.	73
19	For the regime I ( $\Upsilon < 1$ ) the % deviation of the zero <sup>th</sup> -order value from the exact value. For clarity, the upper bound of viscosity (or $\Upsilon$ ) is taken to be the value by which deviation grows to -1%.	74
20	Región I ( $\Upsilon < 1$ ): desviación porcentual de los valores de orden cero con respecto a los valores exactos. Por claridad, el límite superior de la viscosidad (o $\Upsilon$ ) se muestra hasta el valor de la desviación porcentual de -1%.	75
21	For the regime II ( $\Upsilon > 1$ ) the comparison of the exact (eq 90) and zero <sup>th</sup> -order values (eq 126) of the torsional resonance and temporal attenuation frequencies associated with the fast process. The blue and red curves are the exact resonance, $\frac{\Re\omega_1(1,1)}{\omega_0(1,1)}$ , and temporal attenuation, $\frac{\Im\omega_1(1,1)}{\omega_0(1,1)}$ , frequencies respectively. The superimposed dashed-black curves on the respective exact curves are the zero <sup>th</sup> -order values.	80
22	Región II ( $\Upsilon > 1$ ): comparación de los valores exactos (ec 90) y de orden cero (ec 126) de las frecuencias de resonancia y atenuación temporal torsional correspondientes al proceso rápido. Las curvas exactas de la frecuencia de resonancia, $\frac{\Re\omega_1(1,1)}{\omega_0(1,1)}$ , y la atenuación temporal, $\frac{\Im\omega_1(1,1)}{\omega_0(1,1)}$ , se muestran en azul y rojo, respectivamente. Sobre las respectivas curvas exactas se superimponen las curvas de las frecuencias de resonancia y la atenuación temporal de orden cero en líneas punteadas negras.	81

Figure		Page
23	For the regime II ( $\Upsilon > 1$ ) the % deviation from the exact values of the zero <sup>th</sup> -order resonance frequency associated with the fast process.	82
24	Regi_ II ( $\Upsilon > 1$ ): desviación porcentual de los valores de orden cero con respecto a los valores exactos de la frecuencia de resonancia asociada con el proceso rápido.	83
25	For the regime II ( $\Upsilon > 1$ ) the % deviation from the exact values of the zero <sup>th</sup> -order temporal attenuation frequency associated with the fast process.	84
26	Región II ( $\Upsilon > 1$ ): desviación porcentual de los valores de orden cero con respecto a los valores exactos de la frecuencia de atenuación temporal asociada con el proceso rápido.	85
27	For the regime II ( $\Upsilon > 1$ ) the comparison of exact (eq 90) and approximate expression of the torsional resonance and temporal attenuation frequencies associated with the fast process. The exact resonance, $\frac{\Re\omega_1(1,1)}{\omega_0(1,1)}$ , and temporal attenuation, $\frac{\Im\omega_1(1,1)}{\omega_0(1,1)}$ , frequencies are presented as blue and red curves, respectively. On the respective exact curves, the approximate resonance frequency (eq 128) is superimposed as dashed-black line and the temporal attenuation frequencies, eq (130) and eq (132), are superimposed as dashed-black and dashed-green lines.	88
28	Región II ( $\Upsilon > 1$ ): comparación de los valores exactos (ec 90), y de las fórmulas de aproximación para la frecuencia de resonancia y la frecuencia de atenuación temporal correspondientes al proceso rápido. Las curvas exactas de la frecuencia de resonancia, $\frac{\Re\omega_1(1,1)}{\omega_0(1,1)}$ , y la atenuación temporal, $\frac{\Im\omega_1(1,1)}{\omega_0(1,1)}$ , se muestran en azul y rojo, respectivamente. Sobre las respectivas curvas exactas se superimponen la curva de la fórmula aproximada para la frecuencia de resonancia (ec 128) en líneas punteadas negras y para la frecuencia de atenuación temporal se superimponen las curvas de las fórmulas aproximadas, ec (130) y ec (132), en líneas punteadas negras y verdes respectivamente.	89
29	For the regime II ( $\Upsilon > 1$ ) the comparison of the exact (eq 92) and zero <sup>th</sup> -order (eq 135) values of the temporal attenuation frequency associated with the slow process, $\Im\omega_3(1,1)$ . The exact temporal attenuation frequency is presented as a red curve and the zero <sup>th</sup> -order values are superimposed as dashed-black line.	92

Figure		Page
30	Región II ( $\Upsilon > 1$ ): comparación de los valores exactos (ec 92) y de orden cero (ec 135) de la frecuencia de atenuación temporal torsional correspondiente al proceso lento. La curva exacta de la frecuencia de atenuación temporal, $\Im\omega_3(1,1)$ , se muestran en rojo. Sobre la curva exacta se superimpone la curva de la frecuencia de atenuación temporal de orden cero en líneas punteadas negras.	93
31	For the regime II ( $\Upsilon > 1$ ) the % deviation of the zero <sup>th</sup> -order value from the exact value associated with the slow process.	94
32	Región II ( $\Upsilon > 1$ ): desviación porcentual de los valores de orden cero con respecto a los valores exactos de la frecuencia de atenuación temporal asociada con el proceso lento.	95
33	The plot of extensional phase velocity (blue-solid curve) and attenuation (red-solid curve) versus frequency; obtained from the first root of eq (240). The fast-P and fast-S waves phase velocity are presented as purple- and black- solid curves, respectively, and the fast-P and fast-S waves attenuation are shown by purple- and black- dashed curves, respectively. For clarity the crossover frequencies A and B (whose explicit representations are given later in section VI.10) and modified Biot critical frequency ( $\Omega$ ), are also marked.	129
34	Gráfica de la velocidad de fase extensional (curva continua azul) y la atenuación (curva continua roja) contra la frecuencia; obtenidas a partir de la primera raíz de la ec (240). Las velocidades de fase de las ondas rápidas P y S se presentan en curvas continuas moradas y negras, respectivamente, y la atenuación de las ondas rápidas P y S se muestran en curvas punteadas moradas y negras, respectivamente. Por claridad también se muestran las frecuencias de frontera A y B (cuyas fórmulas están dadas en la sección VI.10) y la frecuencia crítica de Biot modificada ( $\Omega$ ).	130
35	The blue-solid curve shows the real part of the second complex velocity of eq (240). The red-solid curve is the ratio of the imaginary to real part of this complex velocity. The slow-P and slow-S waves phase velocity are presented as purple- and black- solid curves, respectively, and the slow-P and slow-S wave attenuation are shown by purple- and black-dashed curves, respectively.	131
36	La curva continua azul representa la parte real de la segunda raíz de la velocidad dada en la ec (240). La curva continua roja representa la razón de la parte imaginaria y la real de dicha velocidad. La velocidad de fase de las ondas lentas P y S se muestran en curvas continuas morada y negra, respectivamente y la atenuación de las ondas lentas P y S se muestran en curvas punteadas moradas y negras, respectivamente.	132

Figure		Page
37	The blue curve shows the real part of the third complex velocity of eq (240). The red curve is the ratio of the imaginary to real part of this complex velocity. The slow-P and slow-S waves phase velocity are presented as purple- and black- solid curves, respectively, and the slow-P and slow-S wave attenuation are shown by purple- and black- dashed curves, respectively.	133
38	La curva continua azul representa la parte real de la tercera raíz de la velocidad dada en la ec (240). La curva continua roja representa la razón de la parte imaginaria y la real de dicha velocidad. La velocidad de fase de las ondas lentas P y S se muestran en curvas continuas morada y negra, respectivamente y la atenuación de las ondas lentas P y S se muestran en curvas punteadas moradas y negras, respectivamente.	134
39	The blue curve shows the real part of the fourth complex velocity of eq (240). The red curve is the ratio of the imaginary to real part of this complex velocity. The slow-P and slow-S waves phase velocity are presented as purple- and black- solid curves, respectively, and the slow-P and slow-S wave attenuation are shown by purple- and black- dashed curves, respectively.	135
40	La curva continua azul representa la parte real de la tercera raíz de la velocidad dada en la ec (240). La curva continua roja representa la razón de la parte imaginaria y la real de dicha velocidad. La velocidad de fase de las ondas lentas P y S se muestran en curvas continuas morada y negra, respectivamente y la atenuación de las ondas lentas P y S se muestran en curvas punteadas moradas y negras, respectivamente.	136
41	The comparison of exact (the first root of eq 240) and approximate expression (eq 254) for extensional phase velocity and attenuation, $V_{E_{o_1}}$ , $\frac{1}{Q_{o_1}}$ , respectively. The exact phase velocity and attenuation are presented as blue and red curves, respectively. On the respective exact curves, the approximate extensional phase velocity and attenuation are superimposed as dashed-black lines.	142
42	Comparación de los valores exactos para la velocidad de fase y la atenuación (la primera raíz de la ec 240) y los valores obtenidos para la velocidad de fase, $V_{E_{o_1}}$ , y la atenuación, $\frac{1}{Q_{o_1}}$ , de la fórmula aproximada (ec 254). Los valores exactos de la velocidad de fase y la atenuación se representan mediante las curvas continuas azul y roja, respectivamente. Sobre las respectivas curvas se superimponen los valores obtenidos de la fórmula aproximada en curvas punteadas negras.	143

Figure		Page
43	<p>The comparison of exact (the second root of eq 240) and approximate expression (eq 255) for <math>\Re V</math> and <math>\frac{1}{Q}</math>, respectively. The exact values for <math>\Re V</math> and <math>\frac{1}{Q}</math> are presented as blue and red curves, respectively. On the respective exact curves, the approximate values for <math>\Re V</math> and <math>\frac{1}{Q}</math> are superimposed as dashed-black lines.</p>	144
44	<p>Comparación de los valores exactos (la segunda raíz de la ec 240) y los valores obtenidos usando la fórmula aproximada (ec 255) para <math>\Re V</math> y <math>\frac{1}{Q}</math>, respectivamente. Los valores exactos para <math>\Re V</math> y <math>\frac{1}{Q}</math> se representan mediante las curvas continuas azul y roja, respectivamente. Sobre las respectivas curvas se superimponen los valores obtenidos de la fórmula aproximada para <math>\Re V</math> y <math>\frac{1}{Q}</math> en curvas punteadas negras.</p>	145
45	<p>The comparison of exact (eq 240) and approximate expression of the extensional phase velocity and attenuation in the region below crossover frequency B. The exact extensional phase velocity and attenuation are presented as blue and red curves, respectively. On the respective exact curves, the approximate extensional phase velocity and attenuation are superimposed as dashed-black lines for the region below A and as dashed-green lines for the region above A.</p>	153
46	<p>Comparación de los valores exactos para la velocidad de fase y la atenuación (ec 240) y los valores obtenidos mediante las fórmulas de aproximación de la velocidad de fase y la atenuación en la región por debajo de la frecuencia de frontera B. La velocidad de fase y la atenuación exactas se representan por las curvas continuas azul y roja, respectivamente. Sobre las respectivas curvas exactas se superimponen en líneas continuas punteadas negras los valores aproximados de la velocidad de fase y la atenuación para la región por debajo de A y en líneas punteadas verdes para la región por arriba de A.</p>	154

Figure		Page
47	The comparison of exact (the first root of eq 240) and approximate expression of the extensional phase velocity and attenuation in the region above B. The exact extensional phase velocity and attenuation are presented as blue and red curves, respectively. On the respective exact curves, the approximate extensional phase velocity and attenuation are superimposed as dashed-green lines for the region above $\Omega$ , eqs (312) and (313) respectively. Because the crossover frequency has no signature on phase velocity only the attenuation has an approximate line which is represented as dashed-black lines, eq (314).	158
48	Comparación de los valores exactos para la velocidad de fase y la atenuación (ec 240) y los valores obtenidos mediante las fórmulas de aproximación para la región arriba de B. La velocidad de fase y la atenuación exactas se representan por las curvas continuas azul y roja, respectivamente. Sobre las respectivas curvas exactas se superimponen en líneas punteadas verdes los valores aproximados de la velocidad de fase y la atenuación para la región por arriba de $\Omega$ , ecs (312) y (313) respectivamente. Debido a que la frecuencia de frontera B no afecta a la velocidad de fase solamente la atenuación tiene una línea de aproximación la cual esta representada por la línea punteada negra, ec (314).	159
49	The plot of extensional phase velocity (blue-solid curve) and attenuation (red-solid curve) versus frequency; obtained from the first root of eq (344). For clarity the crossover frequency the modified Biot critical frequency, $\Omega$ , is marked.	169
50	Gráfica de la velocidad de fase extensional (curva continua azul) y la atenuación (curva continua roja) contra la frecuencia; obtenida a partir de la primera raíz de la ec (344). Por claridad también se muestra la frecuencia crítica de Biot modificada, $\Omega$ .	170
51	The plot of extensional phase velocity (blue-solid curve) and attenuation (red-solid curve) versus frequency; obtained from the second root of eq (344). For clarity the crossover frequency the modified Biot critical frequency, $\Omega$ , is marked.	171

Figure		Page
52	Gráfica de la velocidad de fase extensional (curva continua azul) y la atenuación (curva continua roja) contra la frecuencia; obtenida a partir de la segunda raíz de la ec (344). Por claridad también se muestra la frecuencia crítica de Biot modificada, $\Omega$ .	172
53	The plot of extensional phase velocity (blue-solid curve) and attenuation (red-solid curve) versus frequency; obtained from the third root of eq (344). For clarity the crossover frequency the modified Biot critical frequency, $\Omega$ , is marked.	173
54	Gráfica de la velocidad de fase extensional (curva continua azul) y la atenuación (curva continua roja) contra la frecuencia; obtenida a partir de la tercera raíz de la ec (344). Por claridad también se muestra la frecuencia crítica de Biot modificada, $\Omega$ .	174
55	The plot of extensional phase velocity (blue curve) and attenuation (red curve) versus frequency; obtained from the first root of eq (344) for the frequency regime below $\Omega$ .	175
56	Gráfica de la velocidad de fase extensional (curva continua azul) y la atenuación (curva continua roja) contra la frecuencia; obtenida a partir de la primera raíz de la ec (344) para la región por debajo de $\Omega$ .	176
57	The plot of extensional phase velocity (blue curve) and attenuation (red curve) versus frequency; obtained from the second root of eq (344) for the frequency regime below $\Omega$ .	177
58	Gráfica de la velocidad de fase extensional (curva continua azul) y la atenuación (curva continua roja) contra la frecuencia; obtenida a partir de la segunda raíz de la ec (344) para la región por debajo de $\Omega$ .	178
59	The plot of extensional phase velocity (blue curve) and attenuation (red curve) versus frequency; obtained from the third root of eq (344) for the frequency regime below $\Omega$ .	179
60	Gráfica de la velocidad de fase extensional (curva continua azul) y la atenuación (curva continua roja) contra la frecuencia; obtenida a partir de la tercera raíz de la ec (344) para la región por debajo de $\Omega$ .	180
61	The comparison of the exact (344) and the approximate expression for the extensional phase velocity (382) and attenuation (383) in the region below crossover frequency $\Omega$ . The exact extensional phase velocity and attenuation are presented as blue and red solid curves, respectively. On the respective exact curves, the approximate extensional phase velocity and attenuation are superimposed as black-dashed curves.	185



---

Figure		Page
62	Comparación de los valores exactos para la velocidad de fase y la atenuación (ec 344) y los valores obtenidos mediante las fórmulas de aproximación de la velocidad de fase (ec 382) y la atenuación (ec 383) en la región por debajo de la frecuencia de frontera $\Omega$ . La velocidad de fase y la atenuación exactas se representan por las curvas continuas azul y roja, respectivamente. Sobre las respectivas curvas exactas se superimponen en líneas punteadas negras los valores aproximados de la velocidad de fase y la atenuación.	186

# List of Tables

Table		Page
I	Pore-scale field quantities .....	xxxvi
II	Cantidades a escala del poro .....	xxxvi
III	Macroscopic field quantities .....	xxxvii
IV	Cantidades macroscópicas .....	xxxvii
V	Dynamical field quantities .....	xxxviii
VI	Cantidades dinámicas .....	xxxviii
VII	Parameters .....	xxxix
VIII	Parámetros .....	xl
IX	Derived quantities .....	xli
X	Cantidades derivadas .....	xlii
XI	Velocities .....	xliii
XII	Velocidades .....	xliii
XIII	Transform domain quantities .....	xliv
XIV	Cantidades en el dominio transformado .....	xliv
XV	Torsional wave notation .....	xlv
XVI	Notación para las ondas torsionales .....	xlvi
XVII	Extensional wave notation .....	xlvii
XVIII	Notación para las ondas extensionales .....	xlviii

# Tables of Notation

Symbols	Description
$u_j^s$	solid displacement field
$u_{jk}^s$	solid strain tensor
$\tilde{u}_{jk}^s$	trace-free part of solid strain tensor
$\sigma_{jk}^s$	solid stress tensor
$v_j^f$	fluid velocity field
$v_{jk}^f$	fluid strain-rate tensor
$\tilde{v}_{jk}^f$	trace-free part of fluid strain-rate tensor
$\sigma_{jk}^f$	fluid stress tensor
$\pi_{jk}^f$	viscous stress tensor
$p^f$	fluid pressure

Table I. Pore-scale field quantities

Símbolos	Descripción
$u_j^s$	desplazamiento del sólido
$u_{jk}^s$	tensor de deformación del sólido
$\tilde{u}_{jk}^s$	tensor de deformación del sólido sin elementos de la traza
$\sigma_{jk}^s$	tensor de esfuerzo del sólido
$v_j^f$	velocidad del fluido
$v_{jk}^f$	tensor de deformación del fluido
$\tilde{v}_{jk}^f$	tensor de deformación del fluido sin elementos de la traza
$\sigma_{jk}^f$	tensor de esfuerzo del fluido
$\pi_{jk}^f$	tensor de esfuerzo de viscosidad
$p^f$	presión del fluido

Table II. Cantidades a escala del poro

Symbols		Description
$\bar{u}_j^s$	$-\eta_0(\bar{u}_{j,j}^f - \bar{u}_{j,j}^s)$	solid-frame displacement
$\bar{u}_j^f$		fluid (macroscopic) displacement
$\bar{u}_{jk}^s$		solid-frame strain tensor
$\tilde{\bar{u}}_{jk}^s$		trace-free part of solid-frame strain tensor
$\bar{u}_{j,j}^f$		fluid (macroscopic) volumetric-strain tensor
$\zeta$		increase of fluid content
$\bar{\tau}_{jk}^s$		macroscopic solid stress tensor
$\bar{\tau}_{jk}^f$		macroscopic fluid stress tensor
$\bar{p}_j^s$		macroscopic solid pressure
$\bar{p}_j^f$		macroscopic fluid pressure

Table III. Macroscopic field quantities

Símbolos		Descripción
$\bar{u}_j^s$	$-\eta_0(\bar{u}_{j,j}^f - \bar{u}_{j,j}^s)$	desplazamiento del sólido
$\bar{u}_j^f$		desplazamiento del fluido
$\bar{u}_{jk}^s$		tensor de deformación del sólido
$\tilde{\bar{u}}_{jk}^s$		tensor de deformación del sólido sin elementos de la traza
$\bar{u}_{j,j}^f$		tensor de deformación volumétrica del fluido
$\zeta$		incremento del contenido del fluido
$\bar{\tau}_{jk}^s$		tensor de esfuerzo del sólido
$\bar{\tau}_{jk}^f$		tensor de esfuerzo del fluido
$\bar{p}_j^s$		presión del sólido
$\bar{p}_j^f$		presión del fluido

Table IV. Cantidades macroscópicas

Symbols		Description
$\bar{\mathbf{u}}_j^m$	$m^s \bar{\mathbf{u}}_j^s + m^f \bar{\mathbf{u}}_j^f$	centre-of-mass displacement field
$\bar{\mathbf{u}}_j^i$	$\bar{\mathbf{u}}_j^s - \bar{\mathbf{u}}_j^f$	internal displacement field
$\bar{\mathbf{u}}_{jk}^m$		centre-of-mass strain tensor
$\bar{\mathbf{u}}_{jk}^i$		internal strain tensor
$\tilde{\bar{\mathbf{u}}}_{jk}^m$		trace-free part of centre-of-mass strain tensor
$\tilde{\bar{\mathbf{u}}}_{jk}^i$		trace-free part of internal strain tensor
$\bar{\boldsymbol{\tau}}_{jk}^m$		total stress tensor of the porous medium
$\bar{\boldsymbol{\tau}}_{jk}^i$		stress tensor associated with the relative acceleration
$\mathbf{u}_j$	$(\bar{\mathbf{u}}_j^m, \bar{\mathbf{u}}_j^i)^T$	
$\mathbf{u}_{jk}$	$(\bar{\mathbf{u}}_{jk}^m, \bar{\mathbf{u}}_{jk}^i)^T$	
$\boldsymbol{\tau}_{jk}$	$(\bar{\boldsymbol{\tau}}_{jk}^m, \bar{\boldsymbol{\tau}}_{jk}^i)^T$	

Table V. Dynamical field quantities

Símbolos		Descripción
$\bar{\mathbf{u}}_j^m$	$m^s \bar{\mathbf{u}}_j^s + m^f \bar{\mathbf{u}}_j^f$	desplazamiento del centro de masa
$\bar{\mathbf{u}}_j^i$	$\bar{\mathbf{u}}_j^s - \bar{\mathbf{u}}_j^f$	desplazamiento relativo
$\bar{\mathbf{u}}_{jk}^m$		tensor de deformación del centro de masa
$\bar{\mathbf{u}}_{jk}^i$		tensor de deformación relativo
$\tilde{\bar{\mathbf{u}}}_{jk}^m$		tensor de deformación del centro de masa sin elementos de la traza
$\tilde{\bar{\mathbf{u}}}_{jk}^i$		tensor de deformación relativo sin elementos de la traza
$\bar{\boldsymbol{\tau}}_{jk}^m$		tensor de esfuerzo total del medio poroso
$\bar{\boldsymbol{\tau}}_{jk}^i$		tensor de esfuerzo asociado con la aceleración relativa
$\mathbf{u}_j$	$(\bar{\mathbf{u}}_j^m, \bar{\mathbf{u}}_j^i)^T$	
$\mathbf{u}_{jk}$	$(\bar{\mathbf{u}}_{jk}^m, \bar{\mathbf{u}}_{jk}^i)^T$	
$\boldsymbol{\tau}_{jk}$	$(\bar{\boldsymbol{\tau}}_{jk}^m, \bar{\boldsymbol{\tau}}_{jk}^i)^T$	

Table VI. Cantidades dinámicas

Symbols		Description
		<b>Pore-scale parameters</b>
$\rho_0^s$		solid density
$K^s$		solid-mineral bulk modulus
$\mu^s$		solid-mineral shear modulus
$\rho_0^f$		fluid density
$K^f$		fluid bulk modulus
$\xi^f$		fluid bulk viscosity
$\mu^f$		fluid shear viscosity
		<b>Macroscopic parameters</b>
$\eta_0$		unperturbed porosity
$K^0$		solid-frame bulk modulus
$\mu^0$		solid-frame shear modulus
$\alpha$	$1 - \frac{K^0}{K^s}$	Biot coefficient
$\beta$	$1 - \frac{\mu^0}{\mu^s}$	Biot shear coefficient
M	$(\frac{\alpha - \eta_0}{K^s} + \frac{\eta_0}{K^f})^{-1}$	fluid bulk storage coefficient
K		permeability
S		tortuosity factor

Table VII. Parameters

Símbolos		Descripción
		<b>Parámetros a escala del poro</b>
$\rho_0^s$		densidad del sólido
$K^s$		módulo volumétrico del mineral
$\mu^s$		módulo de cizalla del mineral
$\rho_0^f$		densidad del fluido
$K^f$		módulo volumétrico del fluido
$\xi^f$		viscosidad volumétrica del fluido
$\mu^f$		viscosidad de cizalla del fluido
		<b>Parámetros macroscópicos</b>
$\eta_0$		porosidad sin perturbar
$K^0$		módulo volumétrico del sólido
$\mu^0$		módulo de cizalla del sólido
$\alpha$	$1 - \frac{K^0}{K^s}$	Coefficiente de Biot
$\beta$	$1 - \frac{\mu^0}{\mu^s}$	Coefficiente de cizalla de Biot
M	$(\frac{\alpha - \eta_0}{K^s} + \frac{\eta_0}{K^f})^{-1}$	Coefficiente de almacenamiento volumétrico del fluido
K		permeabilidad
S		factor de tortuosidad

Table VIII. Parámetros

Symbols		Description
$H^0$	$K^0 + \frac{4}{3}\mu^0$	dry-frame P-wave elastic modulus
$K^c$	$K^0 + \alpha^2 M$	saturated (Gassmann) bulk modulus
$H^c$	$K^c + \frac{4}{3}\mu^0$	saturated ( Gassmann) P-wave elastic modulus
$\rho^{12}$	$-(S - 1)\eta_0\rho_0^f$	induced mass-coefficient
$\phi_0$	$1 - \eta_0$	solid volume fraction
$\rho_0^m$	$\phi_0\rho_0^s + \eta_0\rho_0^f$	total density
$\rho_0^r$	$(\frac{1}{\phi_0\rho_0^s} + \frac{1}{\eta_0\rho_0^f})^{-1}$	reduced density
$\rho_0^i$	$\rho_0^r - \rho^{12} = \rho_0^r (1 + \frac{S-1}{m^s})$	modified reduced density
$m^s$	$\frac{\phi_0\rho_0^s}{\rho_0^m}$	solid mass fraction
$m^f$	$\frac{\eta_0\rho_0^f}{\rho_0^m}$	fluid mass fraction
$d^s$	$\frac{\phi_0\rho_0^s}{\rho_0^i} = \frac{\rho_0^m}{\rho_0^i} m^s = \frac{m^s}{m^f} \frac{1}{S-m^f}$	
$d^f$	$\frac{\eta_0\rho_0^f}{\rho_0^i} = \frac{\rho_0^m}{\rho_0^i} m^f = \frac{1}{S-m^f}$	
$\nu^f$	$\frac{\mu^f}{\rho_0^f}$	kinematic viscosity of the fluid
$f_c$	$\frac{\eta_0\mu^f}{\rho_0^f K} = \eta_0 \frac{\nu^f}{K}$	Biot critical frequency
$\Omega$	$\frac{\eta_0^2\mu^f}{\rho_0^f K} = d^f f_c$	Darcian relaxation frequency = $d^f \times$ Biot critical frequency

Table IX. Derived quantities



Símbolos		Descripción
$H^0$	$K^0 + \frac{4}{3}\mu^0$	módulo de elasticidad de la onda P de la matriz porosa sin fluido
$K^c$	$K^0 + \alpha^2 M$	módulos volumétrico saturado con un fluido (Gassmann)
$H^c$	$K^c + \frac{4}{3}\mu^0$	módulo de elasticidad de la onda P saturado con un fluido (Gassmann)
$\rho^{12}$	$-(S-1)\eta_0\rho_0^f$	coeficiente de masa inducido
$\phi_0$	$1 - \eta_0$	fracción de volumen del sólido
$\rho_0^m$	$\phi_0\rho_0^s + \eta_0\rho_0^f$	densidad total
$\rho_0^r$	$(\frac{1}{\phi_0\rho_0^s} + \frac{1}{\eta_0\rho_0^f})^{-1}$	densidad reducida
$\rho_0^i$	$\rho_0^r - \rho^{12} = \rho_0^r (1 + \frac{S-1}{m^s})$	densidad reducida modificada
$m^s$	$\frac{\phi_0\rho_0^s}{\rho_0^m}$	fracción de masa del sólido
$m^f$	$\frac{\eta_0\rho_0^f}{\rho_0^m}$	fracción de masa del fluido
$d^s$	$\frac{\phi_0\rho_0^s}{\rho_0^i} = \frac{\rho_0^m}{\rho_0^i} m^s = \frac{m^s}{m^f} \frac{1}{S-m^f}$	
$d^f$	$\frac{\eta_0\rho_0^f}{\rho_0^i} = \frac{\rho_0^m}{\rho_0^i} m^f = \frac{1}{S-m^f}$	
$\nu^f$	$\frac{\mu^f}{\rho_0^f}$	viscosidad cinemática del fluido
$f_c$	$\frac{\eta_0\mu^f}{\rho_0^f K} = \eta_0 \frac{\nu^f}{K}$	frecuencia crítica de Biot
$\Omega$	$\frac{\eta_0^2\mu^f}{\rho_0^f K} = d^f f_c$	frecuencia de relajación Darciana = $d^f \times$ frecuencia crítica de Biot

Table X. Cantidades derivadas

Symbols		Description
$\alpha_s^2$	$\frac{K^s + \frac{4}{3}\mu^s}{\rho_0^s}$	mineral P-wave velocity (squared)
$\beta_s^2$	$\frac{\mu^s}{\rho_0^s}$	mineral S-wave velocity (squared)
$\alpha_0^2$	$\frac{H^0}{\phi_0 \rho_0^s}$	dry P-wave velocity (squared)
$\beta_0^2$	$\frac{\mu^0}{\phi_0 \rho_0^s}$	dry-frame S-wave velocity (squared)
$\alpha_c^2$	$\frac{H^c}{\rho_0^m}$	saturated (Gassmann) P-wave velocity (squared)
$\beta_c^2$	$\frac{\mu^0}{\rho_0^m}$	saturated (Gassmann) S-wave velocity (squared)
$\alpha_I^2$		Fast P-wave velocity (squared)
$\alpha_{II}^2$		Slow P-wave velocity (squared)
$\beta_I^2$		Fast S-wave velocity (squared)
$\beta_{II}^2$		Slow S-wave velocity (squared)

Table XI. Velocities

Símbolos		Descripción
$\alpha_s^2$	$\frac{K^s + \frac{4}{3}\mu^s}{\rho_0^s}$	velocidad (cuadrada) de la onda P en el mineral
$\beta_s^2$	$\frac{\mu^s}{\rho_0^s}$	velocidad (cuadrada) de la onda S en el mineral
$\alpha_0^2$	$\frac{H^0}{\phi_0 \rho_0^s}$	velocidad (cuadrada) de la onda P de la matriz porosa sin fluido
$\beta_0^2$	$\frac{\mu^0}{\phi_0 \rho_0^s}$	velocidad (cuadrada) de la onda S de la matriz porosa sin fluido
$\alpha_c^2$	$\frac{H^c}{\rho_0^m}$	velocidad (cuadrada) de la onda P de la matriz porosa saturada (Gassmann)
$\beta_c^2$	$\frac{\mu^0}{\rho_0^m}$	velocidad (cuadrada) de la onda S de la matriz porosa saturada (Gassmann)
$\alpha_I^2$		velocidad (cuadrada) de la onda P rápida
$\alpha_{II}^2$		velocidad (cuadrada) de la onda P lenta
$\beta_I^2$		velocidad (cuadrada) de la onda S rápida
$\beta_{II}^2$		velocidad (cuadrada) de la onda S lenta

Table XII. Velocidades

Symbols		Description
$\omega$		frequency (in radians)
$k_l$	$\frac{\pi l}{L}$	axial wavenumber for torsional case ( $l = \text{integer}$ )
$q_p$	$\frac{N_p}{a}$	radial wavenumber for torsional case
$N_p$		$p^{\text{th}}$ root of the Bessel function of second-order
$a$		radius of the cylindrical core
$L$		length of the cylindrical core
$k$		axial wavenumber for extentional case
$q_{\alpha_I}, q_{\alpha_{II}}, q_{\beta_I}, q_{\beta_{II}}$		radial wavenumbers for extensional case

Table XIII. Transform domain quantities

Símbolos		Descripción
$\omega$		frecuencia (radianes)
$k_l$	$\frac{\pi l}{L}$	número de onda axial para el caso torsional ( $l = \text{entero}$ )
$q_p$	$\frac{N_p}{a}$	número de onda radial para el caso torsional
$N_p$		$p$ -ésima raíz de la función Bessel de segundo orden
$a$		radio del cilindro
$L$		longitud del cilindro
$k$		número de onda axial para el caso extensional
$q_{\alpha_I}, q_{\alpha_{II}}, q_{\beta_I}, q_{\beta_{II}}$		números de onda radiales para el caso extensional

Table XIV. Cantidades en el dominio transformado

Symbols	Description
$\mathbf{u}_\theta(r, z, t)$ $\mathbf{U}_\theta(q_p, k_l, t)$  $\omega_1(q_p, k_l) = \omega_1(p, l)$ and $\omega_2(q_p, k_l) = \omega_2(p, l)$ $\omega_3(q_p, k_l) = \omega_3(p, l)$ and $\omega_4(q_p, k_l) = \omega_4(p, l)$ $\Re\omega_1(p, l), \Re\omega_2(p, l)$ $\Im\omega_1(p, l), \Im\omega_2(p, l)$  $\Im\omega_3(p, l), \Im\omega_4(p, l)$  $\omega_0(q_p, k_l) = \omega_0(p, l)$  A, B, C  $\Upsilon = \frac{d^f m^f}{2\sqrt{m^s} (1+d^f m^f)^{3/2}} \frac{\Omega}{\omega_0(p, l)}$ $\epsilon = \frac{1}{4} \left( \frac{m^f}{S} \right)^3 \frac{1}{\Upsilon^2}$	<p><b>Displacements</b>  angular displacement field in <math>(r, z, t)</math> domain  angular displacement field in <math>(q_p, k_l, t)</math> domain</p> <p><b>Torsional frequencies</b>  fast processes  slow processes  torsional resonance frequency of the fast processes  torsional temporal attenuation frequency  of the fast processes  torsional temporal attenuation frequency  of the slow processes  torsional resonance frequency of the dry-frame</p> <p><b>Crossover viscosities</b></p> <p><b>Dimensionless parameters</b></p>

Table XV. Torsional wave notation

Símbolos	Descripción
$\mathbf{u}_\theta(r, z, t)$ $\mathbf{U}_\theta(q_p, k_l, t)$	<p><b>Desplazamientos</b>  desplazamiento angular en el dominio <math>(r, z, t)</math>  desplazamiento angular en el dominio <math>(q_p, k_l, t)</math></p>
$\omega_1(q_p, k_l) = \omega_1(p, l)$ y $\omega_2(q_p, k_l) = \omega_2(p, l)$ $\omega_3(q_p, k_l) = \omega_3(p, l)$ y $\omega_4(q_p, k_l) = \omega_4(p, l)$ $\Re\omega_1(p, l), \Re\omega_2(p, l)$ $\Im\omega_1(p, l), \Im\omega_2(p, l)$ $\Im\omega_3(p, l), \Im\omega_4(p, l)$ $\omega_0(q_p, k_l) = \omega_0(p, l)$	<p><b>Frecuencias torsionales</b></p> <p>procesos rápidos</p> <p>procesos lentos</p> <p>frecuencia de resonancia para los procesos rápidos</p> <p>frecuencia de atenuación temporal para los procesos rápidos</p> <p>frecuencia de atenuación temporal para los procesos lentos</p> <p>frecuencia de resonancia de la matriz porosa sin fluido</p>
<p>A, B, C</p>	<p><b>Viscosidades de frontera</b></p>
$\Upsilon = \frac{d^f m^f}{2\sqrt{m^s} (1+d^f m^f)^{3/2}} \frac{\Omega}{\omega_0(p, l)}$ $\epsilon = \frac{1}{4} \left( \frac{m^f}{S} \right)^3 \frac{1}{\Upsilon^2}$	<p><b>Parámetros adimensionales</b></p>

Table XVI. Notación para las ondas torsionales

Symbols	Description
$\mathbf{u}_r(r, z, \omega)$ $\mathbf{u}_z(r, z, \omega)$	<p><b>Displacements</b>                      radial displacement field in <math>(r, z, \omega)</math> domain                      axial displacement field in <math>(r, z, \omega)</math> domain</p>
$\Theta_{\alpha\text{I}}$ $\Theta_{\alpha\text{II}}$ $\Theta_{\beta\text{I}}$ $\Theta_{\beta\text{II}}$	<p><b><math>\Theta</math> functions</b>                      function associated to fast-P wave                      function associated to slow-P wave                      function associated to fast-S wave                      function associated to slow-S wave</p>
$\mathbf{l}^{\beta\text{I}} \cdot \mathbf{r}^{\alpha\text{I}}$ $\mathbf{l}^{\beta\text{I}} \cdot \mathbf{r}^{\alpha\text{II}}$ $\mathbf{l}^{\beta\text{II}} \cdot \mathbf{r}^{\alpha\text{I}}$ $\mathbf{l}^{\beta\text{II}} \cdot \mathbf{r}^{\alpha\text{II}}$	<p><b>Relations between P and S wave motions</b>                      fast-S and fast-P motion                      fast-S and slow-P motion                      slow-S and fast-P motion                      slow-S and slow-P motion</p>
A, B	<p><b>Crossover frequencies</b></p>
$V = \frac{\omega}{k}$	<p><b>Complex velocity</b></p>
$E^0$ $E^c$	<p><b>Young's modulus</b>                      Young's modulus related to dry-frame                      Young's modulus related to saturated-frame (Gassmann)</p>

Table XVII. Extensional wave notation

Símbolos	Descripción
$\mathbf{u}_r(r, z, \omega)$ $\mathbf{u}_z(r, z, \omega)$	<p><b>Desplazamientos</b>  desplazamiento radial en el dominio <math>(r, z, \omega)</math>  desplazamiento axial en el dominio <math>(r, z, \omega)</math></p>
$\Theta_{\alpha I}$ $\Theta_{\alpha II}$ $\Theta_{\beta I}$ $\Theta_{\beta II}$	<p><b>Funciones <math>\Theta</math></b>  función asociada a la onda P rápida  función asociada a la onda P lenta  función asociada a la onda S rápida  función asociada a la onda S lenta</p>
$\mathbf{l}^{\beta I} \cdot \mathbf{r}^{\alpha I}$ $\mathbf{l}^{\beta I} \cdot \mathbf{r}^{\alpha II}$ $\mathbf{l}^{\beta II} \cdot \mathbf{r}^{\alpha I}$ $\mathbf{l}^{\beta II} \cdot \mathbf{r}^{\alpha II}$	<p><b>Relaciones entre los movimientos de las ondas P y S</b>  relación entre las ondas rápida S y rápida P  relación entre las ondas rápida S y lenta P  relación entre las ondas lenta S y rápida P  relación entre las ondas lenta S and lenta P</p>
A, B	<p><b>Frecuencias de frontera</b></p>
$V = \frac{\omega}{k}$	<p><b>Velocidad compleja</b></p>
$E^0$ $E^c$	<p><b>Módulos de Young</b>  módulo de Young asociado a la matriz porosa sin fluido  módulo de Young asociado a la matriz porosa saturada con un fluido (Gassmann)</p>

Table XVIII. Notación para las ondas extensionales

# Chapter I

## Introduction

### I.1 Introduction

The resonance-bar technique is often used to determine the elastic moduli of a solid. In this method a cylindrical or rectangle core of finite length is excited into a characteristic mode of standing wave, such as torsional or longitudinal, and the resonance frequency is recorded. The resonance frequency for the case of the torsional mode of vibration is linked to rigidity. For the longitudinal mode it is related to Young's modulus and Poisson's ratio.

When this method is applied to a poroelastic sample, (i.e. a solid matrix saturated with viscous fluid), one also observes attenuation of the wavefield. The likely mechanism of attenuation in porous material are:

- 1) motion of the fluid with respect to the solid-frame, and
- 2) viscous loss within the pore-fluid.

Thus, the attenuation values must be linked to fluid properties, porosity and permeability. In order to appropriately link the observed velocity and attenuation to the properties of the solid, fluid constituents and permeability one must work-out the boundary-value problems in the framework of the equations of motion for the poroelasticity approach.



Since 1962 various scientist have attempted to work-out boundary-value problems associated with torsional and longitudinal mode in the frame work of poroelastic theory, however success in establishing formulas linking porous medium properties to observed velocity and attenuation in a clear and transparent way have not been realized yet. In this thesis I have reworked the torsional and longitudinal boundary-value problems in a cylindrical geometric figure and worked-out the equations which link velocity and attenuation to porous cilinder properties in a clear and transparent manner. These now be may be used to interpret torsional and longitudinal data properly.

The torsional and longitudinal modes are two-dimensional motions. For the elastic case the particle motion in the longitudinal case is in both the axial and radial directions, therefore two displacements are considered which are independent of the azimuth, and both compressional and shear motions exist as coupled motion such that they propagate at the same velocity. For porous cylinder this mode becomes complicated because the axial and radial motions exist for both the solid and fluid phases, therefore four displacement are considered. To avoid the longitudinal boundary value problem becoming mathematically intractable because of the coupling of the compressional and shear motions traveling in the same direction a special kind of longitudinal motion was considered for porous cylinders only, namely extensional motion, wherein the axial motion is compressional in nature, (i.e. the direction of propagation is along axial direction), and the radial motion is shear in nature, as it being executed perpendicular of the direction of propagation.

When the extensional wave propagates in porous medium which is fully-saturated an attenuation peak around the Biot critical frequency, namely Biot's attenuation peak,

occurs due to the energy dissipation on account of the fluid movement with respect to the solid-frame. This energy dissipation varies depending on the frequencies. According to accepted present day literature on the subject, when the viscosity effect is dominant at low frequencies, fluid moves is almost in unison with the solid-frame, thus resulting in very little energy dissipation. This energy dissipation reaches its maximum when the fluid viscous skin depth is comparable to pore size. As frequency increases the viscous coupling gets weaker resulting in very little fluid movement relative to the solid-frame, thus creating small energy dissipation. Apart from the Biot's attenuation peak an additional attenuation peak is present for the case of open-pore stress-free boundary condition. In this case the zero pressure condition on the outer curved surface results into dissipation of fluid pressure within the cylindrical core, if the half time period of wave process is bigger than time required for fluid pressure to dissipate over the radius of the cylindrical core.

The nature of vibration in the elastic torsional mode is the same as shear motion. In the porous case, based on Biot theory the role of fluid shear motion is ignored giving that the torsional motion is taken to be the same as the shear motion of the solid-frame which is valid for the frequency regime below Biot critical frequency. The modified Biot theory incorporates in a natural way the fluid shear motion into the torsional vibration giving the torsional motion for the region above Biot critical frequency.

In addition a description of the previous work in extensional and torsional wave propagation in a fully-saturated porous circular cylinder will be presented, followed by the presentation of the objectives of this thesis. A brief description of the poroelastic theory on which this work is based is presented in the following section, and finally, the outline of the thesis is presented.

---

## I.2 Previous work

The problem of longitudinal wave propagation in an isotropic elastic solid (non-porous) circular cylinder was studied by Pochhammer (1876). At this time, the longitudinal boundary value problem was very difficult due the transcendental nature of the functions involved. Pochhammer developed a rudimentary form of cylindrical vector harmonics decomposition to the governing system of coupled partial differential equations to obtain a set of decoupled scalar wave equations thereby the general form of solution valid for the infinite domain was deduced. Pochhammer also worked-out the underlying dispersion relation for longitudinal boundary value dictated by stress-free boundary conditons on radial surface of the cylinder. The resulting dispersion relation is a transcendental equation. It suggested the decoupled P and S motions, for infinite medium case, are now coupled because of the boundary conditions.

Chree (1889) showed how to approximate this transcendental equation to an algebraic equation for the lowest order of the extensional mode, wherein compressional particle motion is along the axial direction and the shear particle motion is along the radial direction (and propagate with same velocity), and the axial wavelength is order of magnitude larger than the radii of cylinder. By solving the resulting algebraic equation Chree showed that the velocity of the mode is basically controlled by Young's modulus which is slightly modified by the square of the radii of the cylinder and Poisson's ratio.

Numerical study of Pochhammer transcendental equation was so complicated that it was over seventy years later, when electronic computing starting shaping up, that the numerical study was undertaken. Bancroft (1941), rewrote in a proper form Pochhammer's equation showing analytically that when the axial wavelength is very small compared to

radii, the velocity of the extensional mode is the same as Rayleigh wave velocity. He also presented a numerical analysis of the displacement for the extensional wave through the cylinder showing how the motion is confined in the cylinder surface as the wavelength becomes infinitesimal, giving in this manner that the extensional wave velocity equals the Rayleigh wave velocity.

Davies (1948) corroborates all the results obtained by Bancroft. In addition, he presented a set of experiments comparing the results derived from Pochhammer's theory with laboratory experimental results obtaining an acceptable agreement between both.

Following Davies work, the boundary value problem of extensional wave propagation for fully-saturated, homogeneous, isotropic, porous, circular cylinders was first studied by Gardner (1962) using the framework of the Biot theory.

In a porous cylinder the relative motion between the solid and fluid in the surface of the cylinder determine the boundary condition of the problem under consideration. When in the fully-saturated porous boundary the fluid moves freely in and out of the boundary and this is called the open-pore boundary; when the fluid and solid moves in unison along the surface so that the fluid is not permitted to move in and out of the surface it is called the closed-pore boundary.

Gardner studied only the case of the open-pore stress-free boundary value problem. Because Gardner approach is based on Biot theory, he worked with a theory which ignores two of the degrees of freedom which are associated with the non-propagating fluid shear motion. This gave instead of a  $4 \times 4$  vanishing determinant for the dispersion relation for extensional mode, a  $3 \times 3$  vanishing determinant. The resulting dispersion

relation from the 3 vanishing determinant is easier than the 4 dispersion relation, however the contribution of the slow S wave is ignored throughout the entire process. The resulting dispersion relation is a transcendental equation due the nature of the functions involved. Gardner used ad hoc approximations for the transcendental functions involved in the dispersion relation to transform them into algebraic equations, reducing in this form, the transcendental dispersion relation to an algebraic dispersion relation, which is mathematically managable.

Under the consideration that the associated axial wavelenght is larger than the radius of the cylinder Gardner obtained equations for the extensional phase velocity and for the attenuation which are valid only in the regime below Biot critical frequency. These equations are linked to the elastic constants of the Biot theory. It can be shown that the Gardner formula for the lowest mode of extensional vibration gives that the phase velocity is controlled by Young's modulus of dry frame and the total mass density, and that the attenuation is controlled by frequency, fluid viscosity, permeability and the square radii of the cylinder.

Gardner also studied the dispersion relation for the region above Biot critical frequency, he introduced the frequency permeability dependency and tried to work-out the equation, although he used the issue that the associated axial wavelength is larger than the radius, which is valid only for frequencies smaller than Biot critical frequency. In the region above Biot critical frequency, he was unable to establish a relation between phase velocity and attenuation with the material properties as was found to exist in the region below Biot critical frequency.

Berryman (1983) solved the extensional open-pore boundary value problem for poroe-

---

lastic cylinders. He took the low-frequency limit, (i.e. in which the associated axial wavelength is larger than the radius of the cylinder), belonging to the region below Biot critical frequency, and reproduced Gardner's formulas. For ultrasonic frequency, the assumption that the associated axial wavelength is larger than the radius of the cylinder is not valid, therefore the transcendental functions involving in the extensional dispersion relation remain, thus its analytical solution becomes complicated and only a numerical solution is possible for ultrasonic frequencies, (i.e. the region above Biot critical frequency). Hence, Berryman only showed numerically that for ultrasonic frequencies, as the wavelength became infinitesimal, the phase velocity value is close to the Rayleigh phase velocity for saturated frame.

Because of the extensional oscillations results being based on Biot theory, Berryman found that for open-pore stress-free boundary conditions the slow extensional wave is not propagated, and it is in contradiction with the results obtained in this thesis which are based on the modified Biot theory. The modified Biot theory considers an viscous loss within the pore-fluid attenuation mechanism which governs the slow extensional wave. The propagating slow extensional wave has a low attenuation and its phase velocity is always less than, but close to, the slow-P phase velocity.

Berryman also solved the closed-pore boundary-value problem for extensional waves in a fully-saturated, porous, circular cylinder. He numerically solved the closed-pore boundary condition dispersion relation for ultrasonic frequencies. Berryman numerically showed that for ultrasonic frequencies, as the wavelength became infinitesimal, the phase velocity value for the closed-pore surface is close to the Rayleigh phase velocity for saturated frame as it is in the open-pore surface case. In the closed-pore stress-free boundary value problem he found a slow wave that propagates with a weak

attenuation and its phase velocity was always lower than, but close to, the slow-P wave phase velocity. Similar results were obtained in this thesis for the open-pore stress-free boundary condition.

Because Berryman only solved numerically the extensional dispersion relation for ultrasonic frequencies for open-pore as well as closed-pore stress-free boundary conditions, the relation between phase velocity and attenuation for properties of the solid and fluid constituents were not developed.

White (1986) presented a clear understanding of the extensional attenuation peak appearing below Biot's attenuation peak and he has clearly shown it numerically using Gardner's formula. He also numerically showed that the relaxation frequency, due to the boundary of the cylinder, is directly proportional to the permeability and is inversely proportional to fluid shear viscosity and radius squared. The magnitude of the attenuation peak changed depending upon the value of the frame compression and shear moduli. Thus, the surface of the cylinder does not affect the magnitude of the attenuation peak, but changes the frequency at which this peak occurs. This demonstrates a numerical analysis but does not address an analytical analysis. In this thesis I will present an analytical analysis of the foregoing numerical results.

Dunn (1986) only presented a systematic mathematical development for the extensional waves in fully-saturated, homogeneous, isotropic, porous circular cylinders subjected to open-pore as well as close-pore stress-free boundary conditions. In the case of the open-pore stress-free boundary condition he showed only the numerical solution, however, no solution to the problem was presented either numerically or analitically in the closed-pore case. Also he did not show the relation between phase velocity and attenuation

with respect to the properties of the solid and fluid constituents, either for the extensional open-pore or the closed-pore boundary-value problems.

Möriq and Burkhardt (1989), using cylinders with the same material properties but changing the radius measured the attenuation of the extensional waves. In the regime below Biot critical frequency the data gathered was in agreement with the Gardner theory for extensional waves. For higher frequencies an additional attenuation mechanism was encountered which was not considered by the Gardner theory. In this thesis this additional attenuation mechanism is considered in a natural manner because the study here presented is based on Biot theory corrected for pore-fluid viscous relaxation, which governs the above mention attenuation mechanism.

Johnson et al (1995) also studied Gardner theory reaching the conclusion that the equations for the low-frequency regime obtained by Gardner are not always applicable to this range. They showed that for the extensional problem below certain permeability value, Gardner's formulas are valid.

The only analysis of the problem of the torsional waves in a finite, fully-saturated, isotropic, homogeneous, porous, circular cylinder was presented by Dunn (1986). Based on Biot theory, he found that the torsional velocity is the same as the shear velocity in an infinite medium.

### **I.3 Objective of the thesis**

The above analytic studies for extensional and torsional boundary-value problems are oriented towards the prediction of material properties of poroelastic cylinders.



Based on Biot theory, Gardner and Dunn obtained formulas that link the material properties of porous cylinders with the observed phase velocity and attenuation measurements for extensional and torsional vibrations, respectively, within the low-frequency regime (i.e. below Biot critical frequency). However, these methodologies are not yet clearly developed. In addition to the above, for the high frequencies regime, the equations that link the material properties with phase velocity and attenuation, for extensional as well as torsional vibrations, have not been developed.

I will present the analytical calculations and numerical computations for the torsional and extensional vibrations of homogeneous, isotropic, fully-saturated, porous circular cylinders. Based upon these results, I will present a systematic and transparent methodology for deducing poroelastic constants from the torsional and the extensional observed measurements for low as well as for high frequencies, (i.e. below and above Biot critical frequency, respectively).

The low-frequency regime equations for torsional and extensional vibrations presented here, are in agreement with those obtained by Dunn and Gardner, respectively.

Based on this work a set of torsional and extensional oscillation experiments are designed, (e.g. frame saturated with two different fluids, and or cylinders of different radius), to determine their material properties values.

---

## I.4 Framework

The theory of wave propagation in porous media was introduced in the middle of the last century by Biot (1956; 1962). In Biot's formulation, the change in porosity during deformation does not appear explicitly in the constitutive relations. It excludes the fluid strain-rate dependence in its fluid stress tensor, otherwise it would have rendered the energy potential non-conservative, which contradicts the assumption on which it is based. This amounts to not taking into consideration the viscous loss within the pore-fluid in the fluid stress tensor of the Biot theory. In addition, it makes the framework mathematically inconsistent because it renders only four degrees of freedom instead of the actual six degrees of freedom.

Recently, by volume averaging pore-scale dynamic equations, a theory of poroelasticity has been developed on a firm basis, (de la Cruz and Spanos (1985; 1989); de la Cruz et al. (1993); Hickey et al. (1995); Sahay (1996) and Sahay et al. (2001)), wherein change in porosity during deformation is explicitly present in the constitutive relations. The constitutive relations of this theory of poroelasticity incorporates the internal viscous loss process as a relaxation term in a natural way, in addition to the usual Darcian dissipation process.

Thus, this theory could be viewed as Biot theory corrected for pore-fluid viscous relaxation, hereafter it will be referred to as the modified Biot theory. It should be noted that this relaxation process gives a wave-number dependent loss whereas the Darcian dissipation loss is independent of wave-number. For a porous sample saturated with highly viscous fluid, such as heavy crude oil or bitumen, this relaxation process is of importance. In addition, it makes the framework consistent by incorporating the two

missing degrees of freedom that the Biot theory did not consider.

In order to properly take into account the change in porosity during deformation and pore-fluid viscous relaxation I carried out the study of extensional and torsional mode of vibrations in the framework of the modified Biot theory.

## I.5 Outline of thesis

In the attempt to present a clear and understandable outline of the thesis I have gone into a detailed description of the different sections of each chapter.

In chapter II, a review of Biot theory is presented and it is also shown that the fluid-strain rate is not taken into account in the fluid stress-tensor causing Biot theory to miss two degrees of freedom making it mathematically inconsistent. In addition, the absence of the fluid-strain rate into the fluid stress-tensor leaves out the viscous loss within pore-fluid mechanisms which is of importance for porous sample saturated with highly viscous fluid. Next, is presented the Biot theory corrected for pore-fluid viscosity, hereafter named the modified Biot theory. By using the volume-average approach the fluid-strain rate and change in porosity is incorporated into the constitutive relations in a natural way making the modified Biot theory mathematically consistent with the incorporation of the two missing degrees of freedom. Then the equations of motions for poroelasticity in the modified Biot framework in terms of solid and fluid displacements are presented.

The analysis on torsional and extensional vibrations of porous cylinders are done in terms of solid and fluid displacement fields, however the natural fields variables are the

centre-of-mass and internal fields variables which have not been yet analyzed.

The centre-of-mass and internal fields are the natural fields variables because in reality geophones track the centre-of-mass field which is associated with the in-phase motion of solid and fluid displacements. The internal field amounts to fluid flow because it is the motion of fluid relative to the solid-frame. While the internal field is not detected directly, its effect is measured via the attenuation of the centre-of-mass field. Therefore, the equations of motions are rewritten in terms of the centre-of-mass and internal fields.

In chapter III the problems for torsional and extensional modes of vibration of an homogeneous and isotropic poroelastic, circular cylinder cast in the framework of modified Biot theory of poroelasticity are stated. The equations of motion in cylindrical coordinates, which is the natural coordinate system for torsional and extensional vibrations of porous cylinders, are also presented. Finally, because the corresponding problems are two dimensional the appropriate two dimensional boundary value problems are therefore presented.

In chapter IV the solution of the boundary-value problem associated with standing torsional oscillations of a finite, poroelastic, circular cylinder cast in the framework of the modified Biot theory is developed. Using the eigenvalue perturbation approach, for the solution of the problem under consideration, the expressions for torsional resonance and temporal attenuation frequencies are found and there expressions are linked in a transparent manner with the material properties of the porous cylinder.

The general solution of the torsional boundary-value problem obtained using an eigenfunction approach is presented. The expressions for the torsional resonance and tempo-

ral attenuation frequencies thus obtained are algebraically complicated when attempting to show the material properties dependence in a transparent manner. These expressions are reworked by the eigenvalue perturbation approach such that the link with material properties is transparent. To obtain this solution of the boundary value problem a transformation of the displacement field vector was chosen, such that the diagonal part of the transformed wave operator is viewed as the unperturbed operator and the off-diagonal part of the transformed wave operator is viewed as the perturbation. The unperturbed operator has the characteristics that its values for the resonance and temporal attenuation frequencies are close to the exact values. Because of the unperturbed operator being diagonal thus the resonance and temporal attenuation frequencies expressions are straightforwardly apparent.

The above analysis shows how the attenuation is controlled by permeability and the fluid's shear viscosity, and how the resonance frequency drops compared to its dry frame value due to the effect of fluid mass.

Chapter V addresses the case in which the excitation of torsional mode is a robust technique for dynamic measurement of the materials rigidity. In this technique a cylindrical core of finite length is excited into a characteristic torsional mode and the resonance and the temporal attenuation frequencies are recorded. Based on the results of the complete analysis of the boundary value problem associated with torsional mode of vibration of a finite, fully-saturated, homogeneous and isotropic porous circular cylinder cast in the modified Biot theory, future torsional mode experiments can be designed to determine the poroelastic material properties.

In a torsional oscillation problem there are seven parameters involved. Four of the

seven constituent properties, namely, fluid and solid mass densities and fluid shear viscosity, and porosity can easily be ascertained by well known standard procedures. Since these four parameters are known, the procedures used to determine the remaining three macroscopic parameters, namely, frame shear modulus, permeability and tortuosity factor based on torsional resonance experiment are presented.

Chapter VI presents the solution of the open-pore stress-free boundary-value problems associated with extensional oscillations of a poroelastic, circular cylinder cast in the framework of the modified Biot theory. The expressions for the extensional phase velocity and for the attenuation, in which the dependence upon the material properties are transparent are developed.

In addition to the above, the general solution for the extensional vibrations of poroelastic cylinders is presented and is followed by the analysis of the open-pore stress-free boundary-value problem.

The dispersion relation of the open-pore stress-free boundary-value problem results in a quartic equation which is algebraically difficult to solve. For this reason a numerical approach was used to obtain and show the four roots of the problem. Although there are four roots, only one represents the extensional vibrations of the cylinders, with the other three representing the extensional diffusion wave processes. These roots are complex numbers in which the real parts are related to phase velocity and the attenuation is related by the ratio of the imaginary part to the real part. In the plot of the extensional phase velocity and attenuation curves a simple dependence of them to the material properties becomes visible.

Thus, based on physical arguments, the quartic order extensional dispersion relation is reduced to a form such that a second order extensional dispersion relation is obtained. In which one of the roots of this second order expression represents the extensional wave propagation for porous cylinders. This is presented by analytical expression, and using this as a basis, the phase velocity and attenuation are linked with material properties in a transparent manner.

This analysis shows how the attenuation is controlled by permeability, fluid shear viscosity and the radius of the cylinder, and how the phase velocity increases compared to Young's modulus of the dry-frame value due to the effect of fluid mass.

Finally, concluding remarks are presented in chapter VII.

# Chapter II

## Poroelasticity Framework: An overview

This chapter presents an overview of the theory of poroelasticity, for a homogeneous and isotropic porous medium as presented in Biot (1956) modified for the pore-fluid viscous relaxation process. This modified Biot framework is the basis for the study in this thesis.

Section II.1 presents a review of the homogeneous and isotropic poroelastic Biot theory (1956). The Biot theory considers only as an attenuation loss mechanism the motion of the fluid with respect to the solid-frame omitting the viscous loss within pore-fluid as a mechanism of attenuation in a porous media. This occurs because the fluid-strain rate, (i. e. pore-fluid viscous relaxation process), is not incorporated into its constitutive relations and as a result it predicts an additional "non propagating" shear process. The existence of this non propagating process renders two degrees of freedom of the theory redundant. In order to carry out a meaningful mathematical analysis in this framework the approach thus far has been to simply ignore these two redundant degrees of freedom, and workout a boundary value problem in the reduced domain of four degrees of freedom.

By incorporating pore-fluid strain-rate term, (i.e. pore-fluid viscous relaxation mech-



anism), in the constitutive relations the "non-propagating" process of the Biot theory can be turned into a propagating wave process, although highly diffusive, and thus there is no longer any mathematical inconsistency.

Section II.2 presents this modified Biot theory. Using the volume-average approach the fluid-strain rate term is incorporated into the Biot constitutive relations in a natural way.

Sahay (1996) showed that the natural dynamical fields for a wave propagation problem, are the centre-of-mass field, which is mass weighted solid and fluid motions, and the internal field, which is the difference of solid and fluid motions. In Section II.3 the reformulation of the modified Biot theory, in terms of centre-of-mass and internal fields, is presented. It is the framework in which boundary value problems are studied in this thesis.

The centre-of-mass and internal field variables are more representative than the solid and fluid displacements because the centre-of-mass field represents the in-phase displacements of the solid and fluid phases, thus in reality the geophones track the centre-of-mass field. The internal field represents the out-of phase displacement of both phases. Although the internal field is not detected directly, its effect is measured via the attenuation of the centre-of-mass field. Therefore, the equations of motion are written in terms of these natural fields.

For the purpose of this thesis, Biot theory of poroelasticity for an homogeneous and isotropic porous medium corrected for pore fluid viscous relaxation process and stated in terms of dynamical variables, centre-of-mass and internal fields, is the theory of

poroelasticity.

## II.1 Biot theory

The porous medium considered in this thesis consists of an homogeneous and isotropic elastic solid matrix permeated by interconnected pores that are filled with a newtonian fluid. In such a medium at macroscopic scale (i.e. for wavelengths that are orders of magnitude larger than the characteristic pore/grain dimension) the governing equations of motion according to Biot (1956, 1962) are:

$$(1 - \eta_0) \rho_0^s \partial_t^2 \bar{u}_j^s = \bar{\tau}_{jk,k}^s + I_j, \quad (1)$$

$$\eta_0 \rho_0^f \partial_t^2 \bar{u}_j^f = \bar{\tau}_{jk,k}^f - I_j, \quad (2)$$

in which  $\bar{u}_j^s$  and  $\bar{u}_j^f$  are the solid frame and the fluid displacement fields, respectively.  $\eta_0$  is the unperturbed porosity.  $\rho_0^s$  and  $\rho_0^f$  are the solid and fluid densities, respectively.

$\bar{\tau}_{jk}^s$  and  $\bar{\tau}_{jk}^f$  are, respectively, the solid and fluid macroscopic stress tensors, Biot suggested these stresses to be

$$\bar{\tau}_{jk}^s = K^0 \bar{u}_{jj}^s \delta_{jk} + 2\mu^0 \bar{u}_{jk}^s - (\alpha - \eta_0) \bar{p}^f, \quad (3)$$

$$\bar{\tau}_{jk}^f = -\eta_0 \bar{p}^f \delta_{jk}, \quad (4)$$

and the fluid pressure,  $\bar{p}^f$ , is expressed as

$$\bar{p}^f = -M\alpha \bar{u}_{jj}^s + M\zeta. \quad (5)$$

The solid-frame strain tensor  $\bar{u}_{jk}^s$  is

$$\bar{u}_{jk}^s = \frac{1}{2} \left( \bar{u}_{j,k}^s + \bar{u}_{k,j}^s \right). \quad (6)$$

$\tilde{u}_{jk}^s$  is the trace free part of solid-frame strain tensor and it is

$$\tilde{u}_{jk}^s = \bar{u}_{jk}^s - \frac{1}{3} \delta_{jk} \bar{u}_{ll}^s. \quad (7)$$

$\zeta$  is interpreted as increase of fluid content and it is the divergence of the difference of fluid and solid displacements, that is

$$\zeta = -\eta_0 \left( \bar{u}_{j,j}^f - \bar{u}_{j,j}^s \right). \quad (8)$$

$K^0$  and  $\mu^0$  are respectively frame bulk- and shear- modulus. The Biot bulk coefficient,  $\alpha$ , and the fluid storage coefficient,  $M$ , are linked to the bulk moduli of the constituent solid,  $K^s$ , and the constituent fluid,  $K^f$ , as

$$\alpha = 1 - \frac{K^0}{K^s}, \quad (9)$$

$$\frac{1}{M} = \frac{\eta_0}{K^f} + \frac{\alpha - \eta_0}{K^s}, \quad (10)$$

with  $\alpha$  bounded between  $\eta_0$  and unity.

$I_j$  is the drag force that the two phases impart on each other in equal but opposite manner. It is taken to be linearly related to the difference in velocity and acceleration of two phases as

$$I_j = -\frac{\eta_0^2 \mu^f}{K} \partial_t \left( \bar{u}_j^s - \bar{u}_j^f \right) + \rho^{12} \partial_t^2 \left( \bar{u}_j^s - \bar{u}_j^f \right), \quad (11)$$

where  $K$  is permeability,  $\mu^f$  is the fluid shear viscosity and  $\rho^{12}$  is the induced mass-coefficient, which is linked to tortuosity,  $S$ , as

$$\rho^{12} = -(S - 1)\eta_0\rho_0^f. \quad (12)$$

Some authors (Johnson et al, 1987; Pride, et al 2002) presented permeability and tortuosity as frequency dependent which essentially have an effect in the frequency band above Biot critical frequency  $\left(= \frac{\eta_0\mu^f}{\rho_0^f K}\right)$ . Being that the frequency range of our interest is below Biot critical frequency, permeability and tortuosity will be considered as frequency independent.

It is apparent the fluid strain-rate dependence is excluded from the macroscopic fluid stress tensor (eq 4), thus leaving out any viscous loss mechanism within the pore fluid. For a porous sample saturated with highly viscous fluid, such as heavy crude oil or bitumen, the viscous loss mechanism within the pore fluid may be of importance.

The absence of the fluid strain-rate in the fluid stress tensor makes the framework inconsistent, because it generates two redundant degrees of freedom in Biot theory. It has been customary, beginning with Biot (1956), just to ignore these redundant degrees and study a boundary value problem in the domain of the remaining four degrees of freedom.

When the fluid strain-rate is incorporated into the constitutive relations, the poroelastic theory should be viewed as the Biot theory corrected for pore-fluid viscosity which is called the modified Biot theory. In addition to the above the modified Biot theory automatically rectifies the redundancy in the degrees of freedom of the Biot theory,

making it a six degree of freedom theory as is expected. Thus, the methodology to find the solutions of the boundary value problems under considerations are now clear and straightforward, and thus the physical implications are transparent.

## II.2 Modified Biot theory

### II.2.1 General form of constitutive relation by volume average approach

The volume-averaging approach brings the missing fluid strain-rate term in Biot's constitutive relation in a natural way by deducing the macroscopic constitutive equations from the constitutive relations for the solid and fluid at pore scale. The constitutive relations for the solid and fluid constituents at pore-scale are, respectively, taken to be described by linear elasticity and newtonian rheology as

$$\sigma_{jk}^s = K^s \delta_{jk} u_{jj}^s + 2\mu^s \tilde{u}_{jk}^s, \quad (13)$$

$$\sigma_{jk}^f = -p^f \delta_{jk} + \Pi_{jk}, \quad (14)$$

and the pore-scale fluid pressure is expressed as

$$p^f = -K^f u_{jj}^f. \quad (15)$$

The viscous strain tensor  $\Pi_{jk}$  is the term that brings the role of pore-fluid viscous relaxation at pore-scale

$$\Pi_{jk} = \xi^f \delta_{jk} \partial_t u_{jj}^f + 2\mu^f \partial_t \tilde{u}_{jk}^f, \quad (16)$$

where  $\xi^f$  and  $\mu^f$  are the bulk and shear viscosities of the fluid.  $\mu^s$  is the shear moduli of the solid.  $K^s$  and  $K^f$  are the bulk and compression of fluid moduli respectively.

In the volume average approach (Whitaker, 1966, 1969; Slattery, 1969) the porous medium is split in regions  $V$  of identical shapes, volumes and orientations, and then assigned an average value for the physical quantities within the volume to a material point which uniquely represents the average value of the regions  $V$ . When the volume average approach is applied the problem is reformulated at a macroscopic scale in such a manner that the over abundance of physical details at the pore-scale is eliminated. Applying the volume average procedure to the constitutes relations for the solid and fluid constituents of the porous medium, eqs (13) and (14), and utilizing the continuity of velocity fields at pore interfaces and linearization, the macroscopic stresses (Sahay et al., 2001), are

$$\bar{\tau}_{jk}^s = (1-\eta_0)\bar{\sigma}_{jk}^s = K^s\delta_{jk}[(1-\eta_0)\bar{u}_{ll}^s - (\eta-\eta_0)] + 2\mu^s((1-\eta_0)\bar{u}_{jk}^s + D_{jk}), \quad (17)$$

$$\bar{\tau}_{jk}^f = \eta_0\bar{\sigma}_{jk}^f = -\eta_0\bar{p}^f\delta_{jk} + \underbrace{\xi^f\delta_{jk}(\eta_0\partial_t\bar{u}_{ll}^f + \partial_t\eta)} + 2\mu^f(\eta_0\partial_t\bar{u}_{jk}^f - \partial_t D_{jk}), \quad (18)$$

and the volume-average fluid pressure equation is

$$\eta_0\bar{p}^f = -K^f(\eta_0\bar{u}_{ll}^f + (\eta - \eta_0)). \quad (19)$$

The term  $\eta - \eta_0$  is

$$\eta - \eta_0 = -\frac{1}{V} \int_{A^{sf}} u_q^s \hat{n}_q dA, \quad (20)$$

where  $A^{\text{sf}}$  represents the pore interfaces in the averaging volume  $V$  and the unit normal  $\hat{n}_q$  points from solid to fluid phase.  $\eta - \eta_0$  is the area integral of dilatational motion, i.e. motion perpendicular to pore boundaries. Hence, it is the sum of motion of pore interfaces in its normal direction, per unit volume of the porous medium.

$D_{ij}$  is the sum over the pore boundary deviatoric motion, i.e. sum of interfacial motion along itself, in a unit volume of the porous medium, which is expressed as

$$D_{ij} = \frac{1}{V} \int_{A^{\text{sf}}} \frac{1}{2} \left( u_i^{\text{s}} \hat{n}_j + u_j^{\text{s}} \hat{n}_i - \frac{2}{3} \delta_{ij} u_q^{\text{s}} \hat{n}_q \right) dA. \quad (21)$$

As a direct result of the above a general form of macroscopic constitutive relations is obtained in which the role of the viscous loss within the pore-fluid is incorporated. The underlined expression in eq (18) shows the presence of the pore fluid viscosity in the constitutive relations which are the missing members of the fluid stress in Biot theory macroscopic constitutive relations.

## II.2.2 Reduction of the general form to Biot constitutive relations corrected for pore-fluid viscous relaxation

If the area integral term of dilatational motion of pore interface,  $\eta - \eta_0$ , is assumed to be linearly related to the difference of the solid and fluid pressures as follows

$$(\eta - \eta_0) = -\frac{(1 - \eta_0)(\alpha - \eta_0)}{K^0} (\bar{p}^{\text{s}} - \bar{p}^{\text{f}}), \quad (22)$$

and the area integral of deviatoric motion of pore interface,  $D_{jk}$ , is taken to be solely linearly dependent of deviatoric part of solid stress,  $\tilde{\tau}_{jk}^{\text{s}}$ , as

$$D_{jk} = -\frac{\beta - \eta_0}{2\mu^0} \tilde{\tau}_{jk}^{\text{s}}. \quad (23)$$

where  $\beta$  is the Biot shear coefficient and its explicit form is

$$\beta = 1 - \frac{\mu^0}{\mu^s}. \quad (24)$$

The general macroscopic constitutive equations (17-19) exactly render the Biot constitutive relations (ignoring contribution due to the underlined expression in eq 18).

Substituting the expression of  $\bar{p}^f$  from eq (19) and the expression for  $\bar{p}^s$  from (17), using the identity  $(1 - \eta_0) \bar{p}^s = -\frac{1}{3} \bar{\tau}_{ll}^s$ , into the porosity equation (22) permits it to be rewritten in terms of solid and fluid macroscopic dilatations as

$$(\eta - \eta_0) = \delta^s \bar{u}_{ll}^s - \delta^f \bar{u}_{ll}^f, \quad (25)$$

where the  $\delta^s$  and  $\delta^f$  are

$$\delta^s = \eta_0 (\alpha - \eta_0) \frac{M}{K^f}, \quad (26)$$

$$\delta^f = \eta_0 (\alpha - \eta_0) \frac{M}{K^s}, \quad (27)$$

and from eq (17) it is obtained that  $\tilde{\tau}_{jk}^s = 2\mu^0 \tilde{u}_{jk}^s$ , thus eq (23) renders the pore-boundary deviatoric term  $D_{jk}$  to be rewritten as

$$D_{jk} = -(\beta - \eta_0) \tilde{u}_{jk}^s. \quad (28)$$

By substituting eq (25) into eq (19) the Biot fluid pressure eq (5) is obtained. When eqs (25) and (28) are substituted into eq (17), Biot solid stress eq (3) is obtained.

The role of the viscous loss within the pore-fluid mechanism was incorporated in the constitutive relations (the underline expression in eq 18) in a transparent manner and



also the link with the Biot theory is established clearly.

Until this point the theory is expressed in terms of solid and fluid displacements, however geophones do not register the movement of solid and fluid phases separately, but they register the in-phase motion of both solid and fluid constituents.

New field variables will be introduced namely the centre-of-mass and internal fields. These new variables are more adequate than the solid and fluid displacements because the centre-of-mass field represents in-phase displacements of the solid and fluid, thus in reality the geophones only track the centre-of-mass field.

## II.3 Modified Biot theory in terms of the centre-of-mass and internal fields

### II.3.1 Dynamical variables

The centre-of-mass,  $\bar{u}_j^m$ , and internal,  $\bar{u}_j^i$ , fields in terms of the solid and fluid motions,  $\bar{u}_j^s$  and  $\bar{u}_j^f$  are (Sahay,1996)

$$\begin{pmatrix} \bar{u}_j^m \\ \bar{u}_j^i \end{pmatrix} = \begin{pmatrix} m^s & m^f \\ 1 & -1 \end{pmatrix} \begin{pmatrix} \bar{u}_j^s \\ \bar{u}_j^f \end{pmatrix}, \quad (29)$$

where the solid- and fluid- mass fractions,  $m^s$  and  $m^f$  respectively, are

$$m^s = \frac{\phi_0 \rho_0^s}{\rho_0^m}, \quad (30)$$

$$m^f = \frac{\eta_0 \rho_0^f}{\rho_0^m}, \quad (31)$$

and the total density of the porous medium,  $\rho_0^m$ , is

$$\rho_0^m = (1 - \eta_0) \rho_0^s + \eta_0 \rho_0^f. \quad (32)$$

The center-of-mass field,  $\bar{u}_j^m$ , is a linear combination of solid and fluid displacements weighted by the solid- and fluid- mass fractions, respectively. Hence the center-of-mass field is associated with total linear-momentum flux whereas the internal field,  $\bar{u}_j^i$ , is associated with the relative acceleration of two phases and it describes spin (angular momentum about the mass center) flux. Since geophones register the field associated with total linear-momentum, they in fact track the centre-of-mass field. The internal field amounts to fluid flow because it is the motion of fluid relative to the solid frame. While the internal field is not detected directly, its effect is measured via the attenuation of the centre-of-mass field. Thus the new field variables are compatible with dynamical measurements. Hereafter they are referred as dynamical variables.

The equations of motion recasted in terms of the centre-of-mass and internal fields are

$$\rho_0^m \partial_t^2 \bar{u}_j^m = \bar{\tau}_{jk,k}^m, \quad (33)$$

$$\rho_0^r \partial_t^2 \bar{u}_j^i = \bar{\tau}_{jk,k}^i + I_j, \quad (34)$$

where  $I_j$  is the drag force term expressed in terms of the natural dynamical fields as

$$I_j = -\frac{\eta_0^2 \mu^f}{K} \partial_t \bar{u}_j^i + \rho^{12} \partial_t^2 \bar{u}_j^i, \quad (35)$$

and  $\bar{\tau}_{jk}^m$  and  $\bar{\tau}_{jk}^i$  are respectively the total stress of the porous medium and the stress associated with the relative acceleration of the two phases which are related to the solid

and fluid stresses by

$$\begin{pmatrix} \bar{\tau}_{jk}^m \\ \bar{\tau}_{jk}^i \end{pmatrix} = \begin{pmatrix} 1 & 1 \\ \frac{\rho_0^r}{\phi_0 \rho_0^s} & \frac{\rho_0^r}{\eta_0 \rho_0^f} \end{pmatrix} \begin{pmatrix} \bar{\tau}_{jk}^s \\ \bar{\tau}_{jk}^f \end{pmatrix}, \quad (36)$$

where  $\rho_0^r$  is the reduced mass density of the porous medium which is given by

$$\rho_0^r = \frac{1}{(1 - \eta_0) \rho_0^s} + \frac{1}{\eta_0 \rho_0^f}. \quad (37)$$

The constitutive relations are reformulated in terms of the natural dynamical fields as

$$\begin{pmatrix} \bar{\tau}_{jk}^m \\ \bar{\tau}_{jk}^i \end{pmatrix} = \begin{pmatrix} K^{mm} & K^{mi} \\ K^{im} & K^{ii} \end{pmatrix} \begin{pmatrix} \bar{u}_{ll}^m \\ \bar{u}_{ll}^i \end{pmatrix} \delta_{jk} + 2 \begin{pmatrix} \mu^{mm} & \mu^{mi} \\ \mu^{im} & \mu^{ii} \end{pmatrix} \begin{pmatrix} \tilde{u}_{jk}^m \\ \tilde{u}_{jk}^i \end{pmatrix}, \quad (38)$$

where the stressess are expressed in the standard representation as the elastic constant follow by the strain-rate tensor.

The constants matrices in eq (38) are defined by

$$\begin{pmatrix} K^{mm} & K^{mi} \\ K^{im} & K^{ii} \end{pmatrix} \equiv \mathbf{K} + \boldsymbol{\xi} \partial_t, \quad (39)$$

$$\begin{pmatrix} \mu^{mm} & \mu^{mi} \\ \mu^{im} & \mu^{ii} \end{pmatrix} \equiv \boldsymbol{\mu} + \boldsymbol{\varsigma} \partial_t. \quad (40)$$

Their explicit expressions in terms of material properties are given by

$$\mathbf{K} = \begin{pmatrix} 1 & m^f \\ m^f & (m^f)^2 \end{pmatrix} \left( 1 - \eta_0 - \eta_0 (\alpha - \eta_0) \frac{M}{K^f} \right) K^s$$

$$\begin{aligned}
& + \begin{pmatrix} 1 & -m^s \\ m^f & -m^f m^s \end{pmatrix} \eta_0 (\alpha - \eta_0) M \\
& + \begin{pmatrix} 1 & m^f \\ -m^s & -m^f m^s \end{pmatrix} \eta_0 (\alpha - \eta_0) M \\
& + \begin{pmatrix} 1 & -m^s \\ -m^s & (m^s)^2 \end{pmatrix} \left( \eta_0 - \eta_0 (\alpha - \eta_0) \frac{M}{K^s} \right) K^f, \tag{41}
\end{aligned}$$

$$\begin{aligned}
\boldsymbol{\xi} & = \begin{pmatrix} 1 & m^f \\ -m^s & -m^f m^s \end{pmatrix} \eta_0 (\alpha - \eta_0) \frac{M}{K^f} \boldsymbol{\xi}^f \\
& + \begin{pmatrix} 1 & -m^s \\ -m^s & (m^s)^2 \end{pmatrix} \left( \eta_0 - \eta_0 (\alpha - \eta_0) \frac{M}{K^s} \right) \boldsymbol{\xi}^f, \tag{42}
\end{aligned}$$

$$\boldsymbol{\mu} = \begin{pmatrix} 1 & m^f \\ m^f & (m^f)^2 \end{pmatrix} \mu^0, \tag{43}$$

$$\boldsymbol{\varsigma} = \begin{pmatrix} 1 & m^f \\ -m^s & -m^f m^s \end{pmatrix} (\beta - \eta_0) \mu^f + \begin{pmatrix} 1 & -m^s \\ -m^s & (m^s)^2 \end{pmatrix} \eta_0 \mu^f. \tag{44}$$

### II.3.2 Extended dynamical variables framework

To simplify the notation the dynamical variables (29) are expressed in a vector form as

$$\mathbf{u}_j = \left( \bar{u}_j^m, \bar{u}_j^i \right)^T, \tag{45}$$

where the two-component vector in the  $j$ th direction  $\mathbf{u}_j$  is named the extended dynamical field vector. Also the constitutive relations (38) can be rewritten in a vector form as

$$\boldsymbol{\tau}_{jk} = \left( \bar{\tau}_{jk}^m, \bar{\tau}_{jk}^i \right)^T. \tag{46}$$

Hence, the equations of motion (33)-(34) in the extended dynamical framework can be rewritten as

$$\boldsymbol{\rho} \partial_t^2 \mathbf{u}_j + \frac{\eta_0^2 \mu^f}{\mathbf{K}} \mathbf{I}_0 \partial_t \mathbf{u}_j = \boldsymbol{\tau}_{jk,k}, \quad (47)$$

where the elements of the second-order  $\boldsymbol{\rho}$  matrix have dimensions of density and the second-order matrix  $\mathbf{I}_0$  has all of its elements equal to zero with the exception of one element. Their explicit expressions are

$$\boldsymbol{\rho} = \begin{pmatrix} \rho_0^m & 0 \\ 0 & \rho_0^i \end{pmatrix}, \quad (48)$$

$$\mathbf{I}_0 = \begin{pmatrix} 0 & 0 \\ 0 & 1 \end{pmatrix}, \quad (49)$$

and the stress  $\boldsymbol{\tau}_{jk}$  term is expressed as

$$\boldsymbol{\tau}_{jk} = (\mathbf{K} + \boldsymbol{\xi} \partial_t) \mathbf{u}_{ll} \delta_{jk} + 2(\boldsymbol{\mu} + \boldsymbol{\varsigma} \partial_t) \tilde{\mathbf{u}}_{jk}. \quad (50)$$

To make the equation of motion (eq 47) notationally akin to elasticity the left hand side of this equation is multiplied by  $\boldsymbol{\rho}^{-1}$ ,

$$\mathbf{I} \partial_t^2 \mathbf{u}_j + \Omega \mathbf{I}_0 \partial_t \mathbf{u}_j = \boldsymbol{\rho}^{-1} \boldsymbol{\tau}_{jk,k}, \quad (51)$$

and the second order matrices are rewritten as  $\mathbf{K} = \boldsymbol{\rho} \left( \mathbf{C}_\alpha - \frac{4}{3} \mathbf{C}_\beta \right)$ ,  $\boldsymbol{\xi} = \boldsymbol{\rho} \left( \mathbf{N}_\alpha - \frac{4}{3} \mathbf{N}_\beta \right)$ ,  $\boldsymbol{\mu} = \boldsymbol{\rho} \mathbf{C}_\beta$  and  $\boldsymbol{\varsigma} = \boldsymbol{\rho} \mathbf{N}_\beta$ . The elements of the second-order  $\mathbf{C}_\alpha$  and  $\mathbf{C}_\beta$  matrices have dimensions of velocity squared and they contain the frame shear modulus and frame and fluid densities. The elements of the second-order  $\mathbf{N}_\alpha$  and  $\mathbf{N}_\beta$  matrices have dimensions of kinematic viscosity and they contain the fluid shear viscosity. The explicit

expressions of these parameters are given in Appendix A.  $\Omega$  is the relaxation frequency corresponding to the dissipation due to fluid flow with respect to the solid-frame and it contains a permeability term. Its explicit expression is

$$\Omega = \frac{\eta_0^2 \mu^f}{\rho_0^i K}, \quad (52)$$

In fact, it is akin to the well known Biot critical frequency.  $\mathbf{I}$  is the  $2 \times 2$  identity matrix associated with the inertial terms.

Substituting the expressions for  $\mathbf{K}$ ,  $\boldsymbol{\xi}$ ,  $\boldsymbol{\mu}$  and  $\boldsymbol{\varsigma}$  in terms of velocities, kinematic viscosity and densities into eq (50), the stress term can be rewritten as

$$\boldsymbol{\tau}_{jk} = \boldsymbol{\rho} \left[ \left\{ \left( \mathbf{C}_\alpha - \frac{4}{3} \mathbf{C}_\beta \right) + \left( \mathbf{N}_\alpha - \frac{4}{3} \mathbf{N}_\beta \right) \partial_t \right\} \mathbf{u}_{ll} \delta_{jk} + 2 \left( \mathbf{C}_\beta + \mathbf{N}_\beta \partial_t \right) \tilde{\mathbf{u}}_{jk} \right]. \quad (53)$$

Taking the divergence of the stress term (eq 53) and substituting it into eq (51), then introducing the following extended dynamical field vector

$$\mathbf{u} = \hat{\mathbf{e}}_j \mathbf{u}_j = \hat{\mathbf{e}}_j (\bar{\mathbf{u}}_j^m, \bar{\mathbf{u}}_j^i)^T = (\mathbf{u}^m, \mathbf{u}^i)^T, \quad (54)$$

where  $\hat{\mathbf{e}}_j$  is the unit vector in  $j$ th direction and  $\mathbf{u}_j$  is the extended dynamical field vector in the  $j$ th direction (eq 45), the poroelasticity equation of motion (eq 51) can be rewritten in terms of the extended dynamical displacement fields in vector notation as

$$\mathbf{I} \partial_t^2 \mathbf{u} + \Omega \mathbf{I}_0 \partial_t \mathbf{u} = (\mathbf{C}_\alpha + \mathbf{N}_\alpha \partial_t) \nabla (\nabla \cdot \mathbf{u}) - (\mathbf{C}_\beta + \mathbf{N}_\beta \partial_t) \nabla \times \nabla \times \mathbf{u}. \quad (55)$$

It should be noted that the matricial representation (55) makes the poroelasticity equations of motion notationally akin to the familiar elasticity theory.

# Chapter III

## Formulation of boundary value problems for torsional and longitudinal standing waves

In this chapter the boundary value problems for torsional and extensional modes of vibration of a homogeneous and isotropic poroelastic, circular cylinder subjected to stress-free boundary conditions are cast in the framework of the theory of poroelasticity as stated in section II.3. The cylindrical coordinate system is the natural framework here.

In a torsional mode of vibration the cylinder undergoes an angular displacement independent of the azimuthal angle and there are no radial and axial displacements. In the longitudinal mode of vibration it undergoes radial and axial displacements independent of the azimuthal angle and there is no angular displacement. These modes are two dimensional vibrations.

Section III.1 lists the equations of motion and constitutive relations in cylindrical coordinates. Section III.2 presents the statement of the boundary value problem associated with torsional-standing waves and the extensional standing wave boundary-value prob-

lem is stated in section III.3.

### III.1 Governing equations in cylindrical coordinates

The equations of motion (51) and constitutive relations (53) expressed in cylindrical coordinates take the form

$$\mathbf{I}\partial_t^2\mathbf{u}_r + \Omega\mathbf{I}_0\partial_t\mathbf{u}_r = \boldsymbol{\rho}^{-1} \left( \boldsymbol{\tau}_{rz,z} + \boldsymbol{\tau}_{rr,r} + \frac{1}{r}\boldsymbol{\tau}_{r\theta,\theta} + \frac{1}{r}(\boldsymbol{\tau}_{rr} - \boldsymbol{\tau}_{\theta\theta}) \right), \quad (56)$$

$$\mathbf{I}\partial_t^2\mathbf{u}_\theta + \Omega\mathbf{I}_0\partial_t\mathbf{u}_\theta = \boldsymbol{\rho}^{-1} \left( \boldsymbol{\tau}_{\theta z,z} + \boldsymbol{\tau}_{r\theta,r} + \frac{1}{r}\boldsymbol{\tau}_{\theta\theta,\theta} + \frac{2}{r}\boldsymbol{\tau}_{r\theta} \right), \quad (57)$$

$$\mathbf{I}\partial_t^2\mathbf{u}_z + \Omega\mathbf{I}_0\partial_t\mathbf{u}_z = \boldsymbol{\rho}^{-1} \left( \boldsymbol{\tau}_{zz,z} + \boldsymbol{\tau}_{rz,r} + \frac{1}{r}\boldsymbol{\tau}_{\theta z,\theta} + \frac{1}{r}\boldsymbol{\tau}_{rz} \right), \quad (58)$$

and

$$\begin{aligned} \boldsymbol{\tau}_{rr} = & \boldsymbol{\rho} \left[ \{(\mathbf{C}_\alpha + \mathbf{N}_\alpha\partial_t) - 2(\mathbf{C}_\beta + \mathbf{N}_\beta\partial_t)\} \left\{ \left( \partial_r + \frac{1}{r} \right) \mathbf{u}_r + \frac{1}{r}\partial_\theta\mathbf{u}_\theta + \partial_z\mathbf{u}_z \right\} \right. \\ & \left. + 2(\mathbf{C}_\beta + \mathbf{N}_\beta\partial_t)\partial_r\mathbf{u}_r \right], \end{aligned} \quad (59)$$

$$\begin{aligned} \boldsymbol{\tau}_{zz} = & \boldsymbol{\rho} \left[ \{(\mathbf{C}_\alpha + \mathbf{N}_\alpha\partial_t) - 2(\mathbf{C}_\beta + \mathbf{N}_\beta\partial_t)\} \left\{ \left( \partial_r + \frac{1}{r} \right) \mathbf{u}_r + \frac{1}{r}\partial_\theta\mathbf{u}_\theta + \partial_z\mathbf{u}_z \right\} \right. \\ & \left. + 2(\mathbf{C}_\beta + \mathbf{N}_\beta\partial_t)\partial_z\mathbf{u}_z \right], \end{aligned} \quad (60)$$

$$\begin{aligned} \boldsymbol{\tau}_{\theta\theta} = & \boldsymbol{\rho} \left[ \{(\mathbf{C}_\alpha + \mathbf{N}_\alpha\partial_t) - 2(\mathbf{C}_\beta + \mathbf{N}_\beta\partial_t)\} \left\{ \left( \partial_r + \frac{1}{r} \right) \mathbf{u}_r + \frac{1}{r}\partial_\theta\mathbf{u}_\theta + \partial_z\mathbf{u}_z \right\} \right. \\ & \left. + 2(\mathbf{C}_\beta + \mathbf{N}_\beta\partial_t)\frac{1}{r}(\partial_\theta\mathbf{u}_\theta + \mathbf{u}_r) \right], \end{aligned} \quad (61)$$

$$\boldsymbol{\tau}_{rz} = \boldsymbol{\rho} [(\mathbf{C}_\beta + \mathbf{N}_\beta\partial_t)(\partial_z\mathbf{u}_r + \partial_r\mathbf{u}_z)], \quad (62)$$

$$\boldsymbol{\tau}_{r\theta} = \boldsymbol{\rho} \left[ (\mathbf{C}_\beta + \mathbf{N}_\beta\partial_t) \left\{ \left( \partial_r - \frac{1}{r} \right) \mathbf{u}_\theta + \frac{1}{r}\partial_\theta\mathbf{u}_r \right\} \right], \quad (63)$$

$$\boldsymbol{\tau}_{\theta z} = \boldsymbol{\rho} \left[ (\mathbf{C}_\beta + \mathbf{N}_\beta\partial_t) \left( \frac{1}{r}\partial_\theta\mathbf{u}_z + \partial_z\mathbf{u}_\theta \right) \right]. \quad (64)$$



## III.2 Torsional problem

In a torsional mode of vibration poroelastic circular cylinders undergo angular displacement,  $\mathbf{u}_\theta$ , independent of the azimuthal angle,  $\theta$ , such that there are no axial or radial displacements, i.e.  $\mathbf{u}_r = \mathbf{u}_z = \mathbf{0}$ . This means that the cross-section of the cylinder rotates without distortion. Because of no dependence on azimuthal angle, the equation of motion (57) for angular displacement simplifies to

$$\mathbf{I}\partial_t^2\mathbf{u}_\theta + \Omega\mathbf{I}_0\partial_t\mathbf{u}_\theta = \boldsymbol{\rho}^{-1} \left( \boldsymbol{\tau}_{\theta z,z} + \boldsymbol{\tau}_{r\theta,r} + \frac{2}{r}\boldsymbol{\tau}_{r\theta} \right), \quad (65)$$

and the stresses (63) and (64) simplifies to

$$\boldsymbol{\tau}_{r\theta} = \boldsymbol{\rho} (\mathbf{C}_\beta + \mathbf{N}_\beta\partial_t) \left( \partial_r - \frac{1}{r} \right) \mathbf{u}_\theta, \quad (66)$$

$$\boldsymbol{\tau}_{\theta z} = \boldsymbol{\rho} (\mathbf{C}_\beta + \mathbf{N}_\beta\partial_t) \partial_z \mathbf{u}_\theta. \quad (67)$$

Substituting the stresses (66) and (67) into eq (65) the governing equation for torsional mode of vibration in terms of the angular displacement field is

$$\mathbf{I}\partial_t^2\mathbf{u}_\theta + \Omega\mathbf{I}_0\partial_t\mathbf{u}_\theta = (\mathbf{C}_\beta + \mathbf{N}_\beta\partial_t) \left[ \frac{1}{r}\partial_r (r\partial_r) + \partial_z^2 - \frac{1}{r^2} \right] \mathbf{u}_\theta. \quad (68)$$

For torsional mode this equation subjected to stress-free boundary conditions, at radial surface ( $r = a$ ), top end-cap ( $z = L$ ) and bottom end-cap ( $z = 0$ ), has to be solved. For stress-free surface condition, tractions are not at all present at the boundary, i.e. traction on both solid and fluid phases are zero. This in turns implies that

$$\boldsymbol{\tau}_{r\theta}|_{r=a} = \mathbf{0}, \quad \boldsymbol{\tau}_{\theta z}|_{z=0} = \mathbf{0}, \quad \boldsymbol{\tau}_{\theta z}|_{z=L} = \mathbf{0}. \quad (69)$$

### III.3 Longitudinal problem

In a longitudinal mode of vibration poroelastic circular cylinders undergo radial,  $\mathbf{u}_r$ , and axial,  $\mathbf{u}_z$ , displacements independent of the azimuthal angle,  $\theta$ , such that there is no angular displacement,  $\mathbf{u}_\theta = \mathbf{0}$ . This means that the motion of each material point is confined to the plane defined by the unit vectors for the radial,  $\hat{\mathbf{e}}_r$ , and axial,  $\hat{\mathbf{e}}_z$ , directions. Because of no dependence on azimuthal angle, the equations of motion (56) and (58) for radial and axial displacements simplifies to

$$\mathbf{I}\partial_t^2\mathbf{u}_r + \Omega\mathbf{I}_0\partial_t\mathbf{u}_r = \boldsymbol{\rho}^{-1} \left( \boldsymbol{\tau}_{rz,z} + \boldsymbol{\tau}_{rr,r} + \frac{1}{r}(\boldsymbol{\tau}_{rr} - \boldsymbol{\tau}_{\theta\theta}) \right), \quad (70)$$

$$\mathbf{I}\partial_t^2\mathbf{u}_z + \Omega\mathbf{I}_0\partial_t\mathbf{u}_z = \boldsymbol{\rho}^{-1} \left( \boldsymbol{\tau}_{zz,z} + \boldsymbol{\tau}_{rz,r} + \frac{1}{r}\boldsymbol{\tau}_{rz} \right), \quad (71)$$

and the stresses (59)-(62) simplifies to

$$\begin{aligned} \boldsymbol{\tau}_{rr} &= \boldsymbol{\rho} \left[ \{(\mathbf{C}_\alpha + \mathbf{N}_\alpha \partial_t) - 2(\mathbf{C}_\beta + \mathbf{N}_\beta \partial_t)\} \left\{ \left( \partial_r + \frac{1}{r} \right) \mathbf{u}_r + \partial_z \mathbf{u}_z \right\} \right. \\ &\quad \left. + 2(\mathbf{C}_\beta + \mathbf{N}_\beta \partial_t) \partial_r \mathbf{u}_r \right], \end{aligned} \quad (72)$$

$$\begin{aligned} \boldsymbol{\tau}_{zz} &= \boldsymbol{\rho} \left[ \{(\mathbf{C}_\alpha + \mathbf{N}_\alpha \partial_t) - 2(\mathbf{C}_\beta + \mathbf{N}_\beta \partial_t)\} \left\{ \left( \partial_r + \frac{1}{r} \right) \mathbf{u}_r + \partial_z \mathbf{u}_z \right\} \right. \\ &\quad \left. + 2(\mathbf{C}_\beta + \mathbf{N}_\beta \partial_t) \partial_z \mathbf{u}_z \right], \end{aligned} \quad (73)$$

$$\begin{aligned} \boldsymbol{\tau}_{\theta\theta} &= \boldsymbol{\rho} \left[ \{(\mathbf{C}_\alpha + \mathbf{N}_\alpha \partial_t) - 2(\mathbf{C}_\beta + \mathbf{N}_\beta \partial_t)\} \left\{ \left( \partial_r + \frac{1}{r} \right) \mathbf{u}_r + \partial_z \mathbf{u}_z \right\} \right. \\ &\quad \left. + 2(\mathbf{C}_\beta + \mathbf{N}_\beta \partial_t) \frac{\mathbf{u}_r}{r} \right], \end{aligned} \quad (74)$$

$$\boldsymbol{\tau}_{rz} = \boldsymbol{\rho} [(\mathbf{C}_\beta + \mathbf{N}_\beta \partial_t) (\partial_z \mathbf{u}_r + \partial_r \mathbf{u}_z)]. \quad (75)$$

Substituting stresses (72)-(75) into eqs (70)-(71) and introducing the notation for the extended dynamical variables in cylindrical coordinates,

$$\mathbf{u} = \hat{\mathbf{e}}_r \mathbf{u}_r + \hat{\mathbf{e}}_z \mathbf{u}_z = (\mathbf{u}^m, \mathbf{u}^i)^T, \quad (76)$$

the governing equation for longitudinal motion is

$$\mathbf{I}\partial_t^2\mathbf{u}+\Omega\mathbf{I}_0\partial_t\mathbf{u}=(\mathbf{C}_\alpha+\mathbf{N}_\alpha\partial_t)\nabla(\nabla\cdot\mathbf{u})-(\mathbf{C}_\beta+\mathbf{N}_\beta\partial_t)\nabla\times\nabla\times\mathbf{u}. \quad (77)$$

For longitudinal mode of vibration equation (77), subjected to open-pore as well as closed-pore boundary conditions at the surface ( $r = a$ ), is solved. For open-pore surface condition the fluid is free to move across the boundary and no traction exist on the surface of the cylinder. This in turns implies that

$$\boldsymbol{\tau}_{rr}|_{r=a} = \mathbf{0}, \quad \boldsymbol{\tau}_{rz}|_{r=a} = \mathbf{0}. \quad (78)$$

For closed-pore surface condition the total force is zero and the fluid is not allowed to escape the surface, i.e. there is no relative motion between solid and fluid displacements at the boundary, which means the internal field is zero on the surface of the cylinder. This in turns implies that

$$\hat{\mathbf{e}}_2\mathbf{u}_r|_{r=a} = \mathbf{0}, \quad \hat{\mathbf{e}}_2\mathbf{u}_z|_{r=a} = \mathbf{0}, \quad \hat{\mathbf{e}}_1\boldsymbol{\tau}_{rr}|_{r=a} = \mathbf{0}, \quad \hat{\mathbf{e}}_1\boldsymbol{\tau}_{rz}|_{r=a} = \mathbf{0}, \quad (79)$$

where  $\hat{\mathbf{e}}_1$  and  $\hat{\mathbf{e}}_2$  are respectively, the unitary two-component vectors  $(1, 0)^T$  and  $(0, 1)^T$ .

In this thesis longitudinal mode of vibrations are solved only for slender cylinders. In a slender cylinder the length of the cylinder is orders of magnitude larger than the radius of the cylinder in such a manner that it is considered as an infinite cylinder. This avoids the elastic (non-porous) longitudinal boundary value problem becoming a non-separable boundary value problem. In the case of a finite elastic cylinder, when the waves hit the end-caps of the cylinder they couple in such a manner that the boundary conditions are not satisfied simultaneously, thus no analytical solution to the problem is

possible. By ensuring the direction of propagation lies along the axial direction for the slender elastic cylinder case the axial and radial motions could be made almost compressional and shear in nature, respectively. Experimentally it is straight forward to setup such standing waves. These modes of vibrations are akin quasi-static extensional or Young's modulus deformation, hence known as extensional modes. The extensional mode is a special longitudinal mode wherein axial motion is compressional in nature, i.e. direction of propagation is along axial direction, and radial motion is shear in nature, as it being executed perpendicular to the direction of propagation. For this reason only solutions for slender porous cylinders are considered in this thesis.

# Chapter IV

## Standing Torsional Waves in Porous Cylinder

This chapter presents the solution of the boundary-value problem associated with standing torsional oscillations of a finite, homogeneous and isotropic, poroelastic, circular cylinder subjected to stress-free boundary conditions cast in the framework of Biot theory modified for pore-fluid viscous relaxation process and expressed in terms of extended dynamical variables as discussed in section II.3.2.

In section IV.1, the general solution is obtained using an eigenfunction approach. The expressions for the torsional resonance and temporal attenuation frequencies thus obtained are algebraically complicated and they do not show the material properties dependence in a transparent manner.

In section IV.2 the expressions for the torsional resonance and temporal attenuation frequencies are reworked by the eigenvalue perturbation approach such that the link with material properties is transparent.

In section IV.3 a summarize of the results of this chapter is presented.

## IV.1 General solution of the problem

The boundary value problem associated with torsional mode is stated in section II.2. The governing equation for angular displacement field,  $\mathbf{u}_\theta = (\bar{\mathbf{u}}_\theta^m, \bar{\mathbf{u}}_\theta^i)^T$ , is eq (68) subjected to boundary conditions (69). The expansion of the solution of the equations of motion is stated in terms of appropriate orthonormal basis functions in radial and axial coordinates that automatically satisfy the boundary conditions. These choices reduce the equations of motion (68) to a system of two coupled, second-order ODEs (in time). The solution is then obtained in a straight forward manner.

### IV.1.1 Eigenfunction expansion

Because of the cylindrical geometry of the problem, one may take the Bessel function of first-order,  $J_1(qr)$ , and the cosine function,  $\cos(kz)$ , as the appropriate basis functions to express the spatial part of displacement fields governed by the differential equation (68).

To satisfy the boundary conditions on the radial surface (eq 69 in conjunction with 66) one requires that  $r\partial_r\left(\frac{J_1(qr)}{r}\right)\Big|_{r=a} = 0$ , which restricts the radial wavenumber  $q$  to be a discrete set defined as  $q_p = \frac{N_p}{a}$ , where  $N_p$  is the  $p^{\text{th}}$  root of the Bessel function of second-order. These Bessel functions form an orthonormal complete set over the interval  $0 \leq r \leq a$ .

In order to satisfy the boundary conditions on the end-caps (eq 69 in conjunction with 67) one requires that the derivative in axial direction of the function  $\cos(kz)$  vanishes at  $z = 0$  and  $z = L$ ; these conditions restrict the axial wavenumber  $k$  to be a discrete set given as  $k_l = \frac{l\pi}{L}$ , where  $l$  is an integer. These cosine functions form an orthonormal complete set over the interval  $0 \leq z \leq L$ .

Hence, the solution is taken to be in the following form

$$\mathbf{u}_\theta(r, z, t) = \sum_{p=1}^{\infty} \sum_{l=1}^{\infty} q_p J_1(q_p r) \cos(k_l z) \mathbf{U}_\theta(t; q_p, k_l) \quad (80)$$

which satisfies the boundary conditions (69).

### IV.1.2 Reduction to a coupled ordinary differential equation system

Substituting the general solution form eq (80) into eq (68), yields the temporal part of displacement field vector,  $\mathbf{U}_\theta = (\mathbf{U}_\theta^m, \mathbf{U}_\theta^i)^\top$ , which is governed by a system of two coupled damped harmonic oscillators

$$\left[ \mathbf{I} \frac{d^2}{dt^2} + (\Omega \mathbf{I}_0 + \boldsymbol{\nu}) \frac{d}{dt} + \mathbf{W} \right] \mathbf{U}_\theta = 0 \quad (81)$$

or in a compact notation

$$\left( \mathbf{I} \frac{d^2}{dt^2} + \mathcal{D} \right) \mathbf{U}_\theta = 0, \quad (82)$$

where

$$\mathbf{W} = (q_p^2 + k_l^2) \mathbf{C}_\beta \quad (83)$$

$$\boldsymbol{\nu} = (q_p^2 + k_l^2) \mathbf{N}_\beta \quad (84)$$

$$\mathcal{D} = (\Omega \mathbf{I}_0 + \boldsymbol{\nu}) \frac{d}{dt} + \mathbf{W}. \quad (85)$$

The matrix  $\mathbf{W}$ , which is the matrix  $\mathbf{C}_\beta$  weighted by the square of the wavenumber, has dimensions of frequency squared. As it is associated with the elastic stiffness, it may be regarded as the fundamental-frequency (squared) matrix of the system. The matrix  $\boldsymbol{\nu}$ , which is the kinematic viscosity matrix  $\mathbf{N}_\beta$  weighted by the square of the

wavenumber, also has dimensions of frequency. Thus, it is the wavenumber-dependent damping matrix due to viscous loss within the pore fluid. The explicit expressions of these matrices are given in appendix A.

### IV.1.3 Eigenfrequency

A solution is sought for eq (82) in the form of  $e^{-i\omega(q_p, k_l)t}$  in order to obtain the 4th-order characteristic polynomial

$$\omega \left\{ \omega^3 + i [\Omega + Tr(\boldsymbol{\nu})] \omega^2 - [Tr(\mathbf{W}) + \Omega \nu^{mm}] \omega - i [\Omega W^{mm} + Tr(\mathbf{W}) Tr(\boldsymbol{\nu}) - Tr(\mathbf{W}\boldsymbol{\nu})] \right\} = 0. \quad (86)$$

Hereafter,  $Tr()$  stands for the trace of the matrix within the braces.  $\omega = 0$  is the trivial root of eq (86) (hereafter it is labelled as  $\omega_4$ ). The remaining three discrete (complex) frequencies associated with torsional-eigen vibrations are determined by solving the cubic polynomial within the curly braces ( $\{ \}$ ) in eq (86).

#### IV.1.3.1 The solutions of the characteristic polynomial

Utilizing the CRC standard mathematical tables (Selby, 1971; p. 103) the roots were found to be

$$\begin{aligned} \omega_1(q_p, k_l) &= -\frac{A+B}{2} + i \left( \sqrt{3} \frac{A-B}{2} - \frac{h}{3} \right) \\ \omega_2(q_p, k_l) &= A+B - i \frac{h}{3} \\ \omega_3(q_p, k_l) &= -\frac{A+B}{2} - i \left( \sqrt{3} \frac{A-B}{2} + \frac{h}{3} \right) \end{aligned} \quad (87)$$



where  $A$  and  $B$  are complex numbers as expressed below

$$\begin{aligned} A &= i^{(1/3)} \left( -\frac{d}{2} + \sqrt{\frac{d^2}{4} - \frac{b^3}{27}} \right)^{(1/3)} \\ B &= -i^{(1/3)} \left( \frac{d}{2} + \sqrt{\frac{d^2}{4} - \frac{b^3}{27}} \right)^{(1/3)} \end{aligned} \quad (88)$$

and the real constants are expressed as follows

$$\begin{aligned} b &= \frac{1}{3} (3f + h^2) \\ d &= \frac{1}{27} (27g - 2h^3 - 9hf) \\ h &= \Omega + Tr(\boldsymbol{\nu}) \\ f &= -[Tr(\mathbf{W}) + \Omega\nu^{mm}] \\ g &= -[\Omega W^{mm} + Tr(\mathbf{W})Tr(\boldsymbol{\nu}) - Tr(\mathbf{W}\boldsymbol{\nu})]. \end{aligned} \quad (89)$$

Using that  $i^{(1/3)} = \frac{1}{2}(\sqrt{3} + i)$  then  $\Re A = \sqrt{3} \Im A$  and  $B = -\frac{1}{3}\frac{b}{A}$ , hereafter  $\Re$  and  $\Im$  stand for the real and imaginary parts of the quantity, respectively, and adopting the standard notation for discrete functions,  $\omega_j(\mathbf{p}, l) \equiv \omega_j(q_{\mathbf{p}}, k_l)$  (where  $j = 1, 2, 3$ ), the three complex roots (eqs 87) expressed in their real and imaginary parts explicitly are found to be

$$\begin{aligned} \omega_1(\mathbf{p}, l) &= \Re A \frac{b - 3 [(\Re A)^2 + (\Im A)^2]}{3 [(\Re A)^2 + (\Im A)^2]} \\ &\quad - \frac{i}{3} \left[ h - \Im A \frac{b + 3 [(\Re A)^2 + (\Im A)^2]}{3 [(\Re A)^2 + (\Im A)^2]} \right], \end{aligned} \quad (90)$$

$$\begin{aligned} \omega_2(\mathbf{p}, l) &= -\Re A \frac{b - 3 [(\Re A)^2 + (\Im A)^2]}{3 [(\Re A)^2 + (\Im A)^2]} \\ &\quad - \frac{i}{3} \left[ h - \Im A \frac{b + 3 [(\Re A)^2 + (\Im A)^2]}{3 [(\Re A)^2 + (\Im A)^2]} \right], \end{aligned} \quad (91)$$

$$\omega_3(p, l) = -\frac{i}{3} \left[ h + 2\Im A \frac{b + 3 [(\Re A)^2 + (\Im A)^2]}{(\Re A)^2 + (\Im A)^2} \right]. \quad (92)$$

For realistic parameters in regard to geomaterials, the quantity  $\frac{d^2}{4} - \frac{b^3}{27} > 0$  and  $d < 0$ , which implies the real and imaginary parts of  $A$  are positive and

$$h > \Im A \frac{b + 3 [(\Re A)^2 + (\Im A)^2]}{3 [(\Re A)^2 + (\Im A)^2]} > 0, \quad (93)$$

for which the pair  $\omega_1(p, l)$  and  $\omega_2(p, l)$  have the same (negative) imaginary parts and equal but opposite real parts. The root  $\omega_3(p, l)$  is purely (negative) imaginary.

It should be noted that the real and imaginary parts of the root are, respectively, the resonance frequency and the temporal attenuation frequency of the process. The first pair, those with the same negative imaginary part and equal but opposite real parts, correspond to an underdamped harmonic oscillation and they represent torsional-waves propagating in opposite directions. The other two roots, the purely (negative) imaginary  $\omega_3(p, l)$  and the trivial root  $\omega_4(p, l) = 0$  correspond to an overdamped harmonic oscillation and they represent a diffusive torsional process.

In the usual nomenclature, the former pair is the fast-wave process and the later pair is the slow-wave process. Clearly if a porous sample is set into torsional resonance, it is the fast process that goes into vibration because only its eigenfrequencies have non-zero real parts.

#### IV.1.4 Some numerical results

Although the eigenfrequency expressions (90-92) are exact, the dependence on the material properties are not transparent in them. In order to get some insight, numerical

computations of eigenfrequencies are presented, corresponding to the first harmonics in radial ( $q_1$ ) and axial ( $k_1$ ) directions, for the fast and slow processes of a sample of Berea Sandstone for a wide range of viscosity values. The poroelastic sample used for numerical computation has a radius of  $1.9 \times 10^{-2}$  (m) and length of  $40 \times 10^{-2}$  (m), hence the first harmonics are  $q_1 = 270.296$  and  $k_1 = 7.854$ . The other physical properties used are listed in appendix B.

The computation with respect to viscosity is motivated by the fact that, in a laboratory setting, torsional experiments are often carried out on the same sample saturated with different fluids. It should be noted that in this calculation, for numerical purposes, the fluid density is kept the same while the viscosity value is varied. The range of viscosity values may seem unphysical but they are used in this manner in order to exhibit the entire spectrum of behavior.

The resonance frequency and temporal attenuation frequency plots of the fast process, i.e. the real and imaginary parts of the (either  $\omega_1(1,1)$  or  $\omega_2(1,1)$ ) eigenfrequency, are in Fig. 1 (marked as blue and red curves, respectively). Because the real part of the eigenfrequency,  $\Re\omega$ , is zero for a part of the data so attenuation has been plotted as the imaginary part of the eigenfrequency,  $\Im\omega$ , rather than its usual representation as quality factor  $Q$ , which is  $\frac{\Re\omega}{\Im\omega}$ .

For clarity, both resonance and temporal attenuation frequencies values are scaled by  $\omega_0(1,1)$ , the resonance frequency for the dry-frame for the corresponding mode, eq (421). The details about  $\omega_0(1,1)$  are in appendix C. The temporal attenuation frequency curve of the slow process ( $\omega_3(1,1)$ ) is presented in Fig. 2. In this case the real part of the eigenfrequency is always zero.

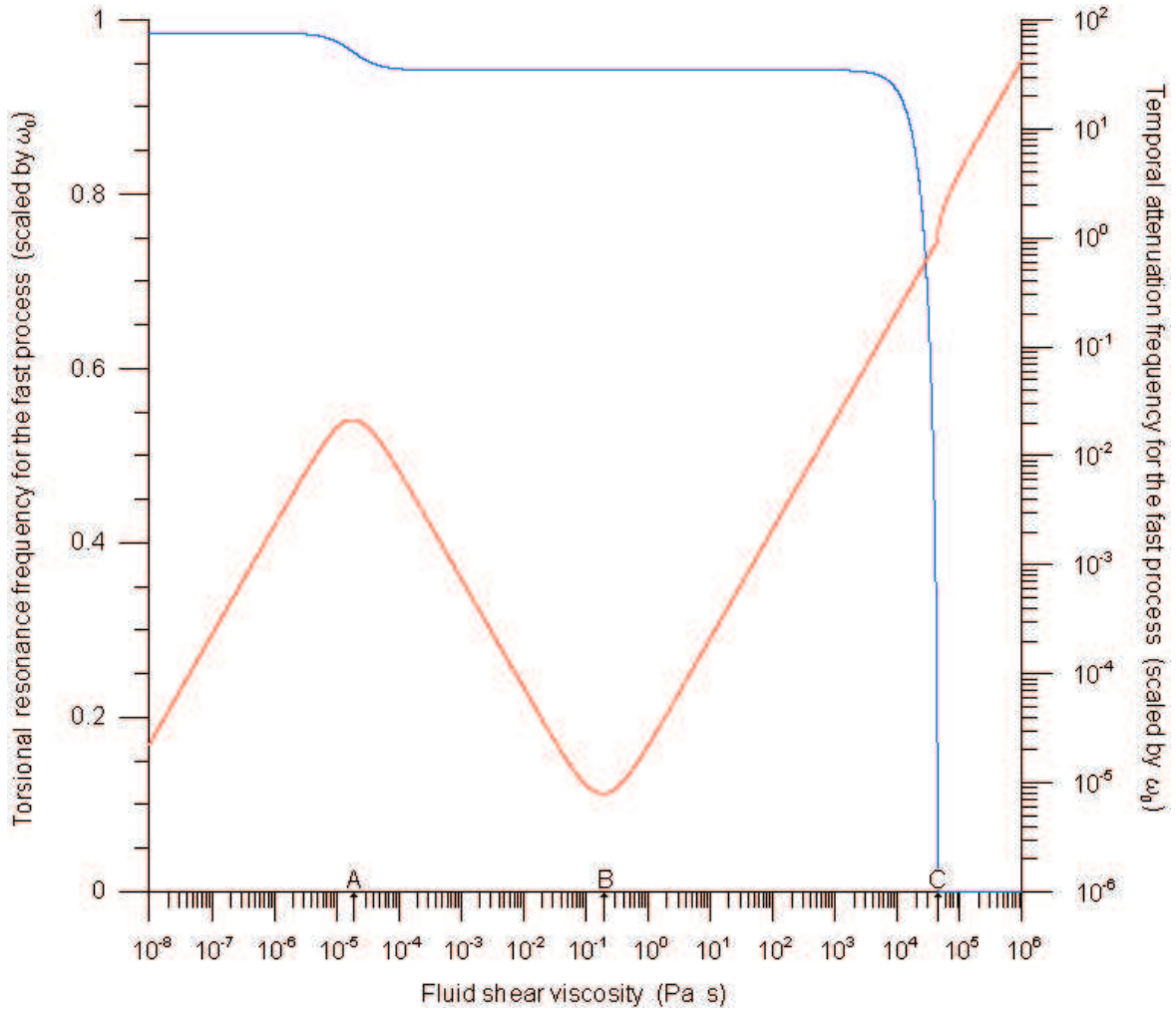


Figure 1. The plot of torsional resonance frequency,  $\Re\omega_1(1,1)$ , the blue curve and temporal attenuation frequency,  $\Im\omega_1(1,1)$ , the red curve versus fluid viscosity associated with the fast process corresponding to the first harmonics in radial and axial directions, eq (90). Both curves are scaled by the resonance frequency of the dry-frame,  $\omega_0(1,1)$ , and its corresponding equation is given in (421). For clarity the crossover viscosities A, B and C, whose explicit representations are given later in section IV.2.4.4, are also marked.

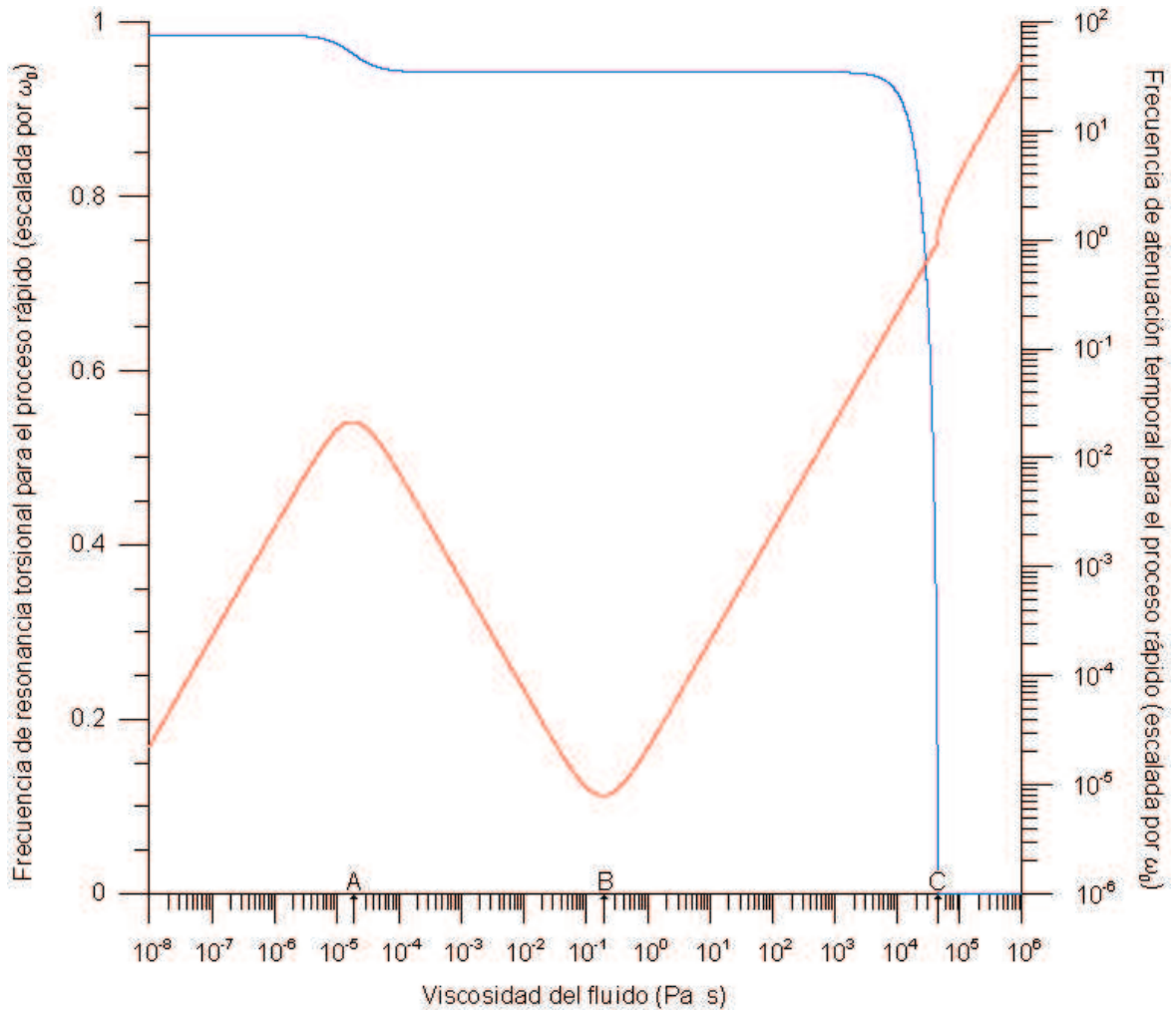


Figure 2. Gráfica de la frecuencia de resonancia torsional en azul,  $\Re\omega_1(1, 1)$ , y de la frecuencia de atenuación temporal en rojo,  $\Im\omega_1(1, 1)$ , contra la viscosidad del fluido correspondiente al proceso rápido asociado con los primeros armónicos en las direcciones radial y axial, ec (90). Ambas curvas están escaladas con la frecuencia de resonancia asociada a la matriz porosa sin fluido,  $\omega_0(1, 1)$ , cuya correspondiente ecuación es 421. Por claridad también se muestran las viscosidades de frontera A, B y C, cuyas expresiones están dadas en la sección 4.2.4.4.

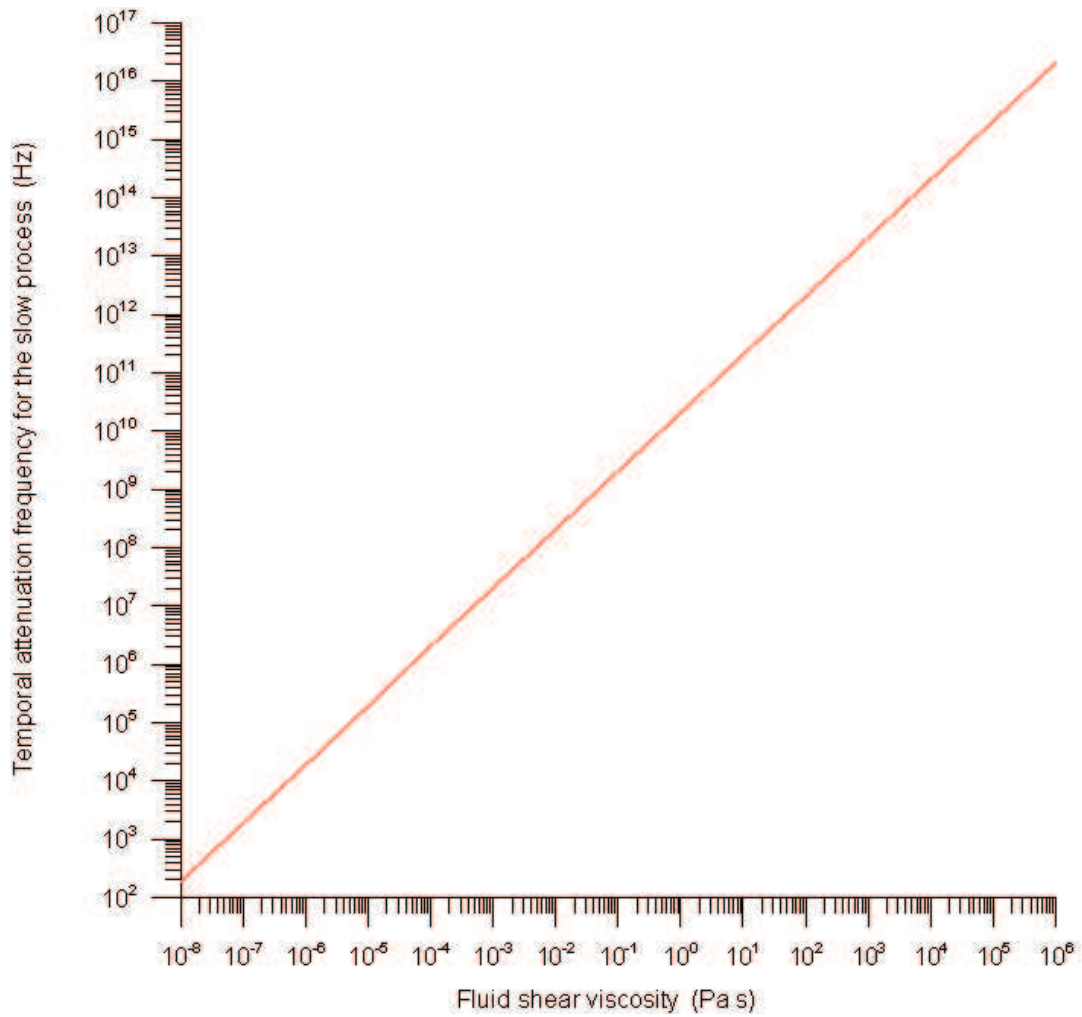


Figure 3. The plot of temporal attenuation frequency,  $\Im\omega_3(1,1)$ , versus fluid shear viscosity for the slow process corresponding to the first harmonics in radial and axial directions, eq (92). In this process the real part of the eigenfrequency is zero, therefore it is not plotted.

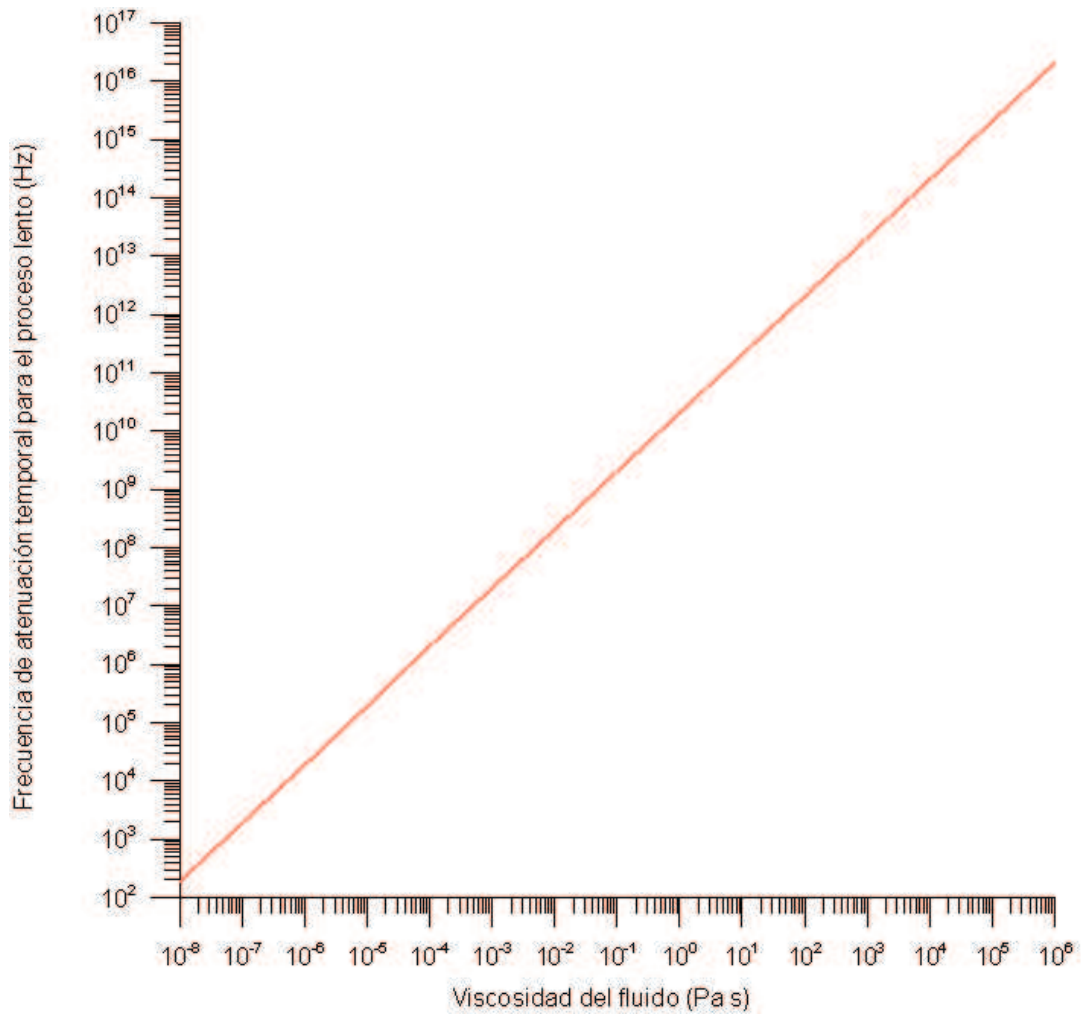


Figure 4. Gráfica de la frecuencia de atenuación temporal,  $\Im\omega_3(1, 1)$ , contra la viscosidad del fluido correspondiente al proceso lento asociado con los primeros armónicos en las direcciones radial y axial, ec (92). En este proceso la parte real de las frecuencias características son cero, por lo que no se muestran.

#### IV.1.4.1 Description of plots

The plots in Fig. 1 are characterized by three crossover viscosity values referred to as A, B and C, whose explicit expressions are defined in section IV.2.4.4. In the resonance frequency plot the third crossover viscosity, C, marks the transition from an underdamped to an overdamped state of vibration. Above C there is no resonance vibration. Below C there are two regimes defined by the first crossover viscosity marked as A. In each of these two regimes the resonance frequency drops below the value for the dry-frame ( $\omega_0(1, 1)$ ) by constant amounts. The drop is less in the regime that lies below A compared to the regime that lies between A and C. The second crossover viscosity, B, does not have any signature on the resonance plot.

The red curve in Fig. 1, the temporal attenuation frequency plot shows segmented linear trends with viscosity. Above the crossover viscosity C, it increases linearly as expected of an overdamped system. Below the crossover viscosity A, the trend is also linearly increasing. At the crossover viscosity A its trend, after forming a smooth crest, becomes linearly decreasing. This trend continues until the crossover viscosity B at which it again becomes linearly increasing after forming a smooth trough.

The temporal attenuation frequency for the slow process presented in Fig. 2 shows the expected increasing linear trend with viscosity.

## IV.2 The eigenvalue perturbation approach

There are altogether eight material parameters in this problem: four constituent properties, namely, fluid ( $\rho_0^f$ ) and solid ( $\rho_0^s$ ) mass densities, fluid shear viscosity ( $\mu^f$ ) and shear modulus of the solid-grain ( $\mu^s$ ), and four averaged parameters, namely, unper-



turbed porosity ( $\eta_0$ ), permeability (K), induced-mass-coefficient (or tortuosity factor S) and the frame shear modulus ( $\mu^0$ ).

Although in the plots (Figs. 1 and 2) only the variation with respect to fluid viscosity is presented, it can be found that the variations due to the other parameters do not alter the trends of the curves. A variation in either solid or fluid density simply alters the magnitude of the drop (from the  $\omega_0(1, 1)$  value) on the resonance curve. The tortuosity factor variation only alters the drop value of the resonance frequency curve in the regime below the crossover viscosity  $A$ .

A change in either frame shear modulus ( $\mu^0$ ) or solid-grain shear modulus ( $\mu^s$ ) amounts to a variation in  $\omega_0(1, 1)$ . Since  $\omega_0(1, 1)$  is the scale factor of the resonance frequency plot, the trend of curve remains the same, although, the crossover viscosity  $A$  moves to a lower value as  $\omega_0(1, 1)$  increases. It is found that the inverse of permeability has essentially identical effect on the plots as that of viscosity.

For any given set of material-parameters, the numerical computations show their simple dependence on resonance and temporal attenuation frequencies, although in the exact expressions given by eqs (90-92) the dependences are not apparent. In the following section using the perturbation theory as applied to eigenvalue problems, approximate eigenvalues of the operator  $\mathcal{D}$  (eq 82) can be deduced that are nearly equal to their exact values. This procedure results in rendering the approximate expressions for resonance and temporal attenuation frequencies such that the implicit relations with material properties become transparent.

### IV.2.1 The framework

A transformation of the wave field vector  $\mathbf{U}_\theta = \mathbf{E}\mathbf{V}$  is sought so that eq (82) is transformed to

$$\left(\mathbf{I}\frac{d^2}{dt^2} + \mathcal{L}\right)\mathbf{V} = 0, \text{ where } \mathcal{L} \equiv \mathbf{E}^{-1} \mathcal{D} \mathbf{E}. \quad (94)$$

The similarity transformation ensures that the eigenvalues of the resulting transformed operator  $\mathcal{L}$  stays the same as that of the operator  $\mathcal{D}$ . Splitting the operator  $\mathcal{L}$  in its diagonal part  $\mathcal{L}^{(0)}$  and off-diagonal part  $\mathbf{Q}$  and transforming eq (94) into an eigenvalue perturbation problem

$$\left(\mathbf{I}\frac{d^2}{dt^2} + \mathcal{L}^{(0)} + \mathbf{Q}\right)\mathbf{V} = 0, \quad (95)$$

by imposing the transformation matrix  $\mathbf{E}$  to be such that

(a) the eigenvalues of the diagonal part  $\mathcal{L}^{(0)}$ , of the resulting transformed operator  $\mathcal{L}$  as given by

$$\left(\mathbf{I}\frac{d^2}{dt^2} + \mathcal{L}^{(0)}\right)\mathbf{V}^{(0)} = 0, \quad (96)$$

are close to the exact eigenvalues of the operator  $\mathcal{L}$  (i.e.  $\mathcal{D}$ ), which shall be henceforth referred as zero<sup>th</sup>-order eigenvalues and  $\mathbf{V}^{(0)} = \mathbf{E}^{-1}\mathbf{U}_\theta$  as zero<sup>th</sup>-order eigenvectors, and

(b) the perturbations to the zero<sup>th</sup>-order eigenvalues due to the off-diagonal part  $\mathbf{Q}$  of the transformed operator  $\mathcal{L}$  are practically negligible which is achieved by ensuring the Frobenius norm of the  $\mathbf{Q}$  is orders of magnitude smaller than that of the  $\mathcal{L}^{(0)}$ .

The Frobenius norm of a matrix  $\mathbf{A}$  of order  $m \times n$  is  $\|\mathbf{A}\| = \sqrt{\sum_{i=1}^m \sum_{j=1}^n |a_{ij}|^2}$  where  $a_{ij}$ 's are the elements of the matrix (Golub and Van Loan 1996; section 2.3).

Hereafter,  $\mathcal{L}^{(0)}$  and  $\mathbf{Q}$  shall be referred to as unperturbed and perturbed operators, respectively. The zero<sup>th</sup>-order eigenvalues thus constructed lead to the expressions for resonance and temporal attenuation frequencies in which dominant material properties become distinct.

It turns out the material-parameters space can be split into two regimes. In the first regime the elastic part  $\mathbf{W}$  is the dominant piece in the wave operator  $\mathcal{D}$  (eq 82) whereas in the second regime the anelastic parts,  $\Omega\mathbf{I}_0$  and  $\boldsymbol{\nu}$ , also become important. A dimensionless parameter, which is named  $\Upsilon$ , marks the boundary of these two regimes.

## IV.2.2 The dimensionless parameter $\Upsilon$

For the torsional mode case, the domain  $\Upsilon < 1$  pertains to the regime in which the elastic part is dominant and in Fig. 1 it lies below of the crossover-viscosity A. The domain  $\Upsilon > 1$  corresponds to the regime in which anelastic parts also become important and in Fig. 1 it lies above of the crossover-viscosity A. They can be regarded as inertia dominated and viscosity dominated regimes, respectively.

In the inertia dominated regime the fluid mass partially participates in the inertia associated with the wave process meanwhile in the viscosity dominated regime the fluid mass imparts its mass completely to the inertia associated with the wave process. The boundary of these two regimes are marked by the dimensionless parameter  $\Upsilon$  which is related to the ratio of the modified Biot critical frequency,  $\Omega$ , to the resonance frequency of the dry porous frame,  $\omega_0(p, l)$ , as

$$\Upsilon = \text{R} \frac{\Omega}{\omega_0(p, l)}, \quad (97)$$

the weighting parameter  $R$  is dimensionless and it is

$$R = \frac{d^f m^f}{2\sqrt{m^s} (1 + d^f m^f)^{3/2}}. \quad (98)$$

The above suggests that for realistic geomaterials saturated with light fluids such as air or light hydrocarbon the likely scenario is  $\Upsilon < 10^{-2}$ . For low-permeability rocks saturated with water  $\Upsilon < 10^{-2}$  still holds true but for the high-permeability case  $10^{-2} < \Upsilon < 1$  is more likely. For heavy hydrocarbons such as crude oil and tar  $\Upsilon > 1$  is likely to hold true.

### IV.2.3 Regime I : $\Upsilon < 1$ (inertia dominated regime)

#### IV.2.3.1 The transformation matrix

In the operator  $\mathcal{D}$  (eq 82), if the viscosity is small, the elastic part  $\mathbf{W}$  will be dominant over the anelastic parts, namely, the Darcian dissipation term  $\Omega \mathbf{I}_0$  and the kinematic viscosity term  $\nu$ . In this case the transformation  $\mathbf{E}^I$  (the superscript<sup>I</sup> labels the regime under consideration) should be such that  $(\mathbf{E}^I)^{-1} \mathbf{W} \mathbf{E}^I$  is a diagonal matrix so that the elastic part,  $\mathbf{W}$ , is completely incorporated in the diagonal part,  $\mathcal{L}^{(0,I)}$  (the first superscript<sup>0</sup> indicates the unperturbed operator and the second superscript<sup>I</sup> the regime under consideration) of the transformed operator  $\mathcal{L}^I ((\mathbf{E}^I)^{-1} \mathcal{D} \mathbf{E}^I)$  for this regime.

The resulting diagonal terms of  $(\mathbf{E}^I)^{-1} \mathbf{W} \mathbf{E}^I$ , i.e. the two eigenvalues of the matrix  $\mathbf{W}$  namely  $(W^{mm} + W^{ii})$  and 0, may be viewed as the two fundamental-frequencies (squared) of the system. Therefore, the transformation matrix  $\mathbf{E}^I$  must be the eigenvector matrix of  $\mathbf{W}$  and it is found to be

$$\mathbf{E}^I = \frac{1}{1 + \frac{W^{ii}}{W^{mm}}} \begin{pmatrix} 1 & -\frac{W^{mi}}{W^{mm}} \\ \frac{W^{ii}}{W^{mi}} & 1 \end{pmatrix}, \quad (99)$$

and using eq(83) and (413) it is simplified to

$$\mathbf{E}^I = \frac{1}{1 + d^f m^f} \begin{pmatrix} 1 & -m^f \\ d^f & 1 \end{pmatrix}. \quad (100)$$

The entries in the above matrix are dimensionless parameters and they are defined in table V.

#### IV.2.3.2 The transformed operator $\mathcal{L}^I$

The transformed operator  $\mathcal{L}^I$  is split into its diagonal  $\mathcal{L}^{(0,I)}$  and off-diagonal  $\mathbf{Q}^I$  pieces

$$\mathcal{L}^I = (\mathbf{E}^I)^{-1} \mathcal{D} \mathbf{E}^I = \mathcal{L}^{(0,I)} + \mathbf{Q}^I, \quad (101)$$

where

$$\begin{aligned} \mathcal{L}^{(0,I)} = & \frac{1}{1 + d^f m^f} \left[ \Omega \begin{pmatrix} d^f m^f & 0 \\ 0 & 1 \end{pmatrix} + \right. \\ & \left. \begin{pmatrix} \nu^{mm} + d^f \nu^{mi} + m^f \nu^{im} + d^f m^f \nu^{ii} & 0 \\ 0 & d^f m^f \nu^{mm} - d^f \nu^{mi} - m^f \nu^{im} + \nu^{ii} \end{pmatrix} \right] \frac{d}{dt} \\ & + \begin{pmatrix} W^{mm} + W^{ii} & 0 \\ 0 & 0 \end{pmatrix}, \end{aligned} \quad (102)$$

and

$$\mathbf{Q}^I = \frac{1}{1 + d^f m^f} \left[ \Omega \begin{pmatrix} 0 & m^f \\ d^f & 0 \end{pmatrix} + \begin{pmatrix} 0 \\ -d^f \nu^{mm} - d^{f^2} \nu^{mi} + \nu^{im} + d^f \nu^{ii} \end{pmatrix} \right]$$

$$\left. \begin{array}{c} -m^f \nu^{mm} + \nu^{mi} - m^{f2} \nu^{im} + m^f \nu^{ii} \\ 0 \end{array} \right] \frac{d}{dt}. \quad (103)$$

### IV.2.3.3 Simplification of the unperturbed operator $\mathcal{L}^{(0,I)}$ and the perturbed operator $\mathbf{Q}^I$ for inertial dominated regime

It turns out for the domain  $\Upsilon < 1$ , the kinematic viscosity terms ( $\nu^{mm}$  etc.) are orders of magnitude smaller than  $\Omega$ , hence, they can be ignored and the unperturbed (or diagonal) part is simply

$$\mathcal{L}^{(0,I)} \approx \frac{\Omega}{1 + d^f m^f} \begin{pmatrix} d^f m^f & 0 \\ 0 & 1 \end{pmatrix} \frac{d}{dt} + \begin{pmatrix} W^{mm} + W^{ii} & 0 \\ 0 & 0 \end{pmatrix}, \quad (104)$$

and

$$\left( \mathbf{I} \frac{d^2}{dt^2} + \mathcal{L}^{(0,I)} \right) \mathbf{V}^{(0,I)} = 0, \quad (105)$$

thus yielding the eigenvalues that are regarded as zero<sup>th</sup>-order. The perturbed (or off-diagonal) part reads

$$\mathbf{Q}^I \approx \frac{\Omega}{1 + d^f m^f} \begin{pmatrix} 0 & m^f \\ d^f & 0 \end{pmatrix} \frac{d}{dt}. \quad (106)$$

The zero<sup>th</sup>-order vector field for this regime is  $\mathbf{V}^{(0,I)} = (\mathbf{E}^I)^{-1} \mathbf{U}$ , and using eq (29) it can be express in terms of solid and fluid motions as

$$\mathbf{V}^{(0,I)} = \begin{pmatrix} V_{\text{fast}}^{(0,I)} \\ V_{\text{slow}}^{(0,I)} \end{pmatrix} = \begin{pmatrix} 1 & m^f \\ -d^f & 1 \end{pmatrix} \begin{pmatrix} U_{\theta}^m \\ U_{\theta}^i \end{pmatrix} = \begin{pmatrix} U_{\theta}^s \\ \frac{S-1}{S-m^f} U_{\theta}^s - \frac{S}{S-m^f} U_{\theta}^f \end{pmatrix}. \quad (107)$$

#### IV.2.3.4 Eigenvalues of the unperturbed operator $\mathcal{L}^{(0,I)}$

##### IV.2.3.4.1 Fast process

From eq (107) the fast process, i.e the first component of the transformed field, is found to be simply the solid motion  $U_\theta^s$ . Naturally the first row of eq (105) is its governing equation. It is an equation of a damped harmonic oscillator. Its dispersion relation yields a frequency pair

$$\omega_1^{(0,I)}(p, l), \omega_2^{(0,I)}(1, 1) = -\frac{i}{2} \Omega \frac{d^f m^f}{(1 + d^f m^f)} \pm \sqrt{W^{mm} + W^{ii} - \left( \frac{\Omega}{2} \frac{d^f m^f}{(1 + d^f m^f)} \right)^2} \quad (108)$$

which are regarded as the zero<sup>th</sup>-order eigenfrequencies, for the first harmonics in radial and axial directions, of the fast process in the regime I, and have been labelled with the superindices of eigenfrequencies accordingly. Obviously they represent wave processes propagating in opposite directions. Utilizing the expressions of W's (eq 83 in conjunction with 413 and 421) and  $\Upsilon$  (eq 97) the above can be rewritten as

$$\omega_1^{(0,I)}(p, l), \omega_2^{(0,I)}(p, l) = -\frac{i}{2} \Omega \frac{d^f m^f}{(1 + d^f m^f)} \pm \omega_0(p, l) \sqrt{m^s (1 + d^f m^f)} \sqrt{1 - \Upsilon^2}, \quad (109)$$

and employing the expression of  $d^f$  (table V) it is further simplified to

$$\omega_1^{(0,I)}(p, l), \omega_2^{(0,I)}(p, l) = -\frac{i}{2} \Omega \frac{m^f}{S} \pm \omega_0(p, l) \sqrt{\frac{m^s}{1 - \frac{m^f}{S}}} \sqrt{1 - \Upsilon^2}. \quad (110)$$

##### IV.2.3.4.1.1 $\Re\omega_1^{(0,I)}(p, l)$ and $\Im\omega_1^{(0,I)}(p, l)$ for the fast process

The real and (negative) imaginary parts of  $\omega_1^{(0,I)}(p, l)$  ( or  $\omega_2^{(0,I)}(p, l)$ ) are read as zero<sup>th</sup>-order resonance and temporal attenuation frequencies for the torsional resonance process. In Fig. 3 they are superimposed on the respective exact curves and are plotted as dashed-black lines.

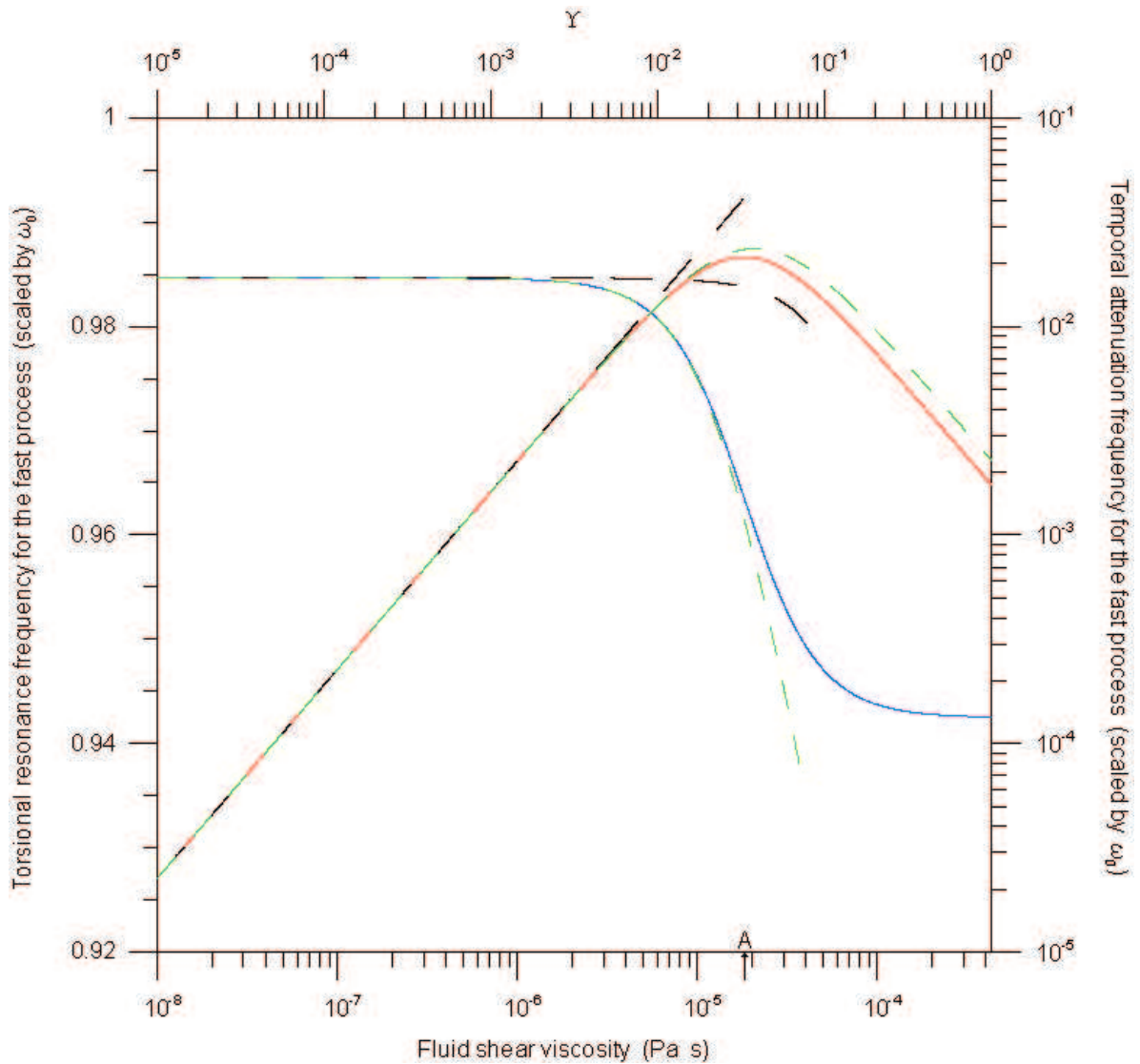


Figure 5. For the regime I ( $\Upsilon < 1$ ) the comparison of exact (eq 90), zero<sup>th</sup>-order (eq 108), and second-order (eq 436) corrected values of the torsional resonance and temporal attenuation frequencies associated with the fast process. The exact resonance,  $\frac{\Re\omega_1(1,1)}{\omega_0(1,1)}$ , and temporal attenuation,  $\frac{\Im\omega_1(1,1)}{\omega_0(1,1)}$ , frequencies are presented as blue and red curves, respectively. On the respective exact curves, the zero<sup>th</sup>-order resonance and temporal attenuation frequencies are superimposed as dashed-black lines, and the dashed-green curves are their second-order corrected values.



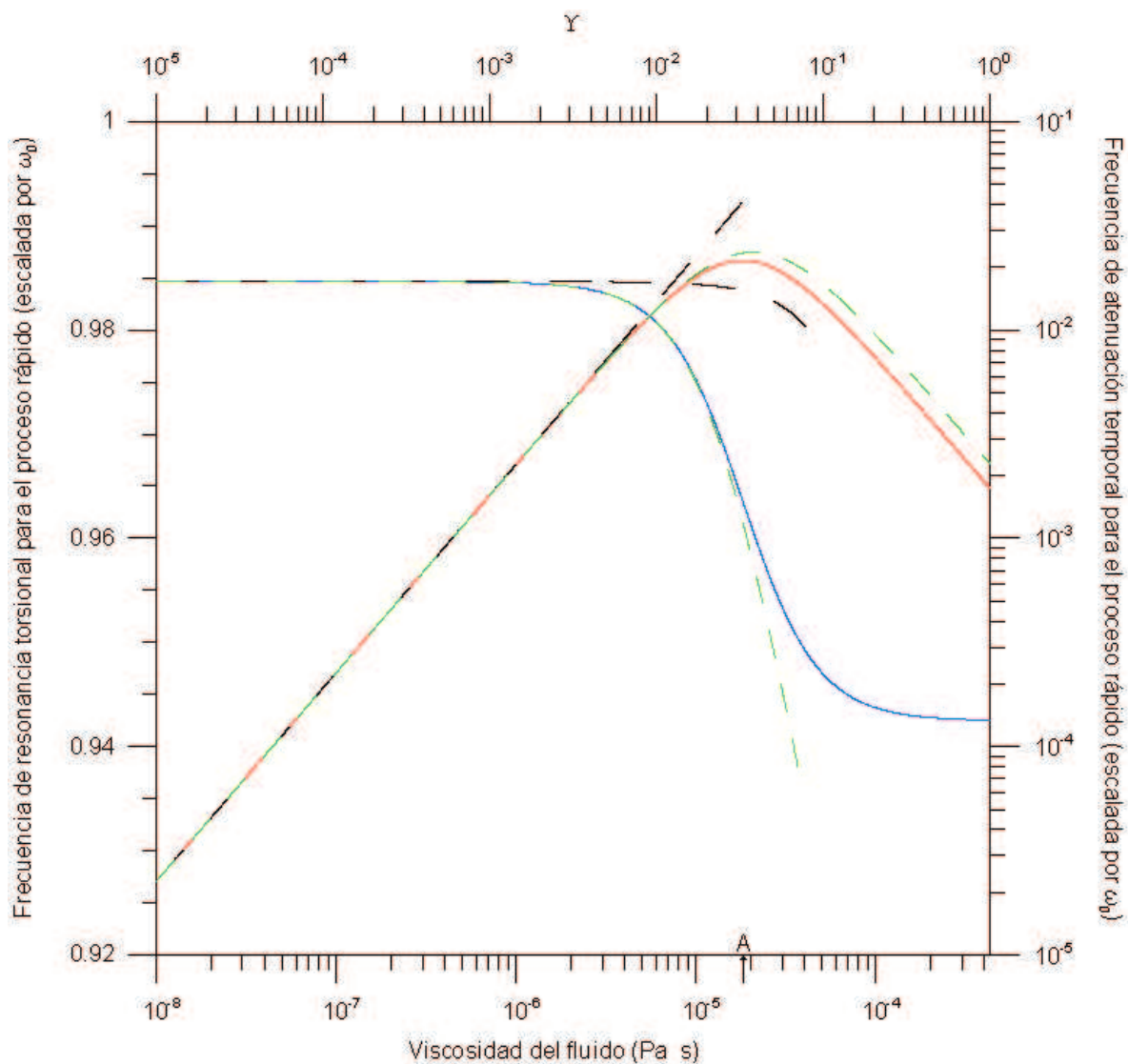


Figure 6. Región I ( $\Upsilon < 1$ ): comparación de los valores exactos (ec 90), de orden cero (ec 108), y segundo orden (ec 436) de las frecuencias de resonancia y atenuación torsional correspondientes al proceso rápido. Las curvas exactas de la frecuencia de resonancia,  $\frac{\Re\omega_1(1,1)}{\omega_0(1,1)}$ , y la atenuación temporal,  $\frac{\Im\omega_1(1,1)}{\omega_0(1,1)}$ , se muestran en azul y rojo, respectivamente. Sobre las respectivas curvas exactas se superimponen las curvas de las frecuencias de resonancia y la atenuación temporal de orden cero en líneas punteadas negras, y las curvas de segundo orden están representadas por líneas punteadas verdes.

To do a quantitative comparison of exact and approximate values the per cent deviation is computed as

$$\% \text{deviation} = \frac{\text{approx} - \text{exact}}{\text{exact}} \times 100. \quad (111)$$

The % deviation of the zero<sup>th</sup>-order and second-order resonance and temporal attenuation frequencies from their exact values are plotted in Figs. 4-7. These plots show them to be essentially in agreement with the exact values for the viscosity value satisfying the inequality  $\Upsilon \ll 1$ .

In fact for  $\Upsilon \ll 1$ , the real part of (110), i.e. the resonance frequency, can be approximated as

$$\Re \omega_1^{(0,1)}(p, l) \approx \omega_0(p, l) \sqrt{\frac{m^s}{1 - \frac{m^f}{S}}}. \quad (112)$$

The above result demonstrates that this approximate resonance frequency expression is valid up to the point where the first flat part of the resonance curve starts bending downwards. It turns out for realistic geomaterials saturated with low-viscosity fluids such as air or light hydrocarbons  $\Upsilon$  is indeed orders of magnitude smaller than unity. The dimensionless factor  $\sqrt{\frac{m^s}{1 - \frac{m^f}{S}}}$  can be viewed as the measure of the drop in the value of resonance frequency for the wet case over its value for the dry-frame. Obviously this drop factor is controlled by the tortuosity factor ( $S$ ) and the fluid mass fraction.

Using eq (421), followed by some algebraic manipulations, eq (112) can be rewritten as

$$\Re \omega_1^{(0,1)}(p, l) \approx \sqrt{q_p^2 + k_l^2} \sqrt{\frac{\mu^0}{\phi_0 \rho_0^s + \eta_0 \rho_0^f \left(1 - \frac{1}{S}\right)}}. \quad (113)$$

Thus, controlled by tortuosity factor, the fluid mass partially participates in the inertia associated with this wave process. The effective density associated with the process is

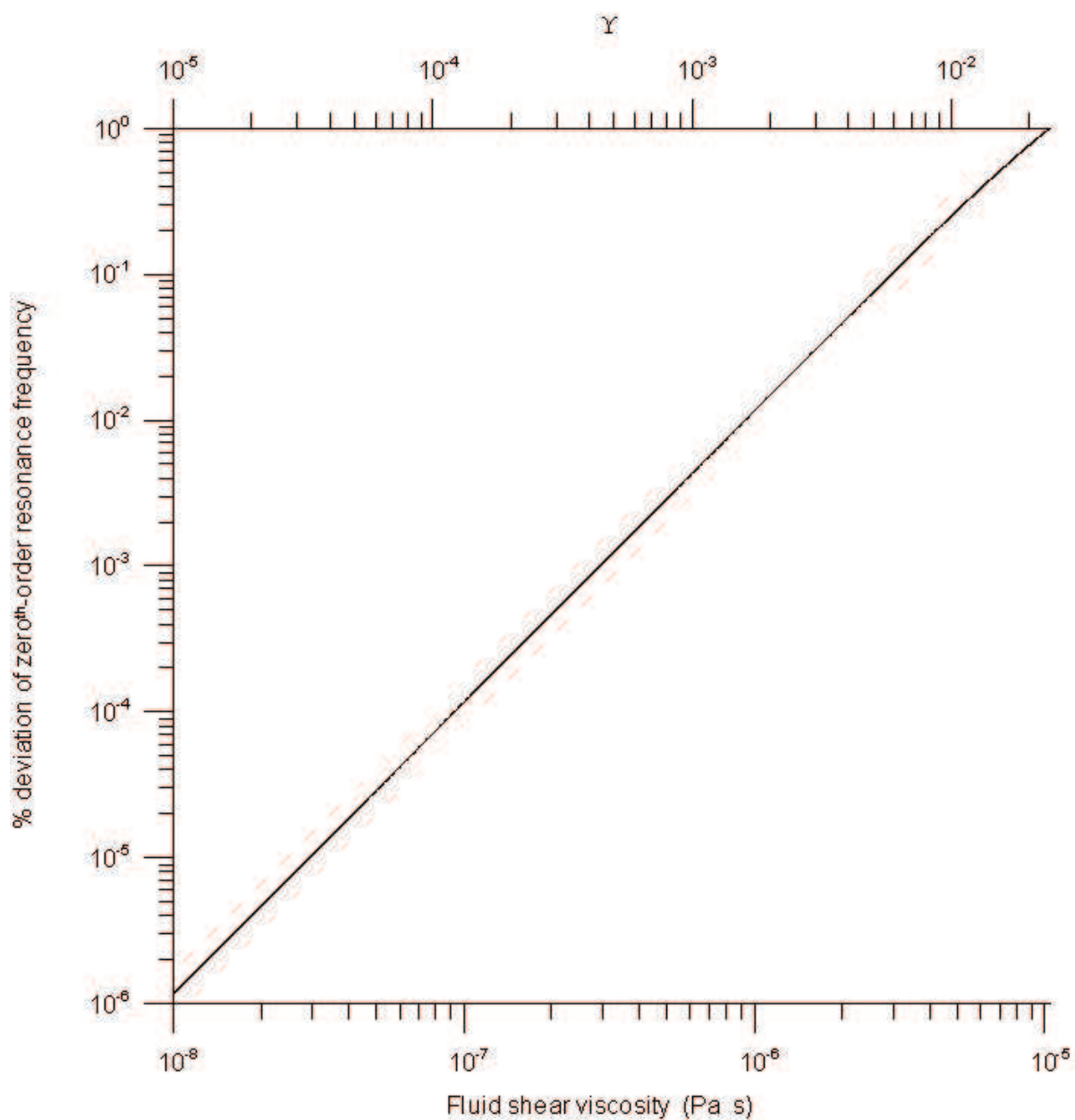


Figure 7. In the regime I ( $\Upsilon < 1$ ) the % deviation from the exact values of the zero<sup>th</sup>-order resonance frequency associated with the fast process. The deviation curves are monotone functions. On the plots the upper bounds of viscosity (or  $\Upsilon$ ) correspond to the deviation being 1%.

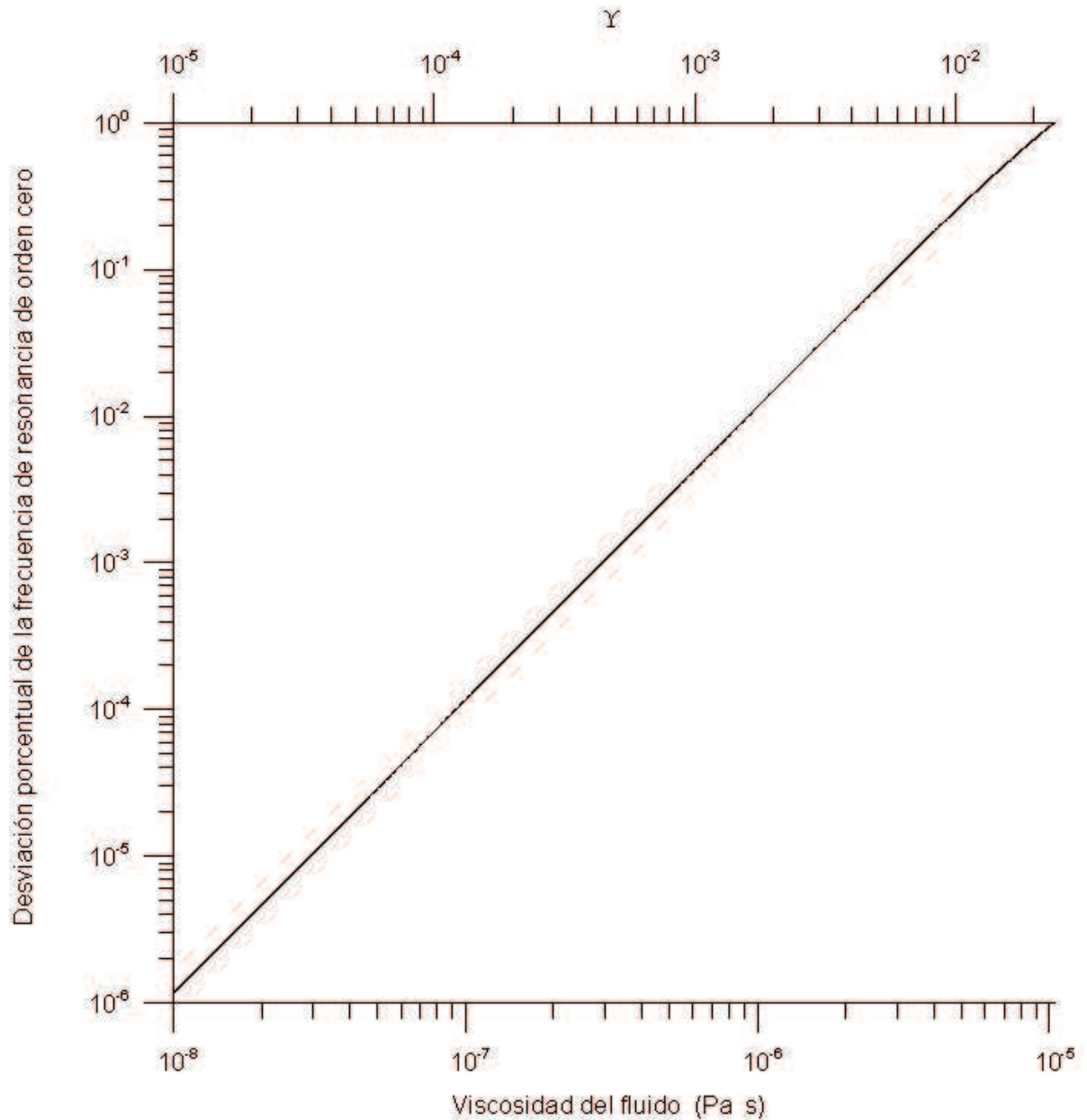


Figure 8. Región I ( $\Upsilon < 1$ ): desviación porcentual de los valores de orden cero con respecto a los valores exactos de la frecuencia de resonancia asociados con el proceso rápido. La curva de la desviación porcentual muestra una tendencia monótona creciente. En la gráfica el límite superior de la viscosidad (o  $\Upsilon$ ) corresponde a la desviación porcentual del 1%.

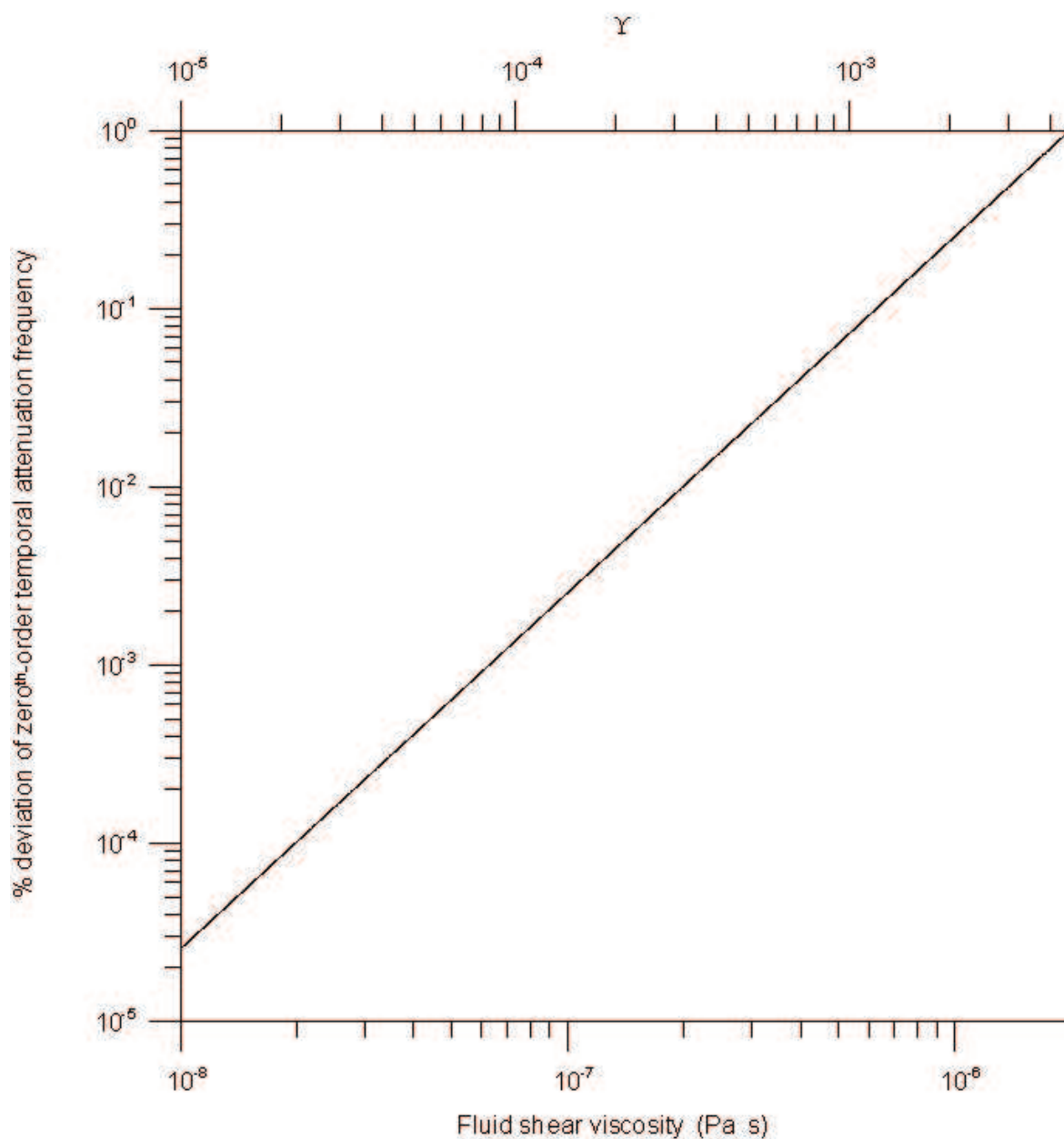


Figure 9. In the regime I ( $\Upsilon < 1$ ) the % deviation from the exact values of the zero<sup>th</sup>-order temporal attenuation frequency associated with the fast process. The deviation curves are monotone functions. On the plots the upper bounds of viscosity (or  $\Upsilon$ ) correspond to the deviation being 1%.

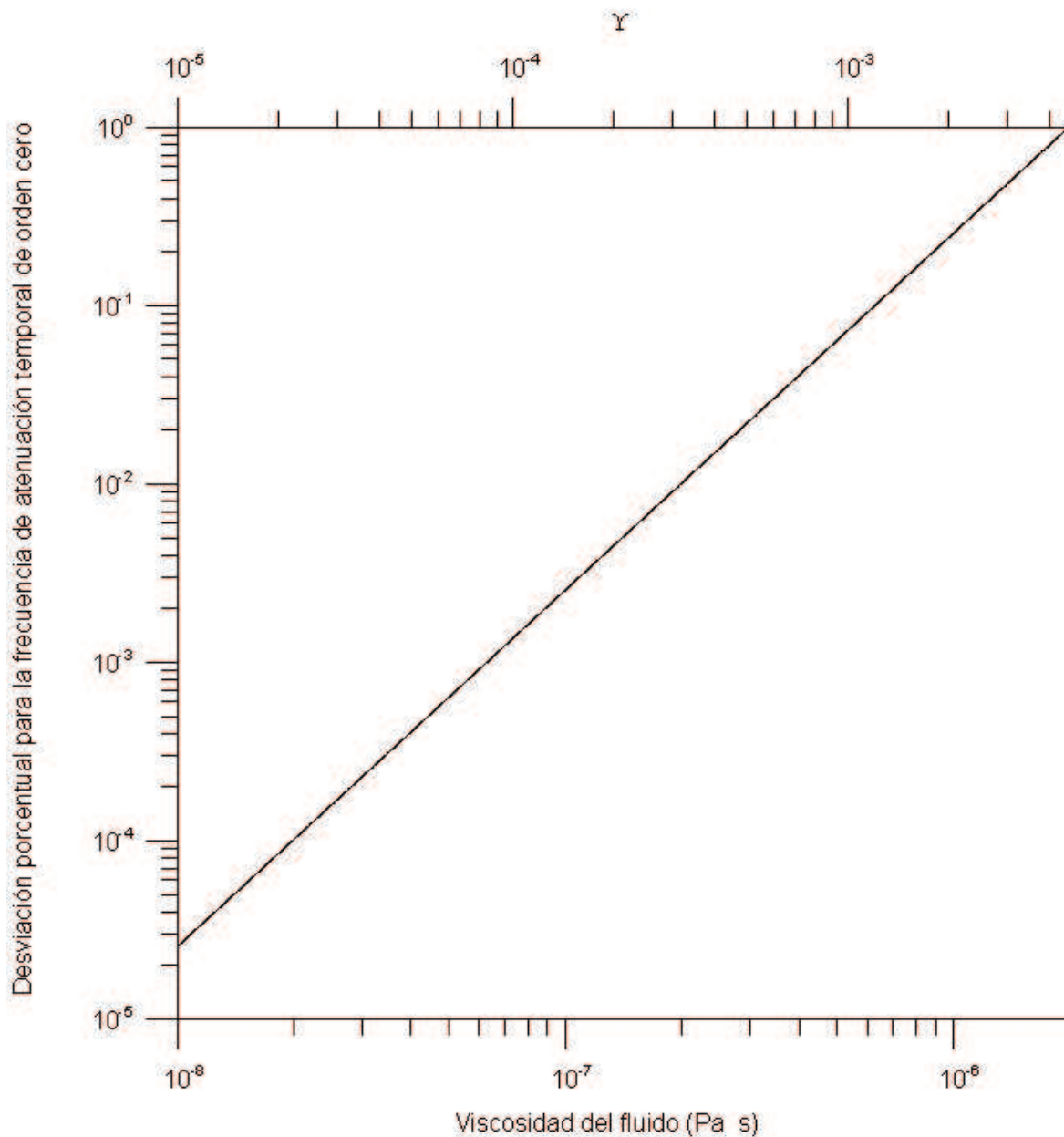


Figure 10. Región I ( $\Upsilon < 1$ ): desviación porcentual de los valores de orden cero con respecto a los valores exactos de la frecuencia de atenuación temporal asociados con el proceso rápido. La curva de la desviación porcentual muestra una tendencia monótona creciente. En la gráfica el límite superior de la viscosidad (o  $\Upsilon$ ) corresponde a la desviación porcentual del 1%.

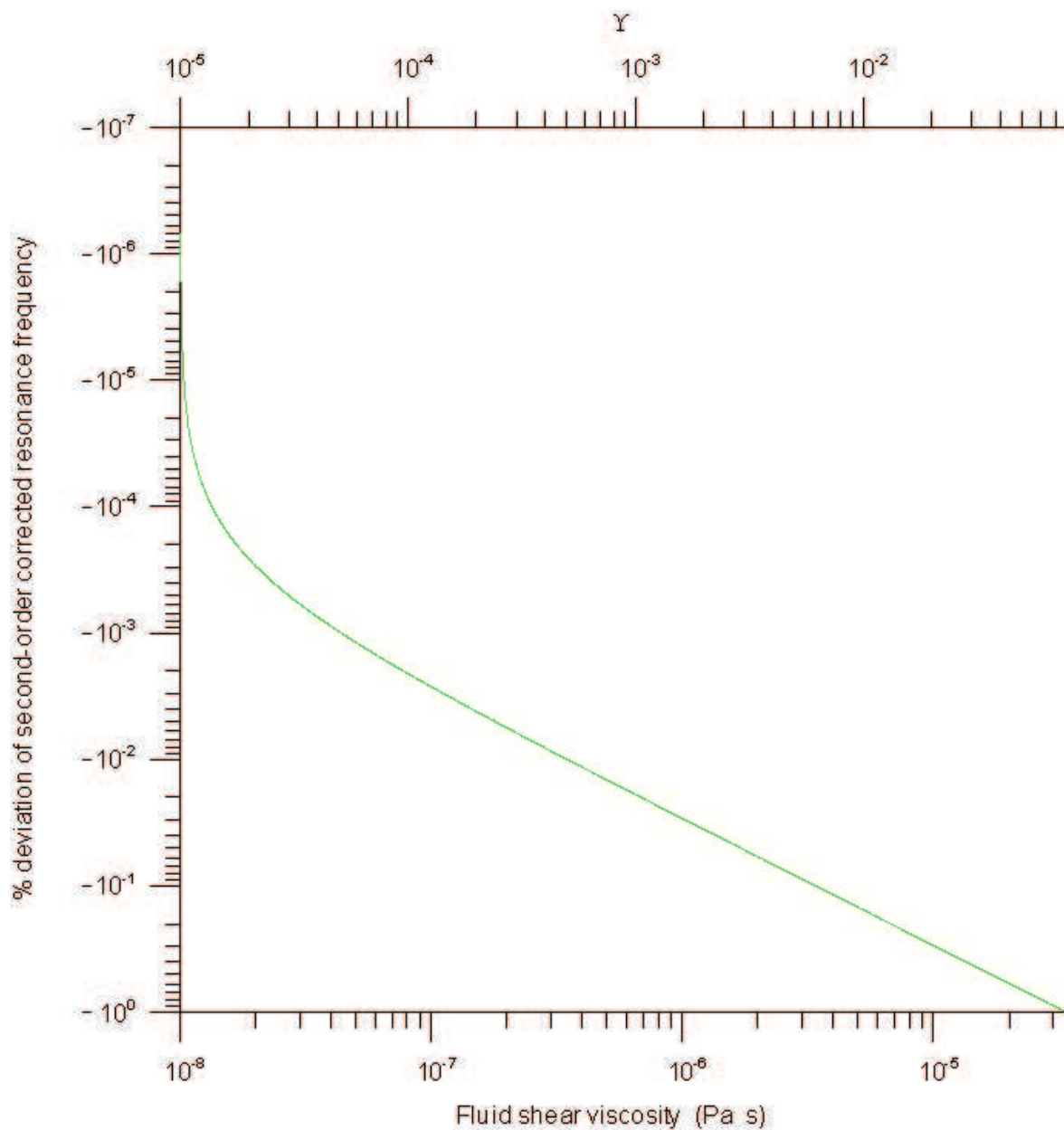


Figure 11. In the regime I ( $\Upsilon < 1$ ) the % deviation from the exact values of the second-order corrected resonance frequency associated with the fast process. The deviation curves are monotone functions. On the plots the upper bounds of viscosity (or  $\Upsilon$ ) correspond to the deviation being 1%.

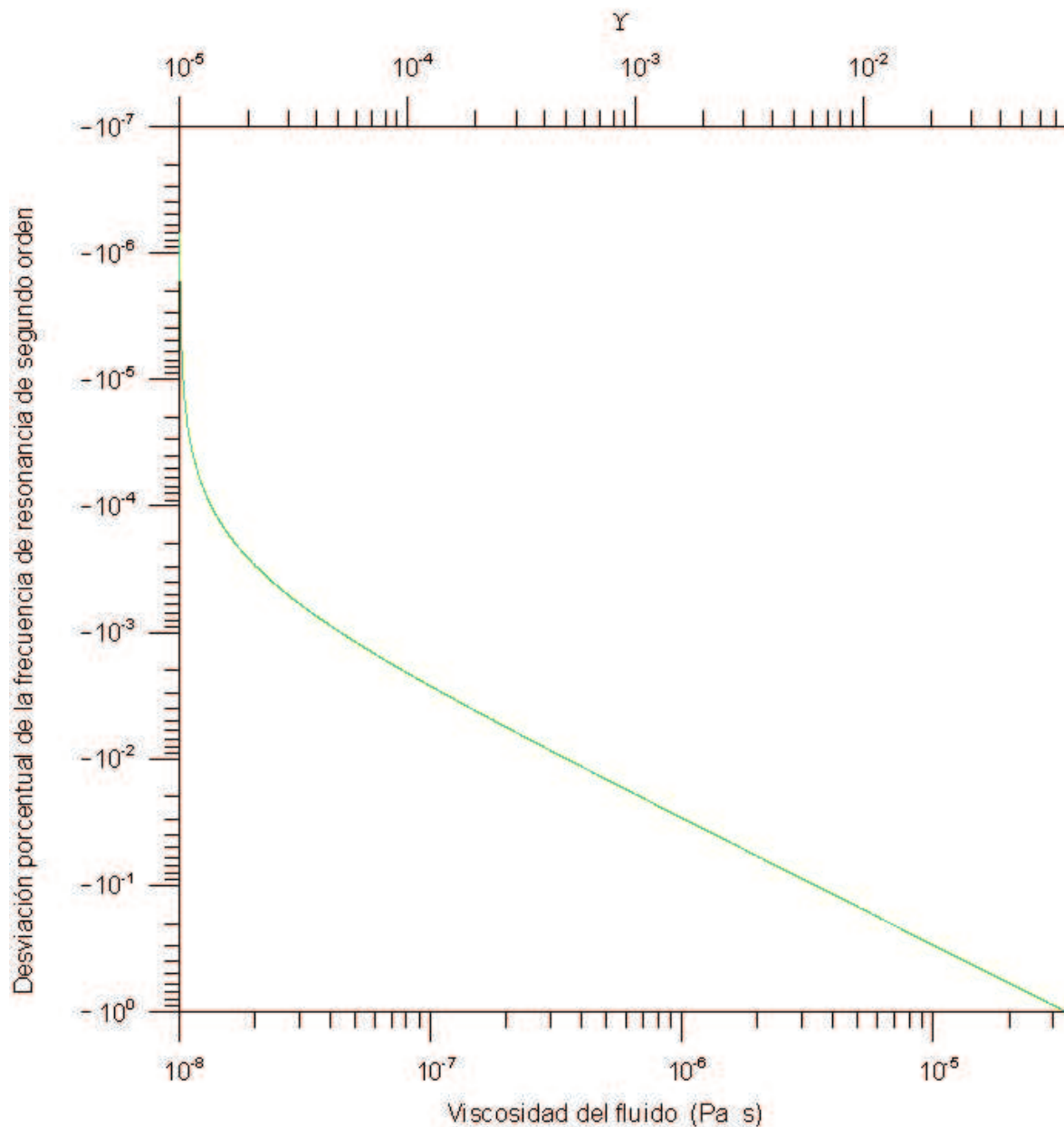


Figure 12. Región I ( $\Upsilon < 1$ ): desviación porcentual de los valores de segundo orden con respecto a los valores exactos de la frecuencia de resonancia asociados con el proceso rápido. La curva de la desviación porcentual muestra una tendencia monótona creciente. En la gráfica el límite superior de la viscosidad (o  $\Upsilon$ ) corresponde a la desviación porcentual del 1%.



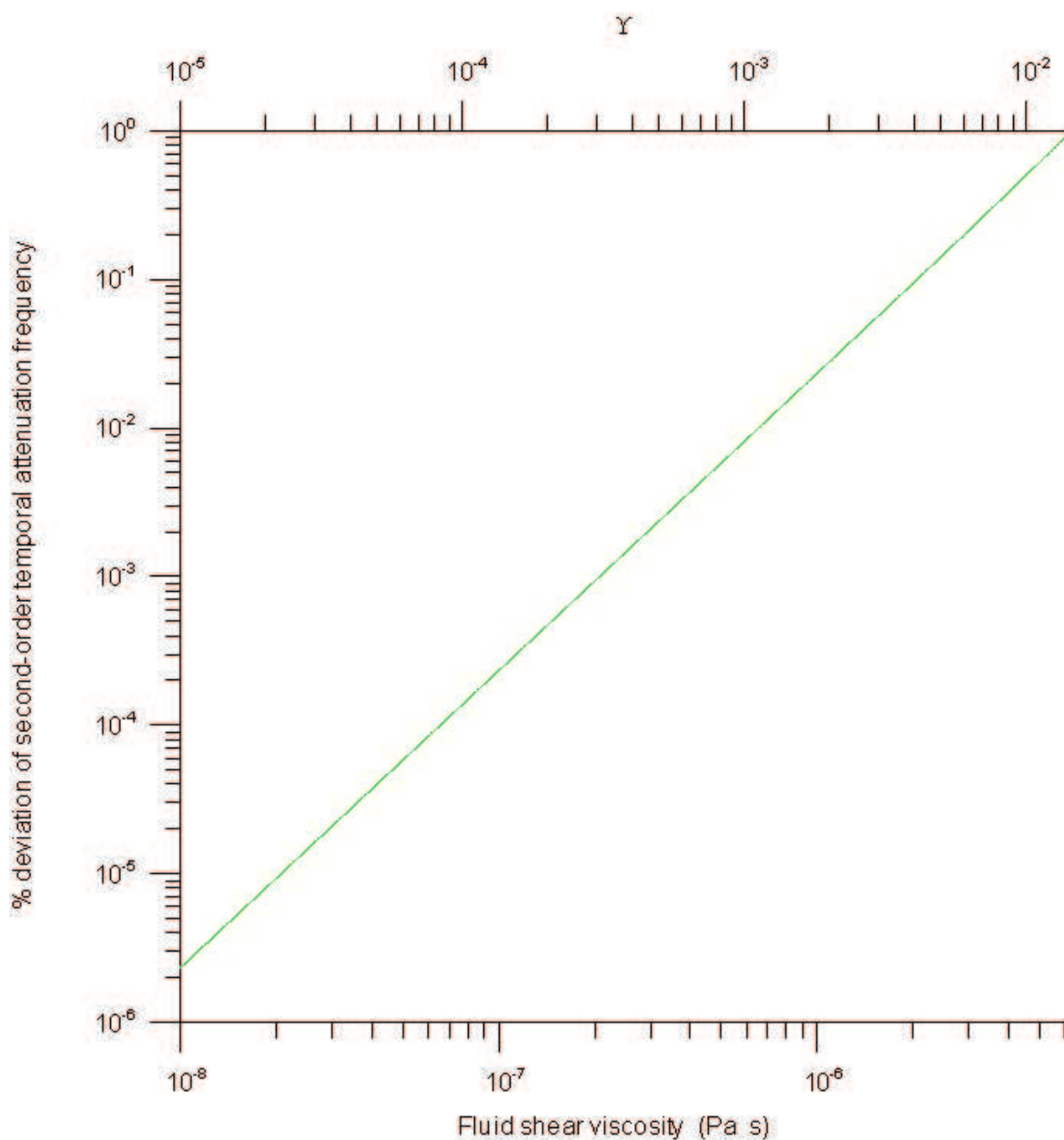


Figure 13. In the regime I ( $\Upsilon < 1$ ) the % deviation from the exact values of the second-order corrected temporal attenuation frequency associated with the fast process. The deviation curves are monotone functions. On the plots the upper bounds of viscosity (or  $\Upsilon$ ) correspond to the deviation being 1%.

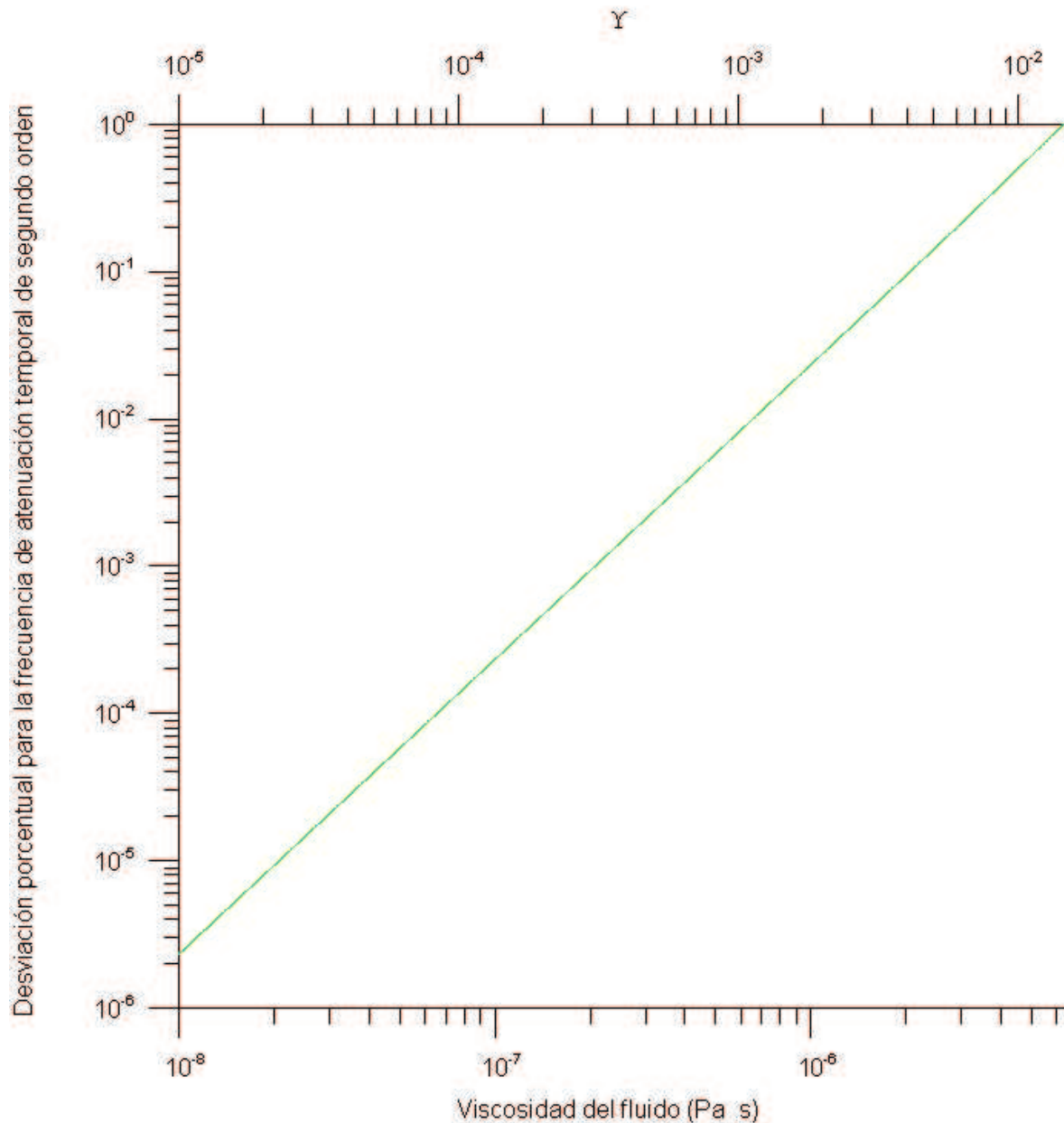


Figure 14. Región I ( $\Upsilon < 1$ ): desviación porcentual de los valores de segundo orden con respecto a los valores exactos de la frecuencia de atenuación temporal asociados con el proceso rápido. La curva de la desviación porcentual muestra una tendencia monótona creciente. En la gráfica el límite superior de la viscosidad (o  $\Upsilon$ ) corresponde a la desviación porcentual del 1%.

$$\phi_0 \rho_0^s + \eta_0 \rho_0^f \left(1 - \frac{1}{S}\right).$$

Utilizing the expression for  $\Omega$  (eq 52), followed by some algebraic rearrangements, the (negative) imaginary part of (110), i.e., the temporal attenuation frequency can be rewritten as

$$-\Im \omega_1^{(0,1)}(p, l) = \frac{1}{2} \frac{\left(\frac{\eta_0}{S}\right)^2}{\phi_0 \rho_0^s + \eta_0 \rho_0^f \left(1 - \frac{1}{S}\right)} \frac{\mu^f}{K}. \quad (114)$$

It is apparent that, in eq (114), the temporal attenuation frequency is inversely proportional to fluid mobility (ratio of permeability to fluid viscosity) where the proportionality constant is a function of constituent masses and tortuosity factor. Also it is independent of wave-numbers, hence, for different modes the same temporal attenuation will be observed.

In Fig. 8 the approximate expression for torsional resonance frequency, eq (113), and temporal attenuation frequency, eq (114), are plotted as dashed-black lines and superimposed on the respective exact curves.

For geomaterial saturated with air  $\Upsilon$  is likely to be under  $10^{-2}$ , thus, the resonance frequency formula given by eq (113) is applicable. Due to the density of air being over 3 orders in magnitude smaller than the solid density, hence, contribution of the tortuosity factor term in (113) is negligible and the resonance frequency for air saturated sample is essentially the same as  $\omega_0(p, l)$ . Furthermore in eq (114), because of the shear viscosity of air being of the order of  $10^{-5}$ , practically no temporal attenuation for the air saturated sample is predictable. Therefore, in this case if any loss is observed it might be attributed to grain to grain friction loss in the solid frame.

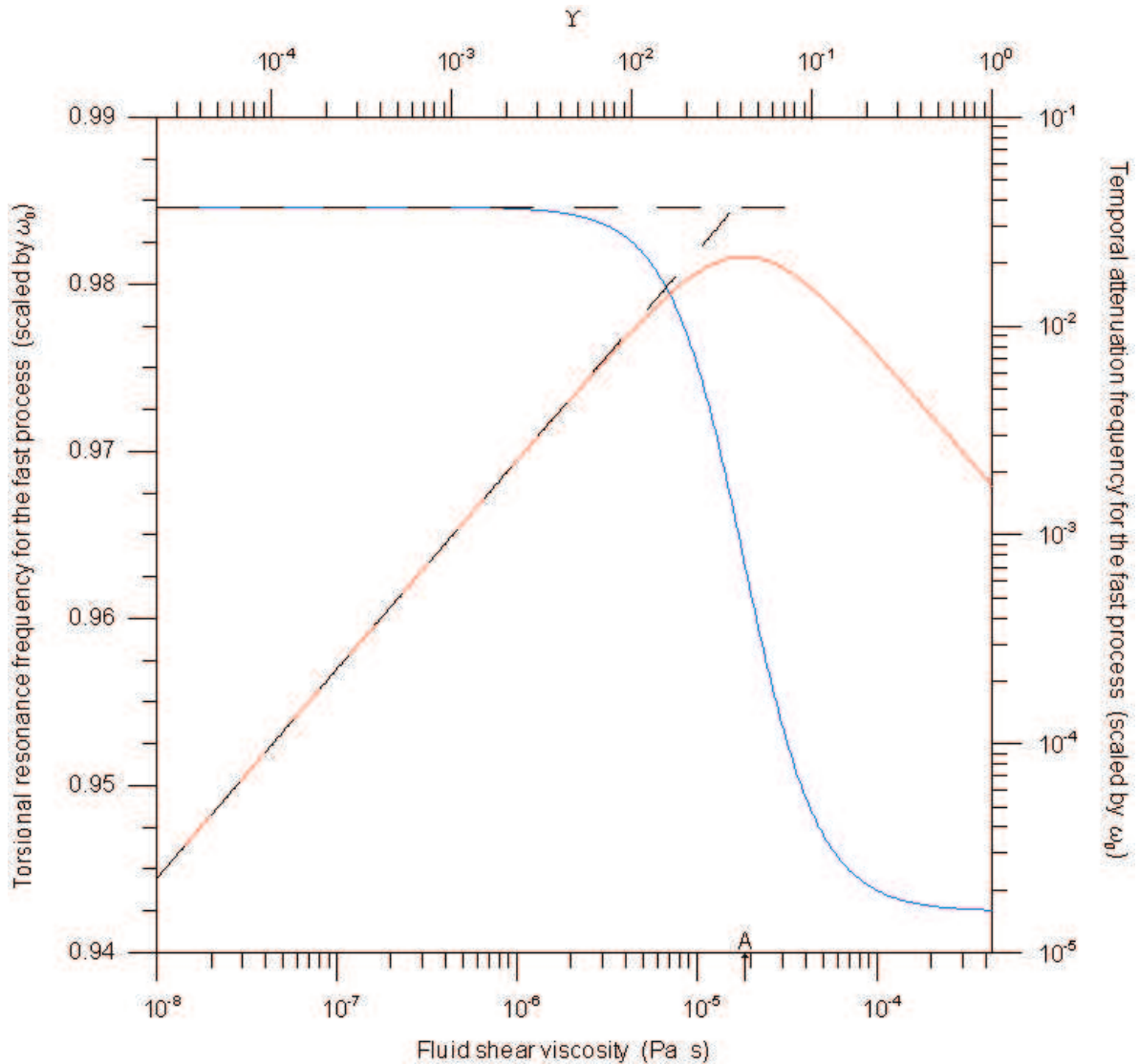


Figure 15. In the regime I ( $\Upsilon < 1$ ) the comparison of exact (eq 90) and approximate expression of the torsional resonance (eq 113) and temporal attenuation (eq 114) frequencies associated with the fast process. The exact resonance,  $\frac{\Re\omega_1(1,1)}{\omega_0(1,1)}$ , and temporal attenuation,  $\frac{\Im\omega_1(1,1)}{\omega_0(1,1)}$ , frequencies are presented as blue and red curves, respectively. On the respective exact curves, the approximate resonance and temporal attenuation frequencies are superimposed as dashed-black lines.

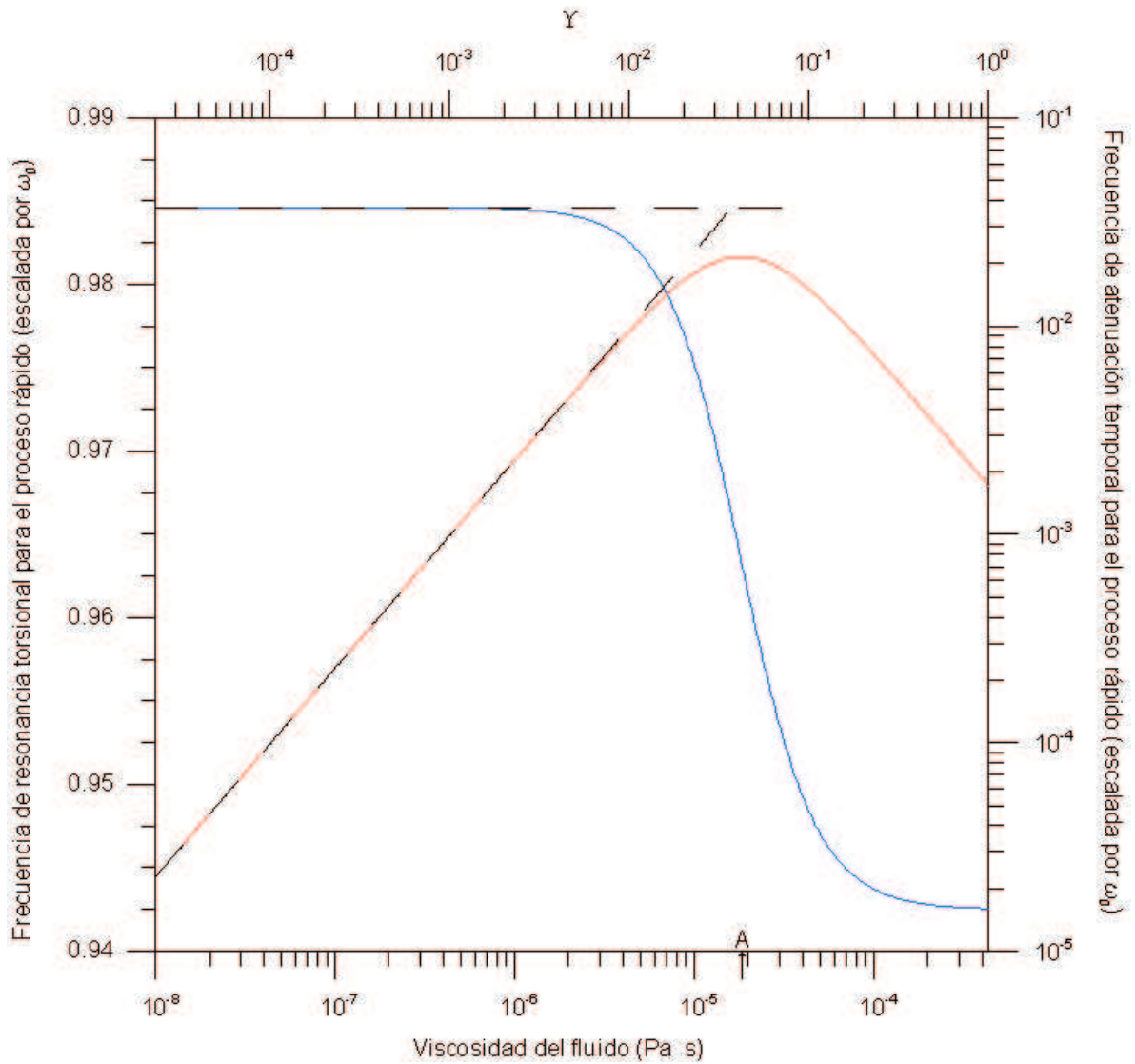


Figure 16. Región I ( $\Upsilon < 1$ ): comparación de los valores exactos (ec 90), y de las fórmulas de aproximación para la frecuencia de resonancia (ec 113), y la frecuencia de atenuación temporal (ec 114) correspondientes al proceso rápido. Las curvas exactas de la frecuencia de resonancia,  $\frac{\Re\omega_1(1,1)}{\omega_0(1,1)}$ , y la atenuación temporal,  $\frac{\Im\omega_1(1,1)}{\omega_0(1,1)}$ , se muestran en azul y rojo, respectivamente. Sobre las respectivas curvas exactas se superimponen las curvas de las fórmulas aproximadas para las frecuencias de resonancia y atenuación temporal en líneas punteadas negras.

#### IV.2.3.4.2 Slow process

Similarly it can be found from eq (107) that the second component of the transformed field or slow process is  $-d^f U_\theta^m + U_\theta^i$  which may be viewed as a motion of fluid accompanied by solid-frame,  $\frac{S-1}{S-m^f} U_\theta^s - \frac{S}{S-m^f} U_\theta^f$ . The second row of eq (105) yields its eigenfrequency pair which are expressed as

$$\omega_3^{(0,1)}(p, l), \omega_4^{(0,1)}(p, l) = -i \Omega \frac{1}{1 + d^f m^f}, \quad 0, \quad (115)$$

and are regarded as the zero<sup>th</sup>-order eigenfrequencies of the slow process in the regime I. The subindex of eigenfrequency is as per notation introduced in section IV.1.3.1.

Clearly the first mode, being devoid of a real part, is a diffusive process, and the second is a non-propagating mode. It is almost possible to reproduce the temporal attenuation frequency curve for this regime as shown in Fig. 9. Its % deviation from the exact value is plotted in Fig. 10.

#### IV.2.3.5 The correction due to the perturbation operator $\mathbf{Q}^I$

##### IV.2.3.6.1 Fast process

It was found that up to the point where viscosity reaches the value so that  $\Omega$  equals to  $\sqrt{W^{ii}}$ , the 2<sup>nd</sup>-order perturbative correction (eq 436) of  $\mathbf{Q}^I$  is able to approximately reproduce the exact graphs as shown in Fig. 3 represented by dashed-green lines. The % deviation from the exact values are shown in Figs. 6 and 7.

Beyond that point this correction also fails since the perturbation part,  $\mathbf{Q}^I$ , becomes comparable to the unperturbed part,  $\mathcal{L}^{(0,1)}$ . It implies that the transformation defined by eq (100) is no longer valid and, therefore, beyond this point another transformation

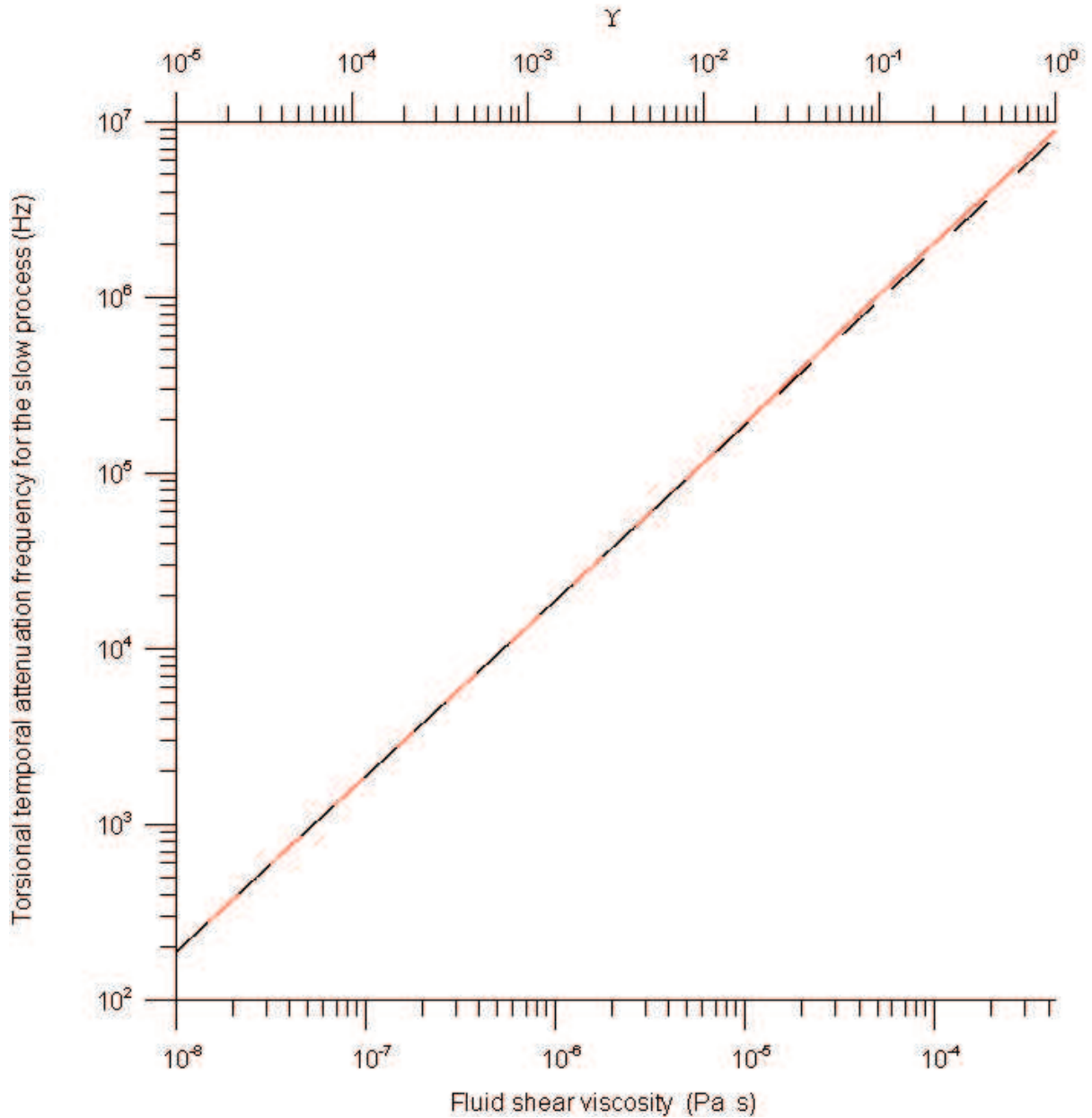


Figure 17. For the regime I ( $\Upsilon < 1$ ) the comparison of the exact (eq 92) and the zero<sup>th</sup>-order (eq 115) values of the temporal attenuation frequency associated with the slow process,  $\Im\omega_3(1,1)$ . The exact temporal attenuation frequency is presented as red curve, on the exact curve the zero<sup>th</sup>-order values are superimposed as dashed-black line.

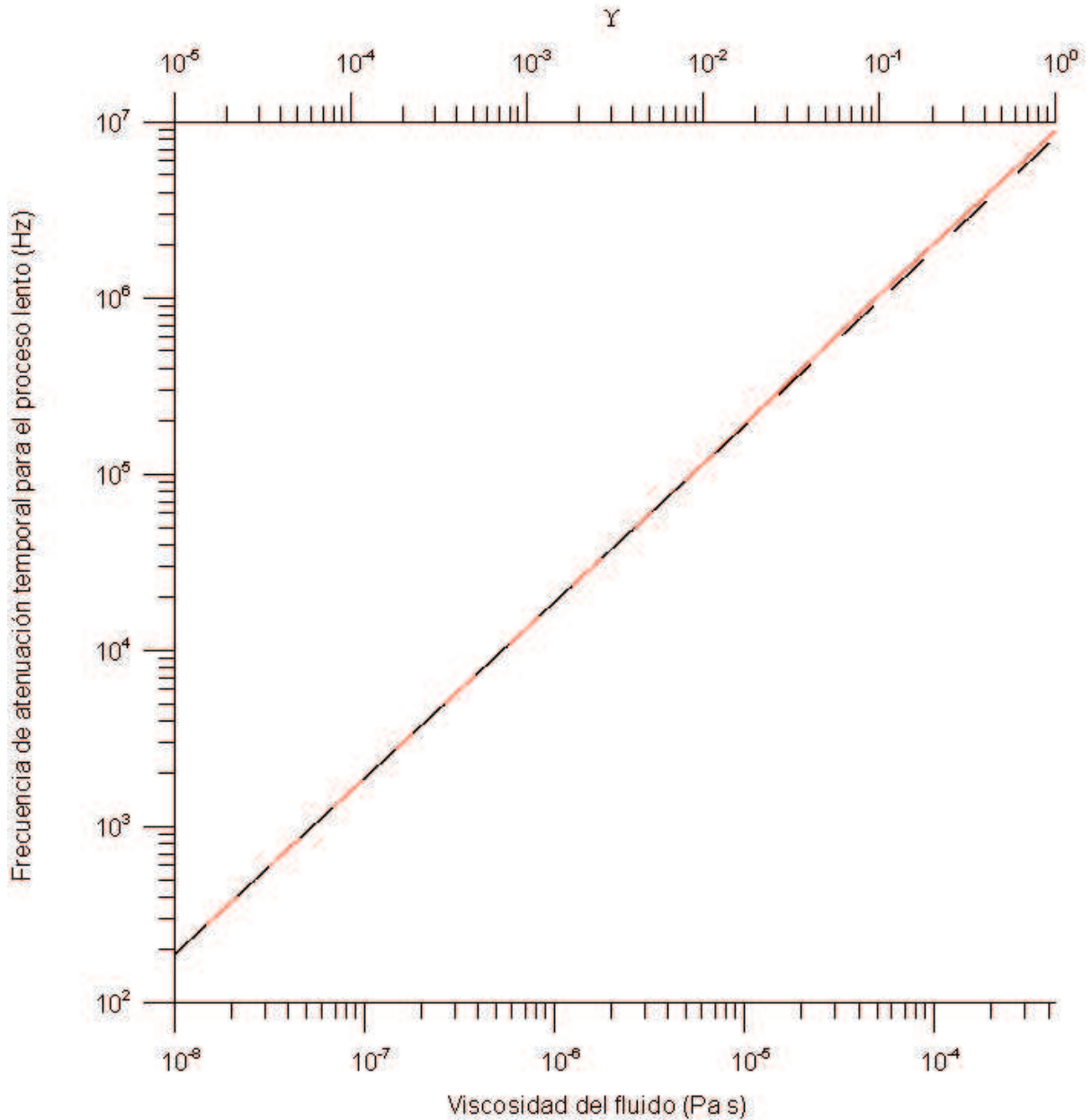


Figure 18. Región I ( $\Upsilon < 1$ ): comparación de los valores exactos (ec 92) y de orden cero (ec 115) de la frecuencia de atenuación temporal torsional correspondientes al proceso lento,  $\Im\omega_3(1, 1)$ . La curva exacta de la atenuación temporal se muestra en rojo y sobre la respectiva curva exacta se superimpone la curva de la atenuación temporal de orden cero en líneas punteadas negras.



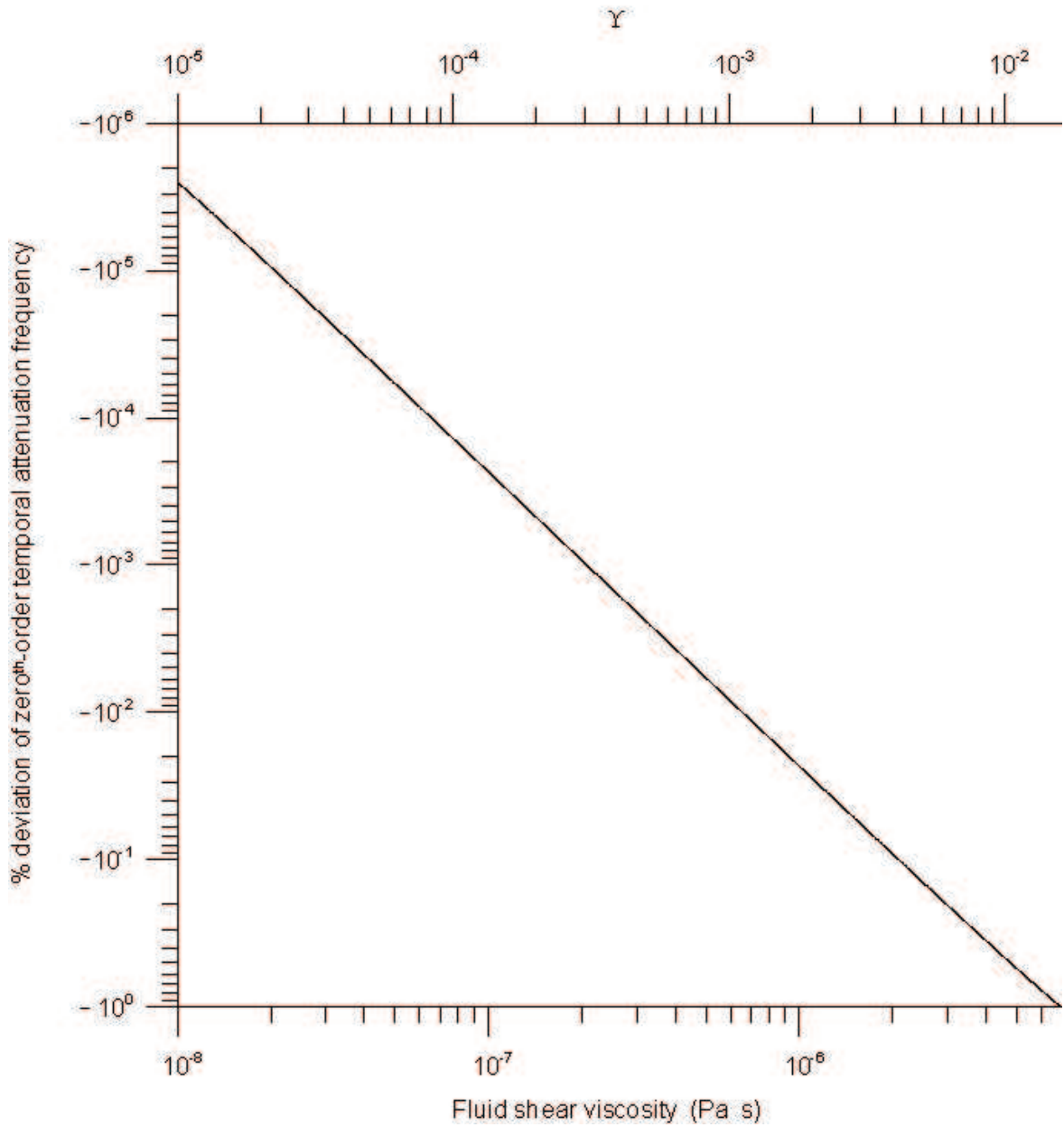


Figure 19. For the regime I ( $\Upsilon < 1$ ) the % deviation of the zero<sup>th</sup>-order value from the exact value. For clarity, the upper bound of viscosity (or  $\Upsilon$ ) is taken to be the value by which deviation grows to -1%.

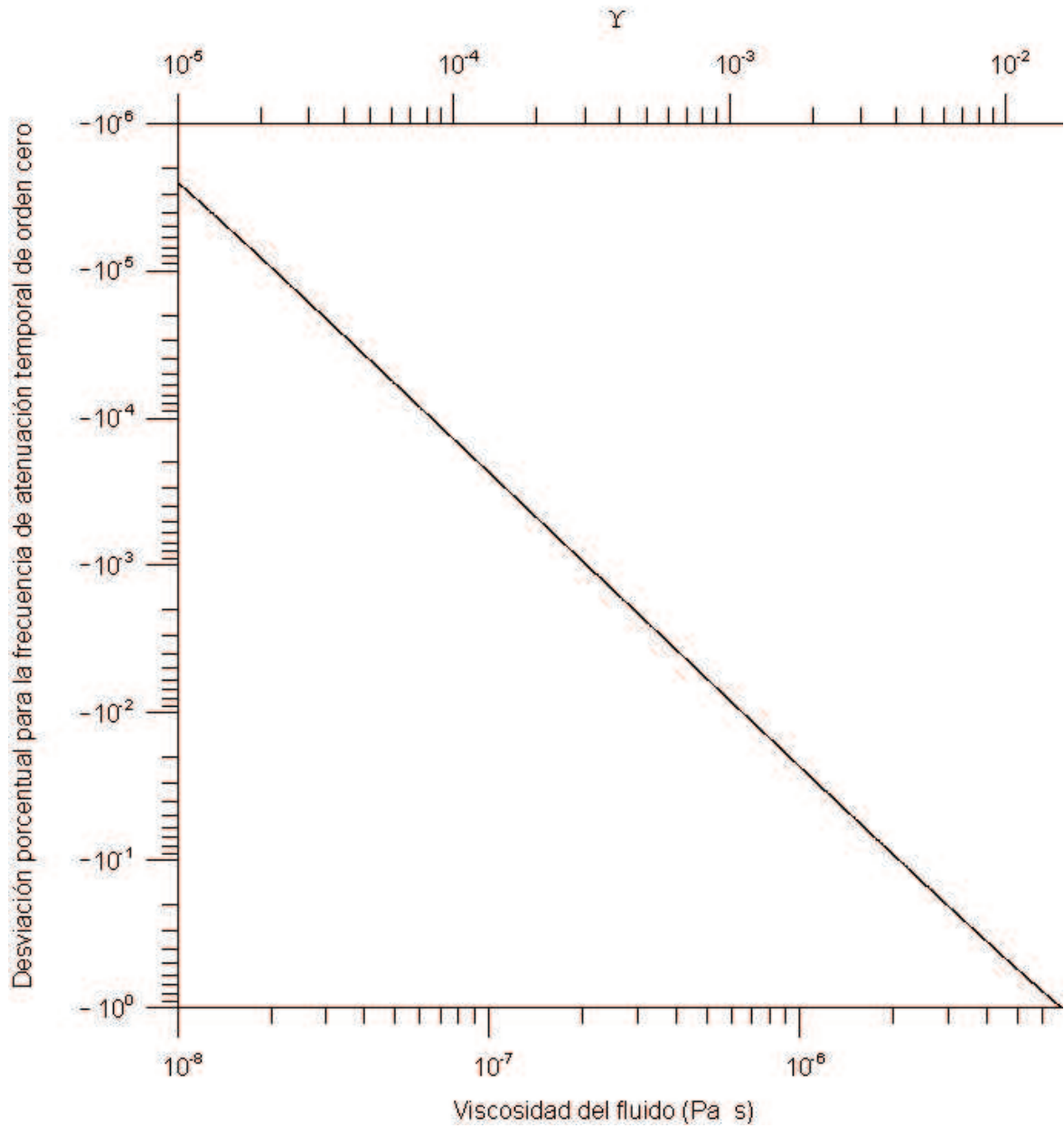


Figure 20. Región I ( $\Upsilon < 1$ ): desviación porcentual de los valores de orden cero con respecto a los valores exactos. Por claridad, el límite superior de la viscosidad (o  $\Upsilon$ ) se muestra hasta el valor de la desviación porcentual de -1%.

matrix has to be reworked by incorporating the  $\Omega$  term appropriately.

#### IV.2.3.6.2 Slow process

The zero<sup>th</sup>-order curve is essentially in agreement with the exact curve. The correction introduced by carrying the perturbation up to second-order (eq 438) is insignificant, hence for the sake of clarity of Fig. 9 it is not shown.

### IV.2.4 Regime II : $\Upsilon > 1$ (viscosity dominated regime)

#### IV.2.4.1 The transformation matrix

The appropriate transformation matrix for this regime turns out to be

$$\mathbf{E}^{\text{II}} = (1 - \epsilon) \begin{pmatrix} 1 & \sqrt{\frac{\epsilon}{1-\epsilon}} \\ -\sqrt{\frac{\epsilon}{1-\epsilon}} & 1 \end{pmatrix}. \quad (116)$$

The superscript<sup>II</sup> labels the regime and the parameter  $\epsilon$  is defined as

$$\epsilon = \frac{W^{\text{ii}}}{\Omega^2}. \quad (117)$$

It contains viscosity as an inverse squared term, since  $\Omega$  is directly proportional to viscosity. Eq (83) in conjunction with eqs (413) and (421) yields  $W^{\text{ii}}$  to be  $d^f m^f m^s \omega_0^2(p, l)$ . Using eq (97)  $\Omega$  is expressed in terms of  $\Upsilon$ . The above expression is rewritten as

$$\epsilon = \frac{1}{4} \left( \frac{m^f}{S} \right)^3 \frac{1}{\Upsilon^2}. \quad (118)$$

At the lower bound of this regime  $\Upsilon = 1$ , for which  $\epsilon$  is  $\frac{1}{4} \left( \frac{m^f}{S} \right)^3$  and for a realistic set of geomaterial parameters it turns out to be less than  $10^{-2}$ . The increment of viscosity,  $\Upsilon$  also increases, and hence  $\epsilon$  dwindles further down ensuring it to be a pertinent

perturbative term.

#### IV.2.4.2 The transformed operator $\mathcal{L}^{\text{II}}$

The transformed operator  $\mathcal{L}^{\text{II}}$  for this regime is split into its diagonal  $\mathcal{L}^{(0,\text{II})}$  and off-diagonal  $\mathbf{Q}^{\text{II}}$  members as

$$\mathcal{L}^{\text{II}} = (\mathbf{E}^{\text{II}})^{-1} \mathcal{D} \mathbf{E}^{\text{II}} = \mathcal{L}^{(0,\text{II})} + \mathbf{Q}^{\text{II}}, \quad (119)$$

where

$$\begin{aligned} \mathcal{L}^{(0,\text{II})} = & \left[ \Omega \begin{pmatrix} \epsilon & 0 \\ 0 & 1 - \epsilon \end{pmatrix} \right. \\ & + \begin{pmatrix} (1 - \epsilon) \nu^{\text{mm}} - \sqrt{\epsilon(1 - \epsilon)} \nu^{\text{mi}} - \sqrt{\epsilon(1 - \epsilon)} \nu^{\text{im}} + \epsilon(1 - \epsilon) \nu^{\text{ii}} & \\ & 0 \\ & 0 \\ & \epsilon(1 - \epsilon) \nu^{\text{mm}} + \sqrt{\epsilon(1 - \epsilon)} \nu^{\text{mi}} + \sqrt{\epsilon(1 - \epsilon)} \nu^{\text{im}} + (1 - \epsilon) \nu^{\text{ii}} \end{pmatrix} \left. \right] \frac{d}{dt} \\ & + \begin{pmatrix} (1 - \epsilon) W^{\text{mm}} - \sqrt{\epsilon(1 - \epsilon)} W^{\text{mi}} - \sqrt{\epsilon(1 - \epsilon)} W^{\text{im}} + \epsilon(1 - \epsilon) W^{\text{ii}} & \\ & 0 \\ & 0 \\ & \epsilon(1 - \epsilon) W^{\text{mm}} + \sqrt{\epsilon(1 - \epsilon)} W^{\text{mi}} + \sqrt{\epsilon(1 - \epsilon)} W^{\text{im}} + (1 - \epsilon) W^{\text{ii}} \end{pmatrix}, \end{aligned} \quad (120)$$

and

$$\mathbf{Q}^{\text{II}} = \left[ \Omega \begin{pmatrix} 0 & -\sqrt{\epsilon(1 - \epsilon)} \\ -\sqrt{\epsilon(1 - \epsilon)} & 0 \end{pmatrix} \right],$$

$$\begin{aligned}
& + \left( \begin{array}{c} 0 \\ \sqrt{\epsilon(1-\epsilon)}\nu^{\text{mm}} - \epsilon(1-\epsilon)\nu^{\text{mi}} + (1-\epsilon)\nu^{\text{im}} - \sqrt{\epsilon(1-\epsilon)}\nu^{\text{ii}} \\ \sqrt{\epsilon(1-\epsilon)}\nu^{\text{mm}} + (1-\epsilon)\nu^{\text{mi}} - \epsilon(1-\epsilon)\nu^{\text{im}} - \sqrt{\epsilon(1-\epsilon)}\nu^{\text{ii}} \\ 0 \end{array} \right) \frac{d}{dt} \\
& + \left( \begin{array}{c} 0 \\ \sqrt{\epsilon(1-\epsilon)}W^{\text{mm}} - \epsilon(1-\epsilon)W^{\text{mi}} + (1-\epsilon)W^{\text{im}} - \sqrt{\epsilon(1-\epsilon)}W^{\text{ii}} \\ \sqrt{\epsilon(1-\epsilon)}W^{\text{mm}} + (1-\epsilon)W^{\text{mi}} - \epsilon(1-\epsilon)W^{\text{im}} - \sqrt{\epsilon(1-\epsilon)}W^{\text{ii}} \\ 0 \end{array} \right). \tag{121}
\end{aligned}$$

#### IV.2.4.3 Simplification of the unperturbed operator $\mathcal{L}^{(0,\text{II})}$ and the perturbed operator $\mathbf{Q}^{\text{II}}$ for the viscosity dominated regime

Since in this regime the value of  $\epsilon$  is orders of magnitude smaller than unity, the unperturbed (diagonal) operator  $\mathcal{L}^{(0,\text{II})}$  is approximated by omitting such terms as,

$$\mathcal{L}^{(0,\text{II})} \approx \left[ \Omega \begin{pmatrix} \epsilon & 0 \\ 0 & 1 \end{pmatrix} + \begin{pmatrix} \nu^{\text{mm}} & 0 \\ 0 & \nu^{\text{ii}} \end{pmatrix} \right] \frac{d}{dt} + \begin{pmatrix} W^{\text{mm}} & 0 \\ 0 & W^{\text{ii}} \end{pmatrix}, \tag{122}$$

and

$$\left( \mathbf{I} \frac{d^2}{dt^2} + \mathcal{L}^{(0,\text{II})} \right) \mathbf{V}^{(0,\text{II})} = 0, \tag{123}$$

which yield the eigenvalues that are regarded as zero<sup>th</sup>-order. The perturbation (off-diagonal) operator is

$$\mathbf{Q}^{\text{II}} \approx \begin{pmatrix} 0 & \nu^{\text{mi}} \\ \nu^{\text{im}} & 0 \end{pmatrix} \frac{d}{dt} + \begin{pmatrix} 0 & W^{\text{mi}} \\ W^{\text{im}} & 0 \end{pmatrix}. \tag{124}$$

The zero<sup>th</sup>-order vector field for this regime is

$$\mathbf{V}^{(0,\text{II})} = \begin{pmatrix} V_{\text{fast}}^{(0,\text{II})} \\ V_{\text{slow}}^{(0,\text{II})} \end{pmatrix} = (\mathbf{E}^{\text{II}})^{-1} \mathbf{U}_\theta = \begin{pmatrix} U_\theta^{\text{m}} - \sqrt{\frac{\epsilon}{1-\epsilon}} U_\theta^{\text{i}} \\ \sqrt{\frac{\epsilon}{1-\epsilon}} U_\theta^{\text{m}} + U_\theta^{\text{i}} \end{pmatrix}. \quad (125)$$

#### IV.2.4.4 Eigenvalues of the unperturbed operator $\mathcal{L}_0^{\text{II}}$

##### IV.2.4.4.1 Fast process

It is obvious from the first row of eq (125) that in this regime the fast process is basically centre-of-mass motion ( $U_\theta^{\text{m}}$ ), and the difference motion of the solid and fluid constituents ( $U_\theta^{\text{i}}$ ) is inconsequential. The first row of eq (123) is its governing equation which yields the eigenvalues for the process as

$$\omega_1^{(0,\text{II})}(p, l), \omega_2^{(0,\text{II})}(p, l) = -\frac{i}{2}(\epsilon\Omega + \nu^{\text{mm}}) \pm \sqrt{W^{\text{mm}} - \left[\frac{1}{2}(\epsilon\Omega + \nu^{\text{mm}})\right]^2}. \quad (126)$$

##### IV.2.4.4.1.1 $\Re\omega_1^{(0,\text{II})}(p, l)$ and $\Im\omega_1^{(0,\text{II})}(p, l)$ for the fast process

The real and (negative) imaginary parts of  $\omega_1^{(0,\text{II})}(p, l)$  ( or  $\omega_2^{(0,\text{II})}(p, l)$ ) are read as zero<sup>th</sup>-order resonance and temporal attenuation frequencies for the torsional resonance process. In Fig. 11, superimposed on the respective exact curves, they are plotted as dashed-black lines. The % deviation from their exact values are plotted in Figs. 12 and 13 which show them to be in agreement.

Just prior to the crossover viscosity  $C$ , for which in Fig. 11 the resonance curve is flat, the inequality  $W^{\text{mm}} \gg \left[\frac{1}{2}(\epsilon\Omega + \nu^{\text{mm}})\right]^2$  holds true. It suggests that for this region the resonance frequency, i.e. the real part of  $\omega_1^{(0,\text{II})}(p, l)$ , can be approximated as

$$\Re\omega_1^{(0,\text{II})}(p, l) \approx \sqrt{W^{\text{mm}}} \quad (127)$$

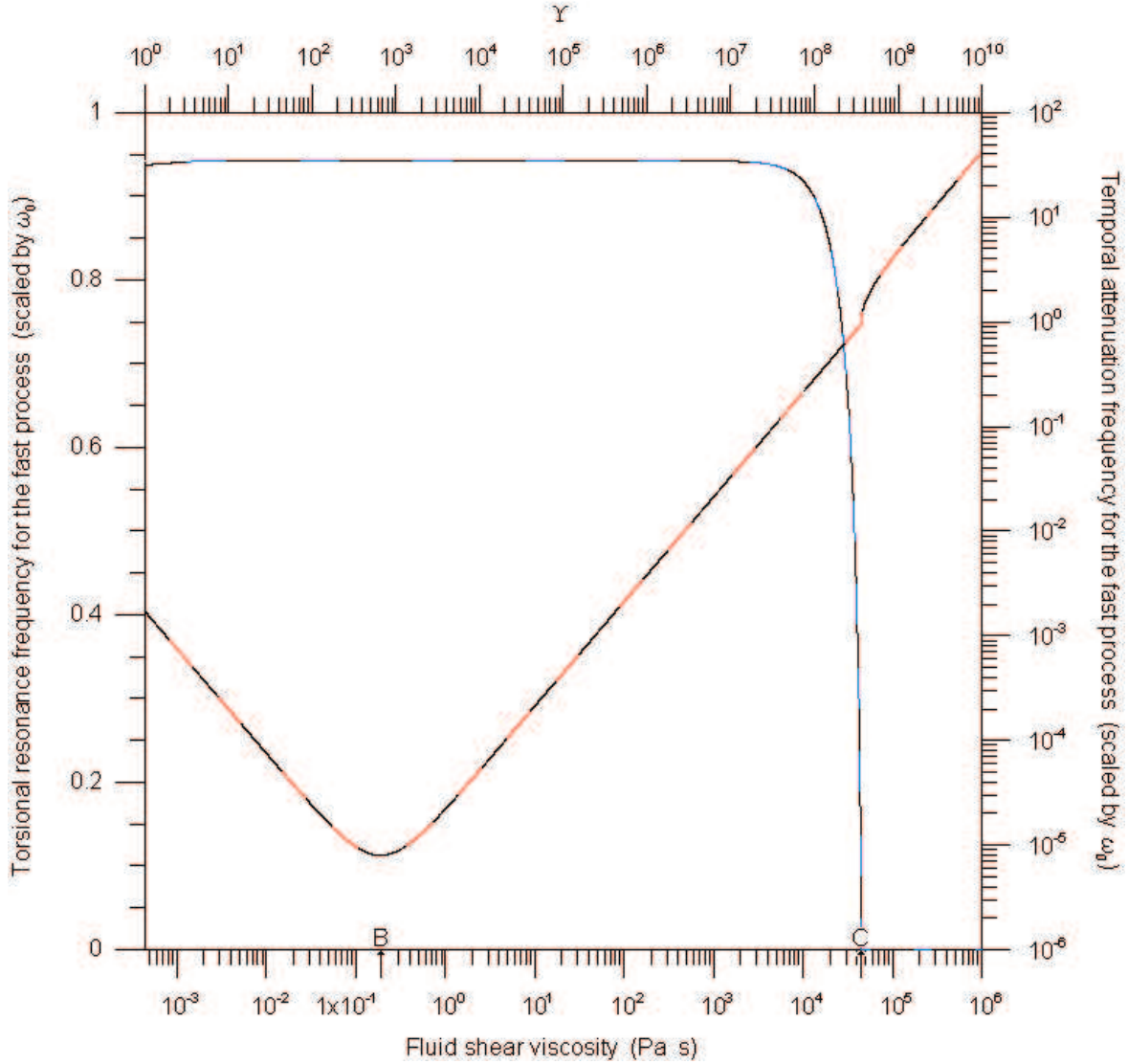


Figure 21. For the regime II ( $\Upsilon > 1$ ) the comparison of the exact (eq 90) and zero<sup>th</sup>-order values (eq 126) of the torsional resonance and temporal attenuation frequencies associated with the fast process. The blue and red curves are the exact resonance,  $\frac{\Re\omega_1(1,1)}{\omega_0(1,1)}$ , and temporal attenuation,  $\frac{\Im\omega_1(1,1)}{\omega_0(1,1)}$ , frequencies respectively. The superimposed dashed-black curves on the respective exact curves are the zero<sup>th</sup>-order values.

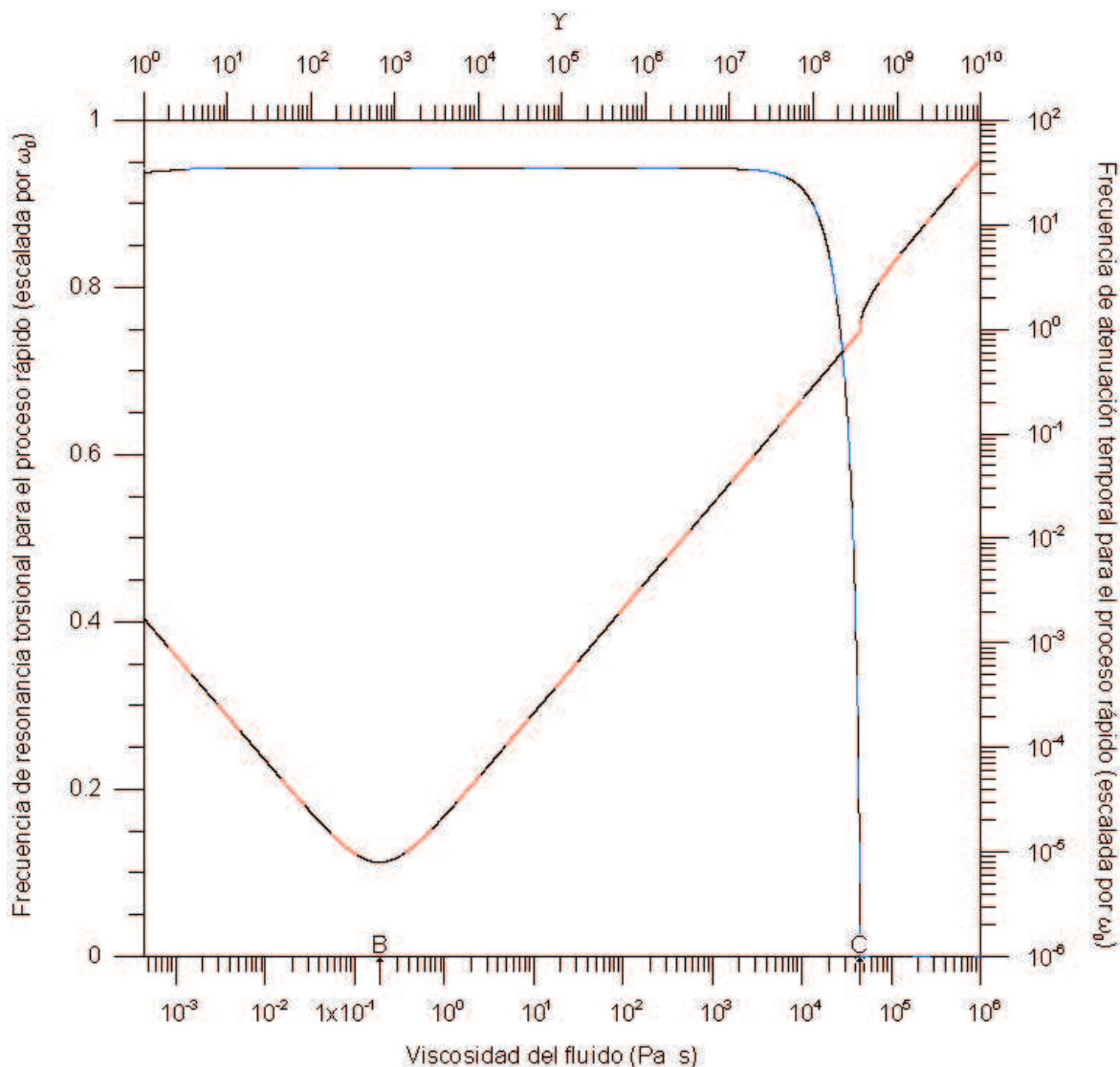


Figure 22. Región II ( $\Upsilon > 1$ ): comparación de los valores exactos (ec 90) y de orden cero (ec 126) de las frecuencias de resonancia y atenuación temporal torsional correspondientes al proceso rápido. Las curvas exactas de la frecuencia de resonancia,  $\frac{\Re\omega_{1(1,1)}}{\omega_{0(1,1)}}$ , y la atenuación temporal,  $\frac{\Im\omega_{1(1,1)}}{\omega_{0(1,1)}}$ , se muestran en azul y rojo, respectivamente. Sobre las respectivas curvas exactas se superimponen las curvas de las frecuencias de resonancia y la atenuación temporal de orden cero en líneas punteadas negras.



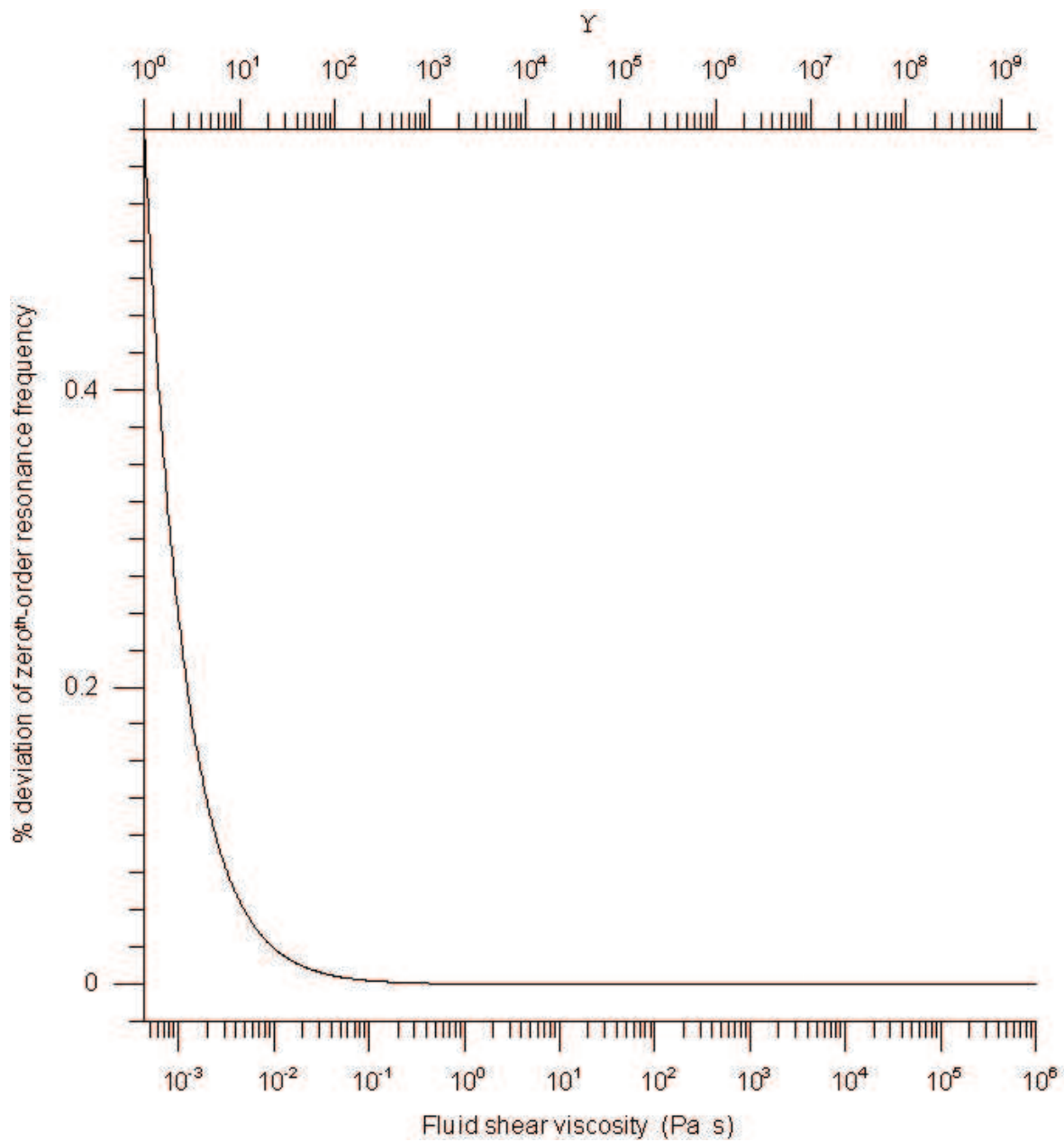


Figure 23. For the regime II ( $\Upsilon > 1$ ) the % deviation from the exact values of the zero<sup>th</sup>-order resonance frequency associated with the fast process.

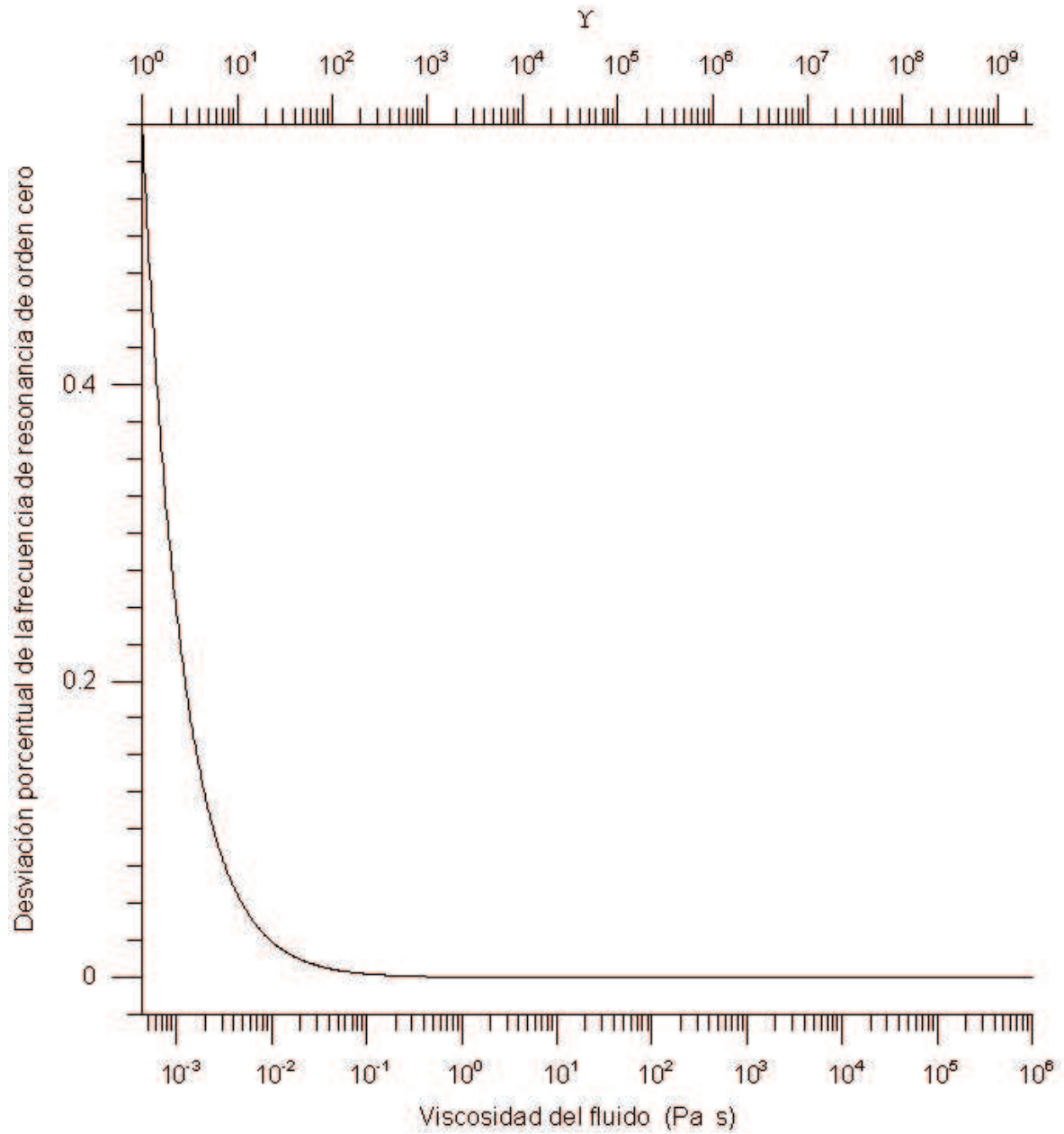


Figure 24. Región II ( $\Upsilon > 1$ ): desviación porcentual de los valores de orden cero con respecto a los valores exactos de la frecuencia de resonancia asociada con el proceso rápido.

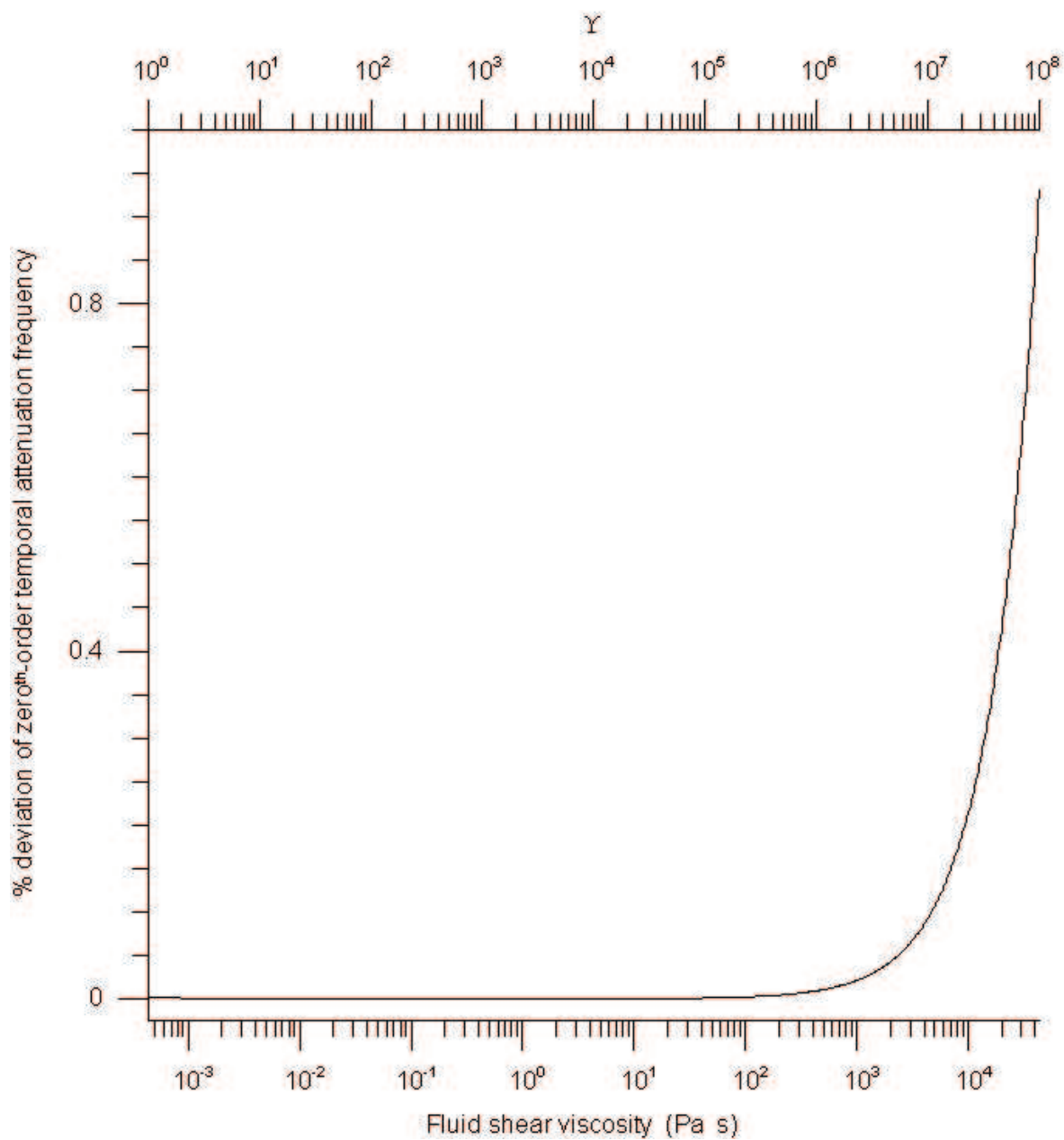


Figure 25. For the regime II ( $\Upsilon > 1$ ) the % deviation from the exact values of the zero<sup>th</sup>-order temporal attenuation frequency associated with the fast process.

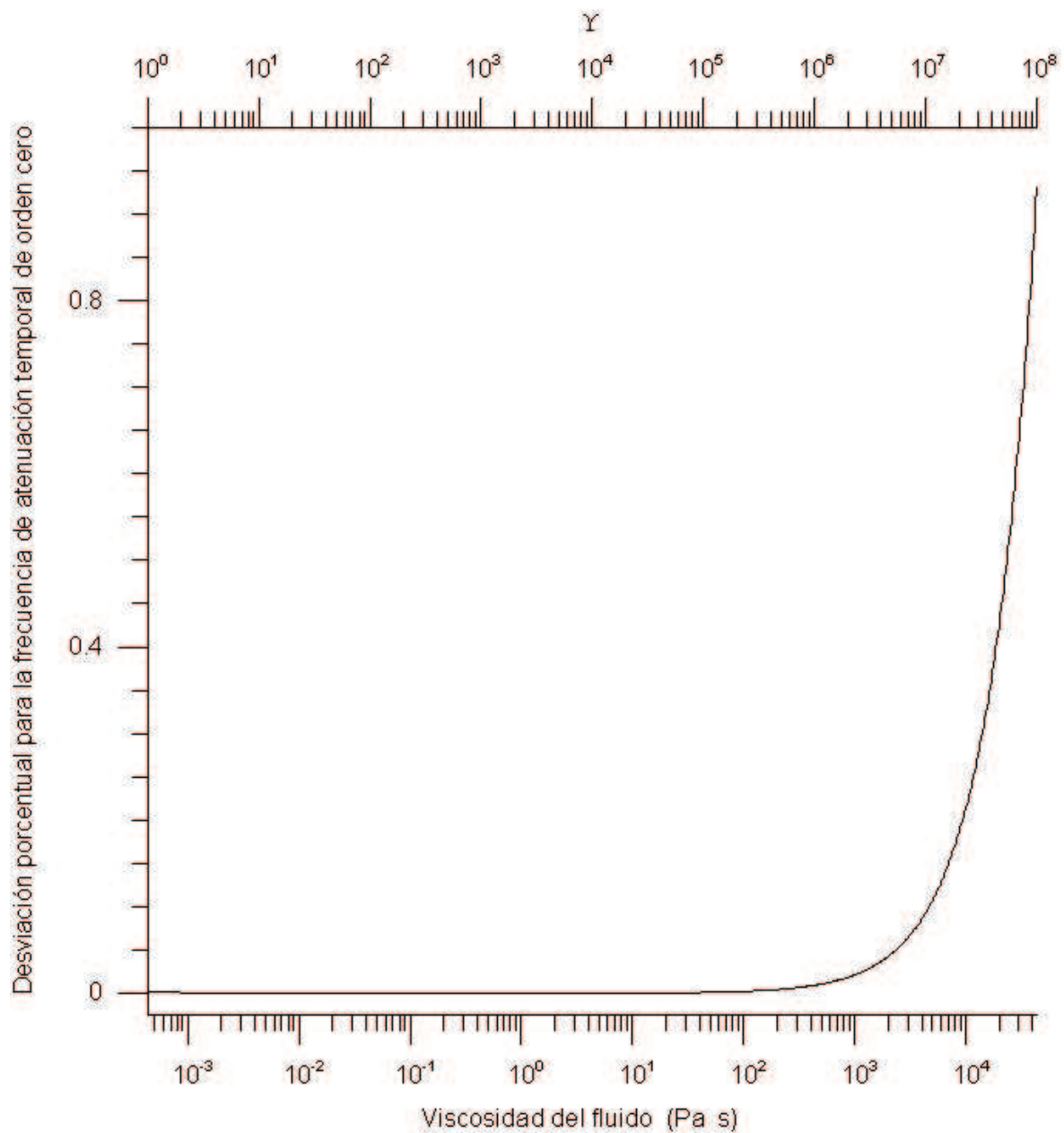


Figure 26. Región II ( $\Upsilon > 1$ ): desviación porcentual de los valores de orden cero con respecto a los valores exactos de la frecuencia de atenuación temporal asociada con el proceso rápido.

and using eq(83) in conjunction with eqs (413) and (421) it is simplified to

$$\Re\omega_1^{(0,II)}(p, l) = \omega_0(p, l)\sqrt{m^s} = \sqrt{q_p^2 + k_l^2} \sqrt{\frac{\mu^0}{\rho_0^m}}. \quad (128)$$

It is found that this approximate resonance frequency expression is valid up to the point (prior to the crossover viscosity C) where the flat part of the resonance curve starts bending downwards. From the first row of eq (125) and eq (128) it is apparent that the wave motion is essentially the unison vibration of solid frame and pore fluid such that the fluid imparts its mass completely to the inertia associated with the process. Hence, it is the total density,  $\rho_0^m$ , that is associated with this process. As opposed to the regime I, in regime II the drop factor of the value of (wet) resonance frequency with respect to  $\omega_0(p, l)$  is independent of the tortuosity factor.

Since  $\epsilon$  is  $\frac{W^{ii}}{\Omega^2}$ , the term  $\epsilon\Omega$  is inversely proportional to viscosity whereas the term  $\nu^{mm}$  is directly proportional to viscosity. At the viscosity value for which  $\Omega = \frac{W^{ii}}{\nu^{mm}}$  holds true these two terms become equal. This viscosity value precisely corresponds to the crossover viscosity B. For the viscosity values less than it, the temporal attenuation frequency for the fast process, i.e. (negative) imaginary part of  $\omega_1^{(0,II)}(p, l)$ , is simply dominated by  $\epsilon\Omega$ . Whereas for the viscosity value greater than it, attenuation is dominated by  $\nu^{mm}$ .

Thus, in the region between A and B, the approximate formula for temporal attenuation of the fast process is

$$-\Im\omega_1^{(0,II)}(p, l) \approx \frac{\epsilon\Omega}{2}, \quad (129)$$

and using eq(118) together with eqs (421), (97), (98) and the expressions for  $d^f$  (table

V) it can be rewritten as

$$-\Im\omega_1^{(0,\text{II})}(\text{p}, l) = \frac{q_{\text{p}}^2 + k_l^2}{2} \left( \frac{\rho_0^{\text{f}}}{\rho_0^{\text{m}}} \right)^2 \mu^0 \frac{\text{K}}{\mu^{\text{f}}}. \quad (130)$$

In contrast of the regime I, in regime II the temporal attenuation frequency is wave number dependent and it is directly proportional to fluid mobility where the proportionality constant is a function of constituent masses and frame shear modulus.

It should be noted that the intersection of eq (114) and eq (130) defines the crossover viscosity A. It turns out to be the point where the viscosity value is such that  $\sqrt{W^{\text{mm}} + W^{\text{ii}}} = \Omega$  holds true.

For the region between B and C the approximate formula for temporal attenuation of the fast process is

$$-\Im\omega_1^{(0,\text{II})}(\text{p}, l) \approx \frac{\nu^{\text{mm}}}{2} \quad (131)$$

and by substituting from eq(84) in conjunction with eq (414) it can be expressed as

$$-\Im\omega_1^{(0,\text{II})}(\text{p}, l) = \frac{q_{\text{p}}^2 + k_l^2}{2} \left( 1 - \frac{\mu^0}{\mu^{\text{s}}} \right) \frac{1}{\rho_0^{\text{m}}} \mu^{\text{f}}. \quad (132)$$

In Fig. 14 the approximate expression for torsional resonance frequency, eq (128), is plotted as dashed-black line superimposed on the respective exact curve.

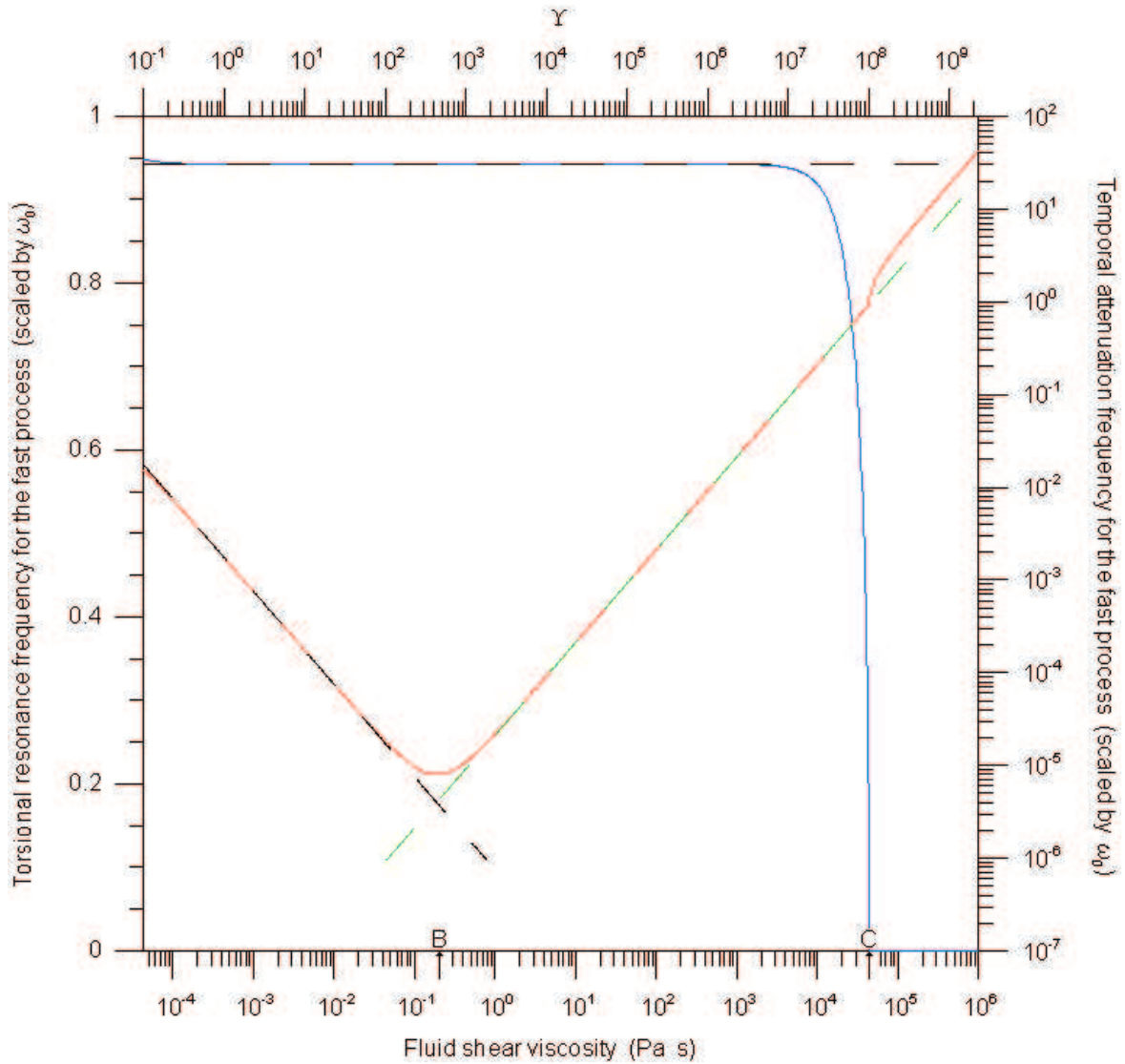


Figure 27. For the regime II ( $\Upsilon > 1$ ) the comparison of exact (eq 90) and approximate expression of the torsional resonance and temporal attenuation frequencies associated with the fast process. The exact resonance,  $\frac{\Re\omega_{1(1,1)}}{\omega_{0(1,1)}}$ , and temporal attenuation,  $\frac{\Im\omega_{1(1,1)}}{\omega_{0(1,1)}}$ , frequencies are presented as blue and red curves, respectively. On the respective exact curves, the approximate resonance frequency (eq 128) is superimposed as dashed-black line and the temporal attenuation frequencies, eq (130) and eq (132), are superimposed as dashed-black and dashed-green lines.

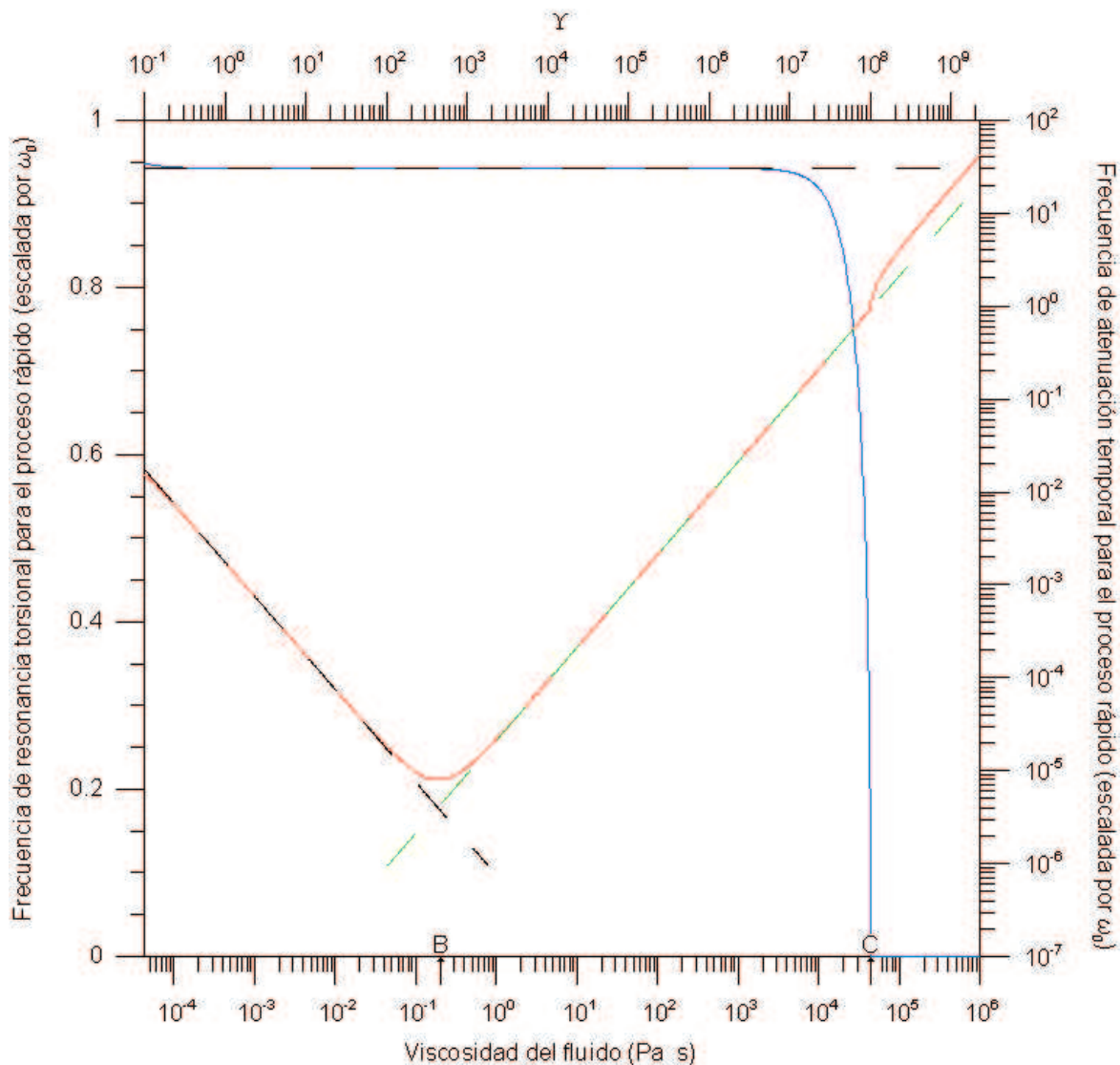


Figure 28. Región II ( $\Upsilon > 1$ ): comparación de los valores exactos (ec 90), y de las fórmulas de aproximación para la frecuencia de resonancia y la frecuencia de atenuación temporal correspondientes al proceso rápido. Las curvas exactas de la frecuencia de resonancia,  $\frac{\Re\omega_1(1,1)}{\omega_0(1,1)}$ , y la atenuación temporal,  $\frac{\Im\omega_1(1,1)}{\omega_0(1,1)}$ , se muestran en azul y rojo, respectivamente. Sobre las respectivas curvas exactas se superimponen la curva de la fórmula aproximada para la frecuencia de resonancia (ec 128) en líneas punteadas negras y para la frecuencia de atenuación temporal se superimponen las curvas de las fórmulas aproximadas, ec (130) y ec (132), en líneas punteadas negras y verdes respectivamente.



The temporal attenuation frequencies in the region between A and B, eq (130), and in the region between B and C, eq (132), are plotted as dashed-black and dashed-green lines respectively.

The crossover viscosity C marks the transition from an underdamped to an overdamped state of vibration. It is the point where the viscosity value is such that  $\sqrt{W^{mm}} = \frac{1}{2}(\epsilon\Omega + \nu^{mm}) \approx \frac{1}{2}\nu^{mm}$  (since  $\epsilon\Omega \ll \nu^{mm}$ ) holds true. Beyond the point C the resonance frequency is zero and the expression for temporal attenuation frequency can be approximated as

$$\begin{aligned} -\Im\omega_1^{(0,II)}(p, l) &\approx \epsilon\Omega + \nu^{mm} \\ &\approx \nu^{mm} = (q_p^2 + k_l^2) \left(1 - \frac{\mu^0}{\mu^s}\right) \frac{1}{\rho_0^m} \mu^f. \end{aligned} \quad (133)$$

It should be noted that for realistic geomaterials parameters eq (133) is not applicable, however, for the sake of completeness of the analysis this was also worked out.

#### IV.2.4.4.2 Slow process

From the second row of eq (125) it is found that the slow wave is basically the difference between the motion of the phases ( $U_\theta^i$ ) with very insignificant amount of center-of-mass motion ( $U_\theta^m$ ), therefore, it can be regarded as a fluid flow process. The second row of eq (123) gives its eigenfrequency pair, which are expressed as

$$\omega_3^{(0,II)}(p, l), \omega_4^{(0,II)}(p, l) = -\frac{i}{2}(\Omega + \nu^{ii}) \pm \sqrt{W^{ii} - \left[\frac{1}{2}(\Omega + \nu^{ii})\right]^2}. \quad (134)$$

Taking into consideration that  $\sqrt{W^{ii}} \ll \frac{\Omega + \nu^{ii}}{2}$ , the above equations can be simplified

as

$$\omega_3^{(0,\text{II})}(\mathbf{p}, l), \omega_4^{(0,\text{II})}(\mathbf{p}, l) \approx -i \left( \Omega + \nu^{\text{ii}} \right), -i \frac{W^{\text{ii}}}{\Omega + \nu^{\text{ii}}}. \quad (135)$$

$\Omega + \nu^{\text{ii}}$  can be regarded as the zero<sup>th</sup>-order temporal attenuation frequency associated with the slow wave. It is almost possible to reproduce the exact temporal attenuation frequency curve for the slow wave in this regime as shown in Fig. 15. The % deviation from its exact value is plotted in Fig. 16. The additional diffusive process with temporal attenuation frequency  $\frac{W^{\text{ii}}}{\Omega + \nu^{\text{ii}}}$  tends to be a non-propagating mode with increasing viscosity.

#### IV.2.4.5 The correction due to the perturbation operator $\mathbf{Q}^{\text{II}}$

For both processes, fast as well as slow, it was found that the correction introduced by carrying the perturbation up to second order are insignificant and as the zero<sup>th</sup>-order curves are essentially in agreement with the exact curves, for the sake of clarity of Figs.11 and 15 it was decided not to plot them.

### IV.2.5 Comparison with the previous work

Dunn (1986) solved the problem of the torsional waves in a finite, fully-saturated, isotropic, homogeneous, porous, circular cylinders in the framework of Biot theory. He found that the complex torsional velocity square is related to the frame-shear modulus by (eq 55, p. 1715)

$$V^2 = \frac{\tau_{22}\mu^0}{\tau_{11}\tau_{22} - \tau_{12}^2}, \quad (136)$$

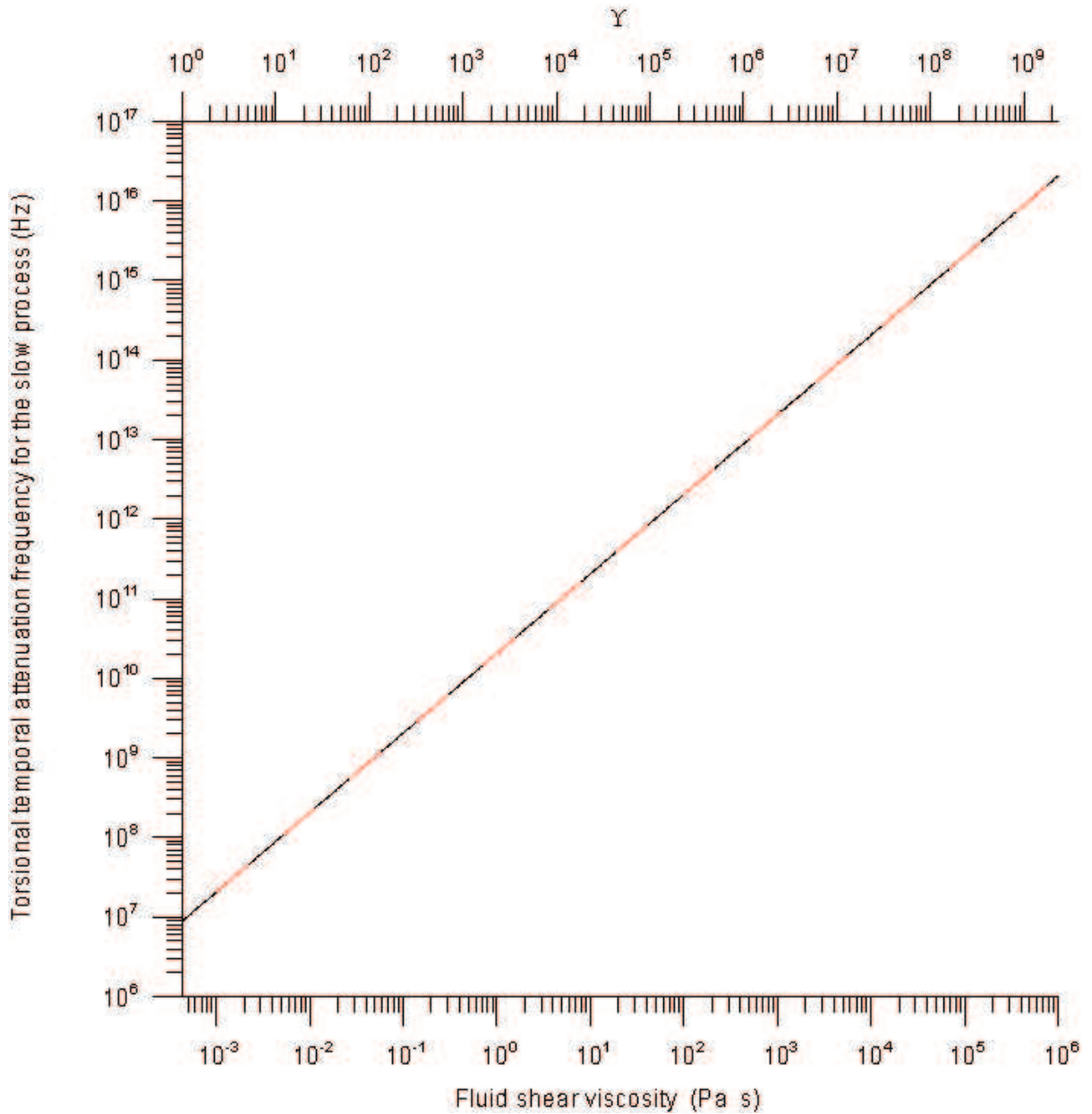


Figure 29. For the regime II ( $\Upsilon > 1$ ) the comparison of the exact (eq 92) and zero<sup>th</sup>-order (eq 135) values of the temporal attenuation frequency associated with the slow process,  $\Im\omega_3(1,1)$ . The exact temporal attenuation frequency is presented as a red curve and the zero<sup>th</sup>-order values are superimposed as dashed-black line.

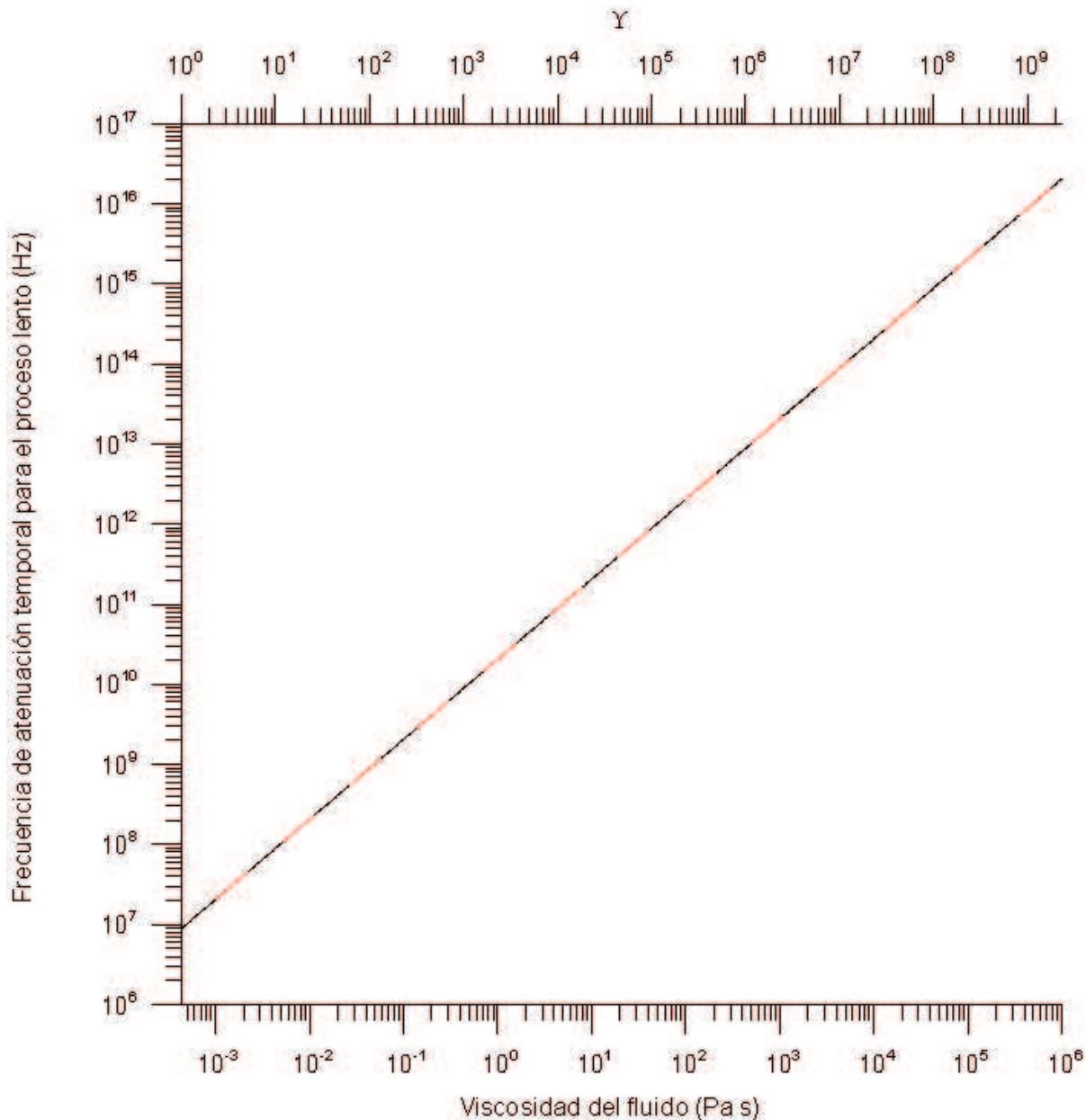


Figure 30. Región II ( $\Upsilon > 1$ ): comparación de los valores exactos (ec 92) y de orden cero (ec 135) de la frecuencia de atenuación temporal torsional correspondiente al proceso lento. La curva exacta de la frecuencia de atenuación temporal,  $\frac{3\omega_1(1,1)}{\omega_0(1,1)}$ , se muestran en rojo. Sobre la curva exacta se superimponen la curva de la frecuencia de atenuación temporal de orden cero en líneas punteadas negras.

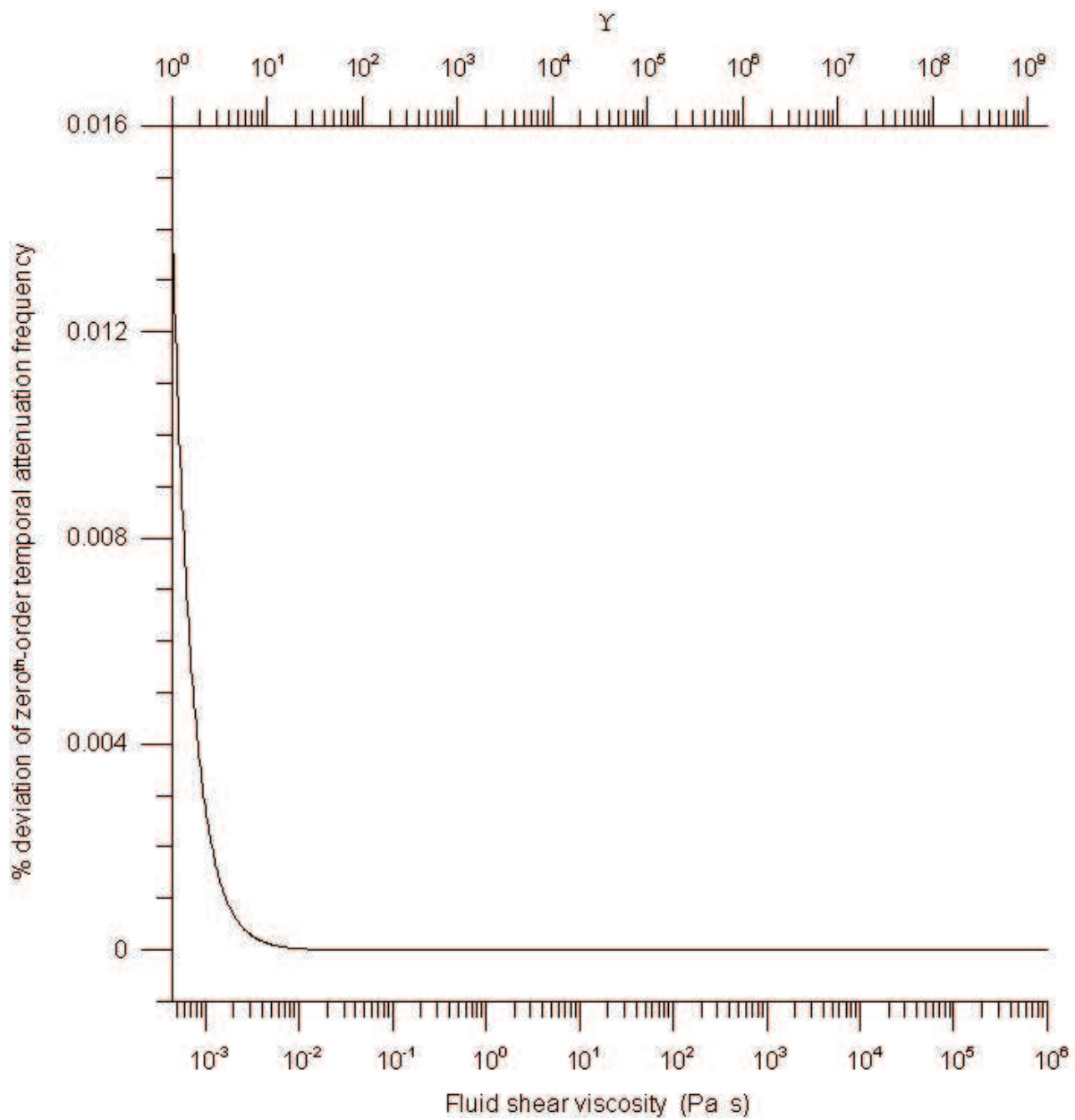


Figure 31. For the regime II ( $\Upsilon > 1$ ) the % deviation of the zero<sup>th</sup>-order value from the exact value associated with the slow process.

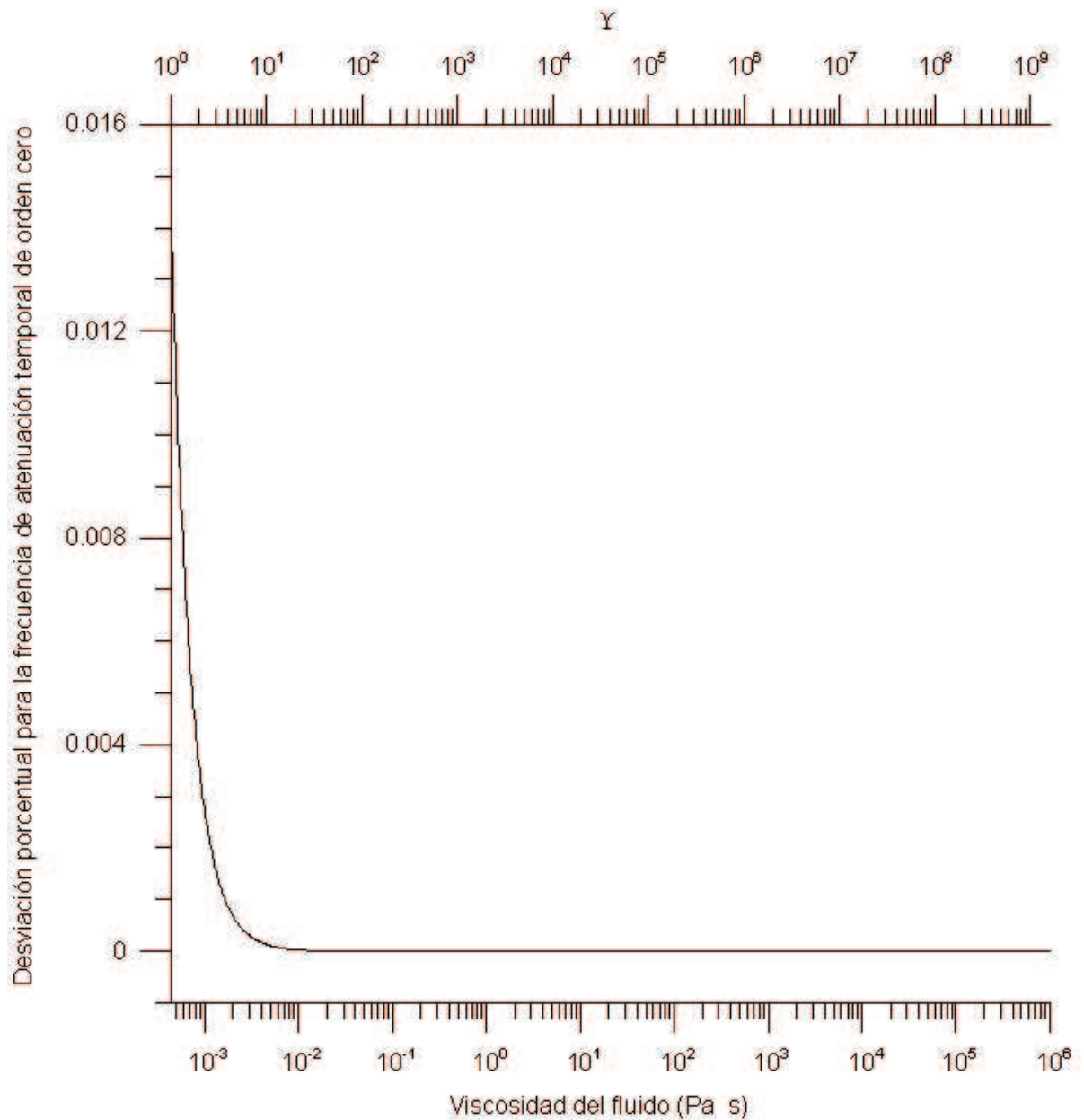


Figure 32. Región II ( $\Upsilon > 1$ ): desviación porcentual de los valores de orden cero con respecto a los valores exactos de la frecuencia de atenuación temporal asociada con el proceso lento.

where

$$\begin{aligned}
\tau_{11} &= (1 - \eta_0) \phi_0^s - \rho^{12} + i \frac{1}{\omega} \frac{\eta_0^2 \mu^f}{K} \\
\tau_{22} &= \eta_0 \phi_0^f - \rho^{12} + i \frac{1}{\omega} \frac{\eta_0^2 \mu^f}{K} \\
\tau_{12} &= \rho^{12} - i \frac{1}{\omega} \frac{\eta_0^2 \mu^f}{K}.
\end{aligned} \tag{137}$$

Substituting eqs (137) into eq (136) and using the complex velocity square is related to frequency and wavenumbers by

$$V^2 = \frac{\omega^2}{q_p^2 + k_l^2}, \tag{138}$$

after rearranging the terms, the following dispersion relation is obtained

$$\omega \left[ \omega^3 + i\Omega\omega^2 - (q_p^2 + k_l^2) \left( \eta_0 \phi_0^f - \rho^{12} + i \frac{1}{\omega} \frac{\eta_0^2 \mu^f}{K} \right) \frac{\mu^0}{\rho_0^m \rho_0^i} - i\Omega (q_p^2 + k_l^2) \frac{\mu^0}{\rho_0^m} \right] = 0, \tag{139}$$

which is the Biot limit case of the dispersion relation (86), which solutions are given by eqs (110) and (115).

Obviously from eqs (138) and (139) it is not clear the contribution of each material parameter in the resonance and temporal attenuation frequencies curves, as the procedure developed throughout this chapter. Moreover, the slow S process is not incorporated in the above analysis, which is of importance for porous samples saturated with highly viscous fluid, like heavy crude oil or bitumen.

Throughout this chapter a methodology in which the link between resonance and temporal attenuation frequencies measurements and material parameters are transparent has been developed.

### IV.3 Summary

The expressions for torsional resonance and temporal attenuation frequencies for a finite, poroelastic, circular cylinder in which dependence upon porous medium material properties are transparent were developed. The summary of these expressions in the different regimes are presented below.

**Regime I** ( $\Upsilon < 10^{-2}$ ):

Torsional resonance frequency

$$\Re\omega_1^{(0,I)}(p, l) = \sqrt{q_p^2 + k_l^2} \sqrt{\frac{\mu^0}{\phi_0 \rho_0^s + \eta_0 \rho_0^f \left(1 - \frac{1}{S}\right)}}. \quad (140)$$

Temporal attenuation frequency

$$-\Im\omega_1^{(0,I)}(p, l) = \frac{1}{2} \frac{\left(\frac{\eta_0}{S}\right)^2}{\phi_0 \rho_0^s + \eta_0 \rho_0^f \left(1 - \frac{1}{S}\right)} \frac{\mu^f}{K}. \quad (141)$$

**Regime II** ( $\Upsilon < 10^{-2}$ ):

Torsional resonance frequency

$$\Re\omega_1^{(0,II)}(p, l) = \sqrt{q_p^2 + k_l^2} \sqrt{\frac{\mu^0}{\rho_0^m}}. \quad (142)$$

Temporal attenuation frequency

*Regime between A and B*

$$-\Im\omega_1^{(0,II)}(p, l) = \frac{q_p^2 + k_l^2}{2} \left(\frac{\rho_0^f}{\rho_0^m}\right)^2 \mu^0 \frac{K}{\mu^f}. \quad (143)$$



*Regime between B and C*

$$-\Im\omega_1^{(0,\text{II})}(\mathbf{p}, l) = \frac{q_{\mathbf{p}}^2 + k_l^2}{2} \left(1 - \frac{\mu^0}{\mu^s}\right) \frac{1}{\rho_0^{\text{m}}} \mu^{\text{f}}. \quad (144)$$

*Regime above C*

$$-\Im\omega_1^{(0,\text{II})}(\mathbf{p}, l) = (q_{\mathbf{p}}^2 + k_l^2) \left(1 - \frac{\mu^0}{\mu^s}\right) \frac{1}{\rho_0^{\text{m}}} \mu^{\text{f}}. \quad (145)$$

Based upon the above expressions there is a firm basis to design torsional oscillation experiments to determine solid frame shear modulus, permeability, and tortuosity factor.

# Chapter V

## Frame Shear Modulus, Permeability and Tortuosity Factor by Torsional Resonance Experiments

In this chapter torsional mode experiments for a finite, poroelastic, circular cylinder are designed to determine the frame shear modulus, permeability and tortuosity factor parameters based on the expressions for torsional resonance and temporal attenuation frequencies developed in chapter IV.

Section V.1 presents how to determine the frame shear modulus parameter. Section V.2 presents how to measure permeability for high and low porosity rocks and section V.3 presents how to determine the tortuosity factor term.

### V.1 Direct measurement of frame shear modulus by air saturated sample

Geomaterial saturated with air  $\Upsilon$ , eq (97), is likely to be under  $10^{-2}$ , thus, the resonance frequency formula given by eq (140) is applicable. Since the density of air is over three orders in magnitude smaller than the solid density the contribution of the tortuosity

factor term in eq (140) is negligible and the resonance frequency for air saturated sample,  $\Re\omega_1^{(0,1)}(p, l)$ , is essentially the same as the resonance frequency of the dry porous frame eq (421),  $\omega_0(p, l)$ .

Thus the frame shear modulus is determined by torsional vibration of air saturated sample as

$$\mu^0 = \frac{\phi_0 \rho_0^s}{q_p^2 + k_l^2} (\omega_0(p, l))^2. \quad (146)$$

On account of the shear viscosity of an air being of the order of  $10^{-5}$ , practically no temporal attenuation is expected here.

## V.2 Measurement of permeability

Since a torsional experiment yields only two measurements, namely, torsional resonance frequency and temporal attenuation frequency and there are three parameters to be resolved: the frame shear modulus, permeability and tortuosity factor, an additional independent measurement is essential.

For the case of high permeability rock which can be drained (and saturated) easily, the torsional excitation of drained/dry core could be an option. The torsional excitation of the same core saturated with a different fluid could also be an another option.

For a low permeability rock, draining may not be feasible. If it is viable to run a set of two excitations on the same core, such that one falls into the inertial mode and the other into viscous mode of torsional vibration, then it could be an option for this case. All of these possibilities are explored.

### V.2.1 High permeability rocks

For the wet (fully mono saturated) core if the resonance frequency drops over its value for the dry-frame (i.e. air saturated) case as per formula

$$\left( \frac{\Re\omega_1^{(0,\text{II})}(\text{p}, l)}{\omega_0(\text{p}, l)} \right)^2 = \frac{\phi_0\rho_0^s}{\phi_0\rho_0^s + \eta_0\rho_0^f}, \quad (147)$$

then, it is indicative that the given mode of vibration belongs to the viscosity dominated regime. In this case using eq (143), the permeability can be deduce from the observed temporal attenuation frequency by

$$K = \frac{2}{q_p^2 + k_l^2} \left( \frac{\rho_0^m}{\rho_0^f} \right)^2 \frac{\mu^f}{\mu^0} \frac{1}{-\Im\omega_1^{(0,\text{II})}(\text{p}, l)}, \quad (148)$$

provided that the frame shear modulus is known, say by torsional mode excitation of the same core saturated with air (eq 146).

If the criterion (147) is not the case, then it is indicative of inertial regime of excitation. In this case by vibrating the sample in a mode with a larger wavenumber, and observing that the attenuation remains the same, one may conclude that the vibration is inertial. In this case the tortuosity factor is deduced from the observed torsional resonance frequency measurement as

$$\frac{1}{S} = \frac{1}{\eta_0\rho_0^f} \left[ \rho_0^m - \phi_0\rho_0^s \left( \frac{\omega_0(\text{p}, l)}{\Re\omega_1^{(0,\text{I})}(\text{p}, l)} \right)^2 \right], \quad (149)$$

and substituting its value in eq (141), the permeability is calculated from observed temporal attenuation frequency as

$$K = \frac{1}{2} \frac{\left(\frac{\eta_0}{S}\right)^2}{\phi_0 \rho_0^s + \eta_0 \rho_0^f \left(1 - \frac{1}{S}\right)} \frac{\mu^f}{-\Im \omega_1^{(0,1)}(p, l)}. \quad (150)$$

### V.2.2 Low permeability rocks

If the mode of excitation is such that  $\Upsilon < 1$ , then eqs (140) and (141) are applicable. By squaring eq (140) and then algebraically manipulating this equation, it can be rewritten as

$$\mu^0 = \frac{\phi_0 \rho_0^s + \eta_0 \rho_0^f \left(1 - \frac{1}{S}\right)}{q_p^2 + k_l^2} \left(\Re \omega_1^{(0,1)}(p, l)\right)^2. \quad (151)$$

By algebraic manipulation of eq (141), it can be rewritten as

$$K = \frac{1}{2} \frac{\left(\frac{\eta_0}{S}\right)^2}{\phi_0 \rho_0^s + \eta_0 \rho_0^f \left(1 - \frac{1}{S}\right)} \frac{\mu^f}{-\Im \omega_1^{(0,1)}(p, l)}. \quad (152)$$

The ratio of eq (140) to eq (141) leads to

$$\mu^0 K S^2 = \frac{1}{2} \left( \frac{\eta_0^2 \mu^f}{q_p^2 + k_l^2} \right) \left[ \frac{\left(\Re \omega_1^{(0,1)}(p, l)\right)^2}{-\Im \omega_1^{(0,1)}(p, l)} \right] \quad (153)$$

where  $q_p$  and  $k_l$  labels the wavenumber of the mode. Either (151) or (152), together with (153), can be taken as a set of two linearly independent equations. Clearly at least one more independent measurement is essential for resolving the three unknown parameters.

If it is possible to excite the same sample in an another mode of vibration such that it pertains to  $\Upsilon > 1$  regime, then there are two additional torsional measurements. In

this case the formula (142) and (143) are operational. By squaring eq (142) and then algebraically manipulating this equation, it can be rewritten as

$$\mu^0 = \left( \frac{\rho_0^m}{q_i^2 + k_j^2} \right) \left( \Re \omega_1^{(0,II)}(i,j) \right)^2. \quad (154)$$

By algebraic manipulation of eq (143), it can be rewritten as

$$K = \frac{2\mu^f}{q_i^2 + k_j^2} \left( \frac{\rho_0^m}{\rho_0^f} \right) \left[ -\Im \omega_1^{(0,II)}(i,j) \right] \quad (155)$$

where  $q_i$  and  $k_j$  labels the wavenumber of the new mode.

Substituting eq (154) and (155) into (153) leads to

$$S = \sqrt{\frac{1}{2} \left( \frac{\eta_0^2 \mu^f}{q_p^2 + k_l^2} \right) \frac{\left( \Re \omega_1^{(0,I)}(p,l) \right)^2 \left( q_i^2 + k_j^2 \right)^2 \rho_0^f}{-\Im \omega_1^{(0,I)}(p,l)} \frac{1}{2\mu^f (\rho_0^m)^2} \frac{1}{-\Im \omega_1^{(0,II)}(i,j)} \left( \Re \omega_1^{(0,II)}(i,j) \right)^2}. \quad (156)$$

Eq (156), in conjunction with either the eqs (151-152) or the eqs (154 - 155) can be used to determine all three parameters.

### V.3 Measurement of tortuosity factor

It should be noted that the appropriate value of tortuosity factor can only be determined if the associated  $\Upsilon$  parameter is smaller than  $10^{-2}$ . This is achieved by saturating the sample with a fluid with appropriate viscosity and exciting the suitable mode. In this case, the tortuosity factor is deduced using eq (140).

# Chapter VI

## Extensional Waves in Porous Cylinder

In this chapter the solution of the open-pore and closed-pore stress-free boundary-value problems associated with extensional oscillations of a poroelastic, circular cylinder cast in the framework of volume-averaged theory of poroelasticity are carried out. Expressions for extensional phase velocity and attenuation in which the dependence upon the material properties are transparent are developed.

Section VI.1 lists the equations of motion for extensional oscillations in frequency domain. Section VI.2 shows the procedure to decouple the equations of motion in two decoupled scalar Helmholtz equations. Section VI.3 presents the solutions of these two decoupled scalar equations. Section VI.4 based on these solutions the expressions of displacements and stresses are presented. Section VI.5 shows the dispersion relation for longitudinal mode for open-pore stress-free boundary condition. Section VI.6 presents a complete analysis of the  $\Theta$  functions which gives the transcendental behavior of the dispersion relation for longitudinal vibrations. Section VI.7 shows the procedure to reduce the transcendental  $\Theta$  functions to algebraic expressions. Section VI.8 presents the dispersion relation for extensional mode for open-pore stress-free boundary condition. Section VI.9 shows the numerical solution of the dispersion relation for the extensional mode. In section VI.10 the extensional phase velocity and attenuation in terms of material properties are stated. Section VI.11 presents the dispersion relation for longi-

tudinal mode for closed-pore stress-free boundary condition. Section VI.12 presents the dispersion relation for extensional mode for closed-pore stress-free boundary condition. Section VI.13 shows the numerical solution of the dispersion relation for the extensional mode for the closed-pore problem. In section VI.14 the extensional phase velocity and attenuation for the closed-pore problem in terms of material properties are stated. Section VI.15 presents the comparison with previous work. In Section VI.16 a summarize of the results of this chapter is presented.

## VI.1 Governing equations

From this point on, the equations of motion (70, 71) are stated in frequency domain, hence the fourier transform with respect to time is implicit. The equations of motion in frequency domain can be written as

$$\Omega^{-1} \boldsymbol{\rho}^{-1} \left( \tau_{rz,z} + \tau_{rr,r} + \frac{1}{r} (\tau_{rr} - \tau_{\theta\theta}) \right) + \omega^2 \mathbf{u}_r = 0, \quad (157)$$

$$\Omega^{-1} \boldsymbol{\rho}^{-1} \left( \tau_{zz,z} + \tau_{rz,r} + \frac{1}{r} \tau_{rz} \right) + \omega^2 \mathbf{u}_z = 0, \quad (158)$$

and stresses (72-75) are

$$\Omega^{-1} \boldsymbol{\rho}^{-1} \tau_{rr} = (\boldsymbol{\alpha} - 2\boldsymbol{\beta}) \left\{ \left( \partial_r + \frac{1}{r} \right) \mathbf{u}_r + \partial_z \mathbf{u}_z \right\} + 2\boldsymbol{\beta} \partial_r \mathbf{u}_r, \quad (159)$$

$$\Omega^{-1} \boldsymbol{\rho}^{-1} \tau_{zz} = (\boldsymbol{\alpha} - 2\boldsymbol{\beta}) \left\{ \left( \partial_r + \frac{1}{r} \right) \mathbf{u}_r + \partial_z \mathbf{u}_z \right\} + 2\boldsymbol{\beta} \partial_z \mathbf{u}_z, \quad (160)$$

$$\Omega^{-1} \boldsymbol{\rho}^{-1} \tau_{\theta\theta} = (\boldsymbol{\alpha} - 2\boldsymbol{\beta}) \left\{ \left( \partial_r + \frac{1}{r} \right) \mathbf{u}_r + \partial_z \mathbf{u}_z \right\} + 2\boldsymbol{\beta} \frac{\mathbf{u}_r}{r}, \quad (161)$$

$$\Omega^{-1} \boldsymbol{\rho}^{-1} \tau_{rz} = \boldsymbol{\beta} (\partial_z \mathbf{u}_r + \partial_r \mathbf{u}_z), \quad (162)$$

where  $\mathbf{u}_p = (\mathbf{u}_p^m, \mathbf{u}_p^i)^T$ ,  $\tau_{jk} = (\tau_{jk}^m, \tau_{jk}^i)^T$ , ( $p = r, z; j, k = r, \theta, z$ ).  $\boldsymbol{\rho}$  is the density matrix given in eq (48).  $\Omega$  is a 2x2 diagonal matrix associated with viscous to inertial transition



frequency  $\Omega$ . It is

$$\mathbf{\Omega} = \mathbf{I} + i\frac{\Omega}{\omega} \mathbf{I}_0, \quad (163)$$

where  $\mathbf{I}$  is a  $2 \times 2$  identity matrix and  $\mathbf{I}_0$  is  $2 \times 2$  matrix whose element  $(2, 2)$  is unity and the rest of the elements are equal to zero, eq (49).  $\boldsymbol{\alpha}$  and  $\boldsymbol{\beta}$  are  $2 \times 2$  matrices associated with P- and S-motion, respectively, whose elements are dimensionally equal to velocity squared. These are

$$\boldsymbol{\alpha} = \mathbf{\Omega}^{-1} (\mathbf{C}_\alpha - i\omega \mathbf{N}_\alpha) \equiv \begin{pmatrix} \alpha^{mm} & \alpha^{mi} \\ \alpha^{im} & \alpha^{ii} \end{pmatrix}, \quad (164)$$

$$\boldsymbol{\beta} = \mathbf{\Omega}^{-1} (\mathbf{C}_\beta - i\omega \mathbf{N}_\beta) \equiv \begin{pmatrix} \beta^{mm} & \beta^{mi} \\ \beta^{im} & \beta^{ii} \end{pmatrix}, \quad (165)$$

where the matrices  $\mathbf{C}$ 's and  $\mathbf{N}$ 's are given in appendix A.

Plugging stresses (159-162) into (157-158) the governing equation for displacement field  $\mathbf{u} = (\mathbf{u}^m, \mathbf{u}^i)^T$  is obtained as

$$\boldsymbol{\alpha} \nabla (\nabla \cdot \mathbf{u}) - \boldsymbol{\beta} \nabla \times \nabla \times \mathbf{u} + \omega^2 \mathbf{u} = 0. \quad (166)$$

The given boundary value problem, eq (166), together with appropriate boundary conditions on stresses, (159-162), have to be solved.

## VI.2 Decoupling

For 2D case under consideration the vector decomposition is

$$\mathbf{u} = \nabla \Phi + \nabla \times \nabla \times (\hat{\mathbf{z}} \Xi), \quad (167)$$

where potential vectors are

$$\mathbf{\Phi} = (\Phi^m, \Phi^i)^T, \quad (168)$$

and

$$\mathbf{\Xi} = (\chi^m, \chi^i)^T, \quad (169)$$

as introduced in (166) which uncouples it into curl-free (compression) and divergence-free (shear) parts by rendering a  $2 \times 2$  matrix Helmholtz equation for each potential vector as follows

$$\alpha \nabla^2 \mathbf{\Phi} + \omega^2 \mathbf{\Phi} = 0, \quad (170)$$

$$\beta \nabla^2 \mathbf{\Xi} + \omega^2 \mathbf{\Xi} = 0. \quad (171)$$

Here  $\alpha$  and  $\beta$  are complex velocity squared matrices associated with P- and S-motion, respectively, as given in eqs (164-165).

The above matrix Helmholtz equations are diagonalized by introducing the transformations

$$\mathbf{\Phi} = \mathbf{r}^\alpha \boldsymbol{\phi} \quad \text{where} \quad \boldsymbol{\phi} = (\phi^I, \phi^{II})^T, \quad (172)$$

and

$$\mathbf{\Xi} = \mathbf{r}^\beta \boldsymbol{\chi} \quad \text{where} \quad \boldsymbol{\chi} = (\chi^I, \chi^{II})^T. \quad (173)$$

Where  $\mathbf{r}^\alpha$  and  $\mathbf{l}^\alpha$  are, respectively, right- and left- eigenvector matrices of  $\boldsymbol{\alpha}$  matrix defined by

$$\mathbf{r}^\alpha = [\mathbf{r}^{\alpha_I}, \mathbf{r}^{\alpha_{II}}], \quad (174)$$

$$\mathbf{l}^\alpha = [\mathbf{l}^{\alpha_I}, \mathbf{l}^{\alpha_{II}}]. \quad (175)$$

They are orthonormal to each other, therefore

$$\mathbf{l}^{\alpha T} \mathbf{r}^\alpha = \mathbf{I}, \quad (176)$$

and they diagonalize the  $\boldsymbol{\alpha}$  matrix by

$$\mathbf{l}^{\alpha T} \boldsymbol{\alpha} \mathbf{r}^\alpha = \boldsymbol{\Lambda}^\alpha \equiv \begin{pmatrix} \alpha_I^2 & 0 \\ 0 & \alpha_{II}^2 \end{pmatrix} \quad (177)$$

where the pair  $(\alpha_I^2, \alpha_{II}^2)$  are eigenvalues of  $\boldsymbol{\alpha}$  matrix, and the pairs  $(\mathbf{r}^{\alpha_I}, \mathbf{r}^{\alpha_{II}})$  and  $(\mathbf{l}^{\alpha_I}, \mathbf{l}^{\alpha_{II}})$  are associated right- and left- eigenvectors, respectively. Likewise right- and left- eigenvector matrices of  $\boldsymbol{\beta}$  matrix are, respectively,

$$\mathbf{r}^\beta = [\mathbf{r}^{\beta_I}, \mathbf{r}^{\beta_{II}}] \quad (178)$$

and

$$\mathbf{l}^\beta = [\mathbf{l}^{\beta_I}, \mathbf{l}^{\beta_{II}}]. \quad (179)$$

They satisfy that

$$\mathbf{l}^{\beta T} \mathbf{r}^\beta = \mathbf{I}, \quad (180)$$

and

$$\mathbf{l}^{\beta^T} \boldsymbol{\beta} \mathbf{r}^\beta = \boldsymbol{\Lambda}^\beta \equiv \begin{pmatrix} \beta_I^2 & 0 \\ 0 & \beta_{II}^2 \end{pmatrix}, \quad (181)$$

where the pair  $(\beta_I^2, \beta_{II}^2)$  are the eigenvalues of  $\boldsymbol{\beta}$  matrix, and the pairs  $(\mathbf{r}^{\beta_I}, \mathbf{r}^{\beta_{II}})$  and  $(\mathbf{l}^{\beta_I}, \mathbf{l}^{\beta_{II}})$  are the associated right- and left- eigenvectors, respectively.

A detail analysis of eigenvalues and eigenvectors of  $\boldsymbol{\alpha}$  and  $\boldsymbol{\beta}$  matrices are presented in appendices (E and F).

Thus, utilizing the normal co-ordinate transformations discussed above, the set of two decoupled scalar Helmholtz equations for P-motion is obtained as

$$\boldsymbol{\Lambda}^\alpha \nabla^2 \phi + \omega^2 \phi = 0, \quad (182)$$

and for S-motion it is

$$\boldsymbol{\Lambda}^\beta \nabla^2 \chi + \omega^2 \chi = 0. \quad (183)$$

### VI.3 Elemental solutions for decoupled potentials

Since the interest is in axial wave propagation, the wavenumber associated with axial direction ( $k$ ) has to be taken as a free parameter. Because of angular independence of motion, for the radial part, only the zero<sup>th</sup>-order Bessel function is permitted. Furthermore, the second independent solution for the radial part, the Bessel function of the second kind has to be ruled out due to its logarithmic singularity at the origin.

The appropriate elemental solutions for scalar Helmholtz equation pairs (182) and (183)

thus read

$$\boldsymbol{\phi} = \begin{pmatrix} \phi^{\text{I}} \\ \phi^{\text{II}} \end{pmatrix} = \begin{pmatrix} J_0(q_{\alpha\text{I}}r) & 0 \\ 0 & J_0(q_{\alpha\text{II}}r) \end{pmatrix} e^{ikz} \begin{pmatrix} a_{\text{I}} \\ a_{\text{II}} \end{pmatrix}, \quad (184)$$

$$\boldsymbol{\chi} = \begin{pmatrix} \chi^{\text{I}} \\ \chi^{\text{II}} \end{pmatrix} = \begin{pmatrix} J_0(q_{\beta\text{I}}r) & 0 \\ 0 & J_0(q_{\beta\text{II}}r) \end{pmatrix} e^{ikz} \begin{pmatrix} b_{\text{I}} \\ b_{\text{II}} \end{pmatrix}, \quad (185)$$

where the associated radial wave numbers are defined by

$$q_{\alpha\text{I}}^2 = \frac{\omega^2}{\alpha_{\text{I}}^2} - k^2, \quad q_{\alpha\text{II}}^2 = \frac{\omega^2}{\alpha_{\text{II}}^2} - k^2, \quad (186)$$

and

$$q_{\beta\text{I}}^2 = \frac{\omega^2}{\beta_{\text{I}}^2} - k^2, \quad q_{\beta\text{II}}^2 = \frac{\omega^2}{\beta_{\text{II}}^2} - k^2, \quad (187)$$

with  $a_{\text{I}}$ ,  $a_{\text{II}}$ ,  $b_{\text{I}}$ , and  $b_{\text{II}}$  being the arbitrary constants.

## VI.4 Expressions of displacements and stresses

From eqs (167), (159) and (160) radial and axial component of displacements and stresses are expressed as

$$\begin{aligned} \mathbf{u}_r &= \partial_r \Phi + \partial_{rz}^2 \Xi, \\ \mathbf{u}_z &= \partial_z \Phi - \left( \partial_r^2 + \frac{1}{r} \partial_r \right) \Xi, \\ \tau_{rr} &= \Omega \rho \left\{ \left[ (\alpha - 2\beta) \nabla^2 + 2\beta \partial_r^2 \right] \Phi + 2\beta \partial_r^2 \partial_z \Xi \right\}, \\ \tau_{rz} &= \Omega \rho \beta \left\{ 2\partial_{rz}^2 \Phi + \partial_r \left[ \partial_z^2 - \left( \partial_r^2 + \frac{1}{r} \partial_r \right) \right] \Xi \right\}. \end{aligned} \quad (188)$$

Using identities (172) and (173) the above equations are rewritten in terms of decouples potentials  $\phi$  and  $\chi$  as

$$\begin{aligned}
\mathbf{u}_r &= \mathbf{r}^\alpha \partial_r \phi + \mathbf{r}^\beta \partial_{rz}^2 \chi, \\
\mathbf{u}_z &= \mathbf{r}^\alpha \partial_z \phi - \mathbf{r}^\beta \left( \partial_r^2 + \frac{1}{r} \partial_r \right) \chi, \\
\tau_{rr} &= \Omega \rho \left\{ [(\boldsymbol{\alpha} - 2\boldsymbol{\beta}) \mathbf{r}^\alpha \nabla^2 + 2\boldsymbol{\beta} \mathbf{r}^\alpha \partial_r^2] \phi + 2\boldsymbol{\beta} \mathbf{r}^\beta \partial_r^2 \partial_z \chi \right\}, \\
\tau_{rz} &= \Omega \rho \boldsymbol{\beta} \left\{ 2\mathbf{r}^\alpha \partial_{rz}^2 \phi + \mathbf{r}^\beta \partial_r \left[ \partial_z^2 - \left( \partial_r^2 + \frac{1}{r} \partial_r \right) \right] \chi \right\}.
\end{aligned} \tag{189}$$

Plugging in the solutions of the potential equations i.e. (184) and (185) into the above equations, followed by some algebraic manipulations, and utilizing the following notations

$$\begin{aligned}
&\begin{pmatrix} q_{\alpha\text{I}}^2 & 0 \\ 0 & q_{\alpha\text{II}}^2 \end{pmatrix} \equiv \mathbf{Q}^\alpha, \\
&\begin{pmatrix} q_{\beta\text{I}}^2 & 0 \\ 0 & q_{\beta\text{II}}^2 \end{pmatrix} \equiv \mathbf{Q}^\beta, \\
&\begin{pmatrix} \frac{2J_1(rq_{\alpha\text{I}})}{rq_{\alpha\text{I}}J_0(rq_{\alpha\text{I}})} & 0 \\ 0 & \frac{2J_1(rq_{\alpha\text{II}})}{rq_{\alpha\text{II}}J_0(rq_{\alpha\text{II}})} \end{pmatrix} \equiv \begin{pmatrix} \Theta(rq_{\alpha\text{I}}) & 0 \\ 0 & \Theta(rq_{\alpha\text{II}}) \end{pmatrix} \equiv \boldsymbol{\Theta}^\alpha, \\
&\begin{pmatrix} \frac{2J_1(rq_{\beta\text{I}})}{rq_{\beta\text{I}}J_0(rq_{\beta\text{I}})} & 0 \\ 0 & \frac{2J_1(rq_{\beta\text{II}})}{rq_{\beta\text{II}}J_0(rq_{\beta\text{II}})} \end{pmatrix} \equiv \begin{pmatrix} \Theta(rq_{\beta\text{I}}) & 0 \\ 0 & \Theta(rq_{\beta\text{II}}) \end{pmatrix} \equiv \boldsymbol{\Theta}^\beta, \\
&ik^3 (\boldsymbol{\Lambda}^\alpha)^{-1} \begin{pmatrix} J_0(rq_{\alpha\text{I}}) & 0 \\ 0 & J_0(rq_{\alpha\text{II}}) \end{pmatrix} \begin{pmatrix} a_{\text{I}} \\ a_{\text{II}} \end{pmatrix} = \begin{pmatrix} A_{\text{I}} \\ A_{\text{II}} \end{pmatrix} \equiv \mathbf{A}, \\
&\frac{1}{2}k^2 (\boldsymbol{\Lambda}^\beta)^{-1} \mathbf{Q}^\beta \begin{pmatrix} J_0(rq_{\beta\text{I}}) & 0 \\ 0 & J_0(rq_{\beta\text{II}}) \end{pmatrix} \begin{pmatrix} b_{\text{I}} \\ b_{\text{II}} \end{pmatrix} = \begin{pmatrix} B_{\text{I}} \\ B_{\text{II}} \end{pmatrix} \equiv \mathbf{B},
\end{aligned} \tag{190}$$

the expressions of displacements and stresses are obtained as

$$\mathbf{u}_r = -\frac{r}{2ik} \left[ \frac{1}{k^2} \mathbf{r}^\alpha \mathbf{Q}^\alpha \Theta^\alpha \Lambda^\alpha \mathbf{A} - 2\mathbf{r}^\beta \Theta^\beta \Lambda^\beta \mathbf{B} \right] e^{ikz}, \quad (191)$$

$$\mathbf{u}_z = \frac{1}{k^2} \left[ \mathbf{r}^\alpha \Lambda^\alpha \mathbf{A} + 2\mathbf{r}^\beta \Lambda^\beta \mathbf{B} \right] e^{ikz}, \quad (192)$$

$$\begin{aligned} \tau_{rr} = & -\frac{\Omega\rho}{ik} \left[ \left\{ (\alpha - 2\beta) \mathbf{r}^\alpha \frac{\omega^2}{k^2} + 2\beta \mathbf{r}^\alpha \left( \frac{\omega^2}{k^2} \mathbf{I} - \Lambda^\alpha \right) \left( \mathbf{I} - \frac{1}{2} \Theta^\alpha \right) \right\} \mathbf{A} \right. \\ & \left. - 2\beta \mathbf{r}^\beta \Lambda^\beta \left( 2\mathbf{I} - \Theta^\beta \right) \mathbf{B} \right] e^{ikz}, \end{aligned} \quad (193)$$

$$\tau_{rz} = -r\Omega\rho\beta \left[ \mathbf{r}^\alpha \left( \frac{\omega^2}{k^2} \mathbf{I} - \Lambda^\alpha \right) \Theta^\alpha \mathbf{A} + \mathbf{r}^\beta \left( \frac{\omega^2}{k^2} - 2\Lambda^\beta \right) \Theta^\beta \mathbf{B} \right] e^{ikz}. \quad (194)$$

## VI.5 Dispersion relation for longitudinal mode for open-pore stress-free boundary condition

In this problem a cylinder of infinite length in the  $z$ -direction is assumed, for this reason no boundary conditions have to be imposed in the  $z$ -direction, otherwise the problem will be non-separable and intractable. It leads to continuous axial wavenumbers in the  $z$ -direction, instead of discrete as it should be for a finite length along the  $z$ -axis.

Using the radial stress-free boundary condition for the open-pore stress-free boundary condition (78), eqs (193) and (194) are rewritten as,

$$\begin{aligned} 0 = & \left\{ (\alpha - 2\beta) \mathbf{r}^\alpha \frac{\omega^2}{k^2} + 2\beta \mathbf{r}^\alpha \left( \frac{\omega^2}{k^2} \mathbf{I} - \Lambda^\alpha \right) \left( \mathbf{I} - \frac{1}{2} \Theta^\alpha \right) \right\} \mathbf{A} \\ & - 2\beta \mathbf{r}^\beta \Lambda^\beta \left( 2\mathbf{I} - \Theta^\beta \right) \mathbf{B}, \end{aligned} \quad (195)$$

$$0 = \beta \mathbf{r}^\alpha \left( \frac{\omega^2}{k^2} \mathbf{I} - \Lambda^\alpha \right) \Theta^\alpha \mathbf{A} + \beta \mathbf{r}^\beta \left( \frac{\omega^2}{k^2} - 2\Lambda^\beta \right) \Theta^\beta \mathbf{B}, \quad (196)$$

then adding eqs (195), (196), after some algebraic manipulation and using that  $\mathbf{r}^\alpha \Lambda^\alpha = \boldsymbol{\alpha} \mathbf{r}^\alpha$ , the following simplified equation is obtained

$$0 = \left( \boldsymbol{\alpha} \mathbf{r}^\alpha \frac{\omega^2}{k^2} - 2\beta \boldsymbol{\alpha} \mathbf{r}^\alpha \right) \mathbf{A} + \beta \mathbf{r}^\beta \left( \frac{\omega^2}{k^2} \Theta^\beta - 4\Lambda^\beta \right) \mathbf{B}. \quad (197)$$

The above equation is the resultant of the linear combinations of eqs (195)-(196), which is a simpler expression than eq (195). To simplify the computation of the extensional dispersion relation instead of using eq (195), eq (197) will be used.

Applying from the left hand side the operator  $\mathbf{I}^{\beta T}$  in eqs (196) and (197), then using that  $\mathbf{I}^{\beta T} \boldsymbol{\beta} = \Lambda^\beta \mathbf{I}^{\beta T}$  the following equations

$$0 = \Lambda^\beta \mathbf{I}^{\beta T} \mathbf{r}^\alpha \left( \frac{\omega^2}{k^2} \mathbf{I} - \Lambda^\alpha \right) \Theta^\alpha \mathbf{A} + \Lambda^\beta \left( \frac{\omega^2}{k^2} \mathbf{I} - 2\Lambda^\beta \right) \Theta^\beta \mathbf{B}, \quad (198)$$

$$0 = \left( \frac{\omega^2}{k^2} \mathbf{I} - 2\Lambda^\beta \right) \mathbf{I}^{\beta T} \mathbf{r}^\alpha \Lambda^\alpha \mathbf{A} + \Lambda^\beta \left( \frac{\omega^2}{k^2} \Theta^\beta - 4\Lambda^\beta \right) \mathbf{B},$$

are obtained. Then, applying from the left side of eqs (198) the operator  $(\Lambda^\beta)^{-1}$ , the following equations

$$0 = \mathbf{I}^{\beta T} \mathbf{r}^\alpha \left( \frac{\omega^2}{k^2} \mathbf{I} - \Lambda^\alpha \right) \Theta^\alpha \mathbf{A} + \left( \frac{\omega^2}{k^2} \mathbf{I} - 2\Lambda^\beta \right) \Theta^\beta \mathbf{B}, \quad (199)$$

$$0 = \left( \frac{\omega^2}{k^2} \mathbf{I} - 2\Lambda^\beta \right) (\Lambda^\beta)^{-1} \mathbf{I}^{\beta T} \mathbf{r}^\alpha \Lambda^\alpha \mathbf{A} + \left( \frac{\omega^2}{k^2} \Theta^\beta - 4\Lambda^\beta \right) \mathbf{B}, \quad (200)$$

are obtained.

In eqs (199) and (200) all the  $2 \times 2$  matrices are diagonal except the matrix  $\mathbf{I}^{\beta T} \mathbf{r}^\alpha$



which in terms of constituents properties is

$$\mathbf{l}^{\beta^T} \mathbf{r}^{\alpha} = \begin{pmatrix} \mathbf{l}^{\beta_I} \cdot \mathbf{r}^{\alpha_I} & \mathbf{l}^{\beta_I} \cdot \mathbf{r}^{\alpha_{II}} \\ \mathbf{l}^{\beta_{II}} \cdot \mathbf{r}^{\alpha_I} & \mathbf{l}^{\beta_{II}} \cdot \mathbf{r}^{\alpha_{II}} \end{pmatrix}, \quad (201)$$

where each component of the above matrix is expressed by

$$\begin{aligned} \mathbf{l}^{\beta_I} \cdot \mathbf{r}^{\alpha_I} &= N^{\beta_I} N^{\alpha_I} \left( 1 + \frac{\beta^{mi}}{\beta_I^2 - \beta^{ii}} \frac{\alpha_I^2 - \alpha^{mm}}{\alpha^{mi}} \right), \\ \mathbf{l}^{\beta_I} \cdot \mathbf{r}^{\alpha_{II}} &= N^{\beta_I} N^{\alpha_{II}} \left( \frac{\beta^{mi}}{\beta_I^2 - \beta^{ii}} + \frac{\alpha^{mi}}{\alpha_{II}^2 - \alpha^{mm}} \right), \\ \mathbf{l}^{\beta_{II}} \cdot \mathbf{r}^{\alpha_I} &= N^{\beta_{II}} N^{\alpha_I} \left( \frac{\beta_{II}^2 - \beta^{ii}}{\beta^{mi}} + \frac{\alpha_I^2 - \alpha^{mm}}{\alpha^{mi}} \right), \\ \mathbf{l}^{\beta_{II}} \cdot \mathbf{r}^{\alpha_{II}} &= N^{\beta_{II}} N^{\alpha_{II}} \left( 1 + \frac{\beta_{II}^2 - \beta^{ii}}{\beta^{mi}} \frac{\alpha^{mi}}{\alpha_{II}^2 - \alpha^{mm}} \right), \end{aligned} \quad (202)$$

and the normalization factors associated to  $\mathbf{r}^{\alpha}$  and  $\mathbf{l}^{\beta}$  matrices, eqs (178) and (179) respectively, are

$$\begin{aligned} N^{\alpha_I} &= \sqrt{\frac{\alpha_I^2 - \alpha^{ii}}{\alpha_I^2 - \alpha_{II}^2}}, \\ N^{\alpha_{II}} &= \sqrt{\frac{\alpha^{mm} - \alpha_{II}^2}{\alpha_I^2 - \alpha_{II}^2}}, \\ N^{\beta_I} &= \sqrt{\frac{\beta_I^2 - \beta^{ii}}{\beta_I^2 - \beta_{II}^2}}, \\ N^{\beta_{II}} &= \sqrt{\frac{\beta^{mm} - \beta_{II}^2}{\beta_I^2 - \beta_{II}^2}}. \end{aligned} \quad (203)$$

The elements of  $\mathbf{l}^{\beta^T} \mathbf{r}^{\alpha}$  matrix shows the interaction between P- and S- motions. That is, the interaction of fast-S and fast-P motion is represented by the element  $\mathbf{l}^{\beta_I} \cdot \mathbf{r}^{\alpha_I}$ . The slow-S and fast-P motion is given by  $\mathbf{l}^{\beta_{II}} \cdot \mathbf{r}^{\alpha_I}$ . The interaction of fast-S and slow-P motion is represented by  $\mathbf{l}^{\beta_I} \cdot \mathbf{r}^{\alpha_{II}}$  and the relationship of slow-S and slow-P waves are

shown by  $\mathbf{l}^{\beta_{\text{II}} \cdot \mathbf{r}^{\alpha_{\text{II}}}}$ .

Hence, a transparent manner to quantify the interaction of P- and S- motions are presented explicitly in the equations of longitudinal mode of vibration for open-pore stress-free boundary conditions.

Using eqs (177), (181), (190) and (201), the system formed by eqs (199) and (200) in a matrix form is written as

$$0 = \begin{pmatrix} (\mathbf{l}^{\beta_{\text{I}} \cdot \mathbf{r}^{\alpha_{\text{I}}}}) (V^2 - \alpha_{\text{I}}^2) \Theta_{\alpha_{\text{I}}} & (\mathbf{l}^{\beta_{\text{I}} \cdot \mathbf{r}^{\alpha_{\text{II}}}}) (V^2 - \alpha_{\text{II}}^2) \Theta_{\alpha_{\text{II}}} \\ (\mathbf{l}^{\beta_{\text{II}} \cdot \mathbf{r}^{\alpha_{\text{I}}}}) (V^2 - \alpha_{\text{I}}^2) \Theta_{\alpha_{\text{I}}} & (\mathbf{l}^{\beta_{\text{II}} \cdot \mathbf{r}^{\alpha_{\text{II}}}}) (V^2 - \alpha_{\text{II}}^2) \Theta_{\alpha_{\text{II}}} \\ (\mathbf{l}^{\beta_{\text{I}} \cdot \mathbf{r}^{\alpha_{\text{I}}}}) (V^2 - 2\beta_{\text{I}}^2) \frac{\alpha_{\text{I}}^2}{\beta_{\text{I}}^2} & (\mathbf{l}^{\beta_{\text{I}} \cdot \mathbf{r}^{\alpha_{\text{II}}}}) (V^2 - 2\beta_{\text{I}}^2) \frac{\alpha_{\text{II}}^2}{\beta_{\text{I}}^2} \\ (\mathbf{l}^{\beta_{\text{II}} \cdot \mathbf{r}^{\alpha_{\text{I}}}}) (V^2 - 2\beta_{\text{II}}^2) \frac{\alpha_{\text{I}}^2}{\beta_{\text{II}}^2} & (\mathbf{l}^{\beta_{\text{II}} \cdot \mathbf{r}^{\alpha_{\text{II}}}}) (V^2 - 2\beta_{\text{II}}^2) \frac{\alpha_{\text{II}}^2}{\beta_{\text{II}}^2} \\ (V^2 - 2\beta_{\text{I}}^2) \Theta_{\beta_{\text{I}}} & 0 \\ 0 & (V^2 - 2\beta_{\text{II}}^2) \Theta_{\beta_{\text{II}}} \\ (V^2 \Theta_{\beta_{\text{I}}} - 4\beta_{\text{I}}^2) & 0 \\ 0 & (V^2 \Theta_{\beta_{\text{II}}} - 4\beta_{\text{II}}^2) \end{pmatrix} \begin{pmatrix} A_{\text{I}} \\ A_{\text{II}} \\ B_{\text{I}} \\ B_{\text{II}} \end{pmatrix}, \quad (204)$$

where the complex velocity is defined as

$$V = \frac{\omega}{k}, \quad (205)$$

and the  $\Theta^\alpha$  and  $\Theta^\beta$  matrices are rewritten as

$$\Theta^\alpha = \begin{pmatrix} \Theta_{\alpha\text{I}} & 0 \\ 0 & \Theta_{\alpha\text{II}} \end{pmatrix}, \quad (206)$$

$$\Theta^\beta = \begin{pmatrix} \Theta_{\beta\text{I}} & 0 \\ 0 & \Theta_{\beta\text{II}} \end{pmatrix},$$

to simplify the notation.

Interchanging the second and third rows, and then the second and third columns, this system is rearranged as

$$0 = \begin{pmatrix} (\mathbf{l}^{\beta\text{I}} \cdot \mathbf{r}^{\alpha\text{I}}) (V^2 - \alpha_{\text{I}}^2) \Theta_{\alpha\text{I}} & (V^2 - 2\beta_{\text{I}}^2) \Theta_{\beta\text{I}} \\ (\mathbf{l}^{\beta\text{I}} \cdot \mathbf{r}^{\alpha\text{I}}) (V^2 - 2\beta_{\text{I}}^2) \frac{\alpha_{\text{I}}^2}{\beta_{\text{I}}^2} & (V^2 \Theta_{\beta\text{I}} - 4\beta_{\text{I}}^2) \\ (\mathbf{l}^{\beta\text{II}} \cdot \mathbf{r}^{\alpha\text{I}}) (V^2 - \alpha_{\text{I}}^2) \Theta_{\alpha\text{I}} & 0 \\ (\mathbf{l}^{\beta\text{II}} \cdot \mathbf{r}^{\alpha\text{I}}) (V^2 - 2\beta_{\text{II}}^2) \frac{\alpha_{\text{I}}^2}{\beta_{\text{II}}^2} & 0 \end{pmatrix} \quad (207)$$

$$\begin{pmatrix} (\mathbf{l}^{\beta_I} \cdot \mathbf{r}^{\alpha_{II}}) (V^2 - \alpha_{II}^2) \Theta_{\alpha_{II}} & 0 \\ (\mathbf{l}^{\beta_I} \cdot \mathbf{r}^{\alpha_{II}}) (V^2 - 2\beta_I^2) \frac{\alpha_{II}^2}{\beta_I^2} & 0 \\ (\mathbf{l}^{\beta_{II}} \cdot \mathbf{r}^{\alpha_{II}}) (V^2 - \alpha_{II}^2) \Theta_{\alpha_{II}} & (V^2 - 2\beta_{II}^2) \Theta_{\beta_{II}} \\ (\mathbf{l}^{\beta_{II}} \cdot \mathbf{r}^{\alpha_{II}}) (V^2 - 2\beta_{II}^2) \frac{\alpha_{II}^2}{\beta_{II}^2} & (V^2 \Theta_{\beta_{II}} - 4\beta_{II}^2) \end{pmatrix} \begin{pmatrix} A_I \\ B_I \\ A_{II} \\ B_{II} \end{pmatrix}.$$

In compact notation, system (207) is

$$0 = \begin{pmatrix} \mathbf{D}_{11} & \mathbf{D}_{12} \\ \mathbf{D}_{21} & \mathbf{D}_{22} \end{pmatrix} \begin{pmatrix} \mathbf{C}_1 \\ \mathbf{C}_2 \end{pmatrix}, \quad (208)$$

where the  $2 \times 2$   $\mathbf{D}$ 's matrices and the two-component  $\mathbf{C}$ 's vectors are expressed as

$$\begin{aligned} \mathbf{D}_{11} &= \begin{pmatrix} (\mathbf{l}^{\beta_I} \cdot \mathbf{r}^{\alpha_{I1}}) (V^2 - \alpha_{I1}^2) \Theta_{\alpha_{I1}} & (V^2 - 2\beta_{I1}^2) \Theta_{\beta_{I1}} \\ (\mathbf{l}^{\beta_I} \cdot \mathbf{r}^{\alpha_{I1}}) (V^2 - 2\beta_{I1}^2) \frac{\alpha_{I1}^2}{\beta_{I1}^2} & (V^2 \Theta_{\beta_{I1}} - 4\beta_{I1}^2) \end{pmatrix}, \\ \mathbf{D}_{12} &= \begin{pmatrix} (\mathbf{l}^{\beta_I} \cdot \mathbf{r}^{\alpha_{II}}) (V^2 - \alpha_{II}^2) \Theta_{\alpha_{II}} & 0 \\ (\mathbf{l}^{\beta_I} \cdot \mathbf{r}^{\alpha_{II}}) (V^2 - 2\beta_I^2) \frac{\alpha_{II}^2}{\beta_I^2} & 0 \end{pmatrix}, \\ \mathbf{D}_{21} &= \begin{pmatrix} (\mathbf{l}^{\beta_{II}} \cdot \mathbf{r}^{\alpha_{I1}}) (V^2 - \alpha_{I1}^2) \Theta_{\alpha_{I1}} & 0 \\ (\mathbf{l}^{\beta_{II}} \cdot \mathbf{r}^{\alpha_{I1}}) (V^2 - 2\beta_{II}^2) \frac{\alpha_{I1}^2}{\beta_{II}^2} & 0 \end{pmatrix}, \end{aligned} \quad (209)$$

$$\begin{aligned}
\mathbf{D}_{22} &= \begin{pmatrix} (\mathbf{l}^{\beta_{\text{II}}} \cdot \mathbf{r}^{\alpha_{\text{II}}}) (V^2 - \alpha_{\text{II}}^2) \Theta_{\alpha_{\text{II}}} & (V^2 - 2\beta_{\text{II}}^2) \Theta_{\beta_{\text{II}}} \\ (\mathbf{l}^{\beta_{\text{II}}} \cdot \mathbf{r}^{\alpha_{\text{II}}}) (V^2 - 2\beta_{\text{II}}^2) \frac{\alpha_{\text{II}}^2}{\beta_{\text{II}}^2} & (V^2 \Theta_{\beta_{\text{II}}} - 4\beta_{\text{II}}^2) \end{pmatrix}, \\
\mathbf{C}_1 &= \begin{pmatrix} A_{\text{I}} \\ B_{\text{I}} \end{pmatrix}, \\
\mathbf{C}_2 &= \begin{pmatrix} A_{\text{II}} \\ B_{\text{II}} \end{pmatrix}.
\end{aligned}$$

Eq (208) has no trivial solution if its determinant is zero, that is,

$$0 = \begin{vmatrix} \mathbf{D}_{11} & \mathbf{D}_{12} \\ \mathbf{D}_{21} & \mathbf{D}_{22} \end{vmatrix}. \quad (210)$$

The  $2 \times 2$  matrices  $\mathbf{D}_{11}$  and  $\mathbf{D}_{22}$  are full matrices whereas  $\mathbf{D}_{12}$  and  $\mathbf{D}_{21}$  has elements different to zero only in the first column, hence the above determinant has the following form

$$\begin{aligned}
0 &= \text{Det}(\mathbf{D}_{11}) \text{Det}(\mathbf{D}_{22}) \\
&- [\text{Tr}(\mathbf{D}_{11}\mathbf{D}_{12}) - \text{Tr}(\mathbf{D}_{11}) \text{Tr}(\mathbf{D}_{12})] [\text{Tr}(\mathbf{D}_{22}\mathbf{D}_{21}) - \text{Tr}(\mathbf{D}_{22}) \text{Tr}(\mathbf{D}_{21})].
\end{aligned} \quad (211)$$

Hereafter,  $\text{Det}()$  and  $\text{Tr}()$  represent the determinant and trace of the matrix inside the braces. After introducing the following notation

$$\begin{aligned}
P_1 &= \text{Det}(\mathbf{D}_{11}), \\
P_2 &= \text{Det}(\mathbf{D}_{22}), \\
P_3 &= \text{Tr}(\mathbf{D}_{11}\mathbf{D}_{12}) - \text{Tr}\mathbf{D}_{11}\text{Tr}\mathbf{D}_{12}, \\
P_4 &= \text{Tr}(\mathbf{D}_{22}\mathbf{D}_{21}) - \text{Tr}\mathbf{D}_{22}\text{Tr}\mathbf{D}_{21},
\end{aligned} \quad (212)$$

the dispersion relation for longitudinal mode for open-pore stress-free boundary condition is given by

$$P_1 P_2 - P_3 P_4 = 0. \quad (213)$$

Making the algebraic operations in eqs (212) the above P polynomials are expressed in terms of complex velocity squared,  $V^2$ , as

$$\begin{aligned} P_1 &= (\mathbf{l}^{\beta_I} \cdot \mathbf{r}^{\alpha_I}) \left\{ (V^2 - \alpha_I^2) (V^2 \Theta_{\beta_I} - 4\beta_I^2) \Theta_{\alpha_I} - (V^2 - 2\beta_I^2)^2 \frac{\alpha_I^2}{\beta_I^2} \Theta_{\beta_I} \right\}, \\ P_2 &= (\mathbf{l}^{\beta_{II}} \cdot \mathbf{r}^{\alpha_{II}}) \left\{ (V^2 - \alpha_{II}^2) (V^2 \Theta_{\beta_{II}} - 4\beta_{II}^2) \Theta_{\alpha_{II}} - (V^2 - 2\beta_{II}^2)^2 \frac{\alpha_{II}^2}{\beta_{II}^2} \Theta_{\beta_{II}} \right\}, \\ P_3 &= (\mathbf{l}^{\beta_I} \cdot \mathbf{r}^{\alpha_{II}}) \left\{ (V^2 - 2\beta_I^2)^2 \frac{\alpha_{II}^2}{\beta_I^2} \Theta_{\beta_I} - (V^2 - \alpha_{II}^2) (V^2 \Theta_{\beta_I} - 4\beta_I^2) \Theta_{\alpha_{II}} \right\}, \\ P_4 &= (\mathbf{l}^{\beta_{II}} \cdot \mathbf{r}^{\alpha_I}) \left\{ (V^2 - 2\beta_{II}^2)^2 \frac{\alpha_I^2}{\beta_{II}^2} \Theta_{\beta_{II}} - (V^2 - \alpha_I^2) (V^2 \Theta_{\beta_{II}} - 4\beta_{II}^2) \Theta_{\alpha_I} \right\}. \end{aligned} \quad (214)$$

Rearranging the terms as a quadratic polynomial in  $V^2$ , they are

$$\begin{aligned} P_1 &= -\frac{(\mathbf{l}^{\beta_I} \cdot \mathbf{r}^{\alpha_I})}{\beta_I^2} \left[ (\alpha_I^2 - \beta_I^2 \Theta_{\alpha_I}) \Theta_{\beta_I} V^4 - \beta_I^2 \left\{ \alpha_I^2 (4 - \Theta_{\alpha_I}) \Theta_{\beta_I} - 4\beta_I^2 \Theta_{\alpha_I} \right\} V^2 \right. \\ &\quad \left. + 4\alpha_I^2 \beta_I^2 \beta_I^2 (\Theta_{\beta_I} - \Theta_{\alpha_I}) \right], \\ P_2 &= -\frac{(\mathbf{l}^{\beta_{II}} \cdot \mathbf{r}^{\alpha_{II}})}{\beta_{II}^2} \left[ (\alpha_{II}^2 - \beta_{II}^2 \Theta_{\alpha_{II}}) \Theta_{\beta_{II}} V^4 - \beta_{II}^2 \left\{ \alpha_{II}^2 (4 - \Theta_{\alpha_{II}}) \Theta_{\beta_{II}} - 4\beta_{II}^2 \Theta_{\alpha_{II}} \right\} V^2 \right. \\ &\quad \left. + 4\alpha_{II}^2 \beta_{II}^2 \beta_{II}^2 (\Theta_{\beta_{II}} - \Theta_{\alpha_{II}}) \right], \\ P_3 &= \frac{(\mathbf{l}^{\beta_I} \cdot \mathbf{r}^{\alpha_{II}})}{\beta_I^2} \left[ (\alpha_{II}^2 - \beta_I^2 \Theta_{\alpha_{II}}) \Theta_{\beta_I} V^4 - \beta_I^2 \left\{ \alpha_{II}^2 (4 - \Theta_{\alpha_{II}}) \Theta_{\beta_I} - 4\beta_I^2 \Theta_{\alpha_{II}} \right\} V^2 \right. \\ &\quad \left. + 4\alpha_{II}^2 \beta_I^2 \beta_I^2 (\Theta_{\beta_I} - \Theta_{\alpha_{II}}) \right], \\ P_4 &= \frac{(\mathbf{l}^{\beta_{II}} \cdot \mathbf{r}^{\alpha_I})}{\beta_{II}^2} \left[ (\alpha_I^2 - \beta_{II}^2 \Theta_{\alpha_I}) \Theta_{\beta_{II}} V^4 - \beta_{II}^2 \left\{ \alpha_I^2 (4 - \Theta_{\alpha_I}) \Theta_{\beta_{II}} - 4\beta_{II}^2 \Theta_{\alpha_I} \right\} V^2 \right. \end{aligned} \quad (215)$$

$$+ 4\alpha_I^2 \beta_{II}^2 \beta_{II}^2 (\Theta_{\beta_{II}} - \Theta_{\alpha_I})].$$

Eq (213) is the dispersion relation for longitudinal mode of vibration for a fully-saturated, isotropic, homogeneous porous cylinder which is a transcendental equation due to the  $\Theta$  functions.

## VI.6 The $\Theta$ function

The  $\Theta(x)$  function is expressed in terms of Bessel functions of the first kind (Gardner, eq. 2.20) as

$$\Theta(x) = 2 \frac{J_1(x)}{xJ_0(x)}. \quad (216)$$

The series expansion of Bessel function of first kind for the zero<sup>th</sup> and first order (Selby, S. M. 1971, CRC standard mathematical tables, p. 518) are given by

$$J_0(x) = 1 - \left(\frac{x}{2}\right)^2 + \frac{1}{(2!)^2} \left(\frac{x}{2}\right)^4 - \frac{1}{(3!)^2} \left(\frac{x}{2}\right)^6 + \frac{1}{(4!)^2} \left(\frac{x}{2}\right)^8 - \dots, \quad (217)$$

$$J_1(x) = \left(\frac{x}{2}\right) \left[1 - \frac{1}{1!2!} \left(\frac{x}{2}\right)^2 + \frac{1}{2!3!} \left(\frac{x}{2}\right)^4 - \frac{1}{3!4!} \left(\frac{x}{2}\right)^6 + \dots\right], \quad (218)$$

where  $q!$  is the factorial of the quantity  $q$ . Therefore, by substituting eqs (217) and (218) into the  $\Theta$ 's expression (eq 216) is rewritten as

$$\begin{aligned} \Theta(x) &= \frac{2 \left(\frac{x}{2}\right) \left[1 - \frac{1}{1!2!} \left(\frac{x}{2}\right)^2 + \frac{1}{2!3!} \left(\frac{x}{2}\right)^4 - \dots\right]}{x \left[1 - \left(\frac{x}{2}\right)^2 + \frac{1}{(2!)^2} \left(\frac{x}{2}\right)^4 - \dots\right]} \quad (219) \\ &= \left[1 - \frac{1}{1!2!} \left(\frac{x}{2}\right)^2 + \frac{1}{2!3!} \left(\frac{x}{2}\right)^4 - \dots\right] \left[1 - \left(\frac{x}{2}\right)^2 + \frac{1}{(2!)^2} \left(\frac{x}{2}\right)^4 - \dots\right]^{-1}. \end{aligned}$$

The binomial expansion as set forth in the CRC standard mathematical tables, p. 454, is used to rewrite the  $\Theta(x)$  function as a series in  $x$  as

$$\begin{aligned}\Theta(x) &= \left[1 - \frac{1}{1!2!} \left(\frac{x}{2}\right) + \frac{1}{2!3!} \left(\frac{x}{2}\right)^4 - \dots\right] \left[1 + \left(\frac{x}{2}\right)^2 - \frac{1}{(2!)^2} \left(\frac{x}{2}\right)^4 + \dots\right] \\ &= 1 + \frac{1}{8}x^2 - \frac{1}{24}x^4 + \dots\end{aligned}\quad (220)$$

Using eq (220) in the dispersion relation for longitudinal vibrations, eq (213), it is clear that this is a complicated transcendental function and it is not possible to obtain its analytical solutions. This results in the material properties dependence not being transparent. Hence, only the extensional mode of vibration which is a special case of longitudinal oscillation is to be under consideration. In this manner the dispersion relation (213) is reduced to an algebraic polynomial.

## VI.7 Simplification of $\Theta$ 's functions

The  $\Theta$  function associated to the fast P-wave velocity has the argument  $aq_{\alpha_1}$  which can be rewritten in terms of the complex longitudinal velocity squared,  $V^2$ , as

$$aq_{\alpha_1} = a\sqrt{\frac{\omega^2}{\alpha_1^2} - k^2} = a\sqrt{\omega^2 \left(\frac{1}{\alpha_1^2} - \frac{k^2}{\omega^2}\right)} = a\omega\sqrt{\frac{1}{\alpha_1^2} - \frac{1}{V^2}}. \quad (221)$$

The expression of  $q_{\alpha_1}^2$  was stated in eq (186). Substituting eq (221) into the series expansion of  $\Theta$  function, eq (220), and considering only the  $a^0$  through  $a^3$  terms, the  $\Theta$  function associated to fast P-wave is approximated by

$$\Theta(aq_{\alpha_1}) \approx \left[1 - \frac{a^2\omega^2}{8} \left(\frac{1}{\alpha_1^2} - \frac{1}{V^2}\right)\right] \left[1 - \frac{a^2\omega^2}{4} \left(\frac{1}{\alpha_1^2} - \frac{1}{V^2}\right)\right]^{-1}. \quad (222)$$



For geomaterials the norm of  $\frac{a^2\omega^2}{4} \left( \frac{1}{\alpha_1^2} - \frac{1}{V^2} \right)$  is always less than one, i.e.  $\left\| \frac{a^2\omega^2}{4} \left( \frac{1}{\alpha_1^2} - \frac{1}{V^2} \right) \right\| \ll 1$ .

Thus the binomial expansion used to obtain that the  $\Theta(aq_{\alpha_1})$  could be approximated by one, that is

$$\Theta(aq_{\alpha_1}) \approx 1. \quad (223)$$

Analogously, the argument of the  $\Theta$  function associated to fast S-wave is rewritten as

$$aq_{\beta_1} = a\sqrt{\frac{\omega^2}{\beta_1^2} - k^2} = a\sqrt{\omega^2 \left( \frac{1}{\beta_1^2} - \frac{k^2}{\omega^2} \right)} = a\omega\sqrt{\frac{1}{\beta_1^2} - \frac{1}{V^2}}. \quad (224)$$

The expression of  $q_{\beta_1}^2$  was stated in eq (187). Considering only until the  $a^3$  term in the series expansion, eq (220), the  $\Theta(aq_{\beta_1})$  function is approximated by

$$\Theta(aq_{\beta_1}) \approx 1. \quad (225)$$

The argument of the  $\Theta$  function associated to the slow P-wave, (see eq 186), is

$$aq_{\alpha_{II}} = a\sqrt{\frac{\omega^2}{\alpha_{II}^2} \left( 1 - \frac{\alpha_{II}^2}{V^2} \right)}, \quad (226)$$

in which the norm of the slow P wave is always less than the norm of the complex longitudinal velocity, that means  $\left\| \frac{\alpha_{II}}{V} \right\| \ll 1$ , then using the binomial expansion in eq (226), the argument of the  $\Theta$  function associated to the slow P-wave is simplified as

$$aq_{\alpha_{II}} \approx \frac{a\omega}{\alpha_{II}}. \quad (227)$$

Thus, using the above equation in the series expansion expression for  $\Theta$  functions, (220), the series expansion of  $\Theta(aq_{\alpha_{\text{II}}})$  is given by

$$\Theta(aq_{\alpha_{\text{II}}}) \approx 1 + \frac{1}{8} \frac{a^2 \omega^2}{\alpha_{\text{II}}^2} + \dots, \quad (228)$$

analogously, the argument of the  $\Theta$  function associated to the slow S-wave, (see eq 187), is given by

$$aq_{\beta_{\text{II}}} = a \sqrt{\frac{\omega^2}{\beta_{\text{II}}^2} \left(1 - \frac{\beta_{\text{II}}^2}{V^2}\right)} \approx \frac{a\omega}{\beta_{\text{II}}}, \quad (229)$$

and the series expansion of  $\Theta(aq_{\beta_{\text{II}}})$  is approximated as

$$\Theta(aq_{\beta_{\text{II}}}) \approx 1 + \frac{1}{8} \frac{a^2 \omega^2}{\beta_{\text{II}}^2} + \dots \quad (230)$$

Thus, the  $\Theta_{\alpha_{\text{II}}}$  and  $\Theta_{\beta_{\text{II}}}$  functions are independent of  $V^2$ .

## VI.8 The dispersion relation for extensional mode for open-pore stress-free boundary condition

For the extensional mode of vibration the four  $\Theta$  functions (eqs 223, 225, 228 and 230) are independent of the complex velocity squared,  $V$ , thus the P polynomials, eqs (214), can be rewritten in the extensional limit as

$$\begin{aligned} P_1 &= -\frac{(\mathbf{l}^{\beta_{\text{I}}} \cdot \mathbf{r}^{\alpha_{\text{I}}})}{\beta_{\text{I}}^2} (\alpha_{\text{I}}^2 - \beta_{\text{I}}^2) (V^2 - h_1) (V^2 - h_2), \\ P_2 &= -\frac{(\mathbf{l}^{\beta_{\text{II}}} \cdot \mathbf{r}^{\alpha_{\text{II}}})}{\beta_{\text{II}}^2} (\alpha_{\text{II}}^2 - \beta_{\text{II}}^2 \Theta_{\alpha_{\text{II}}}) \Theta_{\beta_{\text{II}}} (V^2 - h_3) (V^2 - h_4), \end{aligned} \quad (231)$$

$$P_3 = \frac{(\mathbf{l}^{\beta_I} \cdot \mathbf{r}^{\alpha_{II}})}{\beta_I^2} (\alpha_{II}^2 - \beta_I^2 \Theta_{\alpha_{II}}) (V^2 - h_5) (V^2 - h_6),$$

$$P_4 = \frac{(\mathbf{l}^{\beta_{II}} \cdot \mathbf{r}^{\alpha_I})}{\beta_{II}^2} (\alpha_I^2 - \beta_{II}^2) \Theta_{\beta_{II}} (V^2 - h_7) (V^2 - h_8),$$

where the h-coefficients are expressed in terms of fast- and slow- P and S velocities squared as

$$h_1 = \frac{\beta_I^2 (4\beta_I^2 - 3\alpha_I^2)}{(\beta_I^2 - \alpha_I^2)}, \quad (232)$$

$$h_2 = 0, \quad (233)$$

$$h_3 = \frac{1}{2} \left[ \frac{\beta_{II}^2 \{ \alpha_{II}^2 (4 - \Theta_{\alpha_{II}}) \Theta_{\beta_{II}} - 4\beta_{II}^2 \Theta_{\alpha_{II}} \}}{(\alpha_{II}^2 - \beta_{II}^2 \Theta_{\alpha_{II}}) \Theta_{\beta_{II}}} \right. \\ \left. + \left\{ \left( \frac{\beta_{II}^2 \{ \alpha_{II}^2 (4 - \Theta_{\alpha_{II}}) \Theta_{\beta_{II}} - 4\beta_{II}^2 \Theta_{\alpha_{II}} \}}{(\alpha_{II}^2 - \beta_{II}^2 \Theta_{\alpha_{II}}) \Theta_{\beta_{II}}} \right)^2 - 16 \frac{\alpha_{II}^2 \beta_{II}^2 \beta_{II}^2 (\Theta_{\beta_{II}} - \Theta_{\alpha_{II}})}{(\alpha_{II}^2 - \beta_{II}^2 \Theta_{\alpha_{II}}) \Theta_{\beta_{II}}} \right\}^{1/2} \right], \quad (234)$$

$$h_4 = \frac{1}{2} \left[ \frac{\beta_{II}^2 \{ \alpha_{II}^2 (4 - \Theta_{\alpha_{II}}) \Theta_{\beta_{II}} - 4\beta_{II}^2 \Theta_{\alpha_{II}} \}}{(\alpha_{II}^2 - \beta_{II}^2 \Theta_{\alpha_{II}}) \Theta_{\beta_{II}}} \right. \\ \left. - \left\{ \left( \frac{\beta_{II}^2 \{ \alpha_{II}^2 (4 - \Theta_{\alpha_{II}}) \Theta_{\beta_{II}} - 4\beta_{II}^2 \Theta_{\alpha_{II}} \}}{(\alpha_{II}^2 - \beta_{II}^2 \Theta_{\alpha_{II}}) \Theta_{\beta_{II}}} \right)^2 - 16 \frac{\alpha_{II}^2 \beta_{II}^2 \beta_{II}^2 (\Theta_{\beta_{II}} - \Theta_{\alpha_{II}})}{(\alpha_{II}^2 - \beta_{II}^2 \Theta_{\alpha_{II}}) \Theta_{\beta_{II}}} \right\}^{1/2} \right], \quad (235)$$

$$h_5 = \frac{1}{2} \left[ \frac{\beta_I^2 \{ \alpha_{II}^2 (4 - \Theta_{\alpha_{II}}) - 4\beta_I^2 \Theta_{\alpha_{II}} \}}{(\alpha_{II}^2 - \beta_I^2 \Theta_{\alpha_{II}})} \right. \\ \left. + \left\{ \left( \frac{\beta_I^2 \{ \alpha_{II}^2 (4 - \Theta_{\alpha_{II}}) - 4\beta_I^2 \Theta_{\alpha_{II}} \}}{(\alpha_{II}^2 - \beta_I^2 \Theta_{\alpha_{II}})} \right)^2 - 16 \frac{\alpha_{II}^2 \beta_I^2 \beta_I^2 (1 - \Theta_{\alpha_{II}})}{(\alpha_{II}^2 - \beta_I^2 \Theta_{\alpha_{II}})} \right\}^{1/2} \right], \quad (236)$$

$$h_6 = \frac{1}{2} \left[ \frac{\beta_I^2 \{ \alpha_{II}^2 (4 - \Theta_{\alpha_{II}}) - 4\beta_I^2 \Theta_{\alpha_{II}} \}}{(\alpha_{II}^2 - \beta_I^2 \Theta_{\alpha_{II}})} \right. \\ \left. - \left\{ \left( \frac{\beta_I^2 \{ \alpha_{II}^2 (4 - \Theta_{\alpha_{II}}) - 4\beta_I^2 \Theta_{\alpha_{II}} \}}{(\alpha_{II}^2 - \beta_I^2 \Theta_{\alpha_{II}})} \right)^2 - 16 \frac{\alpha_{II}^2 \beta_I^2 \beta_I^2 (1 - \Theta_{\alpha_{II}})}{(\alpha_{II}^2 - \beta_I^2 \Theta_{\alpha_{II}})} \right\}^{1/2} \right], \quad (237)$$

$$h_7 = \frac{1}{2} \left[ \frac{\beta_{II}^2 (3\alpha_I^2 \Theta_{\beta_{II}} - 4\beta_{II}^2)}{(\alpha_I^2 - \beta_{II}^2) \Theta_{\beta_{II}}} \right. \\ \left. + \left\{ \left( \frac{\beta_{II}^2 (3\alpha_I^2 \Theta_{\beta_{II}} - 4\beta_{II}^2)}{(\alpha_I^2 - \beta_{II}^2) \Theta_{\beta_{II}}} \right)^2 - 16 \frac{\alpha_I^2 \beta_{II}^2 \beta_{II}^2 (\Theta_{\beta_{II}} - 1)}{(\alpha_I^2 - \beta_{II}^2) \Theta_{\beta_{II}}} \right\}^{1/2} \right], \quad (238)$$

$$\begin{aligned}
h_8 &= \frac{1}{2} \left[ \frac{\beta_{\text{II}}^2 (3\alpha_{\text{I}}^2 \Theta_{\beta_{\text{II}}} - 4\beta_{\text{II}}^2)}{(\alpha_{\text{I}}^2 - \beta_{\text{II}}^2) \Theta_{\beta_{\text{II}}}} \right. \\
&\quad \left. - \left\{ \left( \frac{\beta_{\text{II}}^2 (3\alpha_{\text{I}}^2 \Theta_{\beta_{\text{II}}} - 4\beta_{\text{II}}^2)}{(\alpha_{\text{I}}^2 - \beta_{\text{II}}^2) \Theta_{\beta_{\text{II}}}} \right)^2 - 16 \frac{\alpha_{\text{I}}^2 \beta_{\text{II}}^2 \beta_{\text{II}}^2 (\Theta_{\beta_{\text{II}}} - 1)}{(\alpha_{\text{I}}^2 - \beta_{\text{II}}^2) \Theta_{\beta_{\text{II}}}} \right\}^{1/2} \right]. \tag{239}
\end{aligned}$$

By substituting expressions (231) into eq (213) and after algebraic manipulations, the dispersion relation for the open-pore stress-free boundary value problem for extensional mode of vibration for isotropic, homogeneous and fully-saturated porous circular cylinders simplifies to

$$\begin{aligned}
0 &= (V^2 - h_1) (V^2 - h_2) (V^2 - h_3) (V^2 - h_4) \\
&\quad - \gamma (V^2 - h_5) (V^2 - h_6) (V^2 - h_7) (V^2 - h_8), \tag{240}
\end{aligned}$$

where

$$\gamma = \frac{(\mathbf{l}^{\beta_{\text{I}}} \cdot \mathbf{r}^{\alpha_{\text{II}}}) (\mathbf{l}^{\beta_{\text{II}}} \cdot \mathbf{r}^{\alpha_{\text{I}}}) (\alpha_{\text{II}}^2 - \beta_{\text{I}}^2 \Theta_{\alpha_{\text{II}}}) (\alpha_{\text{I}}^2 - \beta_{\text{II}}^2)}{(\mathbf{l}^{\beta_{\text{I}}} \cdot \mathbf{r}^{\alpha_{\text{I}}}) (\mathbf{l}^{\beta_{\text{II}}} \cdot \mathbf{r}^{\alpha_{\text{II}}}) (\alpha_{\text{I}}^2 - \beta_{\text{I}}^2) (\alpha_{\text{II}}^2 - \beta_{\text{II}}^2 \Theta_{\alpha_{\text{II}}})}. \tag{241}$$

Eq (240) is a quartic equation in  $V^2$ , and as such it has four roots. To each of these four roots their correspond two complex velocities  $V$ , which have the same real parts and equal but opposite imaginary parts. To satisfy the radiation condition, i.e. the imaginary part of the complex velocity is negative, thus only four possible roots for  $V$  exist. Although it is possible to obtained the analytical roots by the standard procedure of solving a quartic equation, the dependence of these roots on material properties are not transparent in them. Instead to show the analytical roots of eq (240), which are complicated expressions, this equation is solved numerically to get some insight of the behavior of these roots for a wide range of frequency values, avoiding the complicated calculus of the analytical procedure.

## VI.9 Numerical solution

Eq (240) is a polynomial of the form  $a_0 + a_1V^2 + a_2V^4 + a_3V^6 + V^8 = 0$  which can be represented as  $Det(V^2\mathbf{I} - \mathbf{M}) = 0$  where  $\mathbf{M}$  is called the companion matrix which has the following form (Golub et. al, 1996 section 7.4.6)

$$\mathbf{M} = \begin{pmatrix} 0 & 0 & 0 & -a_0 \\ 1 & 0 & 0 & -a_1 \\ 0 & 1 & 0 & -a_2 \\ 0 & 0 & 1 & -a_3 \end{pmatrix}. \quad (242)$$

The eigenvalues of matrix (242) are then calculated and they are the roots of eq (240).

In order to get some insight, the numerical computations of the eigenvalues of the companion matrix associated to eq (240) are presented for a sample of Berea Sandstone for a wide range of frequency values. The physical properties used are listed in appendix B. In Figs. 17-20 they are plotted as blue curves the real part of  $V$ , in compact notation it is represented by  $\Re V$ . Instead of plotting the imaginary part of  $V$ , that is represented by  $\Im V$ , the ratio  $\frac{\Im V}{\Re V}$ , which defines the quality factor  $Q$  are plotted as red curves.

It is well known that the extensional-wave has its  $\Re V$  larger than the fast-S wave (black-solid curve) and smaller than the fast-P wave (purple-solid curve) obviously only the blue-solid curve in Fig. 17 satisfy this condition, so it is called the extensional phase velocity and its attenuation is expressed as the inverse of the quality factor  $Q$  (red-solid curve), also the inverse of  $Q$  for fast- S and P waves are presented as black-dashed and purple-dashed curves, respectively. Fig. 17 shows two attenuation peaks, one peaks appears in a lower frequency and a second peak is presented around the modified Biot

critical frequency, which is called Biot's attenuation peak (Gardner, 1962; White, 1986; Dunn, 1986) . If the medium was infinite only the Biot's peak appears, which is larger than the fast-P and smaller than the fast-S attenuation peaks, so an additional attenuation peak is presented due to the open-pore stress-free boundary effect.

In Fig. 18 the  $\Re V$  (blue-solid curve) shows an increasing linear trend with frequency. Its value is larger than the slow-S wave phase velocity value (black-solid curve) but as frequency increases it tends to approach equality to the slow-P wave phase velocity value (purple-solid curve). The attenuation (red-solid curve) shows a decreasing linear trend with frequency becoming equal to the value of the slow-P attenuation (purple-dashed curve). It can be thought as a diffusive extensional process.

In Fig. 19 the  $\Re V$  (blue-solid curve) shows an increasing linear trend with frequency. At the lower frequencies its value is almost similar to the slow-S wave phase velocity value (black-solid curve) but as frequency increases the difference increases but always is limited by the slow-P wave phase velocity value (purple-solid curve). The attenuation (blue-solid curve) shows a decreasing linear trend with frequency equal to the slow-S wave attenuation (black-dashed curve). It can be thought as a diffusive extensional process also.

In Fig. 20 an increasing linear trend with frequency in  $\Re V$  (blue-solid curve) and also in attenuation (blue-solid curve) is shown. It should be noted that for the low-frequency range there is negligible dissipation, however  $\Re V$  is not measurable. It should be noted that only for the high-frequency range this root becomes a diffusive process.

Clearly if a porous sample is set into extensional resonance, it is the curves shown

---

in Fig. 17 that represent this vibration. Hereafter this study will focus on the analysis of these curves. The plots in Fig. 17 are characterized by three crossover frequency values. Below  $\Omega$  there are two regimes defined by the first crossover frequency marked as A. In each of these two regimes the phase velocity increments in value, assumed to be by constant amounts. The increment is less in the regime that lies between A and  $\Omega$  compared to the regime that lies below A. The second crossover frequency, B, does not have any signature on the phase velocity plot. The attenuation plot shows segmented linear trends with frequency. Below the crossover frequency A, the trend is linearly increasing. At the crossover frequency A its trend, after forming a smooth crest, becomes linearly decreasing. This trend continues until the crossover frequency B at which it again becomes linearly increasing. At the crossover frequency  $\Omega$  its trend, after forming a smooth trough crest, becomes linearly decreasing.

For any given set of material-parameters, the numerical computations show their simple dependence on extensional phase velocity and attenuation. In the following section using physical arguments an approximate second order extensional dispersion relations are deduced which are nearly equal to the exact values of those obtained by the four order extensional dispersion relation (240). This approximate second order polynomial gives the first and second roots associated with the extensional mode of vibrations plotted in Figs. 17 and 18. This procedure renders the approximate expressions for the extensional phase velocity and attenuation such that the implicit relations with material properties become transparent.

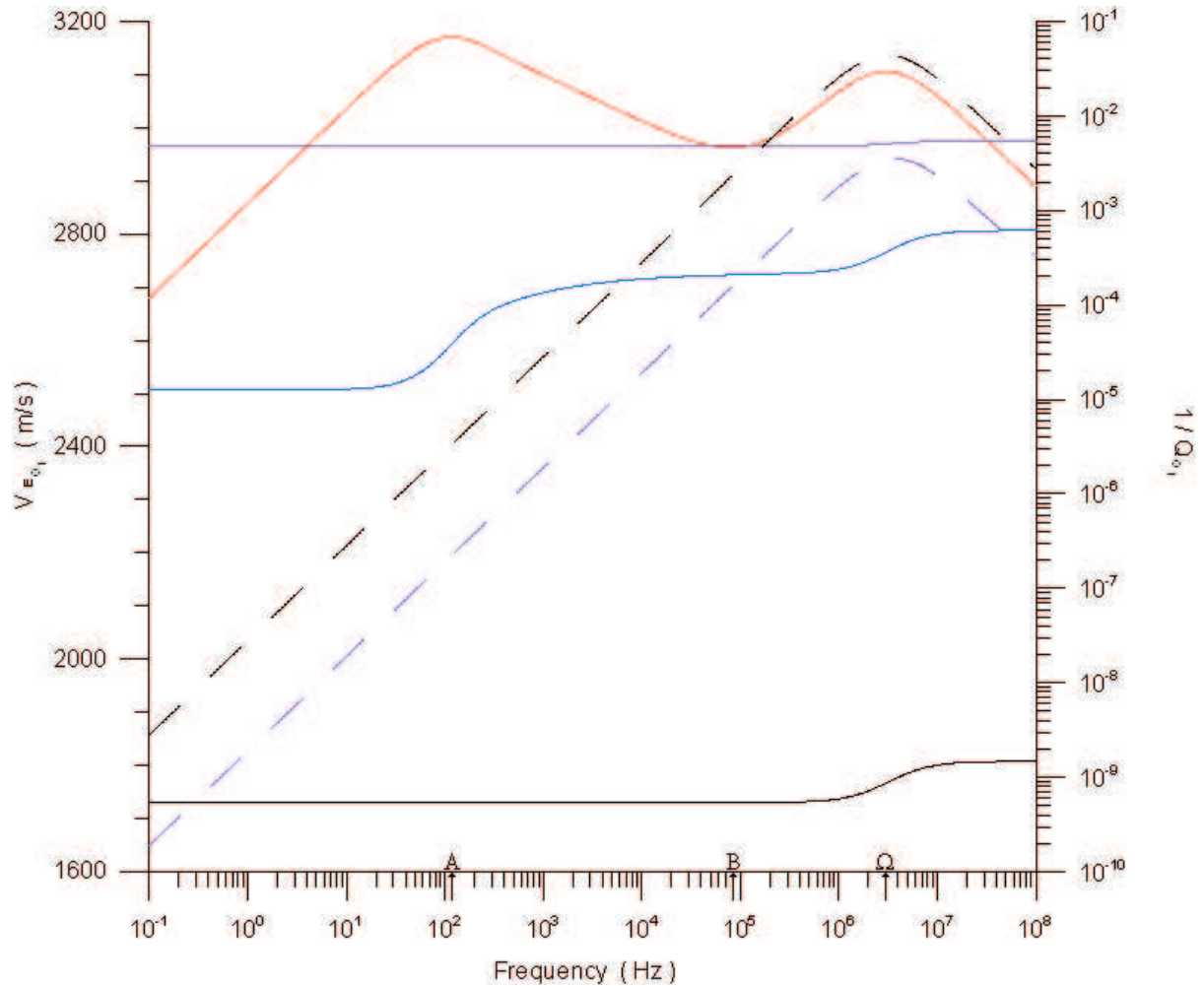


Figure 33. The plot of extensional phase velocity (blue-solid curve) and attenuation (red-solid curve) versus frequency; obtained from the first root of eq (240). The fast-P and fast-S waves phase velocity are presented as purple- and black- solid curves, respectively, and the fast-P and fast-S waves attenuation are shown by purple- and black-dashed curves, respectively. For clarity the crossover frequencies A and B (whose explicit representations are given later in section VI.10) and modified Biot critical frequency ( $\Omega$ ), are also marked.



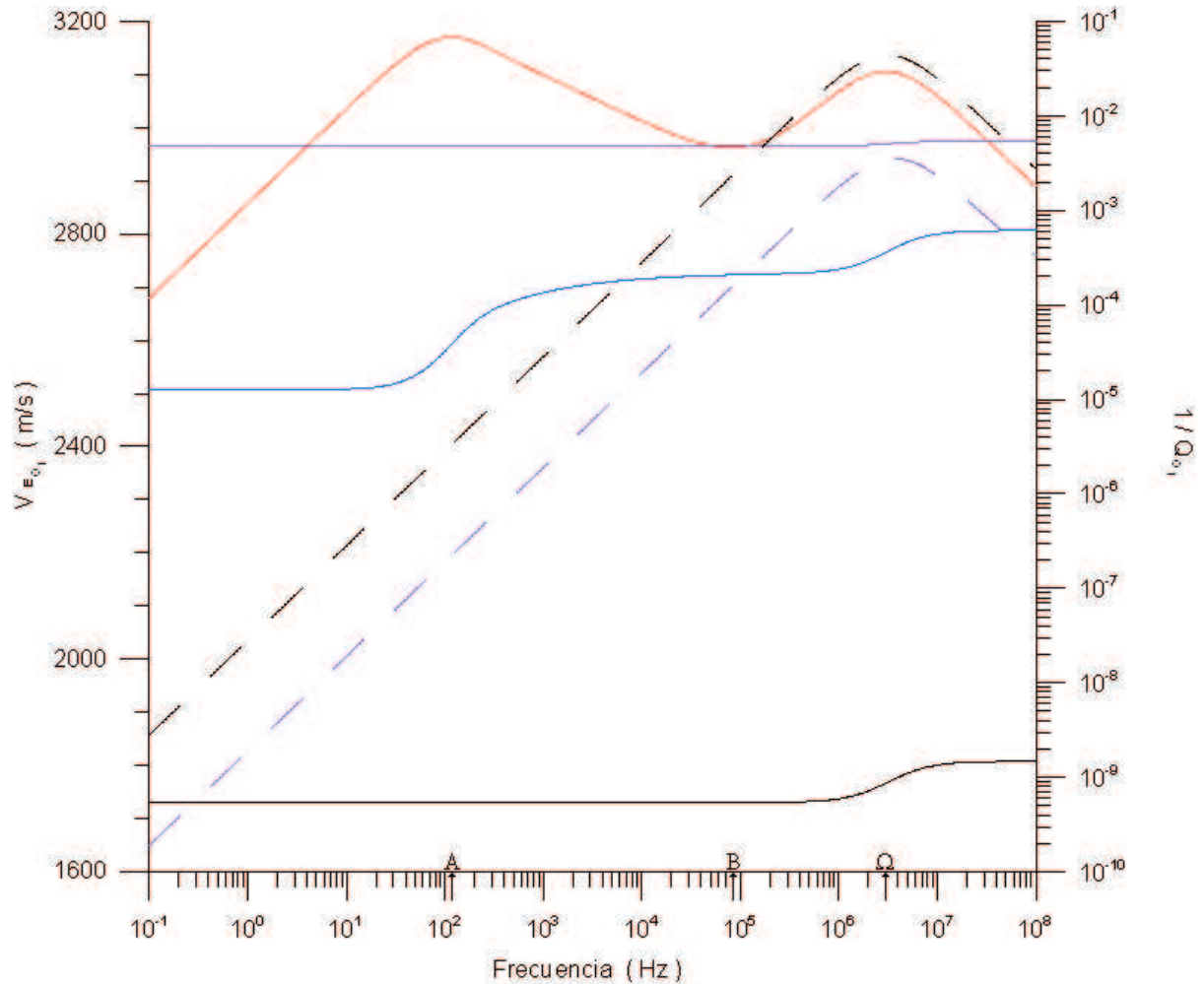


Figure 34. Gráfica de la velocidad de fase extensional (curva continua azul) y la atenuación (curva continua roja) contra la frecuencia; obtenidas a partir de la primera raíz de la ec (240). Las velocidades de fase de las ondas rápidas P y S se presentan en curvas continuas moradas y negras, respectivamente, y la atenuación de las ondas rápidas P y S se muestran en curvas punteadas moradas y negras, respectivamente. Por claridad también se muestran las frecuencias de frontera A y B (cuyas fórmulas están dadas en la sección VI.10) y la frecuencia crítica de Biot modificada ( $\Omega$ ).

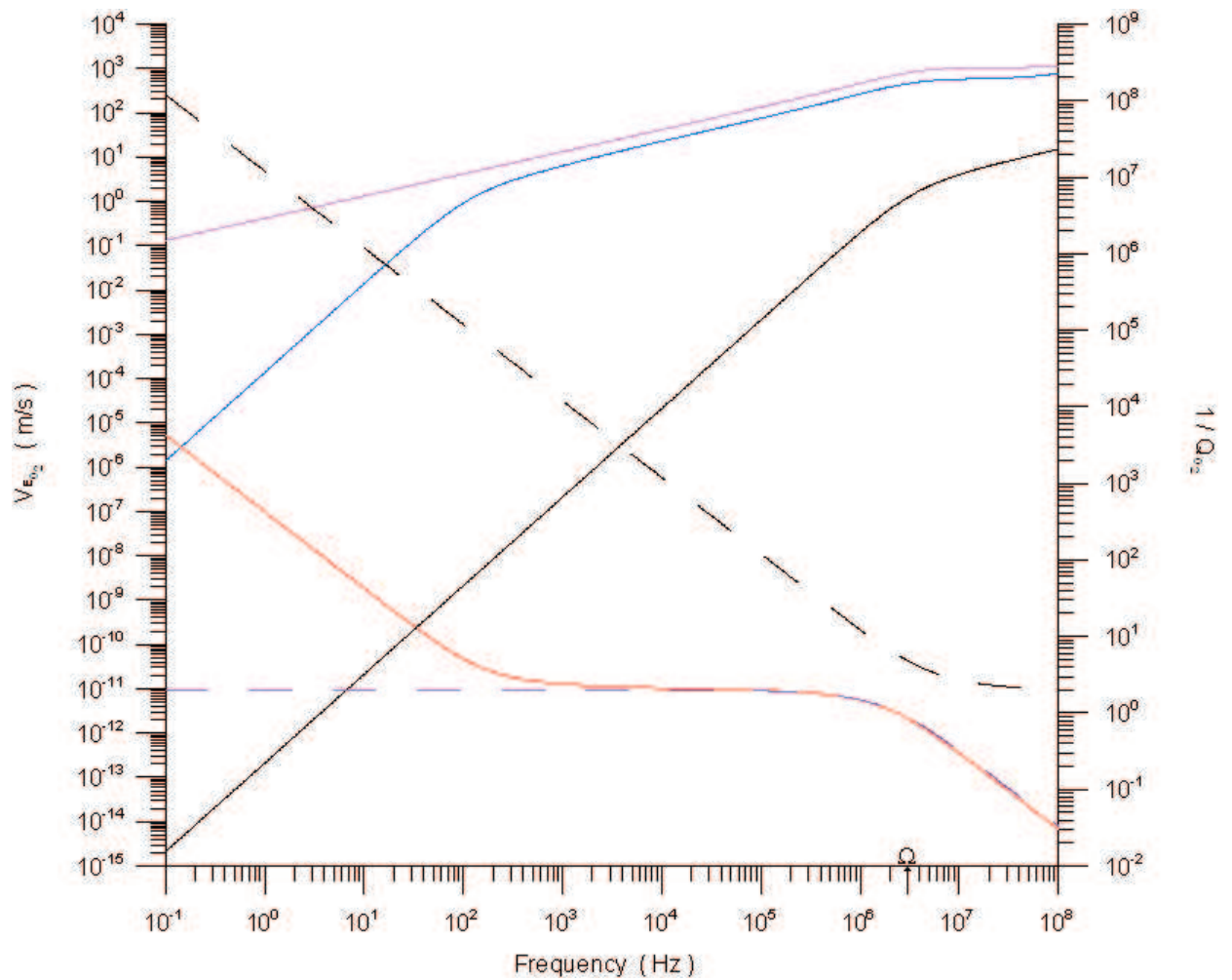


Figure 35. The blue-solid curve shows the real part of the second complex velocity of eq (240). The red-solid curve is the ratio of the imaginary to real part of this complex velocity. The slow-P and slow-S waves phase velocity are presented as purple- and black- solid curves, respectively, and the slow-P and slow-S wave attenuation are shown by purple- and black- dashed curves, respectively.

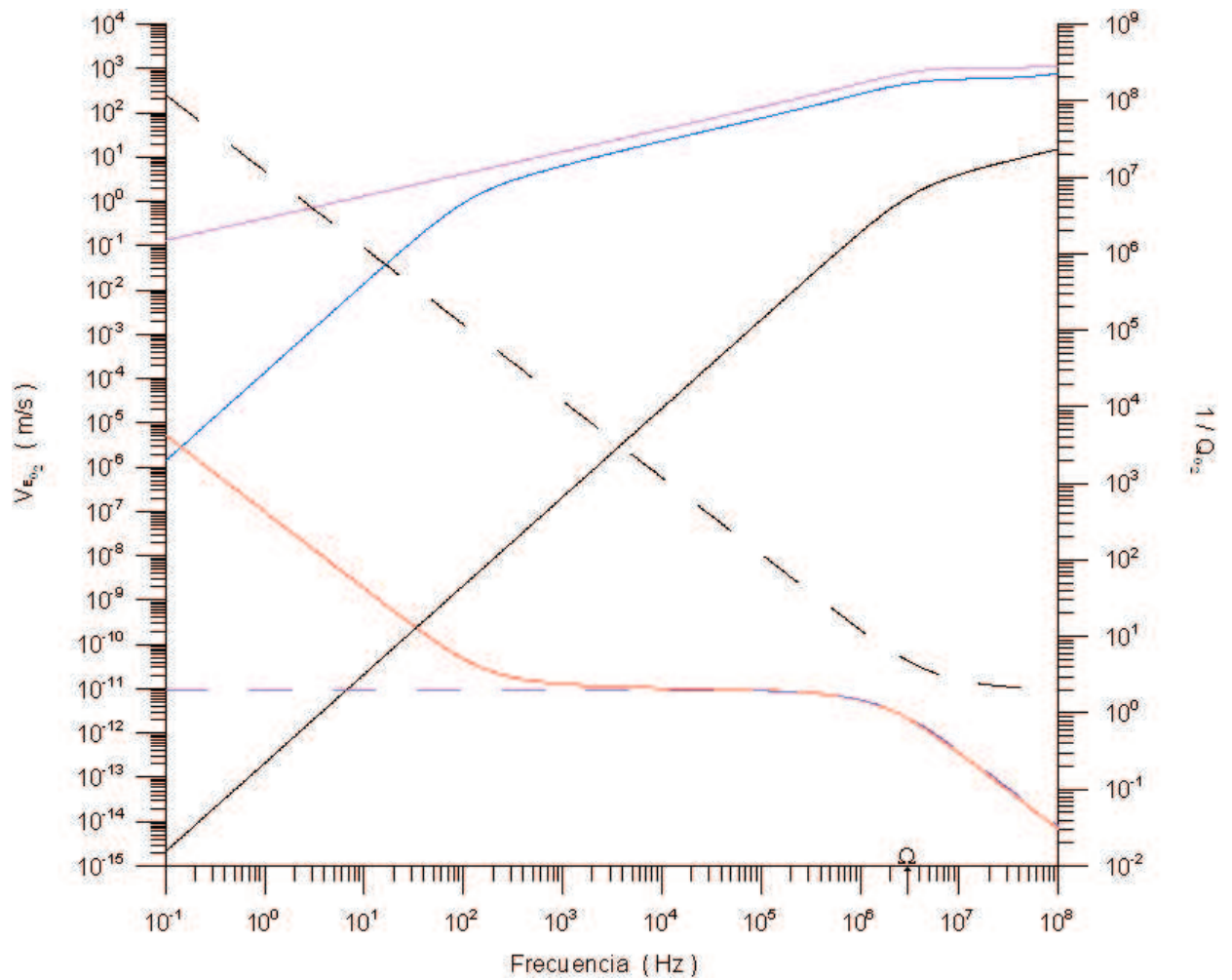


Figure 36. La curva continua azul representa la parte real de la segunda raíz de la velocidad dada en la ec (240). La curva continua roja representa la razón de la parte imaginaria y la real de dicha velocidad. La velocidad de fase de las ondas lentas P y S se muestran en curvas continuas morada y negra, respectivamente y la atenuación de las ondas lentas P y S se muestran en curvas punteadas moradas y negras, respectivamente.

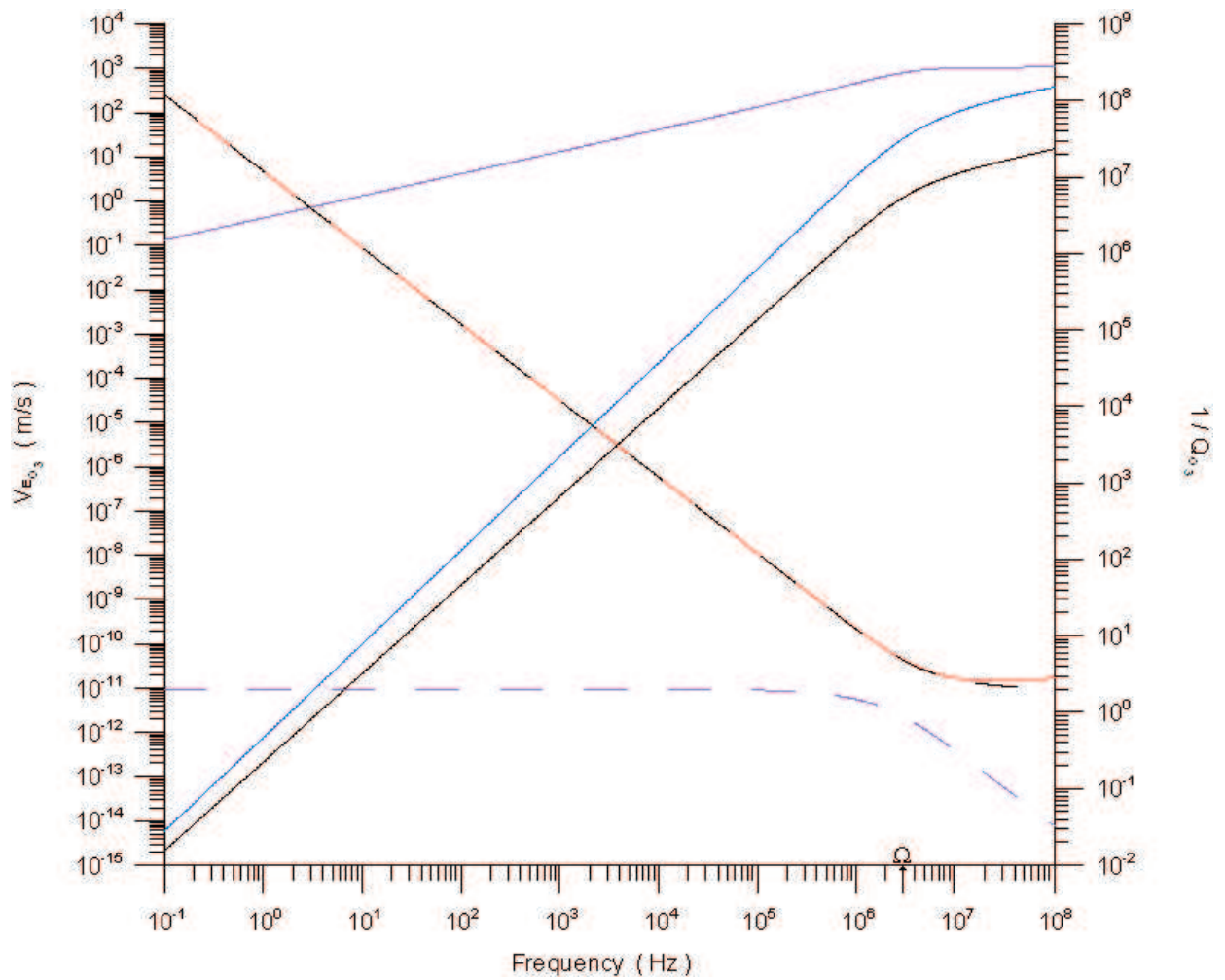


Figure 37. The blue curve shows the real part of the third complex velocity of eq (240). The red curve is the ratio of the imaginary to real part of this complex velocity. The slow-P and slow-S waves phase velocity are presented as purple- and black- solid curves, respectively, and the slow-P and slow-S wave attenuation are shown by purple- and black- dashed curves, respectively.

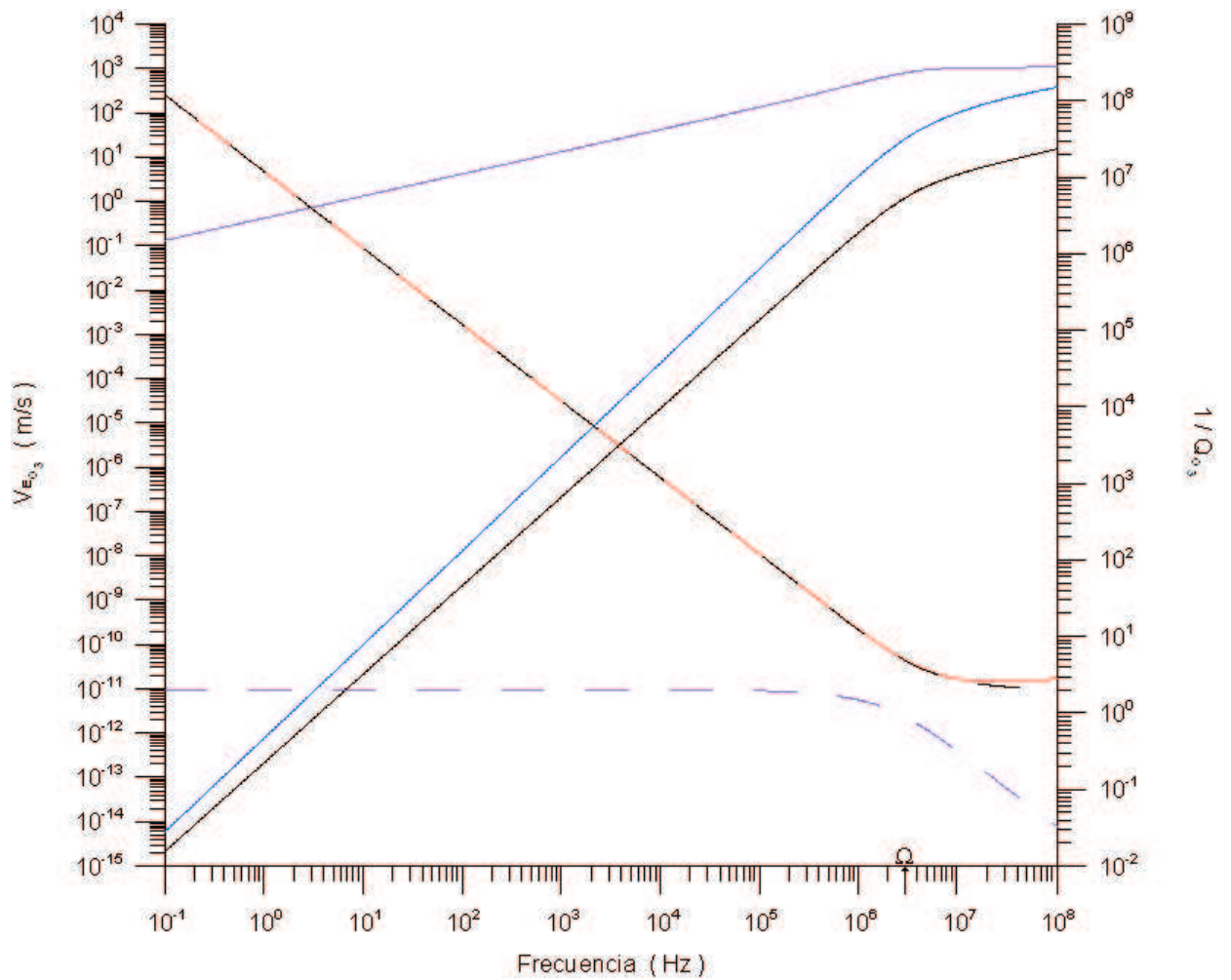


Figure 38. La curva continua azul representa la parte real de la tercera raíz de la velocidad dada en la ec (240). La curva continua roja representa la razón de la parte imaginaria y la real de dicha velocidad. La velocidad de fase de las ondas lentas P y S se muestran en curvas continuas morada y negra, respectivamente y la atenuación de las ondas lentas P y S se muestran en curvas punteadas moradas y negras, respectivamente.

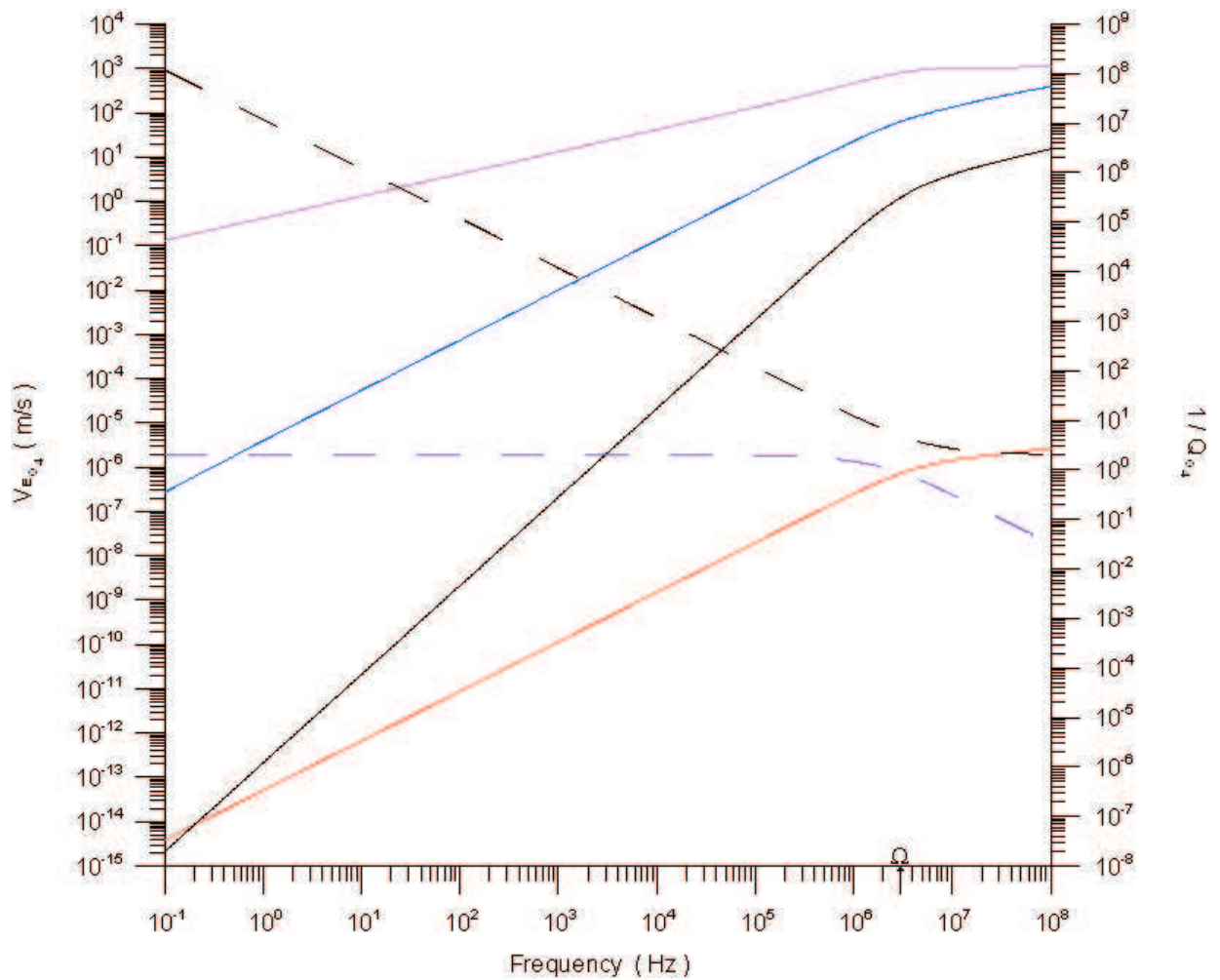


Figure 39. The blue curve shows the real part of the fourth complex velocity of eq (240). The red curve is the ratio of the imaginary to real part of this complex velocity. The slow-P and slow-S waves phase velocity are presented as purple- and black- solid curves, respectively, and the slow-P and slow-S wave attenuation are shown by purple- and black- dashed curves, respectively.

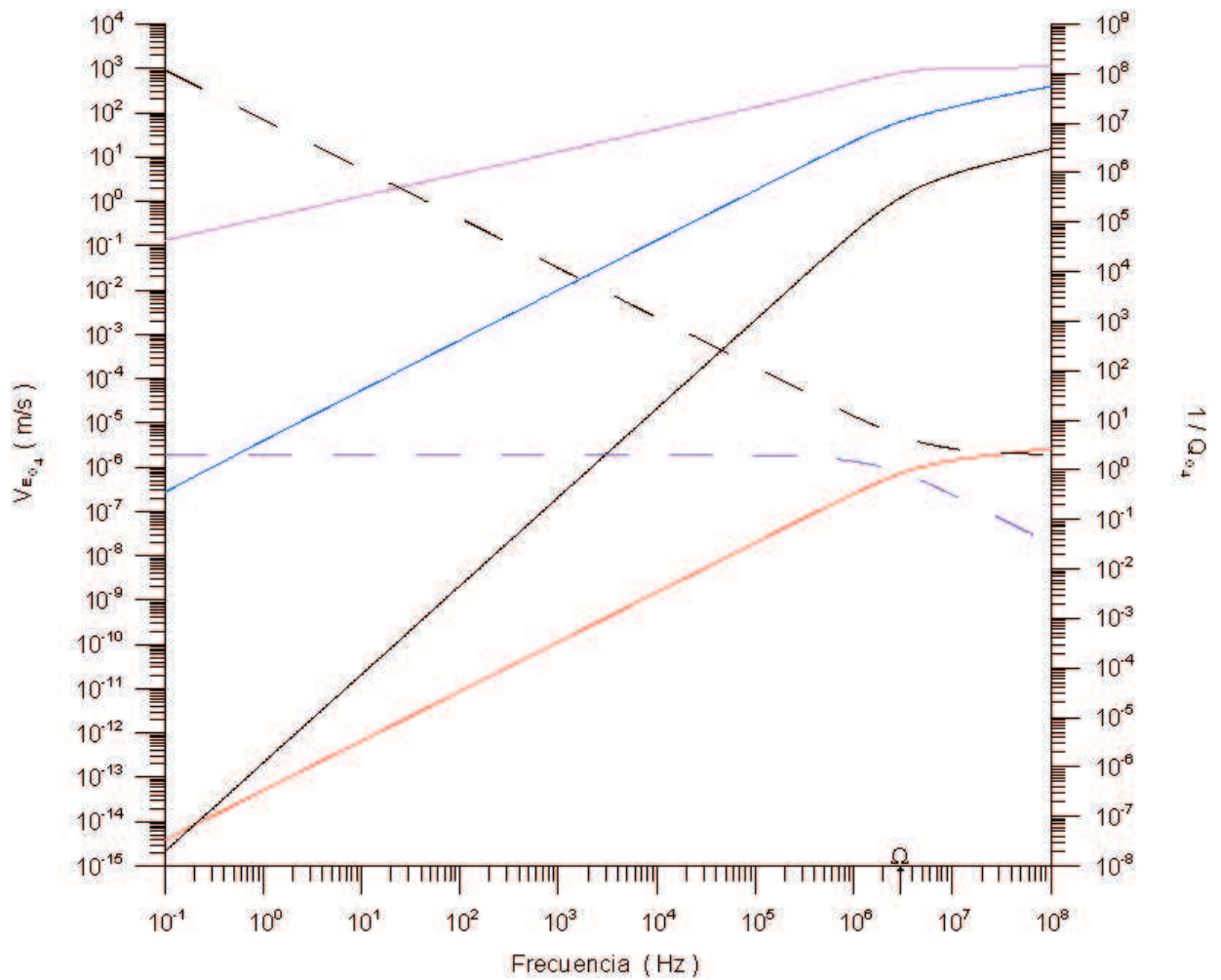


Figure 40. La curva continua azul representa la parte real de la cuarta raíz de la velocidad dada en la ec (240). La curva continua roja representa la razón de la parte imaginaria y la real de dicha velocidad. La velocidad de fase de las ondas lentas P y S se muestran en curvas continuas morada y negra, respectivamente y la atenuación de las ondas lentas P y S se muestran en curvas punteadas moradas y negras, respectivamente.

## VI.10 The complex extensional expression in terms of material properties

To obtain the expressions for phase velocity and attenuation for extensional mode of vibration in which the links with material properties are transparent, it is necessary to suppress the terms that do not contribute in the extensional wave process. For realistic geomaterials the slow S wave,  $\beta_{\text{II}}$ , is very small hence it can be neglected in the coefficients appearing in the extensional dispersion relation, eq (240). Thus, the coefficients  $h_3$ ,  $h_4$ ,  $h_7$  and  $h_8$  can be rewritten.

When the term  $\alpha_{\text{II}}^2$  is factored in the  $h_3$  coefficient, eq (234), can be rewritten as

$$h_3 = \frac{1}{2} \left[ \frac{\beta_{\text{II}}^2 \left\{ (4 - \Theta_{\alpha_{\text{II}}}) \Theta_{\beta_{\text{II}}} - 4 \frac{\beta_{\text{II}}^2}{\alpha_{\text{II}}^2} \Theta_{\alpha_{\text{II}}} \right\}}{\left( 1 - \frac{\beta_{\text{II}}^2}{\alpha_{\text{II}}^2} \Theta_{\alpha_{\text{II}}} \right) \Theta_{\beta_{\text{II}}}} + \left\{ \left( \frac{\beta_{\text{II}}^2 \left\{ (4 - \Theta_{\alpha_{\text{II}}}) \Theta_{\beta_{\text{II}}} - 4 \frac{\beta_{\text{II}}^2}{\alpha_{\text{II}}^2} \Theta_{\alpha_{\text{II}}} \right\}}{\left( 1 - \frac{\beta_{\text{II}}^2}{\alpha_{\text{II}}^2} \Theta_{\alpha_{\text{II}}} \right) \Theta_{\beta_{\text{II}}}} \right)^2 - 16 \frac{\beta_{\text{II}}^2 \beta_{\text{II}}^2 (\Theta_{\beta_{\text{II}}} - \Theta_{\alpha_{\text{II}}})}{\left( 1 - \frac{\beta_{\text{II}}^2}{\alpha_{\text{II}}^2} \Theta_{\alpha_{\text{II}}} \right) \Theta_{\beta_{\text{II}}}} \right\}^{1/2} \right]. \quad (243)$$

Because  $\left\| \frac{\beta_{\text{II}}^2}{\alpha_{\text{II}}^2} \right\| \approx 0$ , it is approximated as

$$h_3 \approx \frac{1}{2} \left[ \beta_{\text{II}}^2 (4 - \Theta_{\alpha_{\text{II}}}) + \beta_{\text{II}}^2 (4 - \Theta_{\alpha_{\text{II}}}) \left\{ 1 - 16 \frac{(\Theta_{\beta_{\text{II}}} - \Theta_{\alpha_{\text{II}}})}{(4 - \Theta_{\alpha_{\text{II}}})^2 \Theta_{\beta_{\text{II}}}} \right\}^{1/2} \right]. \quad (244)$$

Using the binomial expansion (Selby, S. M. 1971, CRC standard mathematical tables, p. 518), it is approximated

$$h_3 \approx 2\beta_{\text{II}}^2 \left[ 1 + \left\{ 1 - \left( 1 - \frac{\Theta_{\alpha_{\text{II}}}}{\Theta_{\beta_{\text{II}}}} \right) \right\}^{1/2} \right]. \quad (245)$$



Hence, the  $h_3$  coefficient can be simplified to

$$h_3 \approx 2\beta_{\text{II}}^2 \left[ 1 + \left( \frac{\Theta_{\alpha_{\text{II}}}}{\Theta_{\beta_{\text{II}}}} \right)^{1/2} \right]. \quad (246)$$

For geomaterial the slow S velocity squared is negligible, that is  $\beta_{\text{II}}^2 \approx 0$ , thus the  $h_3$  coefficient in eq (240) can be neglected, that is

$$h_3 \approx 0. \quad (247)$$

Analogously, the coefficient  $h_4$ , eq (235), is neglected. That is

$$h_4 \approx 2\beta_{\text{II}}^2 \left[ 1 - \left( \frac{\Theta_{\alpha_{\text{II}}}}{\Theta_{\beta_{\text{II}}}} \right)^{1/2} \right] \approx 0. \quad (248)$$

Factorizing the term  $\alpha_{\text{I}}^2$  in the  $h_7$  coefficient, eq (238), is rewritten as

$$\begin{aligned} h_7 = & \frac{1}{2} \left[ \frac{\beta_{\text{II}}^2 \left( 3\Theta_{\beta_{\text{II}}} - 4\frac{\beta_{\text{II}}^2}{\alpha_{\text{I}}^2} \right)}{\left( 1 - \frac{\beta_{\text{II}}^2}{\alpha_{\text{I}}^2} \right) \Theta_{\beta_{\text{II}}}} \right. \\ & \left. + \left\{ \left( \frac{\beta_{\text{II}}^2 \left( 3\Theta_{\beta_{\text{II}}} - 4\frac{\beta_{\text{II}}^2}{\alpha_{\text{I}}^2} \right)}{\left( 1 - \frac{\beta_{\text{II}}^2}{\alpha_{\text{I}}^2} \right) \Theta_{\beta_{\text{II}}}} \right)^2 - 16 \frac{\beta_{\text{II}}^2 \beta_{\text{II}}^2 (\Theta_{\beta_{\text{II}}} - 1)}{\left( 1 - \frac{\beta_{\text{II}}^2}{\alpha_{\text{I}}^2} \right) \Theta_{\beta_{\text{II}}}} \right\}^{1/2} \right]. \end{aligned} \quad (249)$$

Because  $\left\| \frac{\beta_{\text{II}}^2}{\alpha_{\text{I}}^2} \right\| \approx 0$ , it is approximated as

$$h_7 \approx \frac{1}{2} \left[ 3\beta_{\text{II}}^2 - 4 \frac{\beta_{\text{II}}^2}{\sqrt{\Theta_{\beta_{\text{II}}}}} \left\{ 1 + 9\beta_{\text{II}}^2 \right\}^{1/2} \right]. \quad (250)$$

Because the slow S velocity squared is negligible, the  $h_7$  coefficient in eq (240) can be neglected, that is

$$h_7 \approx 0. \quad (251)$$

Analogously, the coefficient  $h_8$ , eq (239), is neglected

$$h_8 \approx -\frac{2\beta_{\text{II}}^2}{\sqrt{\Theta_{\beta_{\text{II}}}}} \approx 0. \quad (252)$$

Hence, essentially the main contribution in the extensional dispersion relation, eq (240), is given by

$$0 \approx V^2 (V^2 - h_1) - \gamma (V^2 - h_5) (V^2 - h_6). \quad (253)$$

Eq (253) is a quadratic equation in  $V^2$ , which solutions are

$$V^2 = \frac{h_1 - \gamma (h_5 + h_6) + [\{h_1 - \gamma (h_5 + h_6)\}^2 + 4(1 - \gamma) \gamma h_5 h_6]^{1/2}}{2(1 - \gamma)}, \quad (254)$$

$$V^2 = \frac{h_1 - \gamma (h_5 + h_6) - [\{h_1 - \gamma (h_5 + h_6)\}^2 + 4(1 - \gamma) \gamma h_5 h_6]^{1/2}}{2(1 - \gamma)}. \quad (255)$$

Figs. 21 and 22 show the comparison of the first and second roots of eq (240) associated with the dispersion relation for extensional waves (obtained numerically by companion matrix methodology, Figs 17 and 18) and the approximated expressions (254) and (255), respectively. The exact  $\Re V$  and attenuation are presented as blue and red curves, respectively. On the respective exact curves, the approximated  $\Re V$  and attenuation are superimposed as dashed-black curves. Eqs (254) and (255) show an acceptable agreement in the region under consideration.

Eq (254) is the only equation which satisfies the extensional-wave characteristic, that is, the phase velocity is larger than the fast-S wave and is smaller than the fast-P wave. Hereafter the analysis is focused on this equation.

To simplify the notation, the extensional wave represented by eq (254) is rewritten as

$$V^2 = \frac{1}{2}h_1 \frac{1-\gamma\delta_1}{(1-\gamma)} \left( 1 + \left[ 1 + \frac{4\gamma\delta_2}{\{1-\gamma\delta_1\}^2} \right]^{1/2} \right), \quad (256)$$

where

$$\begin{aligned} \delta_1 &= \frac{h_5 + h_6}{h_1}, \\ \delta_2 &= \frac{h_5 h_6}{h_1^2}. \end{aligned} \quad (257)$$

Substituting the expressions of  $h_1$  (eq 232),  $h_5$  (eq 236) and  $h_6$  (eq 237) in expressions for  $\delta_1$  and  $\delta_2$ , eqs (257), after algebraic manipulations are rewritten in terms of the fast- and slow- P and S wave complex velocities and  $\Theta$  functions as

$$\delta_1 = \frac{(\beta_I^2 - \alpha_I^2) [4\alpha_{II}^2 - (\alpha_{II}^2 + 4\beta_I^2) \Theta_{\alpha_{II}}]}{(4\beta_I^2 - 3\alpha_I^2) (\alpha_{II}^2 - \beta_I^2 \Theta_{\alpha_{II}})}, \quad (258)$$

$$\delta_2 = -16 \frac{\alpha_{II}^2 (\beta_I^2 - \alpha_I^2)^2 (1 - \Theta_{\alpha_{II}})}{(4\beta_I^2 - 3\alpha_I^2) (\alpha_{II}^2 - \beta_I^2 \Theta_{\alpha_{II}})}. \quad (259)$$

also because  $\beta_{II}$  is so small, the  $\gamma$  term (eq 241) can be approximated as

$$\gamma \approx \frac{(\mathbf{l}^{\beta_I} \cdot \mathbf{r}^{\alpha_{II}}) (\mathbf{l}^{\beta_{II}} \cdot \mathbf{r}^{\alpha_I}) \alpha_I^2 (\alpha_{II}^2 - \beta_I^2 \Theta_{\alpha_{II}})}{(\mathbf{l}^{\beta_I} \cdot \mathbf{r}^{\alpha_I}) (\mathbf{l}^{\beta_{II}} \cdot \mathbf{r}^{\alpha_{II}}) \alpha_{II}^2 (\alpha_I^2 - \beta_I^2)}. \quad (260)$$

For geomaterial it is valid in eq (256) that the norm of the ratio  $\frac{4\gamma\delta_2}{\{1-\gamma\delta_1\}^2}$  is less than one, so the binomial expansion is applied and the square complex extensional velocity is approximated as

$$V^2 \approx h_1 \frac{1-\gamma\delta_1}{(1-\gamma)} \left( 1 + \frac{\gamma\delta_2}{\{1-\gamma\delta_1\}^2} \right). \quad (261)$$

It turns out the material-space can be split into two regimes and the modified Biot critical frequency,  $\Omega$ , marks the boundary of these two regimes.

### VI.10.1 Regime I: $\omega \ll \Omega$

For geomaterial in this regime, it is valid that  $\delta_2 \approx 0$ , hence the complex velocity squared (261) can be approximated as

$$V^2 \approx h_1 \frac{1 - \gamma \delta_1}{(1 - \gamma)}, \quad (262)$$

Thus, the simplest equation for extensional complex velocity squared is obtained in which material properties are linked in a transparent manner. The next operation is to obtain, based on eq (262), the equations to reproduce the segmented linear trends, for extensional phase velocity and attenuation curves, in each frequency region marked by the crossover frequencies A and B.

The approximated expressions of fast- and slow- P and S wave complex velocities for the region below modified Biot critical frequency,  $\Omega$ , are taken to obtain the expressions that represent the linear trend behavior of the extensional phase and attenuation in this region. They are given by

$$\begin{aligned} \alpha_1^2 &\approx C_\alpha^{\text{mm}} - i \left( \frac{\omega}{\Omega} \right) \frac{C_\alpha^{\text{mi}} C_\alpha^{\text{im}}}{C_\alpha^{\text{mm}}}, \\ \beta_1^2 &\approx C_\beta^{\text{mm}} - i \left( \frac{\omega}{\Omega} \right) C_\beta^{\text{ii}}, \\ \alpha_{\text{II}}^2 &\approx -i \left( \frac{\omega}{\Omega} \right) \frac{\text{Det} \mathbf{C}_\alpha}{C_\alpha^{\text{mm}}}. \end{aligned} \quad (263)$$

A complete analysis of the fast- and slow- P and S waves complex velocities are given in appendix E and F, respectively.

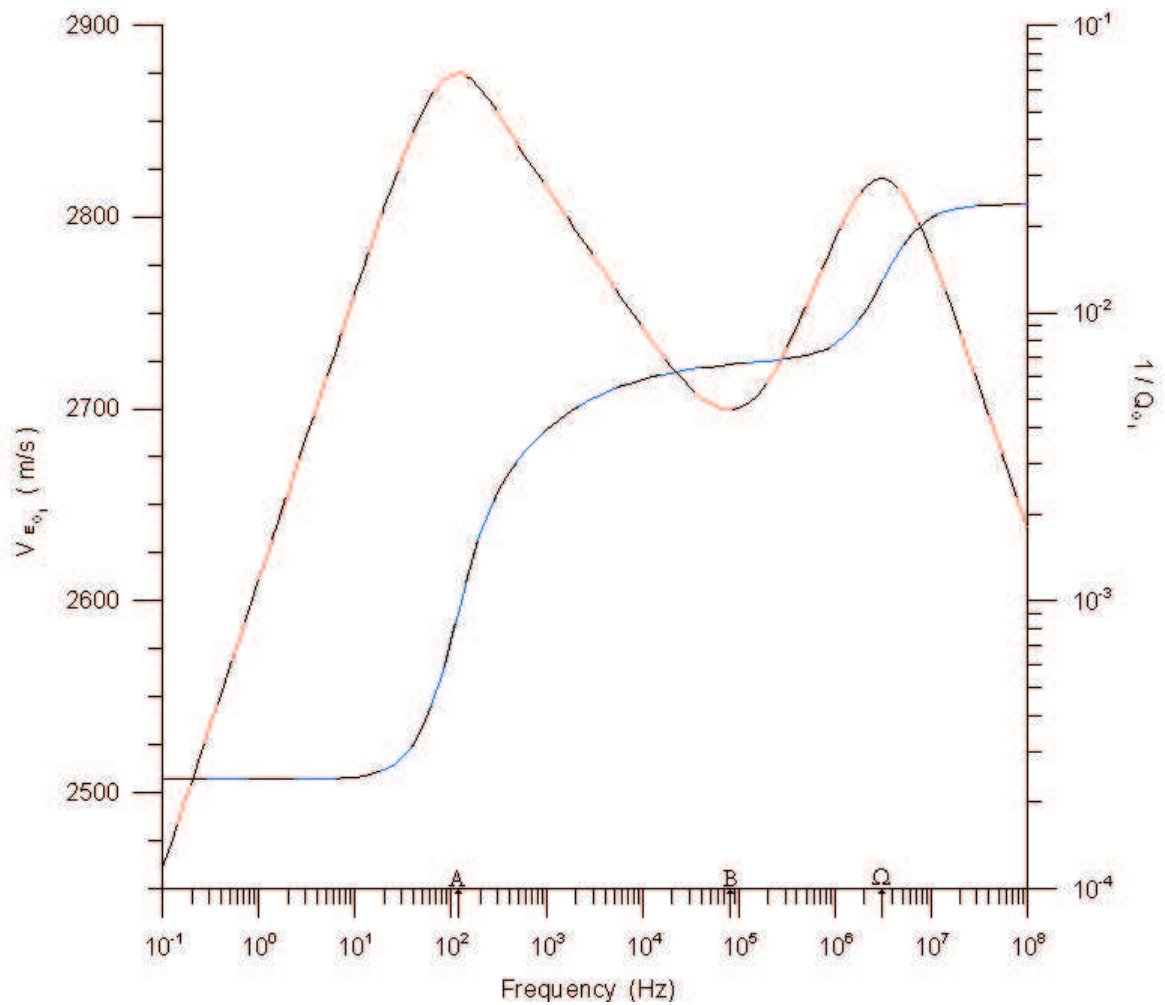


Figure 41. The comparison of exact (the first root of eq 240) and approximate expression (eq 254) for extensional phase velocity and attenuation,  $V_{E_{O_1}}$ ,  $\frac{1}{Q_{O_1}}$ , respectively. The exact phase velocity and attenuation are presented as blue and red curves, respectively. On the respective exact curves, the approximate extensional phase velocity and attenuation are superimposed as dashed-black lines.

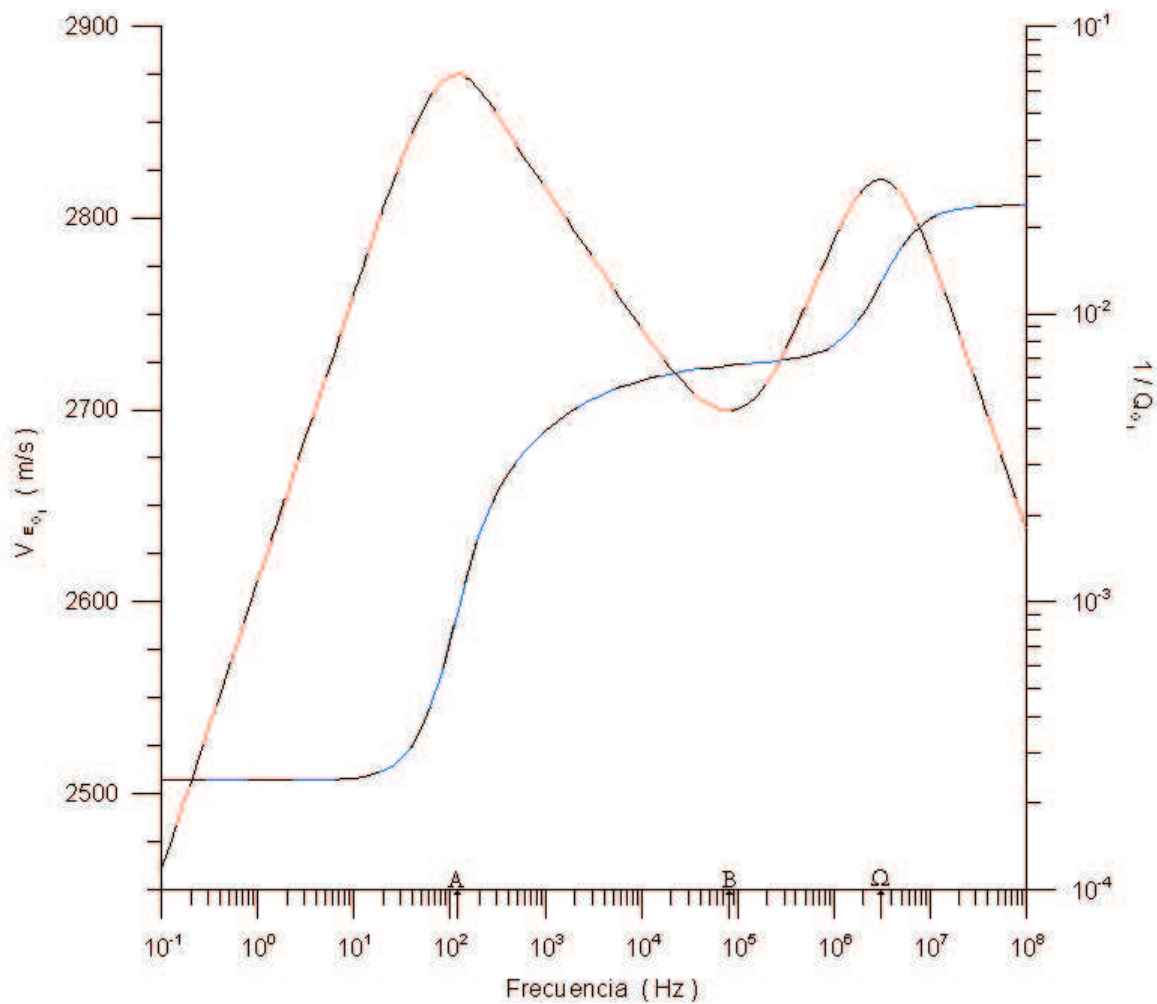


Figure 42. Comparación de los valores exactos para la velocidad de fase y la atenuación (la primera raíz de la ec 240) y los valores obtenidos para la velocidad de fase,  $V_{E_{O_1}}$ , y la atenuación,  $\frac{1}{Q_{O_1}}$ , de la fórmula aproximada (ec 254). Los valores exactos de la velocidad de fase y la atenuación se representan mediante las curvas continuas azul y roja, respectivamente. Sobre las respectivas curvas se superimponen los valores obtenidos de la fórmula aproximada en curvas punteadas negras.

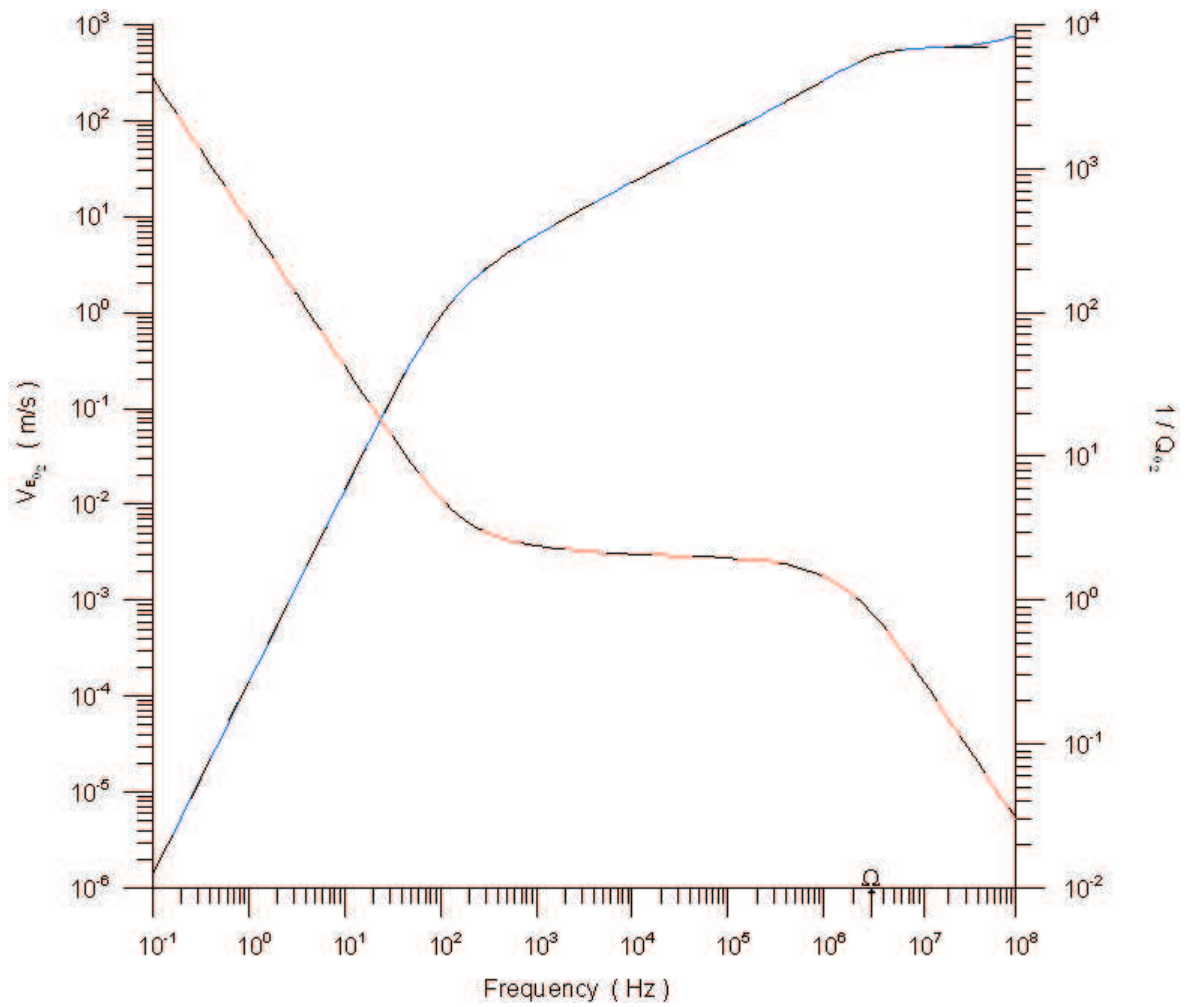


Figure 43. The comparison of exact (the second root of eq 240) and approximate expression (eq 255) for  $\Re V$  and  $\frac{1}{Q}$ , respectively. The exact values for  $\Re V$  and  $\frac{1}{Q}$  are presented as blue and red curves, respectively. On the respective exact curves, the approximate values for  $\Re V$  and  $\frac{1}{Q}$  are superimposed as dashed-black lines.

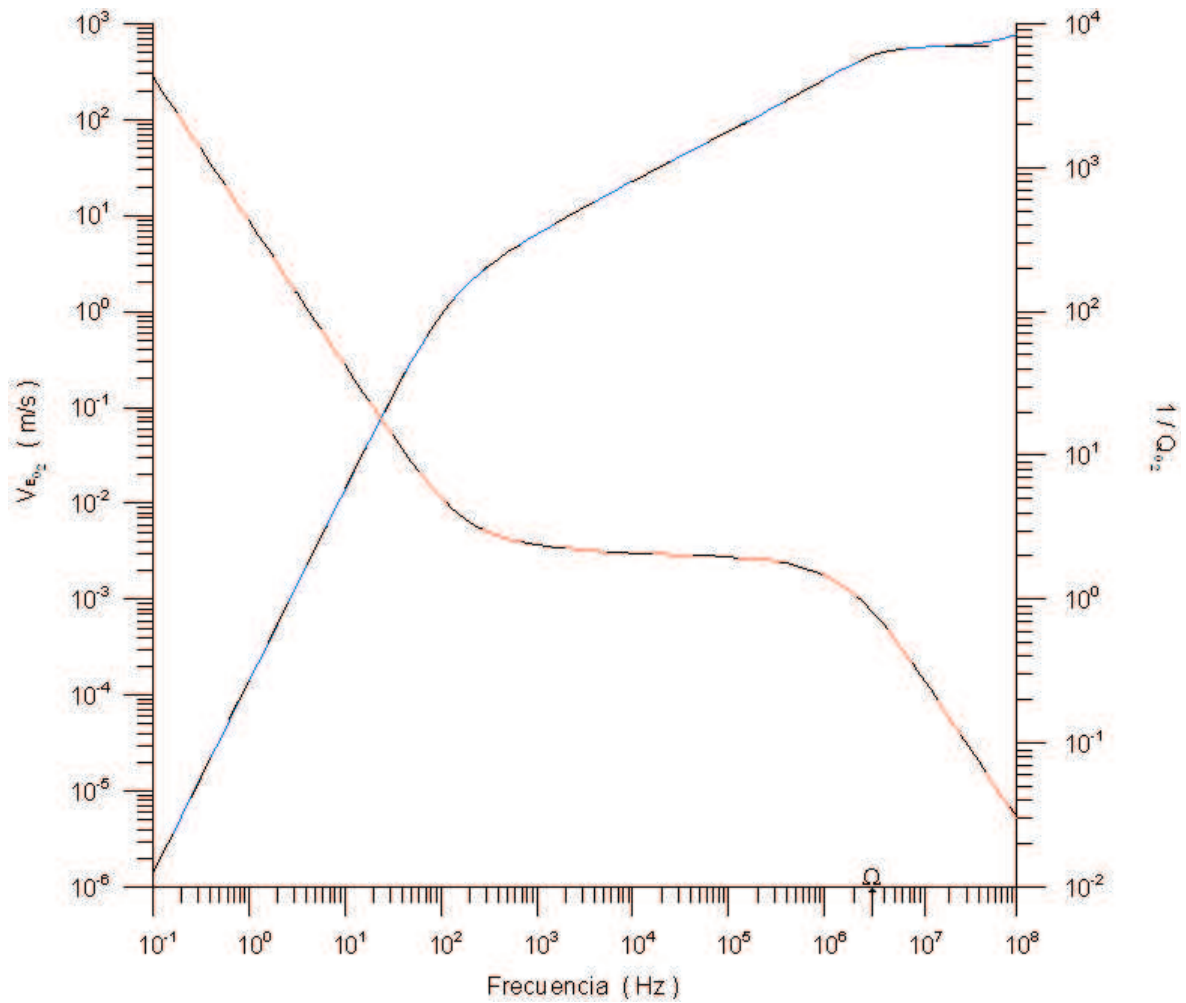


Figure 44. Comparación de los valores exactos (la segunda raíz de la ec 240) y los valores obtenidos usando la fórmula aproximada (ec 255) para  $\Re V$  y  $\frac{1}{Q}$ , respectivamente. Los valores exactos para  $\Re V$  y  $\frac{1}{Q}$  se representan mediante las curvas continuas azul y roja, respectivamente. Sobre las respectivas curvas se superimponen los valores obtenidos de la fórmula aproximada para  $\Re V$  y  $\frac{1}{Q}$  en curvas punteadas negras.



The complex extensional velocity squared, (eq 262), is given in terms of  $h_1$ , (eq 232),  $\delta_1$ , (eq 258) and  $\gamma$ , (eq 260). Substituting eqs (263) in  $h_1$ ,  $\delta_1$  and  $\gamma$ , after algebraic manipulation and leaving only the leading terms, the equations are rewritten in terms of  $C_\alpha$  and  $C_\beta$  matrices as

$$h_1^I \approx \frac{C_\beta^{mm} (3C_\alpha^{mm} - 4C_\beta^{mm}) - \left(\frac{\omega}{\Omega}\right)^2 C_\beta^{ii} \left(3\frac{C_\alpha^{mi}C_\alpha^{im}}{C_\alpha^{mm}} - 4C_\beta^{ii}\right)}{\left(C_\alpha^{mm} - C_\beta^{mm}\right) - i\left(\frac{\omega}{\Omega}\right) \left(\frac{C_\alpha^{mi}C_\alpha^{im}}{C_\alpha^{mm}} - C_\beta^{ii}\right)} - i\left(\frac{\omega}{\Omega}\right) \frac{C_\beta^{ii} (3C_\alpha^{mm} - 4C_\beta^{mm}) + C_\beta^{mm} \left(3\frac{C_\alpha^{mi}C_\alpha^{im}}{C_\alpha^{mm}} - 4C_\beta^{ii}\right)}{\left(C_\alpha^{mm} - C_\beta^{mm}\right) - i\left(\frac{\omega}{\Omega}\right) \left(\frac{C_\alpha^{mi}C_\alpha^{im}}{C_\alpha^{mm}} - C_\beta^{ii}\right)}, \quad (264)$$

$$\delta_1^I \approx \left[ \frac{\left(C_\beta^{mm} - C_\alpha^{mm}\right) - i\left(\frac{\omega}{\Omega}\right) \left(C_\beta^{ii} - \frac{C_\alpha^{mi}C_\alpha^{im}}{C_\alpha^{mm}}\right)}{\left(4C_\beta^{mm} - 3C_\alpha^{mm}\right) - i\left(\frac{\omega}{\Omega}\right) \left(4C_\beta^{ii} - 3\frac{C_\alpha^{mi}C_\alpha^{im}}{C_\alpha^{mm}}\right)} \right] \left[ \frac{4i\left(\frac{\omega}{\Omega}\right) \frac{Det\mathbf{C}_\alpha}{C_\alpha^{mm}} + \left(4C_\beta^{mm} - i\left(\frac{\omega}{\Omega}\right) \left(\frac{Det\mathbf{C}_\alpha}{C_\alpha^{mm}} + 4C_\beta^{ii}\right) \Theta_{\alpha\text{II}}\right)}{i\left(\frac{\omega}{\Omega}\right) \frac{Det\mathbf{C}_\alpha}{C_\alpha^{mm}} + \left(C_\beta^{mm} - i\left(\frac{\omega}{\Omega}\right) C_\beta^{ii}\right) \Theta_{\alpha\text{II}}} \right], \quad (265)$$

$$\gamma^I \approx \frac{\left(\frac{C_\beta^{mi}}{C_\beta^{mm}} - \frac{C_\alpha^{mi}}{C_\alpha^{mm}}\right) \left(\frac{C_\beta^{ii}}{C_\beta^{mi}} - \frac{C_\alpha^{im}}{C_\alpha^{mm}}\right) C_\alpha^{mm} C_\beta^{mm} + i\left(\frac{\omega}{\Omega}\right) \frac{C_\beta^{mi}C_\beta^{ii}}{C_\beta^{mm2}} \left(\frac{C_\beta^{ii}}{C_\beta^{mi}} - \frac{C_\alpha^{im}}{C_\alpha^{mm}}\right) C_\alpha^{mm} C_\beta^{mm}}{\left(\frac{\omega}{\Omega}\right) \frac{Det\mathbf{C}_\alpha}{C_\alpha^{mm}} \left[ \left(1 + \frac{C_\beta^{ii}}{C_\alpha^{mm}} - \frac{C_\beta^{ii}}{C_\beta^{mi}} \frac{C_\alpha^{mi}}{C_\alpha^{mm}}\right) \left(C_\alpha^{mm} - C_\beta^{mm}\right) - \left(\frac{C_\alpha^{mi}C_\alpha^{im}}{C_\alpha^{mm}} - C_\beta^{ii}\right) \right] + i\frac{Det\mathbf{C}_\alpha}{C_\alpha^{mm}} \left(C_\beta^{mm} - C_\alpha^{mm}\right)} \left[ \Im\Theta_{\alpha\text{II}} - i\Re\Theta_{\alpha\text{II}} \right]. \quad (266)$$

The superindex <sup>I</sup> labels the regime under consideration. Expressing them in their real and imaginary part and retaining only the leading terms, they are

$$h_1^I \approx \frac{3C_\alpha^{mm2}C_\beta^{mm} - 7C_\alpha^{mm}C_\beta^{mm2} + 4C_\beta^{mm3}}{\left(C_\alpha^{mm} - C_\beta^{mm}\right)^2} - i\left(\frac{\omega}{\Omega}\right) \frac{3C_\alpha^{mm3}C_\beta^{ii} - 8C_\alpha^{mm2}C_\beta^{mm}C_\beta^{ii} + 4C_\alpha^{mm}C_\beta^{mm2}C_\beta^{ii} + C_\alpha^{mi}C_\alpha^{im}C_\beta^{mm2}}{C_\alpha^{mm} \left(C_\alpha^{mm} - C_\beta^{mm}\right)^2}, \quad (267)$$

$$\delta_1^I \approx \frac{4\left(C_\beta^{mm2} - C_\alpha^{mm}C_\beta^{mm}\right)}{\left(4C_\beta^{mm2} - 3C_\alpha^{mm}C_\beta^{mm}\right)}, \quad (268)$$

$$\gamma^I \approx -\frac{\left(\frac{C_{\beta}^{mi}}{C_{\beta}^{mm}} - \frac{C_{\alpha}^{mi}}{C_{\alpha}^{mm}}\right) \left(\frac{C_{\beta}^{ii}}{C_{\beta}^{mi}} - \frac{C_{\alpha}^{im}}{C_{\alpha}^{mm}}\right) C_{\alpha}^{mm} C_{\beta}^{mm}}{\frac{Det C_{\alpha}}{C_{\alpha}^{mm}} (C_{\beta}^{mm} - C_{\alpha}^{mm})} \Theta_{\alpha II}. \quad (269)$$

In compact notation  $h_1^I$  and  $\gamma^I$  are rewritten as

$$h_1^I = \Re h_1^I - i \left(\frac{\omega}{\Omega}\right) \Im h_1^I, \quad (270)$$

$$\gamma^I = -b \Theta_{\alpha II}, \quad (271)$$

where

$$\Re h_1^I = \frac{3C_{\alpha}^{mm2} C_{\beta}^{mm} - 7C_{\alpha}^{mm} C_{\beta}^{mm2} + 4C_{\beta}^{mm3}}{(C_{\alpha}^{mm} - C_{\beta}^{mm})^2}, \quad (272)$$

$$\Im h_1^I = \frac{3C_{\alpha}^{mm3} C_{\beta}^{ii} - 8C_{\alpha}^{mm2} C_{\beta}^{mm} C_{\beta}^{ii} + 4C_{\alpha}^{mm} C_{\beta}^{mm2} C_{\beta}^{ii} + C_{\alpha}^{mi} C_{\alpha}^{im} C_{\beta}^{mm2}}{C_{\alpha}^{mm} (C_{\alpha}^{mm} - C_{\beta}^{mm})^2}, \quad (273)$$

$$b = \frac{\left(\frac{C_{\beta}^{mi}}{C_{\beta}^{mm}} - \frac{C_{\alpha}^{mi}}{C_{\alpha}^{mm}}\right) \left(\frac{C_{\beta}^{ii}}{C_{\beta}^{mi}} - \frac{C_{\alpha}^{im}}{C_{\alpha}^{mm}}\right) C_{\alpha}^{mm} C_{\beta}^{mm}}{\frac{Det C_{\alpha}}{C_{\alpha}^{mm}} (C_{\beta}^{mm} - C_{\alpha}^{mm})}. \quad (274)$$

Hence, substituting expressions (270) and (271) in the complex extensional velocity squared, eq (262), it simplifies to

$$V^2 \approx \Re h_1^I \frac{(1 + b \delta_1^I \Re \Theta_{\alpha II})}{(1 + b \Re \Theta_{\alpha II})} - i b \Re h_1^I \Im \Theta_{\alpha II} \frac{(1 - \delta_1^I)}{(1 + b \Re \Theta_{\alpha II})^2}. \quad (275)$$

Eq (275) mimics the extensional phase velocity and attenuation for the regime I. Based on this equation the linear equations for the extensional phase velocity and attenuation for the region below and above the crossover frequency  $A$  are obtained in which the dependence with material properties are straightforward.

### VI.10.1.1 region below the crossover frequency A

The argument of the  $\Theta(aq_{\alpha\text{II}})$ , eq (227), in the region below the crossover frequency A is given by

$$aq_{\alpha\text{II}} \approx \frac{a\omega}{\alpha_{\text{II}}} = i^{1/2}\zeta, \quad (276)$$

where  $\zeta = \frac{a\omega}{\sqrt{(\frac{\omega}{\Omega}) \frac{Det(\mathbf{C}_\alpha)}{C_\alpha^{\text{mm}}}}}$ , see eq (444) in appendix E.

Hence, the  $\Theta(aq_{\alpha\text{II}})$  function, eq (230), is approximated as

$$\Theta(aq_{\alpha\text{II}}) \approx 1 + i \frac{a^2\omega\zeta^2}{8} = 1 + i \frac{a^2\omega}{8} \frac{\Omega C_\alpha^{\text{mm}}}{Det\mathbf{C}_\alpha}. \quad (277)$$

Sustituting eq (277) in eq (275) the complex velocity squared is

$$V^2 \approx \Re h_1^{\text{I}} \frac{(1 + b\delta_1^{\text{I}})}{(1 + b)} - i \Re h_1^{\text{I}} \frac{(1 - \delta_1^{\text{I}}) b a^2\omega}{(1 + b)^2} \frac{\Omega C_\alpha^{\text{mm}}}{8 Det\mathbf{C}_\alpha}. \quad (278)$$

Based upon the above equation the complex extensional velocity for the region below A can be obtained in a straightforward manner and its link with material properties is clear. However, it is important to remember that is necessary to satisfy the radiation condition, so the complex extensional velocity satisfies the following form

$$V = \Re V - i\Im V = \Re V \left(1 - i \frac{\Im V}{\Re V}\right) = \Re V \left(1 - i \frac{1}{Q}\right), \quad (279)$$

where

$$\Re V = \sqrt{\frac{1}{2} [||V|| + \Re V^2]}, \quad (280)$$

$$\Im V = \sqrt{\frac{1}{2} [||V|| - \Re V^2]}, \quad (281)$$

and the norm of the complex velocity,  $\|V\|$ , is given by

$$\|V\| = \sqrt{(\Re V^2)^2 + (\Im V^2)^2}. \quad (282)$$

For geomaterial is always true that  $\Im V \ll \Re V$ , hence

$$\|V\| = \Re V^2 \sqrt{1 + \left(\frac{\Im V^2}{\Re V^2}\right)^2}. \quad (283)$$

Using the binomial expansion, the above equation is approximated as

$$\|V\| \approx \Re V^2 \left[ 1 + \frac{1}{2} \left(\frac{\Im V^2}{\Re V^2}\right)^2 \right]. \quad (284)$$

Substituting eq (284) in eqs (280)-(281), the real and imaginary parts of the complex velocity are approximated as

$$\Re V \approx \sqrt{\Re V^2}, \quad (285)$$

$$\Im V \approx \frac{1}{2} \frac{\Im V^2}{\Re V}. \quad (286)$$

Using eqs (285) and (286), the attenuation is given by

$$\frac{1}{Q} = -\frac{\Im V}{\Re V} \approx -\frac{1}{2} \frac{\Im V^2}{\Re V^2}. \quad (287)$$

Hence, from eqs (285) and (287) the extensional phase velocity and attenuation, respectively, for the region below the crossover frequency  $A$ , are

$$V_{\text{ext}} = \sqrt{\frac{(1 + b\delta_1^I)}{(1 + b)}} \Re h_1^I, \quad (288)$$

$$\frac{1}{Q} = \frac{a^2 \omega}{8} \frac{(1 - \delta_1^I) b}{(1 + b)(1 + b\delta_1^I)} \frac{\Omega C_\alpha^{\text{mm}}}{\text{Det}(\mathbf{C}_\alpha)}. \quad (289)$$

Substituting eqs (268), (272) and (274) in eqs (288) and (289), after algebraic manipulation, the extensional phase velocity and attenuation in terms of material properties are

$$V_{\text{ext}} = \sqrt{\frac{E^0}{\rho_0^m}}, \quad (290)$$

$$\frac{1}{Q} = \frac{a^2 \omega}{8} \left( \frac{\mu^f}{K} \right) \left( \frac{\alpha}{3K^0} \right)^2 E^0, \quad (291)$$

where

$$E^0 = 9 \frac{K^0 \mu^0}{\mu^0 + 3K^0}. \quad (292)$$

It is well known that the extensional wave for a elastic sample is related to Young's modulus. Based on that idea,  $E^0$  is interpreted as a poroelastic Young modulus related to dry-frame.

Fig. 23 shows the comparison of the exact extensional phase velocity and attenuation curves (the first root of eq 240) and their approximated expressions, eqs (290) and (291) respectively, for the region below the crossover frequency  $A$ . The exact phase velocity and attenuation are presented, respectively, as continuous blue and red curves whereas their approximations below the crossover frequency  $A$  are given by dashed-black lines. It shows an acceptable agreement between the exact curves and their corresponding approximations in the region under consideration.

### VI.10.1.2 region above the crossover frequency $A$

In the region above  $A$  and below  $\Omega$ , the larger argument approximation for Bessel functions of first kind and zero<sup>th</sup> and first orders shall be taken (CRC standard mathematical

tables, p. 518), that means

$$J_0(aq_{\alpha\text{II}}) \approx \sqrt{\frac{2}{aq_{\alpha\text{II}}\pi}} \cos\left(aq_{\alpha\text{II}} - \frac{1}{4}\pi\right), \quad (293)$$

and

$$J_1(aq_{\alpha\text{II}}) \approx \sqrt{\frac{2}{aq_{\alpha\text{II}}\pi}} \cos\left(aq_{\alpha\text{II}} - \frac{3}{4}\pi\right). \quad (294)$$

Using the above equations in the  $\Theta(aq_{\alpha\text{II}})$  expression, eq (216) is rewritten as

$$\Theta(aq_{\alpha\text{II}}) \approx \frac{2 \cos\left(aq_{\alpha\text{II}} - \frac{3}{4}\pi\right)}{aq_{\alpha\text{II}} \cos\left(aq_{\alpha\text{II}} - \frac{1}{4}\pi\right)} = \frac{2}{aq_{\alpha\text{II}}} \tan\left(aq_{\alpha\text{II}} - \frac{1}{4}\pi\right) \approx \frac{2}{aq_{\alpha\text{II}}}. \quad (295)$$

Using that  $aq_{\alpha\text{II}} \approx i^{1/2} \frac{a\omega}{\sqrt{\left(\frac{\omega}{\Omega}\right) \frac{Det(\mathbf{C}_\alpha)}{C_\alpha^{\text{mm}}}}}$  (eq 276), in the above equation, it follows that

$$\Theta(aq_{\alpha\text{II}}) \approx i^{-1/2} \frac{2\sqrt{Det\mathbf{C}_\alpha}}{a\sqrt{\omega}\sqrt{\Omega C_\alpha^{\text{mm}}}} = \left(\frac{1-i}{\sqrt{2}}\right) \frac{2}{a\sqrt{\omega}} \sqrt{\frac{Det\mathbf{C}_\alpha}{\Omega C_\alpha^{\text{mm}}}}. \quad (296)$$

Hence, substituting eqs (268), (271), (272) and (296) in the complex velocity squared, (275), then after algebraic manipulations, the extensional phase velocity, (285), and attenuation, (287), in terms of material properties are

$$V_{\text{ext}} = \sqrt{\frac{E^c}{\rho^m}}, \quad (297)$$

$$\frac{1}{Q} = \frac{\sqrt{2}}{a\sqrt{\omega}} \left(\frac{\alpha M}{3K^c}\right)^2 E^c \sqrt{\left(\frac{K}{\mu^f}\right) \frac{3K^c + 4\mu^0}{M(3K^0 + 4\mu^0)}}, \quad (298)$$

where

$$E^c = 9 \frac{K^c \mu^0}{\mu^0 + 3K^c}, \quad (299)$$

$$K^c = K^0 + \alpha M. \quad (300)$$

In this regime,  $E^c$  is interpreted as the poroelastic Young's modulus saturated with a fluid, it is related to Gassman low-frequency limit.

Fig. 23 shows the comparison of the exact extensional phase velocity and attenuation curves (the first root of eq 240) and their approximate expressions, respectively, eqs (297) and (298) for the region above the crossover frequency  $A$ . The exact phase velocity and attenuation are presented, respectively, as continuous blue and red curves whereas their approximations are given by dashed-green lines. It shows an acceptable agreement between the exact curves and their corresponding approximations in the region under consideration.

The intersection of eq (291) and eq (298) defines the crossover frequency  $A$ , that is, the frequency such that

$$\omega = \left( \frac{K}{\mu^f} \right) \left\{ \frac{128}{a^6} \left( \frac{MK^0}{K^c} \right)^4 \left( \frac{E^c}{E^0} \right)^2 \left( \frac{3K^c + 4\mu^0}{M(3K^0 + 4\mu^0)} \right) \right\}^{1/3}. \quad (301)$$

To have a complete analysis of the open-pore stress-free boundary value problem, the approximated expressions for extensional phase velocity and attenuation for the region above  $\Omega$  is obtained, this is done in next section.

### VI.10.2 Regime II: $\Omega \ll \omega$

In this regime eq (261) governs the extensional wave motion. Analogously to the procedure developed in the previous section, the approximated expressions for fast- and slow- P and S wave complex velocities in the region under consideration are

$$\alpha_1^2 \approx Tr(\mathbf{C}_\alpha) - \frac{Det(\mathbf{C}_\alpha)}{Tr(\mathbf{C}_\alpha)} - i \left( \frac{\Omega}{\omega} \right) \left[ C_\alpha^{ii} - (Tr(\mathbf{C}_\alpha) + C_\alpha^{ii}) \frac{Det(\mathbf{C}_\alpha)}{\{Tr(\mathbf{C}_\alpha)\}^2} \right],$$

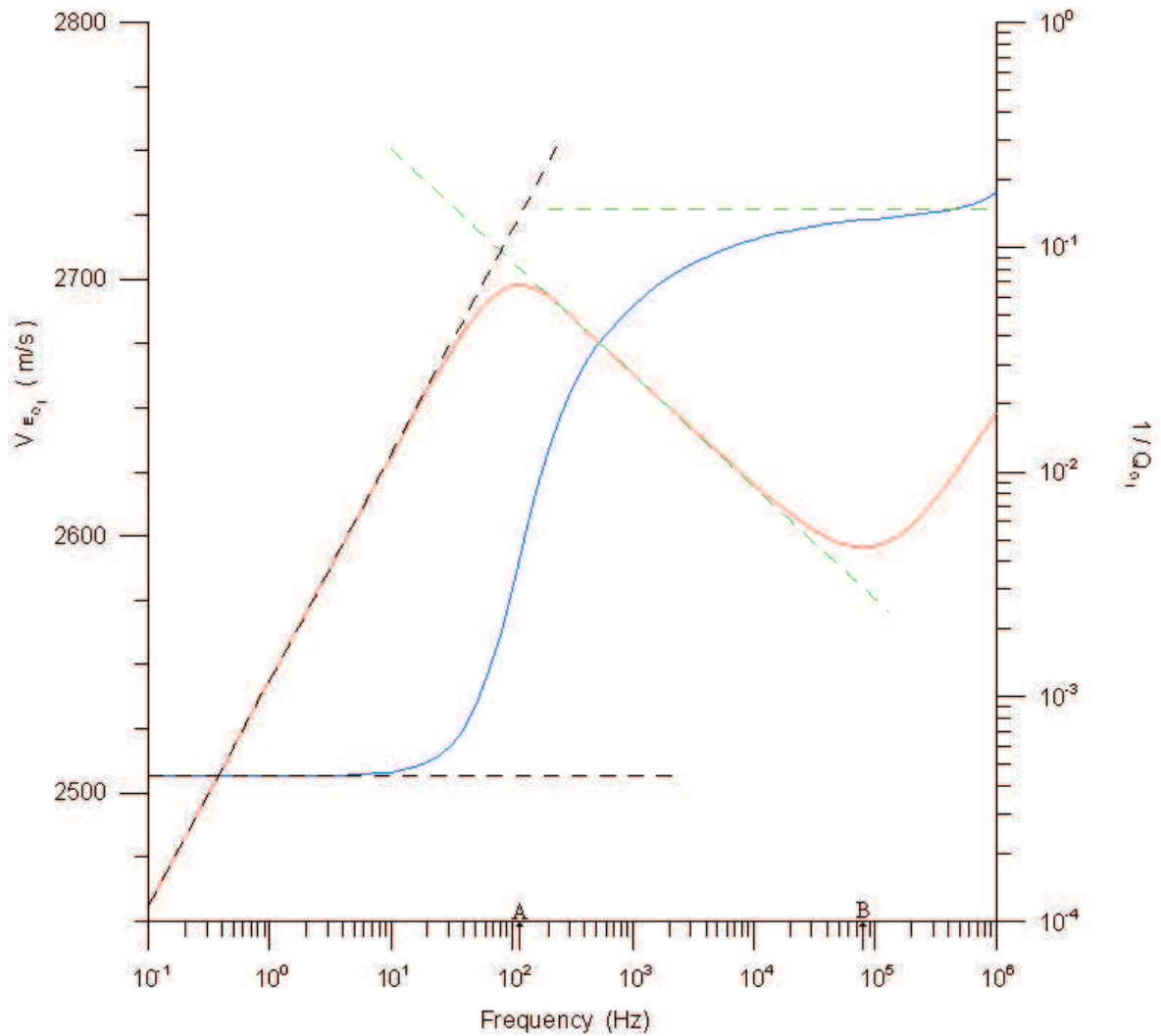


Figure 45. The comparison of exact (eq 240) and approximate expression of the extensional phase velocity and attenuation in the region below crossover frequency B. The exact extensional phase velocity and attenuation are presented as blue and red curves, respectively. On the respective exact curves, the approximate extensional phase velocity and attenuation are superimposed as dashed-black lines for the region below A and as dashed-green lines for the region above A.



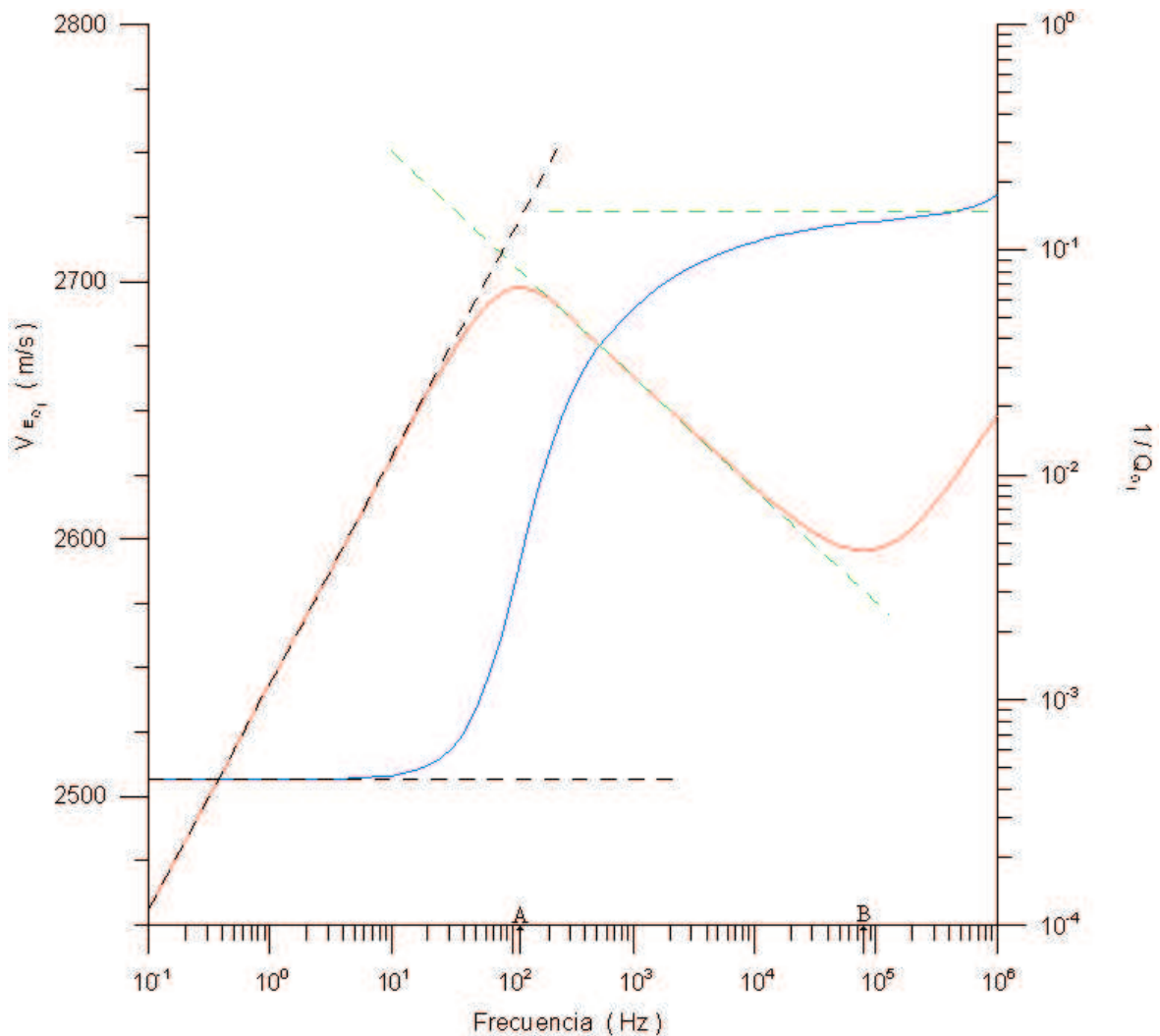


Figure 46. Comparación de los valores exactos para la velocidad de fase y la atenuación (ec 240) y los valores obtenidos mediante las fórmulas de aproximación de la velocidad de fase y la atenuación en la región por debajo de la frecuencia de frontera B. La velocidad de fase y la atenuación exactas se representan por las curvas continuas azul y roja, respectivamente. Sobre las respectivas curvas exactas se superimponen en líneas continuas punteadas negras los valores aproximados de la velocidad de fase y la atenuación para la región por debajo de A y en líneas punteadas verdes para la región por arriba de A.

$$\begin{aligned}
\beta_{\text{I}}^2 &\approx \text{Tr}(\mathbf{C}_\beta) - i \left( \frac{\Omega}{\omega} \right) \mathbf{C}_\beta^{\text{ii}}, & (302) \\
\alpha_{\text{II}}^2 &\approx \frac{\text{Det}(\mathbf{C}_\alpha)}{\text{Tr}(\mathbf{C}_\alpha)} - i \left( \frac{\Omega}{\omega} \right) \left( \text{Tr}(\mathbf{C}_\alpha) + \mathbf{C}_\alpha^{\text{ii}} \right) \frac{\text{Det}(\mathbf{C}_\alpha)}{\{\text{Tr}(\mathbf{C}_\alpha)\}^2}, \\
\beta_{\text{II}}^2 &\approx -i\omega \left( 1 - i \frac{\Omega}{\omega} \right) \frac{\text{Tr}(\mathbf{C}_\beta) \text{Tr}(\mathbf{N}_\beta) - \text{Tr}(\mathbf{C}_\beta \mathbf{N}_\beta)}{\text{Tr}(\mathbf{C}_\beta)}.
\end{aligned}$$

A complete analysis of these velocities are given in appendix E and G.

In the region under consideration the  $\Theta(aq_{\alpha\text{II}})$ , using the large value argument approximation (eq 295), can be rewritten as

$$\Theta(aq_{\alpha\text{II}}) \approx i^{-1/2} \frac{2\sqrt{\text{Det}\mathbf{C}_\alpha}}{a\sqrt{\omega}\sqrt{\Omega\mathbf{C}_\alpha^{\text{mm}}}} = \left( \frac{1-i}{\sqrt{2}} \right) \frac{2}{a\sqrt{\omega}} \sqrt{\frac{\text{Det}\mathbf{C}_\alpha}{\Omega\mathbf{C}_\alpha^{\text{mm}}}}. \quad (303)$$

In this regime the ratio  $\frac{1}{\omega} \approx 0$ , thus

$$\Theta(aq_{\alpha\text{II}}) \approx 0. \quad (304)$$

Substituting eqs (302) and (304) in  $h_1$  (eq 232),  $\delta_1$  (eq 258),  $\delta_2$  (eq 259), and  $\gamma$  (eq 260), after algebraic manipulations and retaining only the leading terms in  $\left(\frac{\Omega}{\omega}\right)$ , they can be rewritten as

$$h_1^{\text{II}} \approx \Re h_1^{\text{II}} - i \left( \frac{\Omega}{\omega} \right) \Im h_1^{\text{II}}, \quad (305)$$

$$\delta_1^{\text{II}} \approx 4 \frac{\text{Tr}(\mathbf{C}_\alpha)^2 - \text{Det}(\mathbf{C}_\alpha) - \text{Tr}(\mathbf{C}_\alpha) \text{Tr}(\mathbf{C}_\beta)}{3\text{Tr}(\mathbf{C}_\alpha)^2 - 3\text{Det}(\mathbf{C}_\alpha) - 4\text{Tr}(\mathbf{C}_\alpha) \text{Tr}(\mathbf{C}_\beta)}, \quad (306)$$

$$\delta_2^{\text{II}} \approx 4 \frac{\text{Tr}(\mathbf{C}_\alpha)^2 - \text{Det}(\mathbf{C}_\alpha) - \text{Tr}(\mathbf{C}_\alpha) \text{Tr}(\mathbf{C}_\beta)}{3\text{Tr}(\mathbf{C}_\alpha)^2 - 3\text{Det}(\mathbf{C}_\alpha) - 4\text{Tr}(\mathbf{C}_\alpha) \text{Tr}(\mathbf{C}_\beta)}, \quad (307)$$

$$\gamma^{\text{II}} \approx -\frac{\mathbf{C}_\alpha^{\text{mi}} \mathbf{C}_\alpha^{\text{im}}}{(\mathbf{C}_\alpha^{\text{mm}})^2}, \quad (308)$$

where the superindex <sup>II</sup> labels the region under consideration and

$$\Re h_1^{\text{II}} = Tr(\mathbf{C}_\beta) \frac{[3\Re(\alpha_1^2) - 4Tr(\mathbf{C}_\beta)]}{\Re(\alpha_1^2) - Tr(\mathbf{C}_\beta)}, \quad (309)$$

$$\Im h_1^{\text{II}} = \frac{3\Re(\alpha_1^2)^2 \Im(\beta_1^2) + 4\Re(\beta_1^2)^2 \Im(\beta_1^2) - 8\Re(\alpha_1^2)\Re(\beta_1^2)\Im(\beta_1^2)}{[\Re(\alpha_1^2) - Tr(\mathbf{C}_\beta)]^2}. \quad (310)$$

Hence, the square complex velocity, eq (261), is

$$V^2 \approx \left( \Re h_1^{\text{II}} - i \left( \frac{\Omega}{\omega} \right) \Im h_1^{\text{II}} \right) \left( \frac{1 - \delta_1^{\text{II}2} \gamma^{\text{II}2}}{1 - \gamma^{\text{II}}} \right). \quad (311)$$

From eq (311), the expressions for the extensional phase velocity, eq (285), and attenuation, eq (287), are rewritten as

$$V_{\text{ext}} = \sqrt{\left( \frac{1 - \delta_1^{\text{II}2} \gamma^{\text{II}2}}{1 - \gamma^{\text{II}}} \right) \Re h_1^{\text{II}}}, \quad (312)$$

$$\frac{1}{Q} = \left( \frac{\Omega}{\omega} \right) \frac{\Im h_1^{\text{II}}}{\Re h_1^{\text{II}}}. \quad (313)$$

The attenuation curve above the crossover frequency B is symmetric. This means the linear trend from the crossover frequency B to  $\Omega$  is inverse to linear trend above  $\Omega$ . So, based upon eq (313) the attenuation, in the region formed by B to  $\Omega$ , is expressed as

$$\frac{1}{Q} = \left( \frac{\omega}{\Omega} \right) \frac{\Im h_1^{\text{II}}}{\Re h_1^{\text{II}}}. \quad (314)$$

The intersection of eq (313) and eq (314) defines the crossover frequency  $\Omega$ . Analogously, the intersection of eq (298) and eq (314) defines the crossover frequency B, that is, the frequency such that

$$\omega = \left[ \left\{ (\delta_1^{\text{I}} - 1) b \frac{\Re h_1^{\text{II}}}{\Im h_1^{\text{II}}} \right\}^2 \frac{2Det(\mathbf{C}_\alpha) \Omega^2}{\Omega C_\alpha^{\text{mm}} a^2} \right]^{1/3}. \quad (315)$$

Fig. 24 shows the comparison of the exact extensional phase velocity and attenuation curves (the first root of eq 240) and their approximated expressions, eqs (312), (313) and (314) for the region above the crossover frequency  $B$ . The exact phase velocity and attenuation are presented, respectively, as continuous blue and red curves whereas their approximations above the crossover frequency  $\Omega$  are given by dashed-green lines. The dashed-black lines represent the approximation for the attenuation in the region below  $\Omega$  and above the crossover frequency  $B$ .

## VI.11 Dispersion relation for longitudinal mode for closed-pore stress-free boundary condition

Using the radial surface does not undergo internal fluid-flow motion in displacement and stresses for the closed-pore stress-free boundary condition (79), from eqs (191)-(194) are obtained that

$$\begin{aligned}
0 &= \left\{ \left( \hat{\mathbf{e}}_2 \cdot \mathbf{r}^{\beta_I} \right) \left( \mathbf{l}^{\beta_I} \cdot \mathbf{r}^{\alpha_I} \right) + \left( \hat{\mathbf{e}}_2 \cdot \mathbf{r}^{\beta_{II}} \right) \left( \mathbf{l}^{\beta_{II}} \cdot \mathbf{r}^{\alpha_I} \right) \right\} \left( V^2 - \alpha_I^2 \right) \Theta_{\alpha_I} A_I \\
&+ \left\{ \left( \hat{\mathbf{e}}_2 \cdot \mathbf{r}^{\beta_I} \right) \left( \mathbf{l}^{\beta_I} \cdot \mathbf{r}^{\alpha_{II}} \right) + \left( \hat{\mathbf{e}}_2 \cdot \mathbf{r}^{\beta_{II}} \right) \left( \mathbf{l}^{\beta_{II}} \cdot \mathbf{r}^{\alpha_{II}} \right) \right\} \left( V^2 - \alpha_{II}^2 \right) \Theta_{\alpha_{II}} A_{II} \\
&- 2 \left( \hat{\mathbf{e}}_2 \cdot \mathbf{r}^{\beta_I} \right) \beta_I^2 \Theta_{\beta_I} B_I - 2 \left( \hat{\mathbf{e}}_2 \cdot \mathbf{r}^{\beta_{II}} \right) \beta_{II}^2 \Theta_{\beta_{II}} B_{II},
\end{aligned} \tag{316}$$

$$\begin{aligned}
0 &= \left\{ \left( \hat{\mathbf{e}}_2 \cdot \mathbf{r}^{\beta_I} \right) \left( \mathbf{l}^{\beta_I} \cdot \mathbf{r}^{\alpha_I} \right) + \left( \hat{\mathbf{e}}_2 \cdot \mathbf{r}^{\beta_{II}} \right) \left( \mathbf{l}^{\beta_{II}} \cdot \mathbf{r}^{\alpha_I} \right) \right\} \alpha_I^2 A_I \\
&+ \left\{ \left( \hat{\mathbf{e}}_2 \cdot \mathbf{r}^{\beta_I} \right) \left( \mathbf{l}^{\beta_I} \cdot \mathbf{r}^{\alpha_{II}} \right) + \left( \hat{\mathbf{e}}_2 \cdot \mathbf{r}^{\beta_{II}} \right) \left( \mathbf{l}^{\beta_{II}} \cdot \mathbf{r}^{\alpha_{II}} \right) \right\} \alpha_{II}^2 A_{II} \\
&+ 2 \left( \hat{\mathbf{e}}_2 \cdot \mathbf{r}^{\beta_I} \right) \beta_I^2 B_I + 2 \left( \hat{\mathbf{e}}_2 \cdot \mathbf{r}^{\beta_{II}} \right) \beta_{II}^2 B_{II},
\end{aligned} \tag{317}$$

$$\begin{aligned}
0 &= \left\{ \left( \hat{\mathbf{e}}_1 \cdot \mathbf{r}^{\beta_I} \right) \left( \mathbf{l}^{\beta_I} \cdot \mathbf{r}^{\alpha_I} \right) \beta_I^2 + \left( \hat{\mathbf{e}}_1 \cdot \mathbf{r}^{\beta_{II}} \right) \left( \mathbf{l}^{\beta_{II}} \cdot \mathbf{r}^{\alpha_I} \right) \beta_{II}^2 \right\} \left( V^2 - \alpha_I^2 \right) \Theta_{\alpha_I} A_I \\
&+ \left\{ \left( \hat{\mathbf{e}}_1 \cdot \mathbf{r}^{\beta_I} \right) \left( \mathbf{l}^{\beta_I} \cdot \mathbf{r}^{\alpha_{II}} \right) \beta_I^2 + \left( \hat{\mathbf{e}}_1 \cdot \mathbf{r}^{\beta_{II}} \right) \left( \mathbf{l}^{\beta_{II}} \cdot \mathbf{r}^{\alpha_{II}} \right) \beta_{II}^2 \right\} \left( V^2 - \alpha_{II}^2 \right) \Theta_{\alpha_{II}} A_{II}
\end{aligned}$$

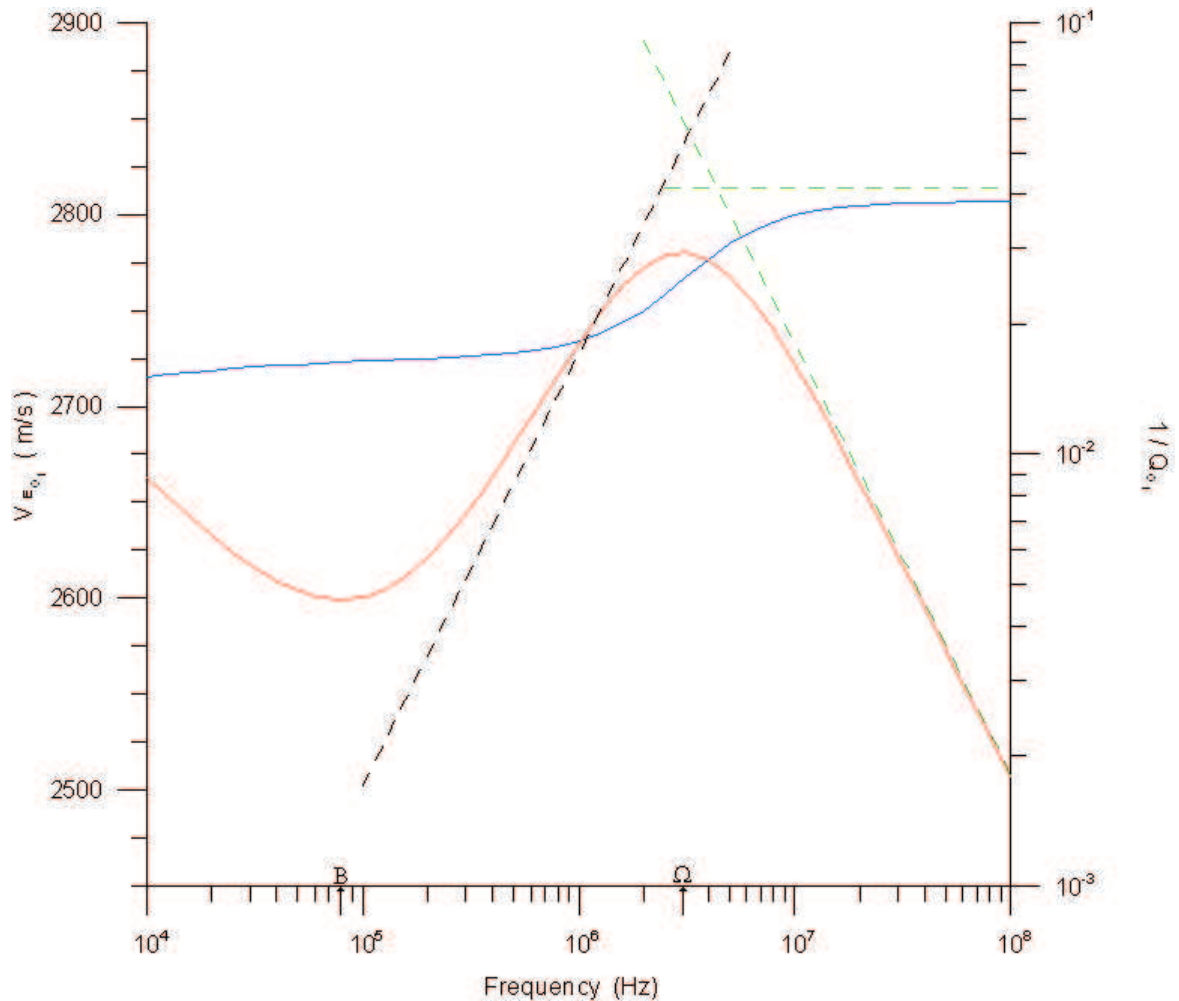


Figure 47. The comparison of exact (the first root of eq 240) and approximate expression of the extensional phase velocity and attenuation in the region above B. The exact extensional phase velocity and attenuation are presented as blue and red curves, respectively. On the respective exact curves, the approximate extensional phase velocity and attenuation are superimposed as dashed-green lines for the region above  $\Omega$ , eqs (312) and eq (313) respectively. Because the crossover frequency B has no signature on phase velocity only the attenuation has an approximate line which is represented as dashed-black lines, eq (314).

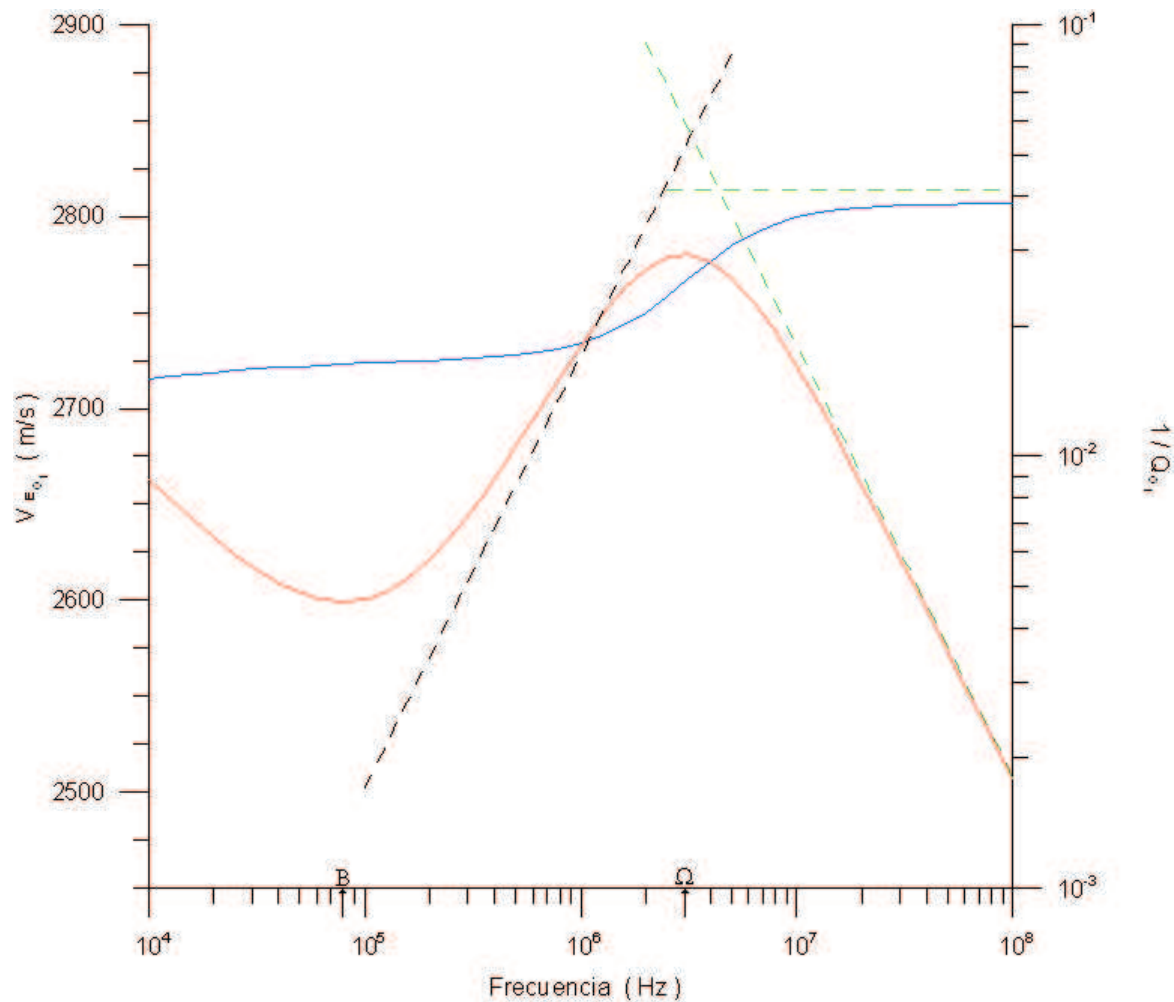


Figure 48. Comparación de los valores exactos para la velocidad de fase y la atenuación (ec 240) y los valores obtenidos mediante las fórmulas de aproximación para la región arriba de B. La velocidad de fase y la atenuación exactas se representan por las curvas continuas azul y roja, respectivamente. Sobre las respectivas curvas exactas se superponen en líneas punteadas verdes los valores aproximados de la velocidad de fase y la atenuación para la región por arriba de  $\Omega$ , ecs (312) y (313) respectivamente. Debido a que la frecuencia de frontera B no afecta a la velocidad de fase solamente la atenuación tiene una línea de aproximación la cual esta representada por la línea punteada negra, ec (314).

$$+ (\hat{\mathbf{e}}_1 \cdot \mathbf{r}^{\beta_1}) (V^2 - 2\beta_1^2) \beta_1^2 \Theta_{\beta_1} B_I + (\hat{\mathbf{e}}_1 \cdot \mathbf{r}^{\beta_{II}}) (V^2 - 2\beta_{II}^2) \beta_{II}^2 \Theta_{\beta_{II}} B_{II}, \quad (318)$$

$$\begin{aligned} 0 &= \left\{ (\hat{\mathbf{e}}_1 \cdot \mathbf{r}^{\beta_1}) (\mathbf{l}^{\beta_1} \cdot \mathbf{r}^{\alpha_1}) (V^2 - 2\beta_1^2) + (\hat{\mathbf{e}}_1 \cdot \mathbf{r}^{\beta_{II}}) (\mathbf{l}^{\beta_{II}} \cdot \mathbf{r}^{\alpha_1}) (V^2 - 2\beta_{II}^2) \right\} \alpha_1^2 A_I \\ &+ \left\{ (\hat{\mathbf{e}}_1 \cdot \mathbf{r}^{\beta_1}) (\mathbf{l}^{\beta_1} \cdot \mathbf{r}^{\alpha_{II}}) (V^2 - 2\beta_1^2) + (\hat{\mathbf{e}}_1 \cdot \mathbf{r}^{\beta_{II}}) (\mathbf{l}^{\beta_{II}} \cdot \mathbf{r}^{\alpha_{II}}) (V^2 - 2\beta_{II}^2) \right\} \alpha_{II}^2 A_{II} \\ &+ (\hat{\mathbf{e}}_1 \cdot \mathbf{r}^{\beta_1}) (V^2 \Theta_{\beta_1} - 4\beta_1^2) \beta_1^2 B_I + (\hat{\mathbf{e}}_1 \cdot \mathbf{r}^{\beta_{II}}) (V^2 \Theta_{\beta_{II}} - 4\beta_{II}^2) \beta_{II}^2 B_{II}. \end{aligned} \quad (319)$$

The system formed by eqs (316)-(319) in a matrix form is written as

$$\begin{aligned} 0 &= \begin{pmatrix} \left\{ (\hat{\mathbf{e}}_2 \cdot \mathbf{r}^{\beta_1}) (\mathbf{l}^{\beta_1} \cdot \mathbf{r}^{\alpha_1}) + (\hat{\mathbf{e}}_2 \cdot \mathbf{r}^{\beta_{II}}) (\mathbf{l}^{\beta_{II}} \cdot \mathbf{r}^{\alpha_1}) \right\} (V^2 - \alpha_1^2) \Theta_{\alpha_1} \\ \left\{ (\hat{\mathbf{e}}_2 \cdot \mathbf{r}^{\beta_1}) (\mathbf{l}^{\beta_1} \cdot \mathbf{r}^{\alpha_1}) + (\hat{\mathbf{e}}_2 \cdot \mathbf{r}^{\beta_{II}}) (\mathbf{l}^{\beta_{II}} \cdot \mathbf{r}^{\alpha_1}) \right\} \alpha_1^2 \\ \left\{ (\hat{\mathbf{e}}_1 \cdot \mathbf{r}^{\beta_1}) (\mathbf{l}^{\beta_1} \cdot \mathbf{r}^{\alpha_1}) \beta_1^2 + (\hat{\mathbf{e}}_1 \cdot \mathbf{r}^{\beta_{II}}) (\mathbf{l}^{\beta_{II}} \cdot \mathbf{r}^{\alpha_1}) \beta_{II}^2 \right\} (V^2 - \alpha_1^2) \Theta_{\alpha_1} \\ \left\{ (\hat{\mathbf{e}}_1 \cdot \mathbf{r}^{\beta_1}) (\mathbf{l}^{\beta_1} \cdot \mathbf{r}^{\alpha_1}) (V^2 - 2\beta_1^2) + (\hat{\mathbf{e}}_1 \cdot \mathbf{r}^{\beta_{II}}) (\mathbf{l}^{\beta_{II}} \cdot \mathbf{r}^{\alpha_1}) (V^2 - 2\beta_{II}^2) \right\} \alpha_1^2 \\ \left\{ (\hat{\mathbf{e}}_2 \cdot \mathbf{r}^{\beta_1}) (\mathbf{l}^{\beta_1} \cdot \mathbf{r}^{\alpha_{II}}) + (\hat{\mathbf{e}}_2 \cdot \mathbf{r}^{\beta_{II}}) (\mathbf{l}^{\beta_{II}} \cdot \mathbf{r}^{\alpha_{II}}) \right\} (V^2 - \alpha_{II}^2) \Theta_{\alpha_{II}} \\ \left\{ (\hat{\mathbf{e}}_2 \cdot \mathbf{r}^{\beta_1}) (\mathbf{l}^{\beta_1} \cdot \mathbf{r}^{\alpha_{II}}) + (\hat{\mathbf{e}}_2 \cdot \mathbf{r}^{\beta_{II}}) (\mathbf{l}^{\beta_{II}} \cdot \mathbf{r}^{\alpha_{II}}) \right\} \alpha_{II}^2 \\ \left\{ (\hat{\mathbf{e}}_1 \cdot \mathbf{r}^{\beta_1}) (\mathbf{l}^{\beta_1} \cdot \mathbf{r}^{\alpha_{II}}) \beta_1^2 + (\hat{\mathbf{e}}_1 \cdot \mathbf{r}^{\beta_{II}}) (\mathbf{l}^{\beta_{II}} \cdot \mathbf{r}^{\alpha_{II}}) \beta_{II}^2 \right\} (V^2 - \alpha_{II}^2) \Theta_{\alpha_{II}} \\ \left\{ (\hat{\mathbf{e}}_1 \cdot \mathbf{r}^{\beta_1}) (\mathbf{l}^{\beta_1} \cdot \mathbf{r}^{\alpha_{II}}) (V^2 - 2\beta_1^2) + (\hat{\mathbf{e}}_1 \cdot \mathbf{r}^{\beta_{II}}) (\mathbf{l}^{\beta_{II}} \cdot \mathbf{r}^{\alpha_{II}}) (V^2 - 2\beta_{II}^2) \right\} \alpha_{II}^2 \\ -2 (\hat{\mathbf{e}}_2 \cdot \mathbf{r}^{\beta_1}) \beta_1^2 \Theta_{\beta_1} & \quad -2 (\hat{\mathbf{e}}_2 \cdot \mathbf{r}^{\beta_{II}}) \beta_{II}^2 \Theta_{\beta_{II}} \\ 2 (\hat{\mathbf{e}}_2 \cdot \mathbf{r}^{\beta_1}) \beta_1^2 & \quad 2 (\hat{\mathbf{e}}_2 \cdot \mathbf{r}^{\beta_{II}}) \beta_{II}^2 \\ (\hat{\mathbf{e}}_1 \cdot \mathbf{r}^{\beta_1}) (V^2 - 2\beta_1^2) \beta_1^2 \Theta_{\beta_1} & \quad (\hat{\mathbf{e}}_1 \cdot \mathbf{r}^{\beta_{II}}) (V^2 - 2\beta_{II}^2) \beta_{II}^2 \Theta_{\beta_{II}} \\ (\hat{\mathbf{e}}_1 \cdot \mathbf{r}^{\beta_1}) (V^2 \Theta_{\beta_1} - 4\beta_1^2) \beta_1^2 & \quad (\hat{\mathbf{e}}_1 \cdot \mathbf{r}^{\beta_{II}}) (V^2 \Theta_{\beta_{II}} - 4\beta_{II}^2) \beta_{II}^2 \end{pmatrix} \begin{pmatrix} A_I \\ A_{II} \\ B_I \\ B_{II} \end{pmatrix}. \end{aligned} \quad (320)$$

Interchanging the second and third rows, and then the second and third columns, this system is rearranged as

$$\begin{aligned}
0 = & \begin{pmatrix} \left\{ (\hat{\mathbf{e}}_2 \cdot \mathbf{r}^{\beta_I}) (\mathbf{l}^{\beta_I} \cdot \mathbf{r}^{\alpha_I}) + (\hat{\mathbf{e}}_2 \cdot \mathbf{r}^{\beta_{II}}) (\mathbf{l}^{\beta_{II}} \cdot \mathbf{r}^{\alpha_I}) \right\} (V^2 - \alpha_I^2) \Theta_{\alpha_I} \\ \left\{ (\hat{\mathbf{e}}_1 \cdot \mathbf{r}^{\beta_I}) (\mathbf{l}^{\beta_I} \cdot \mathbf{r}^{\alpha_I}) \beta_I^2 + (\hat{\mathbf{e}}_1 \cdot \mathbf{r}^{\beta_{II}}) (\mathbf{l}^{\beta_{II}} \cdot \mathbf{r}^{\alpha_I}) \beta_{II}^2 \right\} (V^2 - \alpha_I^2) \Theta_{\alpha_I} \\ \left\{ (\hat{\mathbf{e}}_2 \cdot \mathbf{r}^{\beta_I}) (\mathbf{l}^{\beta_I} \cdot \mathbf{r}^{\alpha_I}) + (\hat{\mathbf{e}}_2 \cdot \mathbf{r}^{\beta_{II}}) (\mathbf{l}^{\beta_{II}} \cdot \mathbf{r}^{\alpha_I}) \right\} \alpha_I^2 \\ \left\{ (\hat{\mathbf{e}}_1 \cdot \mathbf{r}^{\beta_I}) (\mathbf{l}^{\beta_I} \cdot \mathbf{r}^{\alpha_I}) (V^2 - 2\beta_I^2) + (\hat{\mathbf{e}}_1 \cdot \mathbf{r}^{\beta_{II}}) (\mathbf{l}^{\beta_{II}} \cdot \mathbf{r}^{\alpha_I}) (V^2 - 2\beta_{II}^2) \right\} \alpha_I^2 \\ -2 (\hat{\mathbf{e}}_2 \cdot \mathbf{r}^{\beta_I}) \beta_I^2 \Theta_{\beta_I} \\ (\hat{\mathbf{e}}_1 \cdot \mathbf{r}^{\beta_I}) (V^2 - 2\beta_I^2) \beta_I^2 \Theta_{\beta_I} \\ 2 (\hat{\mathbf{e}}_2 \cdot \mathbf{r}^{\beta_I}) \beta_I^2 \\ (\hat{\mathbf{e}}_1 \cdot \mathbf{r}^{\beta_I}) (V^2 \Theta_{\beta_I} - 4\beta_I^2) \beta_I^2 \\ \left\{ (\hat{\mathbf{e}}_2 \cdot \mathbf{r}^{\beta_I}) (\mathbf{l}^{\beta_I} \cdot \mathbf{r}^{\alpha_{II}}) + (\hat{\mathbf{e}}_2 \cdot \mathbf{r}^{\beta_{II}}) (\mathbf{l}^{\beta_{II}} \cdot \mathbf{r}^{\alpha_{II}}) \right\} (V^2 - \alpha_{II}^2) \Theta_{\alpha_{II}} \\ \left\{ (\hat{\mathbf{e}}_1 \cdot \mathbf{r}^{\beta_I}) (\mathbf{l}^{\beta_I} \cdot \mathbf{r}^{\alpha_{II}}) \beta_I^2 + (\hat{\mathbf{e}}_1 \cdot \mathbf{r}^{\beta_{II}}) (\mathbf{l}^{\beta_{II}} \cdot \mathbf{r}^{\alpha_{II}}) \beta_{II}^2 \right\} (V^2 - \alpha_{II}^2) \Theta_{\alpha_{II}} \\ \left\{ (\hat{\mathbf{e}}_2 \cdot \mathbf{r}^{\beta_I}) (\mathbf{l}^{\beta_I} \cdot \mathbf{r}^{\alpha_{II}}) + (\hat{\mathbf{e}}_2 \cdot \mathbf{r}^{\beta_{II}}) (\mathbf{l}^{\beta_{II}} \cdot \mathbf{r}^{\alpha_{II}}) \right\} \alpha_{II}^2 \\ \left\{ (\hat{\mathbf{e}}_1 \cdot \mathbf{r}^{\beta_I}) (\mathbf{l}^{\beta_I} \cdot \mathbf{r}^{\alpha_{II}}) (V^2 - 2\beta_I^2) + (\hat{\mathbf{e}}_1 \cdot \mathbf{r}^{\beta_{II}}) (\mathbf{l}^{\beta_{II}} \cdot \mathbf{r}^{\alpha_{II}}) (V^2 - 2\beta_{II}^2) \right\} \alpha_{II}^2 \\ -2 (\hat{\mathbf{e}}_2 \cdot \mathbf{r}^{\beta_{II}}) \beta_{II}^2 \Theta_{\beta_{II}} \\ (\hat{\mathbf{e}}_1 \cdot \mathbf{r}^{\beta_{II}}) (V^2 - 2\beta_{II}^2) \beta_{II}^2 \Theta_{\beta_{II}} \\ 2 (\hat{\mathbf{e}}_2 \cdot \mathbf{r}^{\beta_{II}}) \beta_{II}^2 \\ (\hat{\mathbf{e}}_1 \cdot \mathbf{r}^{\beta_{II}}) (V^2 \Theta_{\beta_{II}} - 4\beta_{II}^2) \beta_{II}^2 \end{pmatrix} \begin{pmatrix} A_I \\ B_I \\ A_{II} \\ B_{II} \end{pmatrix}. \tag{321}
\end{aligned}$$

In compact notation, system (321) is

$$0 = \begin{pmatrix} \mathbf{D} & \mathbf{E} \\ \mathbf{F} & \mathbf{G} \end{pmatrix} \begin{pmatrix} \mathbf{C}_I \\ \mathbf{C}_{II} \end{pmatrix}, \tag{322}$$



where

$$\mathbf{D} = \begin{pmatrix} D_{11} (V^2 - \alpha_I^2) \Theta_{\alpha_I} & D_{12} \Theta_{\beta_I} \\ D_{21} (V^2 - \alpha_I^2) \Theta_{\alpha_I} & D_{22} (V^2 - 2\beta_I^2) \Theta_{\beta_I} \end{pmatrix}, \quad (323)$$

$$\mathbf{E} = \begin{pmatrix} E_{11} (V^2 - \alpha_{II}^2) \Theta_{\alpha_{II}} & E_{12} \Theta_{\beta_{II}} \\ E_{21} (V^2 - \alpha_{II}^2) \Theta_{\alpha_{II}} & E_{22} (V^2 - 2\beta_{II}^2) \Theta_{\beta_{II}} \end{pmatrix}, \quad (324)$$

$$\mathbf{F} = \begin{pmatrix} F_{11} & F_{12} \\ F_{21} V^2 - 2D_{21} \alpha_I^2 & F_{22} (V^2 \Theta_{\beta_I} - 4\beta_I^2) \end{pmatrix}, \quad (325)$$

$$\mathbf{G} = \begin{pmatrix} G_{11} & G_{12} \\ G_{21} V^2 - 2E_{21} \alpha_{II}^2 & G_{22} (V^2 \Theta_{\beta_{II}} - 4\beta_{II}^2) \end{pmatrix}, \quad (326)$$

in eqs (323)-(326) the coefficients  $D_{pq}$ ,  $E_{pq}$ ,  $F_{pq}$  and  $G_{pq}$  are independent of  $V$  variable, the subindex  $p$  and  $q$  are 1 or 2. Its explicit expressions linked with material properties are

$$D_{11} = (\hat{\mathbf{e}}_2 \cdot \mathbf{r}^{\beta_I}) (\mathbf{l}^{\beta_I} \cdot \mathbf{r}^{\alpha_I}) + (\hat{\mathbf{e}}_2 \cdot \mathbf{r}^{\beta_{II}}) (\mathbf{l}^{\beta_{II}} \cdot \mathbf{r}^{\alpha_I}), \quad (327)$$

$$D_{12} = -2 (\hat{\mathbf{e}}_2 \cdot \mathbf{r}^{\beta_I}) \beta_I^2, \quad (328)$$

$$D_{21} = (\hat{\mathbf{e}}_1 \cdot \mathbf{r}^{\beta_I}) (\mathbf{l}^{\beta_I} \cdot \mathbf{r}^{\alpha_I}) \beta_I^2 + (\hat{\mathbf{e}}_1 \cdot \mathbf{r}^{\beta_{II}}) (\mathbf{l}^{\beta_{II}} \cdot \mathbf{r}^{\alpha_I}) \beta_{II}^2, \quad (329)$$

$$D_{22} = (\hat{\mathbf{e}}_1 \cdot \mathbf{r}^{\beta_I}) \beta_I^2, \quad (330)$$

$$E_{11} = (\hat{\mathbf{e}}_2 \cdot \mathbf{r}^{\beta_I}) (\mathbf{l}^{\beta_I} \cdot \mathbf{r}^{\alpha_{II}}) + (\hat{\mathbf{e}}_2 \cdot \mathbf{r}^{\beta_{II}}) (\mathbf{l}^{\beta_{II}} \cdot \mathbf{r}^{\alpha_{II}}), \quad (331)$$

$$E_{12} = -2 (\hat{\mathbf{e}}_2 \cdot \mathbf{r}^{\beta_{II}}) \beta_{II}^2, \quad (332)$$

$$E_{21} = (\hat{\mathbf{e}}_1 \cdot \mathbf{r}^{\beta_I}) (\mathbf{l}^{\beta_I} \cdot \mathbf{r}^{\alpha_{II}}) \beta_I^2 + (\hat{\mathbf{e}}_1 \cdot \mathbf{r}^{\beta_{II}}) (\mathbf{l}^{\beta_{II}} \cdot \mathbf{r}^{\alpha_{II}}) \beta_{II}^2, \quad (333)$$

$$E_{22} = (\hat{\mathbf{e}}_1 \cdot \mathbf{r}^{\beta_{II}}) \beta_{II}^2, \quad (334)$$

$$F_{11} = \{ (\hat{\mathbf{e}}_2 \cdot \mathbf{r}^{\beta_I}) (\mathbf{l}^{\beta_I} \cdot \mathbf{r}^{\alpha_I}) + (\hat{\mathbf{e}}_2 \cdot \mathbf{r}^{\beta_{II}}) (\mathbf{l}^{\beta_{II}} \cdot \mathbf{r}^{\alpha_I}) \} \alpha_I^2, \quad (335)$$

$$F_{12} = 2 (\hat{\mathbf{e}}_2 \cdot \mathbf{r}^{\beta_I}) \beta_I^2, \quad (336)$$

$$F_{21} = \left\{ (\hat{\mathbf{e}}_1 \cdot \mathbf{r}^{\beta_1}) (\mathbf{l}^{\beta_1} \cdot \mathbf{r}^{\alpha_1}) + (\hat{\mathbf{e}}_1 \cdot \mathbf{r}^{\beta_{II}}) (\mathbf{l}^{\beta_{II}} \cdot \mathbf{r}^{\alpha_1}) \right\} \alpha_1^2, \quad (337)$$

$$F_{22} = (\hat{\mathbf{e}}_1 \cdot \mathbf{r}^{\beta_1}) \beta_1^2, \quad (338)$$

$$G_{11} = \left\{ (\hat{\mathbf{e}}_2 \cdot \mathbf{r}^{\beta_1}) (\mathbf{l}^{\beta_1} \cdot \mathbf{r}^{\alpha_{II}}) + (\hat{\mathbf{e}}_2 \cdot \mathbf{r}^{\beta_{II}}) (\mathbf{l}^{\beta_{II}} \cdot \mathbf{r}^{\alpha_{II}}) \right\} \alpha_{II}^2, \quad (339)$$

$$G_{12} = 2 (\hat{\mathbf{e}}_2 \cdot \mathbf{r}^{\beta_{II}}) \beta_{II}^2, \quad (340)$$

$$G_{21} = \left\{ (\hat{\mathbf{e}}_1 \cdot \mathbf{r}^{\beta_1}) (\mathbf{l}^{\beta_1} \cdot \mathbf{r}^{\alpha_{II}}) + (\hat{\mathbf{e}}_1 \cdot \mathbf{r}^{\beta_{II}}) (\mathbf{l}^{\beta_{II}} \cdot \mathbf{r}^{\alpha_{II}}) \right\} \alpha_{II}^2, \quad (341)$$

$$G_{22} = (\hat{\mathbf{e}}_1 \cdot \mathbf{r}^{\beta_{II}}) \beta_{II}^2. \quad (342)$$

Eq (322) has no trivial solution only if its determinant is zero, that is

$$0 = \begin{vmatrix} \mathbf{D} & \mathbf{E} \\ \mathbf{F} & \mathbf{G} \end{vmatrix}. \quad (343)$$

The  $2 \times 2$  matrices  $\mathbf{D}$ ,  $\mathbf{E}$ ,  $\mathbf{F}$  and  $\mathbf{G}$  are full matrices, so this determinant has a complex form in which the link of the dispersion relation with material properties are not transparent. Thus, physical arguments are used to obtain simple expressions that represent in a transparent manner these relationships.

## VI.12 The dispersion relation for extensional mode for closed-pore stress-free boundary condition

For the extensional mode of vibration the four  $\Theta$  functions (eqs 223, 225, 228 and 230) are independent of the complex velocity squared,  $V$ , hence the closed-pore dispersion relation could be written as

$$0 = a_3 (V^2)^3 + a_2 (V^2)^2 + a_1 V^2 + a_0 \quad (344)$$

where

$$\begin{aligned}
a_3 &= [(-D_{22}E_{11}F_{11}G_{22} + D_{21}E_{11}F_{12}G_{22} + E_{11}E_{22}F_{11}F_{22} - D_{11}E_{21}F_{12}G_{22}) \Theta_{\beta_{\mathbb{I}}} \\
&\quad - D_{21}E_{11}F_{22}G_{12} + D_{11}E_{21}F_{22}G_{12} + D_{22}E_{11}F_{21}G_{12}] \Theta_{\alpha_{\mathbb{I}}} \\
&\quad + (D_{11}D_{22}G_{11}G_{22} - D_{11}E_{22}F_{22}G_{11} + D_{11}E_{22}F_{12}G_{21}) \Theta_{\beta_{\mathbb{I}}} - D_{11}D_{22}G_{12}G_{21}, \tag{345}
\end{aligned}$$

$$\begin{aligned}
a_2 &= \left[ \left\{ (2D_{21}E_{11}E_{22}F_{12} - D_{21}E_{11}F_{12}G_{22} + D_{11}E_{21}F_{12}G_{22}) \alpha_{\mathbb{I}}^2 \right. \right. \\
&\quad + (E_{11}E_{22}F_{21}F_{12} - D_{21}E_{11}F_{12}G_{22} + D_{22}E_{11}F_{11}G_{22} - E_{11}E_{22}F_{11}F_{22} + D_{11}E_{21}F_{12}G_{22}) \alpha_{\mathbb{I}}^2 \\
&\quad + (2D_{22}E_{11}F_{11}G_{22} - 4E_{11}E_{22}F_{11}F_{22}) \beta_{\mathbb{I}}^2 + (-2E_{11}E_{22}F_{11}F_{22} + 2E_{11}E_{22}F_{12}F_{21}) \beta_{\mathbb{I}}^2 \\
&\quad - E_{12}E_{21}F_{11}F_{22} + D_{12}E_{21}F_{11}G_{22} + E_{12}E_{21}F_{12}F_{21} \left. \right\} \Theta_{\beta_{\mathbb{I}}} \\
&\quad + (-2D_{21}D_{22}E_{11}G_{12} - D_{11}E_{21}F_{22}G_{12} + D_{21}E_{11}F_{22}G_{12}) \alpha_{\mathbb{I}}^2 \\
&\quad + (D_{21}E_{11}F_{22}G_{12} - D_{22}E_{11}F_{21}G_{12} - D_{11}E_{21}F_{22}G_{12}) \alpha_{\mathbb{I}}^2 \\
&\quad + (-4D_{11}E_{21}F_{22}G_{12} - 2D_{22}E_{11}F_{21}G_{12} + 4D_{21}E_{11}F_{22}G_{12}) \beta_{\mathbb{I}}^2 \\
&\quad + (-4D_{21}E_{11}F_{12}G_{22} + 4D_{22}E_{11}F_{11}G_{22} + 4D_{11}E_{21}F_{12}G_{22}) \beta_{\mathbb{I}}^2 - D_{12}E_{21}F_{21}G_{12} \left. \right] \Theta_{\alpha_{\mathbb{I}}} \\
&\quad + \left\{ (-D_{11}E_{22}F_{12}G_{21} - D_{11}D_{22}G_{11}G_{22} + D_{11}E_{22}F_{22}G_{11}) \alpha_{\mathbb{I}}^2 - 2D_{11}E_{21}E_{22}F_{12}\alpha_{\mathbb{I}}^2 \right. \\
&\quad + (-2D_{11}D_{22}G_{11}G_{22} + 4D_{11}E_{22}F_{22}G_{11}) \beta_{\mathbb{I}}^2 + (2D_{11}E_{22}F_{22}G_{11} - 2D_{11}E_{22}F_{12}G_{21}) \beta_{\mathbb{I}}^2 \\
&\quad + D_{22}E_{12}F_{11}G_{21} + D_{21}E_{12}G_{11}F_{22} - D_{12}E_{22}F_{11}G_{21} + D_{12}E_{22}F_{21}G_{11} \\
&\quad - D_{22}E_{12}G_{11}F_{21} - D_{21}E_{12}F_{12}G_{21} - D_{21}D_{12}G_{11}G_{22} \left. \right\} \Theta_{\beta_{\mathbb{I}}} + D_{21}D_{12}G_{12}G_{21} \\
&\quad + D_{11}D_{22}G_{12}G_{21}\alpha_{\mathbb{I}}^2 - 4D_{11}D_{22}G_{11}G_{22}\beta_{\mathbb{I}}^2 + 2D_{11}D_{22}E_{21}G_{12}\alpha_{\mathbb{I}}^2 + 2D_{11}D_{22}G_{12}G_{21}\beta_{\mathbb{I}}^2, \tag{346}
\end{aligned}$$

$$\begin{aligned}
a_1 &= \left[ \left\{ (-2D_{21}E_{11}E_{22}F_{12} + D_{21}E_{11}F_{12}G_{22} - D_{11}E_{21}F_{12}G_{22}) \alpha_{\mathbb{I}}^2 \right. \right. \\
&\quad - 4D_{21}E_{11}E_{22}F_{12}\beta_{\mathbb{I}}^2 - 2D_{21}E_{12}E_{21}F_{12} \left. \right\} \alpha_{\mathbb{I}}^2 \\
&\quad + \left( (-2D_{22}E_{11}F_{11}G_{22} + 4E_{11}E_{22}F_{11}F_{22}) \beta_{\mathbb{I}}^2 + (2E_{11}E_{22}F_{11}F_{22} - 2E_{11}E_{22}F_{12}F_{21}) \beta_{\mathbb{I}}^2 \right.
\end{aligned}$$

$$\begin{aligned}
& + (E_{12}E_{21}F_{11}F_{22} - D_{12}E_{21}F_{11}G_{22} - E_{12}E_{21}F_{12}F_{21}) \alpha_{\mathbb{I}}^2 \\
& + (4E_{12}E_{21}F_{11}F_{22} + E_{11}E_{22}F_{11}F_{22}) \beta_{\mathbb{I}}^2 \} \Theta_{\beta_{\mathbb{I}}} \\
& + \left( (-2D_{21}F_{22}E_{11}G_{12} + 2D_{21}D_{22}E_{11}G_{12} + D_{11}E_{21}F_{22}G_{12}) \alpha_{\mathbb{I}}^2 \right. \\
& + (4D_{11}E_{21}F_{22}G_{12} - 4D_{21}E_{11}F_{22}G_{12} + 4D_{21}D_{22}E_{11}G_{12}) \beta_{\mathbb{I}}^2 \\
& + (-4D_{11}E_{21}F_{12}G_{22} + 4D_{21}E_{11}F_{12}G_{22}) \beta_{\mathbb{I}}^2 + 2D_{21}D_{12}E_{21}G_{12} \left. \right) \alpha_{\mathbb{I}}^2 \\
& + \left( (-4D_{21}E_{11}F_{22}G_{12} + 4D_{11}E_{21}F_{22}G_{12} + 2D_{22}E_{11}F_{21}G_{12}) \beta_{\mathbb{I}}^2 \right. \\
& + (4D_{21}E_{11}F_{12}G_{22} - 4D_{22}E_{11}F_{11}G_{22} - 4D_{11}E_{21}F_{12}G_{22}) \beta_{\mathbb{I}}^2 \\
& + D_{12}E_{21}F_{21}G_{12} \left. \right) \alpha_{\mathbb{I}}^2 - 8D_{22}E_{11}F_{11}G_{22}\beta_{\mathbb{I}}^2\beta_{\mathbb{I}}^2 - 4D_{12}E_{21}F_{11}G_{22}\beta_{\mathbb{I}}^2 \left. \right] \Theta_{\alpha_{\mathbb{I}}} \\
& + \left[ \left\{ 2D_{11}E_{22}E_{21}F_{12}\alpha_{\mathbb{I}}^2 + (2D_{11}D_{22}G_{11}G_{22} - 4D_{11}E_{22}F_{22}G_{11}) \beta_{\mathbb{I}}^2 \right. \right. \\
& + (-2D_{11}E_{22}F_{22}G_{11} + 2D_{11}E_{22}F_{12}G_{21}) \beta_{\mathbb{I}}^2 - 2D_{21}D_{12}E_{22}G_{11} + 2D_{21}D_{22}E_{12}G_{11} \\
& - D_{21}E_{12}F_{22}G_{11} + D_{21}D_{12}G_{11}G_{22} + D_{21}E_{12}F_{12}G_{21} \left. \right\} \alpha_{\mathbb{I}}^2 \\
& + (2D_{21}E_{12}E_{21}F_{12} - 2D_{22}E_{12}E_{21}F_{11} + 4D_{11}E_{22}E_{21}F_{12}\beta_{\mathbb{I}}^2 + 2D_{12}E_{21}E_{22}F_{11}) \alpha_{\mathbb{I}}^2 \\
& + (2D_{22}E_{12}F_{21}G_{11} - 4D_{21}E_{12}F_{22}G_{11} - 8D_{11}E_{22}F_{22}G_{11}\beta_{\mathbb{I}}^2 - 2D_{22}E_{12}F_{11}G_{21}) \beta_{\mathbb{I}}^2 \\
& + (-2D_{12}E_{22}F_{21}G_{11} + 2D_{12}E_{22}F_{11}G_{21}) \beta_{\mathbb{I}}^2 \left. \right] \Theta_{\beta_{\mathbb{I}}} \\
& + \left( -D_{21}D_{12}G_{12}G_{21} - 2D_{11}D_{22}G_{12}G_{21}\beta_{\mathbb{I}}^2 + 4D_{11}D_{22}G_{11}G_{22}\beta_{\mathbb{I}}^2 - 2D_{11}D_{22}G_{12}E_{21}\alpha_{\mathbb{I}}^2 \right) \alpha_{\mathbb{I}}^2 \\
& + \left( -2D_{21}D_{12}E_{21}G_{12} - 4D_{11}D_{22}G_{12}E_{21}\beta_{\mathbb{I}}^2 \right) \alpha_{\mathbb{I}}^2 + 4D_{21}D_{12}G_{11}G_{22}\beta_{\mathbb{I}}^2 \\
& + 8D_{11}D_{22}G_{11}G_{22}\beta_{\mathbb{I}}^2\beta_{\mathbb{I}}^2, \tag{347}
\end{aligned}$$

$$\begin{aligned}
a_0 & = \left[ \left\{ (2D_{21}E_{12}E_{21}F_{12} + 4D_{21}E_{11}E_{22}F_{12}\beta_{\mathbb{I}}^2) \alpha_{\mathbb{I}}^2\alpha_{\mathbb{I}}^2 \right. \right. \\
& + (-4E_{21}E_{12}F_{11}F_{22} - 8E_{11}E_{22}F_{11}F_{22}\beta_{\mathbb{I}}^2) \beta_{\mathbb{I}}^2\alpha_{\mathbb{I}}^2 \left. \right\} \Theta_{\beta_{\mathbb{I}}} \\
& + \left\{ (-4D_{11}E_{21}F_{22}G_{12} + 4D_{21}E_{11}F_{22}G_{12} - 4D_{21}D_{22}E_{11}G_{12}) \beta_{\mathbb{I}}^2 \right. \\
& + (4D_{11}E_{21}F_{12}G_{22} - 4D_{21}E_{11}F_{12}G_{22}) \beta_{\mathbb{I}}^2 - 2D_{21}D_{12}E_{21}G_{12} \left. \right\} \alpha_{\mathbb{I}}^2\alpha_{\mathbb{I}}^2 \\
& + \left. \left( 8D_{22}E_{11}F_{11}G_{22}\beta_{\mathbb{I}}^2\beta_{\mathbb{I}}^2 + 4D_{12}E_{21}F_{11}G_{22}\beta_{\mathbb{I}}^2 \right) \alpha_{\mathbb{I}}^2 \right] \Theta_{\alpha_{\mathbb{I}}}
\end{aligned}$$

$$\begin{aligned}
& + \left[ \left\{ \left( -4D_{11}E_{22}E_{21}F_{12}\beta_{\text{II}}^2 - 2D_{21}E_{12}E_{21}F_{12} \right) \alpha_{\text{II}}^2 \right. \right. \\
& + \left( 4D_{21}E_{12}F_{22}G_{11} - 4D_{21}D_{22}E_{12}G_{11} + 8D_{11}E_{22}F_{22}G_{11}\beta_{\text{II}}^2 \right) \beta_{\text{I}}^2 \\
& + \left. 4D_{21}D_{12}E_{22}G_{11}\beta_{\text{II}}^2 \right\} \alpha_{\text{I}}^2 + \left( -4D_{12}E_{22}E_{21}F_{12}\beta_{\text{II}}^2 + 4D_{22}E_{12}E_{21}F_{11}\beta_{\text{I}}^2 \right) \alpha_{\text{II}}^2 \Big] \Theta_{\beta_{\text{II}}} \\
& + \left\{ \left( 2D_{21}D_{12}E_{21}G_{12} + 4D_{11}D_{22}E_{21}G_{12}\beta_{\text{I}}^2 \right) \alpha_{\text{II}}^2 \right. \\
& \left. - 8D_{11}D_{22}G_{11}G_{22}\beta_{\text{I}}^2\beta_{\text{II}}^2 - 4D_{21}D_{12}G_{11}G_{22}\beta_{\text{II}}^2 \right\} \alpha_{\text{I}}^2.
\end{aligned} \tag{348}$$

## VI.13 Numerical solution

Eq (344) can be represented as  $\text{Det}(V^2\mathbf{I} - \mathbf{M}) = 0$  where  $\mathbf{M}$  is the companion matrix which has the following form (Golub et. al, 1996 section 7.4.6)

$$\mathbf{M} = \begin{pmatrix} 0 & 0 & -\frac{a_0}{a_3} \\ 1 & 0 & -\frac{a_1}{a_3} \\ 0 & 1 & -\frac{a_2}{a_3} \end{pmatrix}. \tag{349}$$

The eigenvalues of matrix (349) are then calculated and they are the roots of eq (344). In order to get some insight, the numerical computations of the eigenvalues of the companion matrix associated to eq (349) are presented for a sample of Berea Sandstone for a wide range of frequency values. The physical properties used are listed in appendix B. In Figs. 25-27 they are plotted as blue curves the real part of  $V$ , in compact notation it is represented by  $\Re V$ . Instead of plotting the imaginary part of  $V$ , that is represented by  $\Im V$ , the ratio  $\frac{\Im V}{\Re V}$ , which defines the quality factor  $Q$  are plotted as red curves.

Above the modified Biot critical frequency,  $\Omega$ , Figs 25-27 shows instabilities, thats the reason to reduce the analysis of study to the frequency range below  $\Omega$ , which is the frequency range that is used in laboratory experiments. One of the reason of those instabilities could be the boundary condition established which in reality to have a

closed-pore stress-free condition the boundary value problem to solve is the two concentric cylinders, in which the outer's thin goes to zero. Below  $\Omega$  the solution is taken as properly because the radial boundary is not affected it. Near  $\Omega$ , the curves show a kink that could be interpreted like an artifacts, however above this frequency the curves are unphysical solution of this boundary value problem. So, the three roots of closed-pore boundary value problem are replotted in Figs 28-30 for the frequency range below  $\Omega$ .

Fig. 28 shows a constant behavior of the phase velocity (blue-solid curve) which is larger than the fast-S wave phase velocity (black-solid curve) and smaller than fast-P wave phase velocity (purple-solid curve). The attenuation curve (red-solid curve) shows an increasing linear trend with frequency which is larger than the fast-P attenuation (purple-dashed curve) and smaller than the fast-S attenuation (black-dashed curve). In Fig. 29 the  $\Re V$  (blue-solid curve) shows an increasing linear trend with frequency. At the lower frequencies its value is almost similar to the slow-P wave phase velocity (purple-solid curve) but as frequency increases the difference increases but always is limited by the slow-P wave phase velocity. The attenuation (red-solid curve) shows a decreasing trend with frequency. At the lower frequencies its value is almost similar to the slow-P attenuation (purple-dashed curve) but as frequency increases the difference increases. It can be thought as a diffusive extensional process.

In Fig 30 the  $\Re V$  (blue-solid curve) shows an increasing linear trend with frequency. It is always limited above by the slow-P wave phase velocity (purple-solid curve). The attenuation (red-solid curve) shows a decreasing trend with frequency. It is always limited below by the slow-P attenuation (purple-dashed curve). It can be thought as a diffusive extensional process also.

Although it is easy to obtain the analytical root that give us the extensional closed-pore stress-free wave the dependence on material properties is not transparent in them. For any given set of material-parameters, the phase velocity and attenuation curves show their simple dependence, although in the exact expressions given the dependences are not apparent. In the following section using physical arguments an approximate second order extensional dispersion relation, which roots are nearly equal to the exact values of the cubic extensional dispersion relation roots, are deduced. This procedure renders the approximate expressions for phase velocity and attenuation such that the implicit relations with material properties become transparent.

## VI.14 The complex closed-pore extensional expression in terms of material properties

For realistic geomaterials the slow S velocity is negligible, so it gives that the contribution of  $\Theta_{\beta_{\text{II}}}$  and  $\beta_{\text{II}}$  are negligible. Thus, the  $a$ 's coefficients in the dispersion relation (344) are simplified as

$$a_3 = [-D_{21}E_{11}F_{22} + D_{11}E_{21}F_{22} + D_{22}E_{11}F_{21}] \Theta_{\alpha_{\text{II}}} - D_{11}D_{22}G_{21}, \quad (350)$$

$$\begin{aligned} a_2 = & \left[ (-2D_{21}D_{22}E_{11} - D_{11}E_{21}F_{22} + D_{21}E_{11}F_{22}) \alpha_{\text{I}}^2 \right. \\ & + (D_{21}E_{11}F_{22} - D_{22}E_{11}F_{21} - D_{11}E_{21}F_{22}) \alpha_{\text{II}}^2 \\ & + (-4D_{11}E_{21}F_{22} - 2D_{22}E_{11}F_{21} + 4D_{21}E_{11}F_{22}) \beta_{\text{I}}^2 - D_{12}E_{21}F_{21} \left. \right] \Theta_{\alpha_{\text{II}}} \\ & + D_{21}D_{12}G_{21} + D_{11}D_{22}G_{21}\alpha_{\text{I}}^2 + 2D_{11}D_{22}E_{21}\alpha_{\text{II}}^2 + 2D_{11}D_{22}G_{21}\beta_{\text{I}}^2, \end{aligned} \quad (351)$$

$$a_1 = \left[ \left\{ (-D_{21}F_{22}E_{11} + 2D_{21}D_{22}E_{11} + D_{11}E_{21}F_{22}) \alpha_{\text{II}}^2 \right. \right.$$

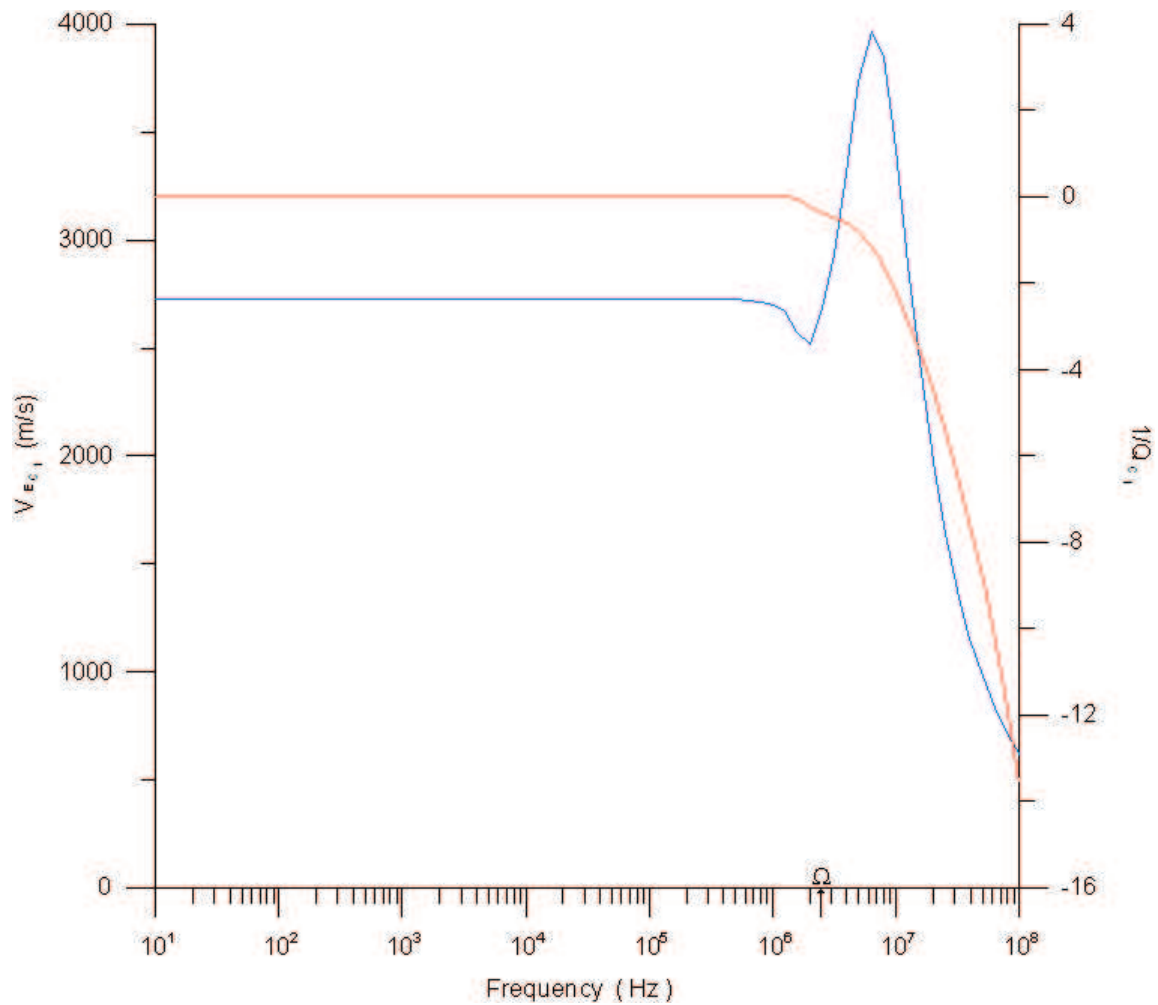


Figure 49. The plot of extensional phase velocity (blue-solid curve) and attenuation (red-solid curve) versus frequency; obtained from the first root of eq (344). For clarity the crossover frequency the modified Biot critical frequency,  $\Omega$ , is marked.



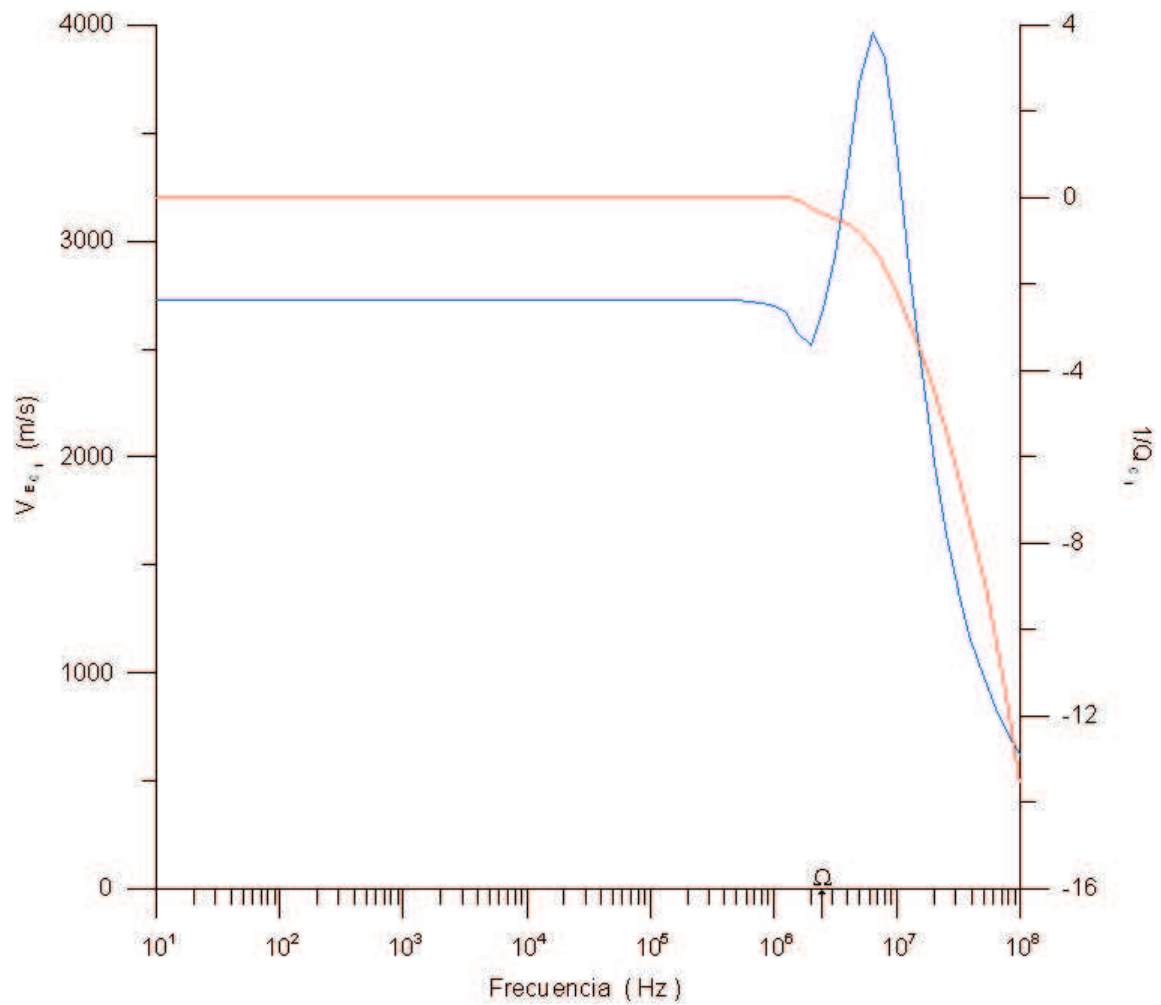


Figure 50. Gráfica de la velocidad de fase extensional (curva continua azul) y la atenuación (curva continua roja) contra la frecuencia; obtenida a partir de la primera raíz de la ec (344). Por claridad también se muestra la frecuencia crítica de Biot modificada,  $\Omega$ .

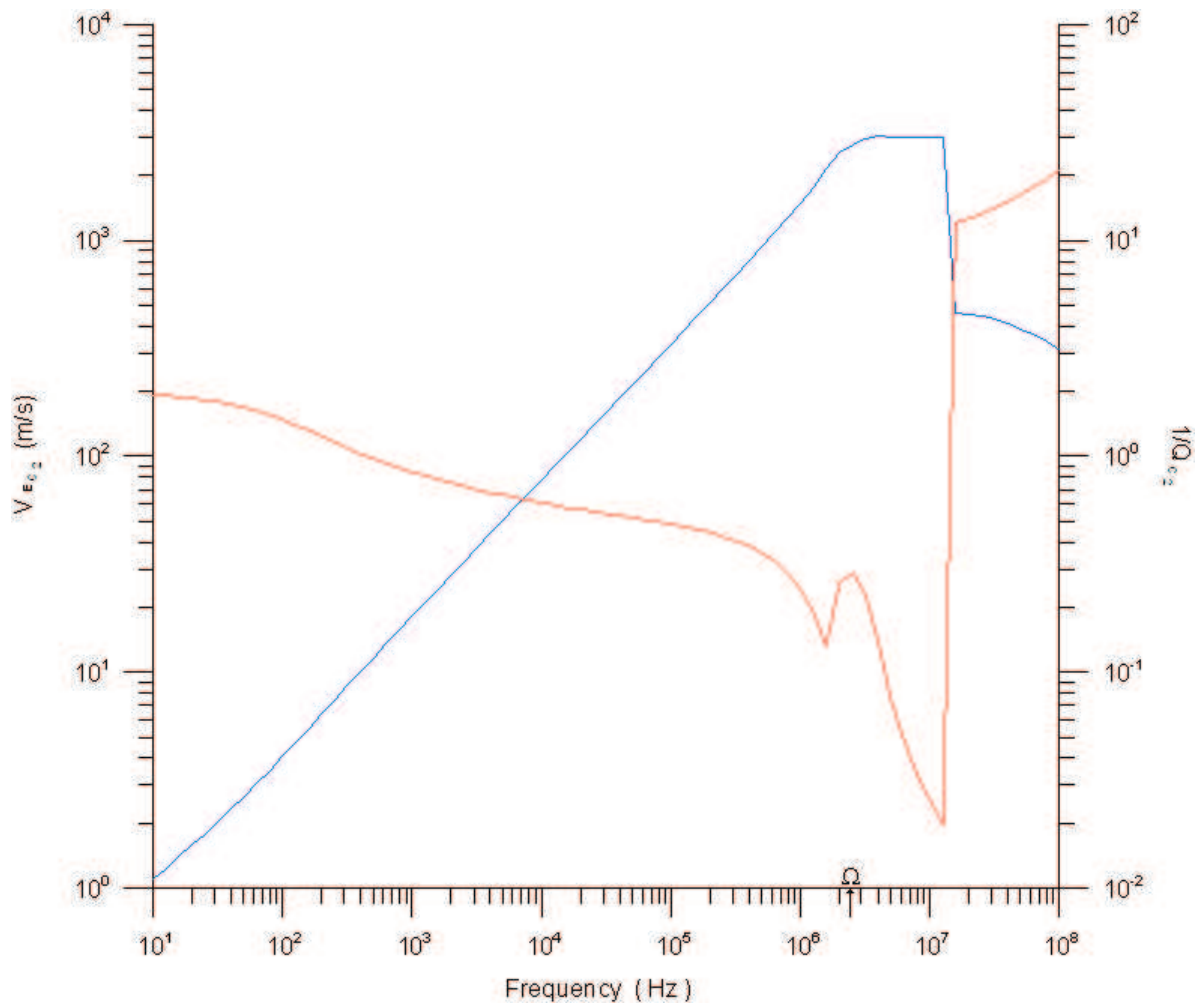


Figure 51. The plot of extensional phase velocity (blue-solid curve) and attenuation (red-solid curve) versus frequency; obtained from the second root of eq (344). For clarity the crossover frequency the modified Biot critical frequency,  $\Omega$ , is marked.

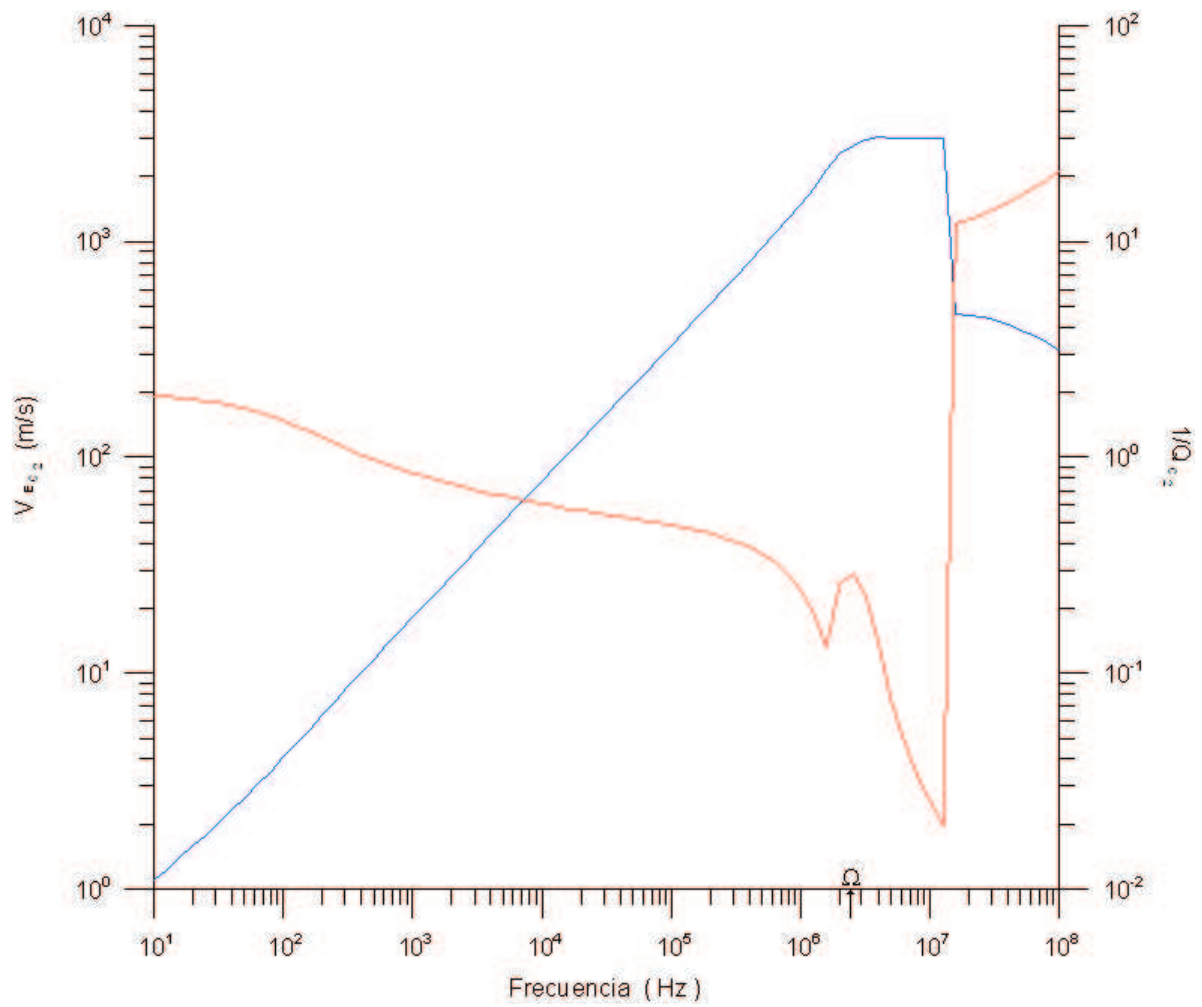


Figure 52. Gráfica de la velocidad de fase extensional (curva continua azul) y la atenuación (curva continua roja) contra la frecuencia; obtenida a partir de la segunda raíz de la ec (344). Por claridad también se muestra la frecuencia crítica de Biot modificada,  $\Omega$ .

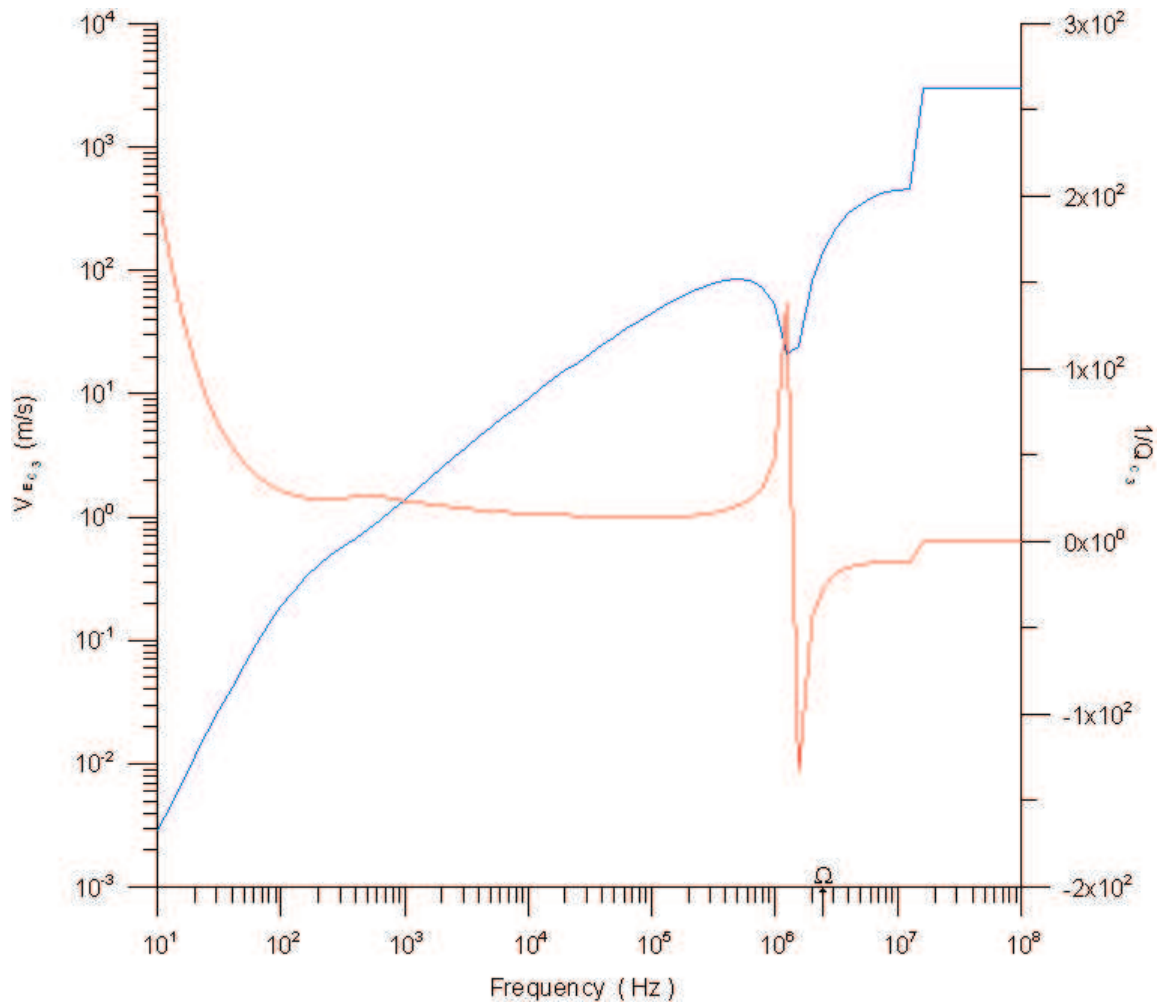


Figure 53. The plot of extensional phase velocity (blue-solid curve) and attenuation (red-solid curve) versus frequency; obtained from the third root of eq (344). For clarity the crossover frequency the modified Biot critical frequency,  $\Omega$ , is marked.

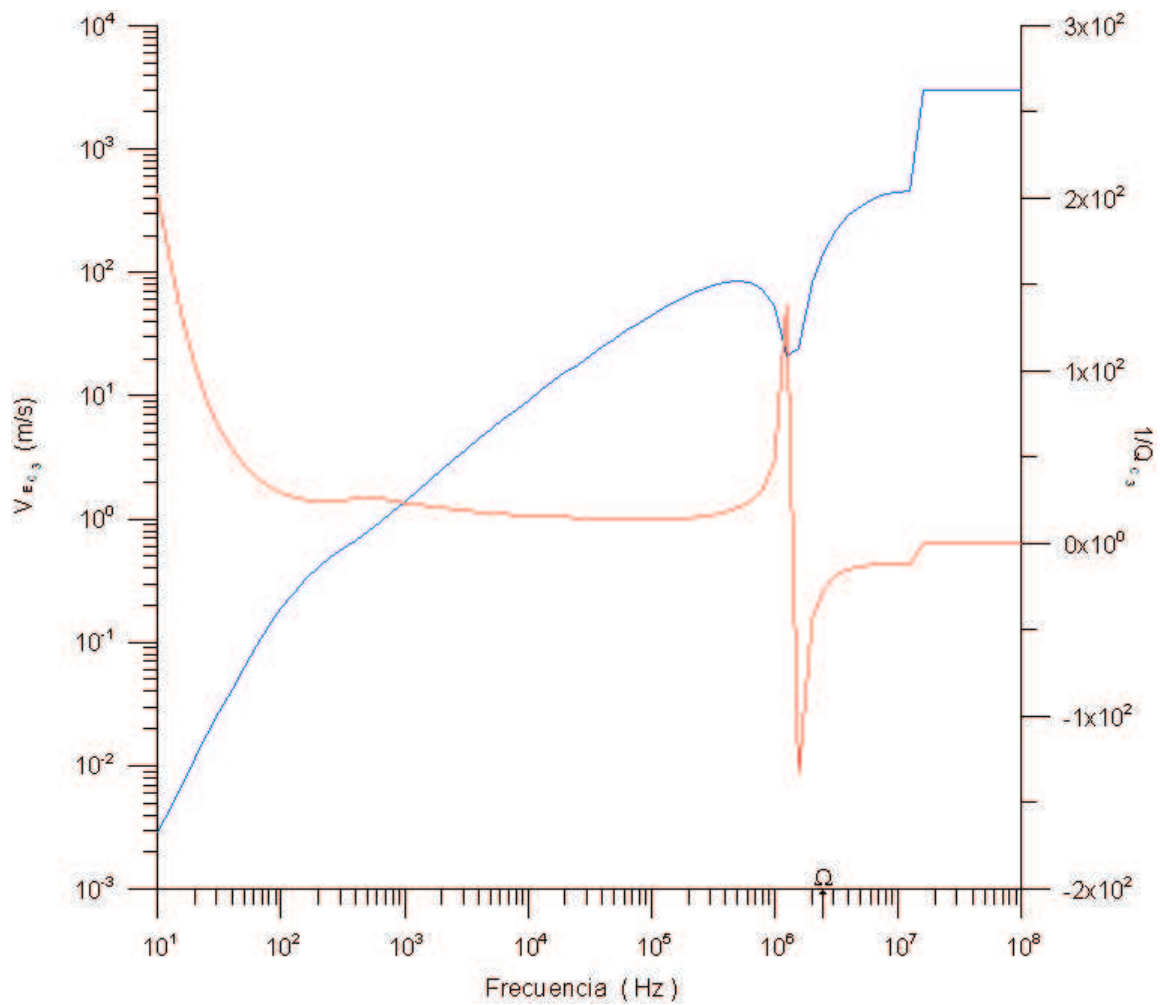


Figure 54. Gráfica de la velocidad de fase extensional (curva continua azul) y la atenuación (curva continua roja) contra la frecuencia; obtenida a partir de la tercera raíz de la ec (344). Por claridad también se muestra la frecuencia crítica de Biot modificada,  $\Omega$ .

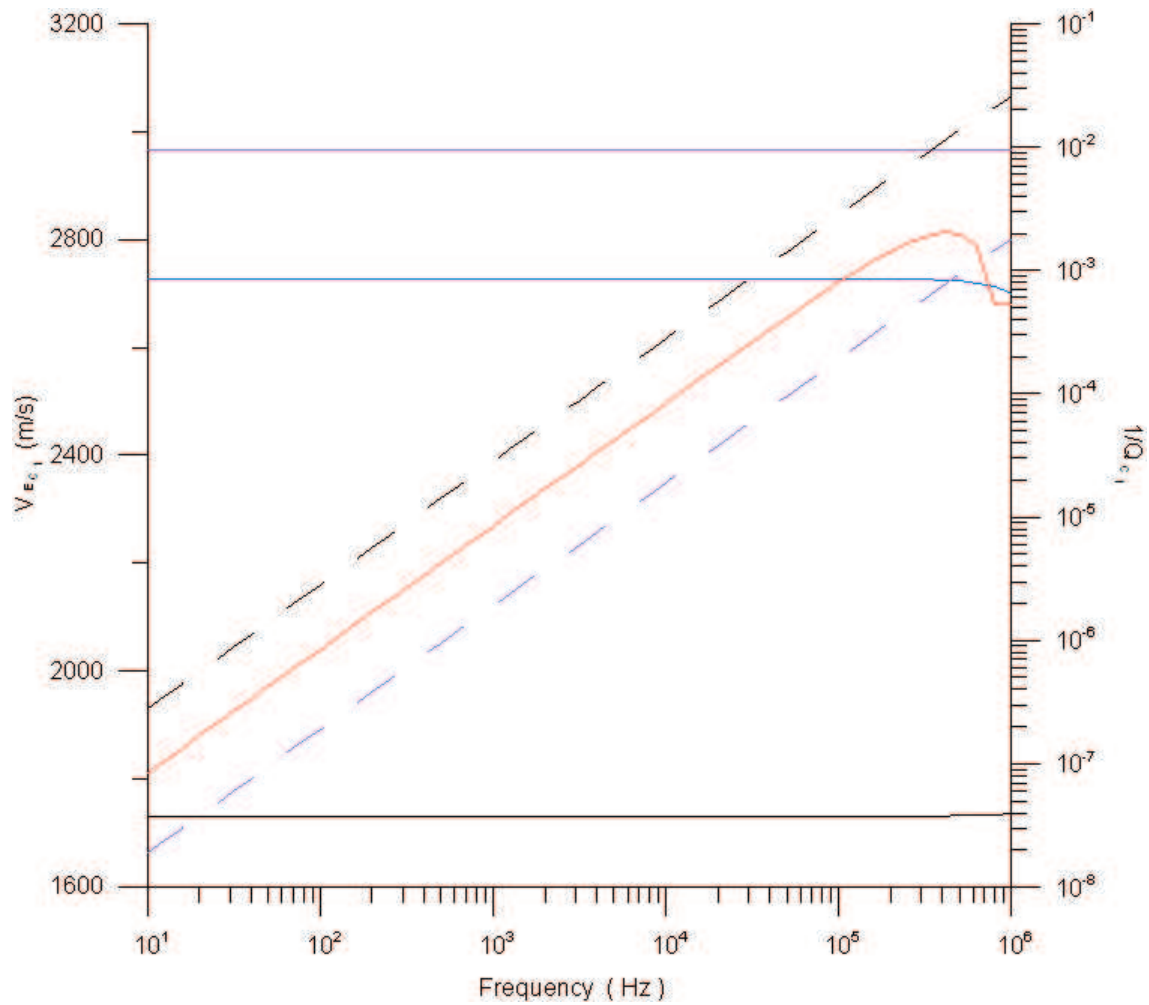


Figure 55. The plot of extensional phase velocity (blue curve) and attenuation (red curve) versus frequency; obtained from the first root of eq (344) for the frequency regime below  $\Omega$ .

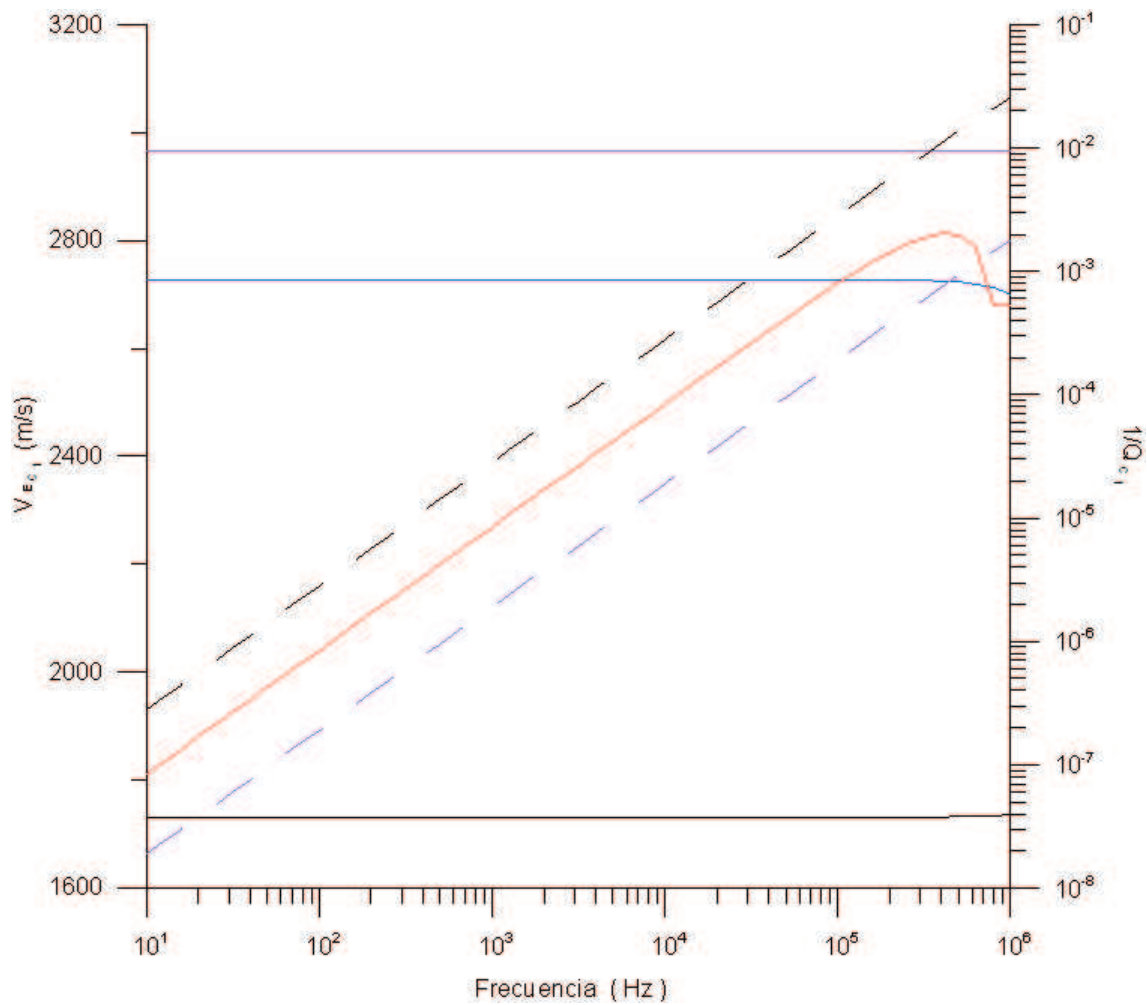


Figure 56. Gráfica de la velocidad de fase extensional (curva continua azul) y la atenuación (curva continua roja) contra la frecuencia; obtenida a partir de la primera raíz de la ec (344) para la región por debajo de  $\Omega$ .

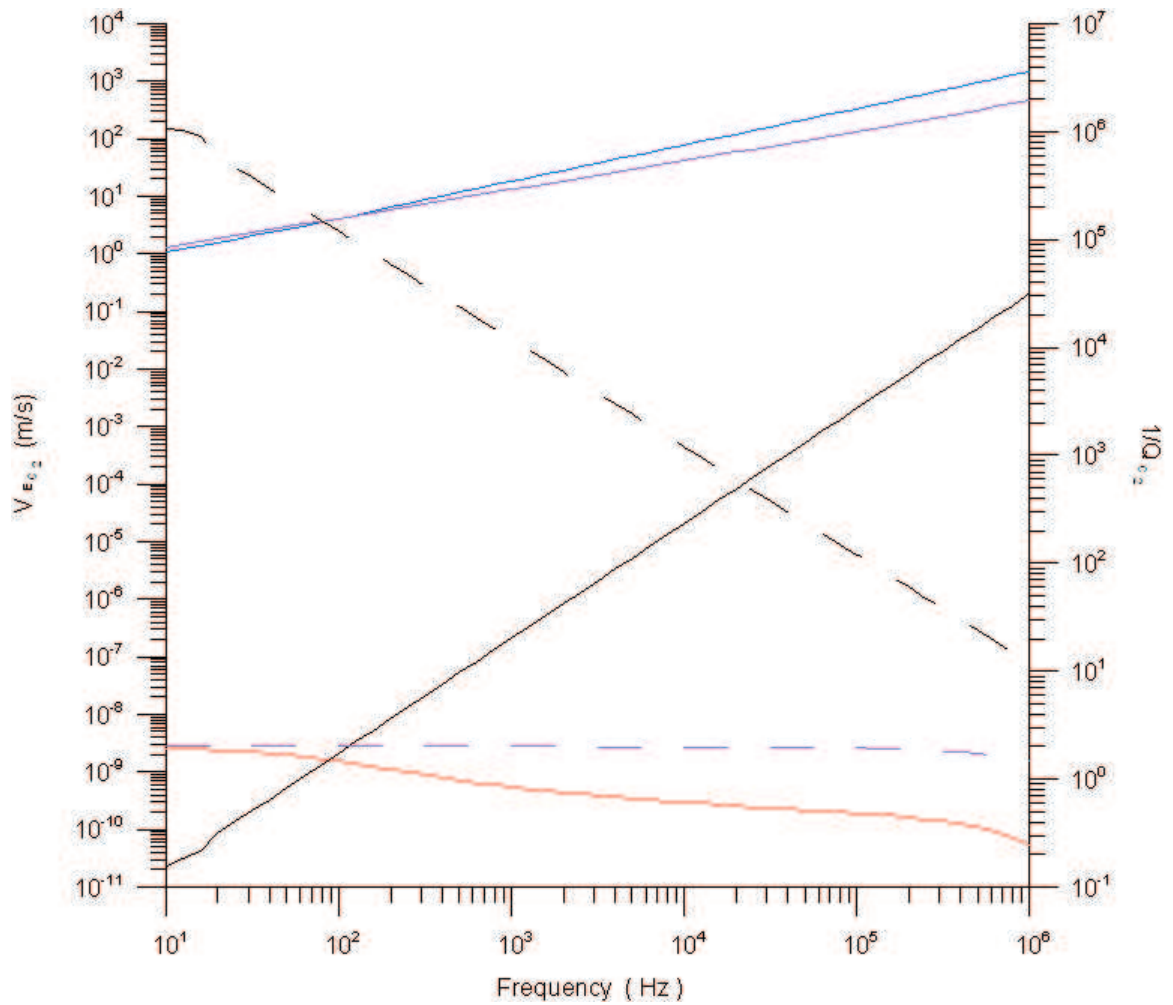


Figure 57. The plot of extensional phase velocity (blue curve) and attenuation (red curve) versus frequency; obtained from the second root of eq (344) for the frequency regime below  $\Omega$ .



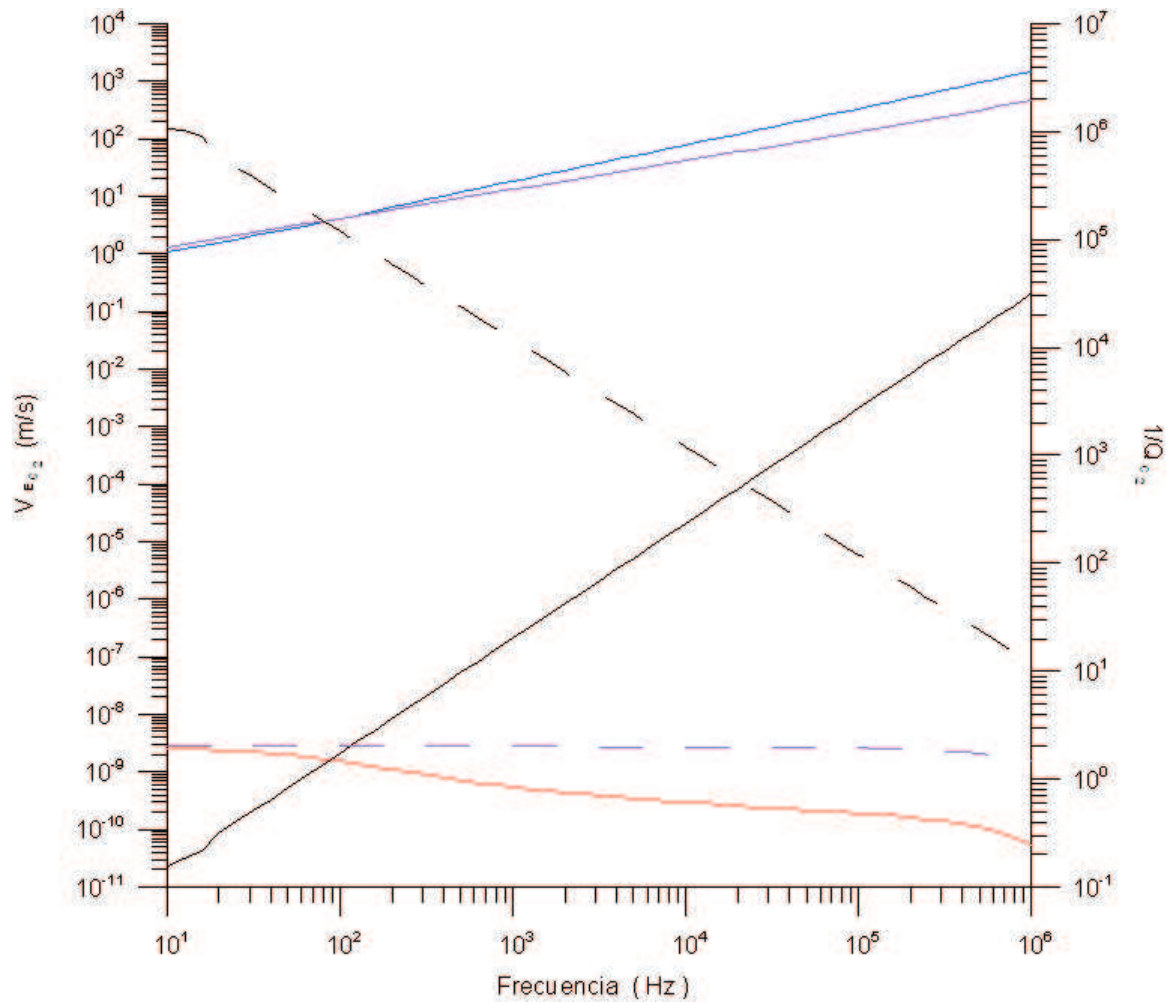


Figure 58. Gráfica de la velocidad de fase extensional (curva continua azul) y la atenuación (curva continua roja) contra la frecuencia; obtenida a partir de la segunda raíz de la ec (344) para la región por debajo de  $\Omega$ .

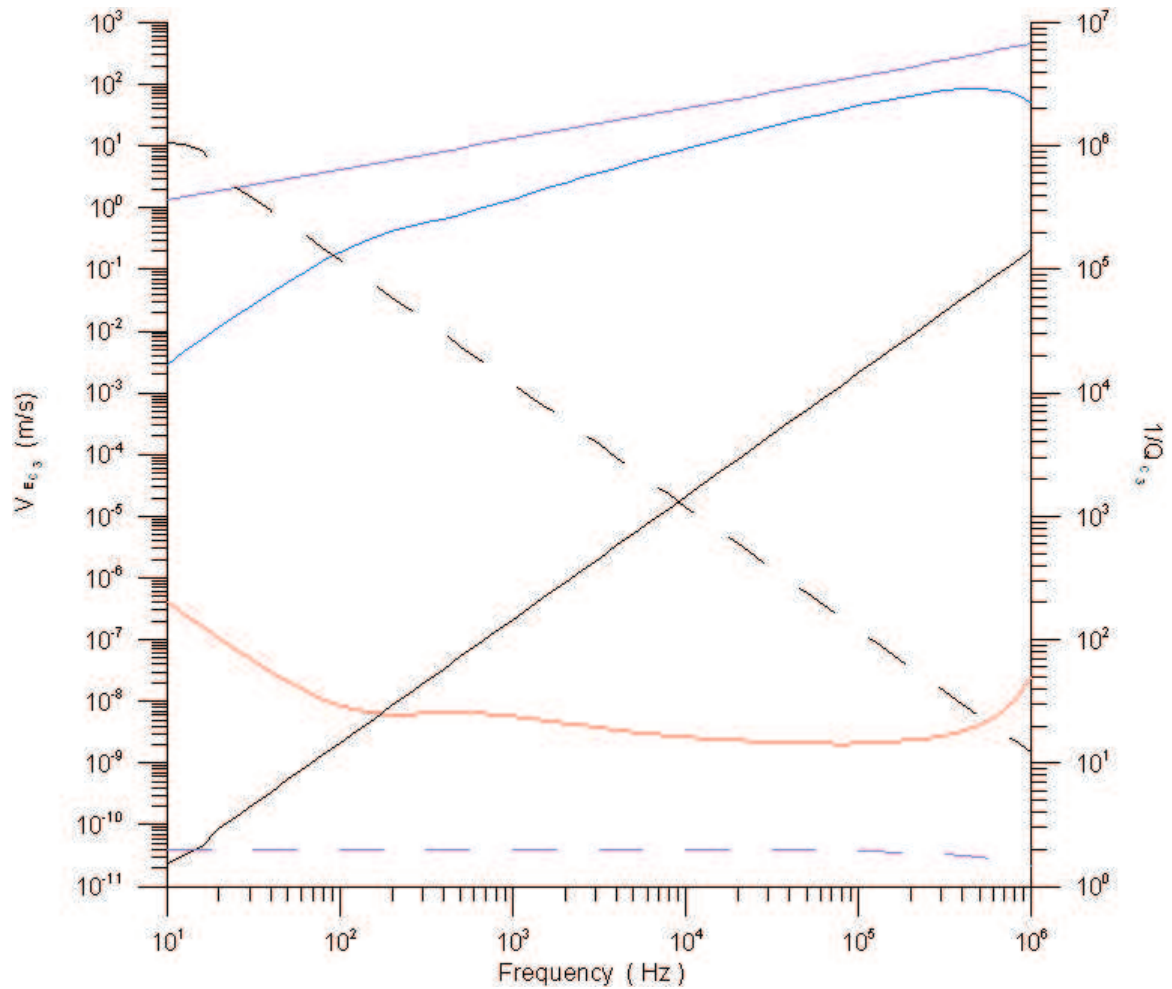


Figure 59. The plot of extensional phase velocity (blue curve) and attenuation (red curve) versus frequency; obtained from the third root of eq (344) for the frequency regime below  $\Omega$ .

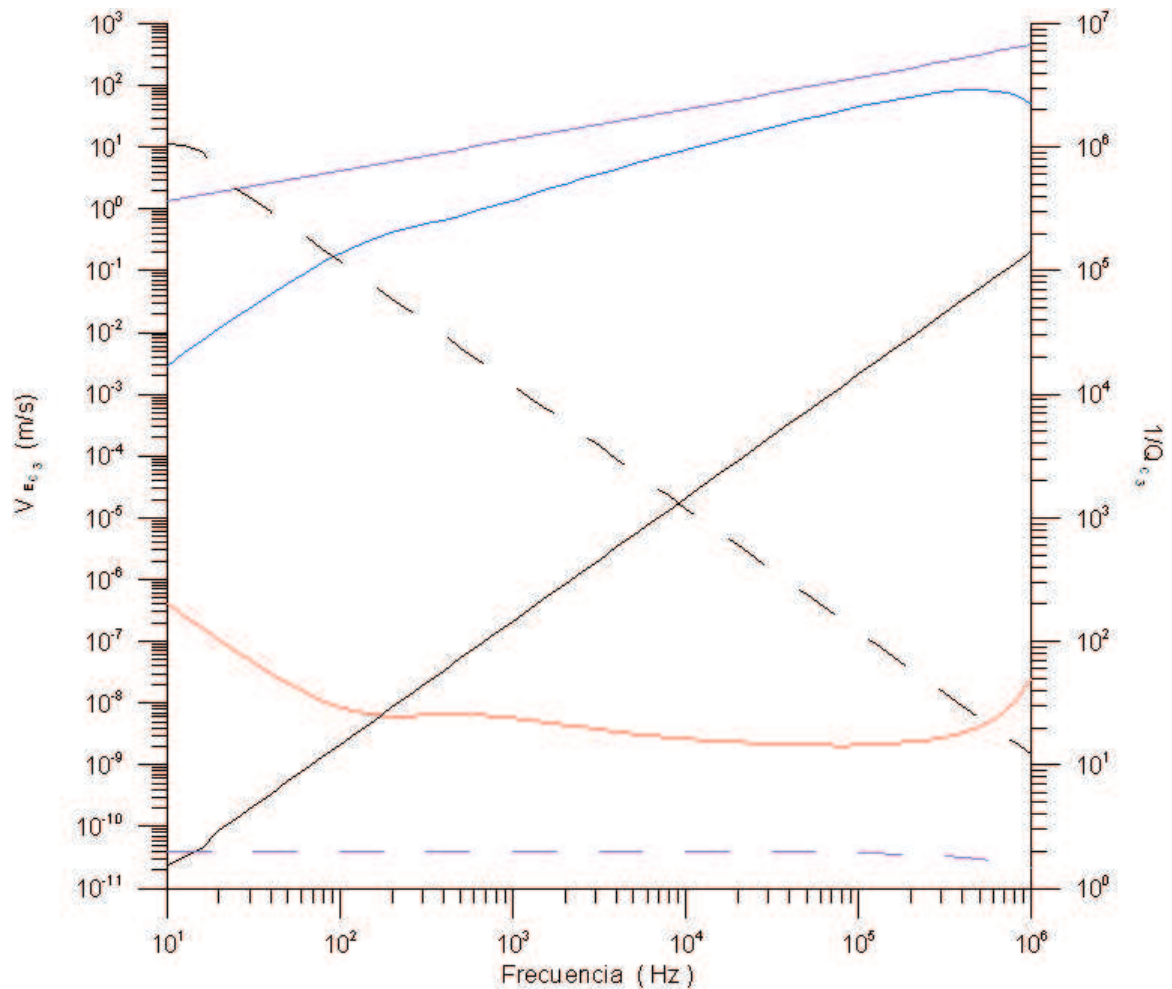


Figure 60. Gráfica de la velocidad de fase extensional (curva continua azul) y la atenuación (curva continua roja) contra la frecuencia; obtenida a partir de la tercera raíz de la ec (344) para la región por debajo de  $\Omega$ .

$$\begin{aligned}
& + (4D_{11}E_{21}F_{22} - 4D_{21}E_{11}F_{22} + 4D_{21}D_{22}E_{11})\beta_I^2 + 2D_{21}D_{12}E_{21}\} \alpha_I^2 \\
& + \left\{(-4D_{21}E_{11}F_{22} + 4D_{11}E_{21}F_{22} + 2D_{22}E_{11}F_{21})\beta_I^2 + D_{12}E_{21}F_{21}\right\} \alpha_{II}^2 \Theta_{\alpha_{II}} \\
& + \left(-D_{21}D_{12}G_{21} - 2D_{11}D_{22}G_{21}\beta_I^2 - 2D_{11}D_{22}E_{21}\alpha_{II}^2\right) \alpha_I^2 \\
& + \left(-2D_{21}D_{12}E_{21} - 4D_{11}D_{22}E_{21}\beta_I^2\right) \alpha_{II}^2, \tag{352}
\end{aligned}$$

$$\begin{aligned}
a_0 & = \left[(-4D_{11}E_{21}F_{22} + 4D_{21}E_{11}F_{22} - 4D_{21}D_{22}E_{11})\beta_I^2 - 2D_{21}D_{12}E_{21}\right] \alpha_I^2 \alpha_{II}^2 \Theta_{\alpha_{II}} \\
& + \left(2D_{21}D_{12}E_{21} + 4D_{11}D_{22}E_{21}\beta_I^2\right) \alpha_{II}^2 \alpha_I^2. \tag{353}
\end{aligned}$$

In the region below Biot critical frequency,  $\Omega$ , the P and S velocities can be approximated as

$$\alpha_I^2 \approx C_\alpha^{mm} - i \frac{\omega}{\Omega} \frac{C_\alpha^{mi} C_\alpha^{im}}{C_\alpha^{mm}}, \tag{354}$$

$$\beta_I^2 \approx C_\beta^{mm} - i \frac{\omega}{\Omega} C_\beta^{ii}, \tag{355}$$

$$\alpha_{II}^2 \approx \left(\frac{\omega}{\Omega}\right)^2 \frac{Det C_\alpha}{C_\alpha^{mm}} \left(1 + \frac{C_\alpha^{ii}}{C_\alpha^{mm}}\right) - i \frac{\omega}{\Omega} \frac{Det C_\alpha}{C_\alpha^{mm}}. \tag{356}$$

A complete analysis of the fast- and slow- P and S waves complex velocities are given in appendix E and F, respectively.

Substituting eqs (354)-(356) into eqs (327)-(342) they are

$$D_{11} \approx -i \left(\frac{\omega}{\Omega}\right) \frac{C_\alpha^{mm} C_\beta^{mi} C_\beta^{im} + C_\alpha^{im} C_\beta^{mm} C_\beta^{mi} - C_\alpha^{mm} C_\beta^{mm} C_\beta^{ii}}{C_\alpha^{mm} C_\beta^{mm} C_\beta^{mi}}, \tag{357}$$

$$D_{12} \approx 2i \left(\frac{\omega}{\Omega}\right) C_\beta^{im}, \tag{358}$$

$$D_{21} \approx C_\beta^{mm} - i \left(\frac{\omega}{\Omega}\right) C_\beta^{ii}, \tag{359}$$

$$D_{22} \approx C_\beta^{mm} - i \left(\frac{\omega}{\Omega}\right) C_\beta^{ii}, \tag{360}$$

$$E_{11} \approx 1 - i \left( \frac{\omega}{\Omega} \right) \frac{C_{\alpha}^{mm} C_{\beta}^{mi} C_{\beta}^{im} - C_{\alpha}^{mi} C_{\beta}^{mm} C_{\beta}^{im}}{C_{\alpha}^{mm} C_{\beta}^{mm2}}, \quad (361)$$

$$E_{12} \approx 0, \quad (362)$$

$$E_{21} \approx \frac{C_{\alpha}^{mm} C_{\beta}^{mi} - C_{\alpha}^{mi} C_{\beta}^{mm}}{C_{\alpha}^{mm} C_{\beta}^{mm}} \left( C_{\beta}^{mm} - i \left( \frac{\omega}{\Omega} \right) C_{\beta}^{ii} \right), \quad (363)$$

$$E_{22} \approx 0, \quad (364)$$

$$F_{11} \approx -i \left( \frac{\omega}{\Omega} \right) \frac{C_{\alpha}^{mm} C_{\beta}^{mi} C_{\beta}^{im} + C_{\alpha}^{im} C_{\beta}^{mm} C_{\beta}^{mi} - C_{\alpha}^{mm} C_{\beta}^{mm} C_{\beta}^{ii}}{C_{\beta}^{mm} C_{\beta}^{mi}}, \quad (365)$$

$$F_{12} \approx -2i \left( \frac{\omega}{\Omega} \right) C_{\beta}^{im}, \quad (366)$$

$$F_{21} \approx C_{\alpha}^{mm} - i \left( \frac{\omega}{\Omega} \right) \frac{C_{\alpha}^{mm} C_{\alpha}^{mi} C_{\alpha}^{im} C_{\beta}^{mi} C_{\beta}^{im} - C_{\alpha}^{mm2} C_{\alpha}^{im} C_{\beta}^{mi} C_{\beta}^{ii} + C_{\alpha}^{mm3} C_{\beta}^{ii2}}{C_{\alpha}^{mm2} C_{\beta}^{mi} C_{\beta}^{im}}, \quad (367)$$

$$F_{22} \approx C_{\beta}^{mm} - i \left( \frac{\omega}{\Omega} \right) C_{\beta}^{ii}, \quad (368)$$

$$G_{11} \approx -i \left( \frac{\omega}{\Omega} \right) \frac{C_{\alpha}^{mm} C_{\alpha}^{ii} - C_{\alpha}^{mi} C_{\alpha}^{im}}{C_{\alpha}^{mm}}, \quad (369)$$

$$G_{12} \approx 0, \quad (370)$$

$$G_{21} \approx -i \left( \frac{\omega}{\Omega} \right) \frac{(C_{\alpha}^{mm} C_{\beta}^{mi} C_{\beta}^{im} - C_{\alpha}^{mi} C_{\beta}^{mm} C_{\beta}^{im} - C_{\alpha}^{mm} C_{\beta}^{mm} C_{\beta}^{ii}) (C_{\alpha}^{mm} C_{\alpha}^{ii} - C_{\alpha}^{mi} C_{\alpha}^{im})}{C_{\alpha}^{mm2} C_{\beta}^{mm} C_{\beta}^{im}}, \quad (371)$$

$$G_{22} \approx 0. \quad (372)$$

Substituting eqs (357)-(372) into eqs (350)-(353) and leaving the leading terms they are

$$\begin{aligned} a_3 \approx & C_{\beta}^{mm} (C_{\alpha}^{mm} - C_{\beta}^{mm}) - i \left( \frac{\omega}{\Omega} \right) \frac{1}{C_{\alpha}^{mm2} C_{\beta}^{mm} C_{\beta}^{mi}} \left( -3C_{\alpha}^{mm2} C_{\beta}^{mm2} C_{\beta}^{im} C_{\beta}^{mi} C_{\beta}^{ii} \right. \\ & + C_{\alpha}^{mm} C_{\alpha}^{mi} C_{\beta}^{mm3} C_{\beta}^{im} C_{\beta}^{ii} + C_{\alpha}^{mm3} C_{\beta}^{mm2} C_{\beta}^{ii2} - C_{\alpha}^{mm2} C_{\alpha}^{mi} C_{\beta}^{mm} C_{\beta}^{mi} C_{\beta}^{im2} \\ & + C_{\alpha}^{mm3} C_{\beta}^{mi2} C_{\beta}^{im2} + C_{\alpha}^{mm} C_{\alpha}^{im} C_{\beta}^{mm2} C_{\beta}^{im} C_{\beta}^{mi2} - C_{\alpha}^{mi} C_{\alpha}^{im} C_{\beta}^{mm3} C_{\beta}^{mi} C_{\beta}^{im} \\ & \left. + C_{\alpha}^{mm} C_{\alpha}^{mi} C_{\alpha}^{im} C_{\beta}^{mm2} C_{\beta}^{im} C_{\beta}^{mi} - C_{\alpha}^{mm2} C_{\alpha}^{im} C_{\beta}^{mm2} C_{\beta}^{mi} C_{\beta}^{ii} \right), \quad (373) \end{aligned}$$

$$\begin{aligned} a_2 \approx & C_{\beta}^{mm2} (3C_{\alpha}^{mm} - 4C_{\beta}^{mm}) - i \left( \frac{\omega}{\Omega} \right) \frac{1}{C_{\alpha}^{mm2} C_{\beta}^{im} C_{\beta}^{mi}} \left( -16C_{\alpha}^{mm2} C_{\beta}^{mm2} C_{\beta}^{im} C_{\beta}^{mi} C_{\beta}^{ii} \right. \\ & + 4C_{\alpha}^{mm} C_{\alpha}^{mi} C_{\beta}^{mm3} C_{\beta}^{im} C_{\beta}^{ii} + 5C_{\alpha}^{mm3} C_{\beta}^{mm} C_{\beta}^{mi} C_{\beta}^{im} C_{\beta}^{ii} + 2C_{\alpha}^{mm3} C_{\beta}^{mm2} C_{\beta}^{ii2} \\ & \left. - 2C_{\alpha}^{mm3} C_{\alpha}^{mi} C_{\beta}^{mm} C_{\beta}^{mi} C_{\beta}^{im2} + 2C_{\alpha}^{mm3} C_{\beta}^{mi2} C_{\beta}^{im2} - C_{\alpha}^{mm2} C_{\alpha}^{ii} C_{\beta}^{mm2} C_{\beta}^{mi} C_{\beta}^{im} \right) \end{aligned}$$

$$\begin{aligned}
& + 3C_{\alpha}^{\text{mm}}C_{\alpha}^{\text{im}}C_{\alpha}^{\text{mi}}C_{\beta}^{\text{mm}2}C_{\beta}^{\text{mi}}C_{\beta}^{\text{im}} + 4C_{\alpha}^{\text{mm}}C_{\alpha}^{\text{im}}C_{\beta}^{\text{mi}2}C_{\beta}^{\text{mi}2}C_{\beta}^{\text{im}} - 4C_{\alpha}^{\text{mi}}C_{\alpha}^{\text{im}}C_{\beta}^{\text{mm}3}C_{\beta}^{\text{mi}}C_{\beta}^{\text{im}} \\
& + C_{\alpha}^{\text{mm}2}C_{\alpha}^{\text{mi}}C_{\beta}^{\text{mm}2}C_{\beta}^{\text{im}}C_{\beta}^{\text{ii}} + C_{\alpha}^{\text{mm}3}C_{\alpha}^{\text{ii}}C_{\beta}^{\text{mm}}C_{\beta}^{\text{mi}}C_{\beta}^{\text{im}} - C_{\alpha}^{\text{mm}2}C_{\alpha}^{\text{mi}}C_{\alpha}^{\text{im}}C_{\beta}^{\text{mm}}C_{\beta}^{\text{mi}}C_{\beta}^{\text{im}} \\
& + C_{\alpha}^{\text{mm}2}C_{\alpha}^{\text{im}}C_{\beta}^{\text{mm}}C_{\beta}^{\text{mi}2}C_{\beta}^{\text{im}} - 2C_{\alpha}^{\text{mm}2}C_{\alpha}^{\text{im}}C_{\beta}^{\text{mm}2}C_{\beta}^{\text{mi}}C_{\beta}^{\text{im}}), \tag{374}
\end{aligned}$$

$$\begin{aligned}
a_1 \approx & -i \left( \frac{\omega}{\Omega} \right) \frac{C_{\beta}^{\text{mm}2}}{C_{\beta}^{\text{mi}}} \left( 4C_{\alpha}^{\text{mi}}C_{\beta}^{\text{mm}}C_{\beta}^{\text{ii}} + 4C_{\alpha}^{\text{im}}C_{\beta}^{\text{mi}2} - 4C_{\alpha}^{\text{mm}}C_{\beta}^{\text{mi}}C_{\beta}^{\text{ii}} + 3C_{\alpha}^{\text{mm}}C_{\alpha}^{\text{ii}}C_{\beta}^{\text{mi}} \right. \\
& \left. - 3C_{\alpha}^{\text{mi}}C_{\alpha}^{\text{im}}C_{\beta}^{\text{mi}} - 4C_{\alpha}^{\text{ii}}C_{\beta}^{\text{mm}}C_{\beta}^{\text{mi}} \right), \tag{375}
\end{aligned}$$

$$a_0 \approx 0. \tag{376}$$

Thus, the polynomial (344) in the region below Biot critical frequency is approximated as

$$0 = V^2 \left[ a_3 (V^2)^2 + a_2 V^2 + a_1 \right], \tag{377}$$

which solutions are

$$V_1^2 = \frac{-a_2 + \sqrt{a_2^2 - 4a_1a_3}}{2a_3}, \tag{378}$$

$$V_2^2 = \frac{-a_2 - \sqrt{a_2^2 - 4a_1a_3}}{2a_3}, \tag{379}$$

$$V_3^2 = 0. \tag{380}$$

The closed-pore stress-free extensional wave is given by eq (378), which is approximated in the region below Biot critical frequency as

$$\begin{aligned}
V^2 & = \frac{-a_2 - a_2 \sqrt{1 - 4 \frac{a_1 a_3}{a_2^2}}}{2a_3} \\
& \approx \frac{-a_2 - a_2 \left( 1 - 2 \frac{a_1 a_3}{a_2^2} \right)}{2a_3}
\end{aligned}$$

$$= -\frac{a_2}{a_3} + \frac{a_1}{a_3}. \quad (381)$$

Using eq (381) into eqs (285) and (287), the closed-pore extensional phase velocity and attenuations in terms of material properties are,

$$V_{\text{ext}} = \sqrt{\frac{E^c}{\rho^m}}, \quad (382)$$

$$\frac{1}{Q} = -\frac{1}{8} \left( \frac{\omega}{\Omega} \right) \frac{\alpha \eta_0^2}{(3MK^c)^2 \rho_0^m \mu^0} E^c \frac{\left[ \mu^0 (\rho_0^s)^2 (K^s + K^0) + 6K^s K^0 (\rho_0^s)^2 + 9\mu^0 (\rho_0^f)^2 (K^s - K^0) \right]}{\rho_0^i \rho_0^m K^s K^f}. \quad (383)$$

Fig. 31 shows the comparison of the exact closed-pore extensional phase velocity and attenuation curves (the first root of eq (344)) and their approximate expressions, respectively, eqs (382) and (383) for the region below crossover frequency  $\Omega$ . The exact phase velocity and attenuation are presented, respectively, as continuous blue and red curves whereas their approximations are given by dashed-black lines. It shows an acceptable agreement between the exact curves and their corresponding approximations in the region under consideration.

## VI.15 Comparison with the previous work

Gardner (1926) solved the extensional open-pore stress-free boundary value problem for a fully-saturated, isotropic and homogeneous porous circular cylinder. He took the low-frequency limit ( $\omega$  close to 0, i.e.  $\omega \rightarrow 0$ ), and found an expression for the complex velocity squared (eq 3.6, p. 38) given by

$$V^2 = \frac{(3v_1^2 - 4v_r^2)(RP - Q^2) - 4(Q + R)^2 v_r^2 \Theta(i^{3/2} a \sqrt{\omega c})}{v_r^2 [(v_1^2 - v_r^2)(RP - Q^2) - (Q + R)^2 v_r^2 \Theta(i^{3/2} a \sqrt{\omega c})]}, \quad (384)$$

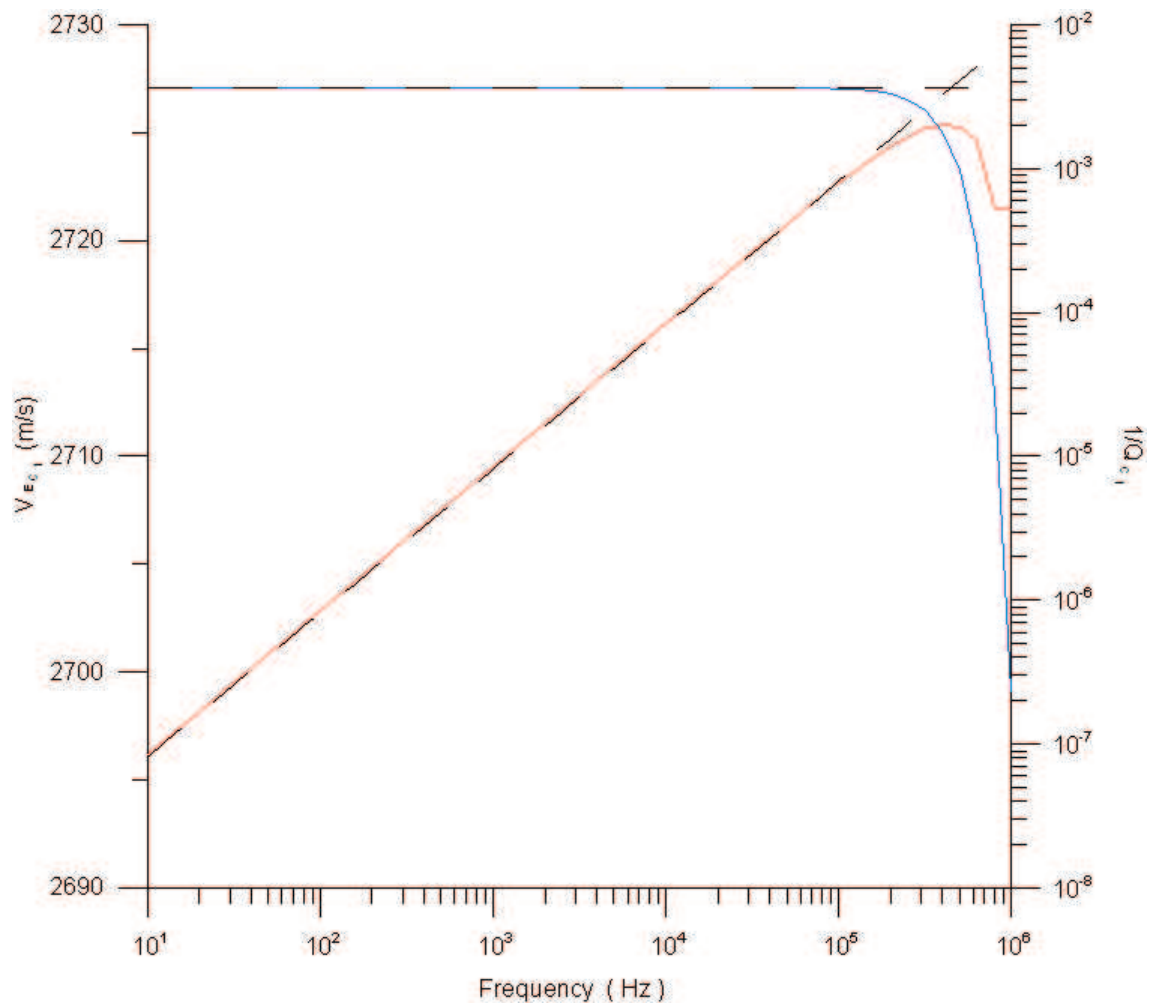


Figure 61. The comparison of the exact (344) and the approximate expression for the extensional phase velocity (382) and attenuation (383) in the region below crossover frequency  $\Omega$ . The exact extensional phase velocity and attenuation are presented as blue and red solid curves, respectively. On the respective exact curves, the approximate extensional phase velocity and attenuation are superimposed as black-dashed curves.



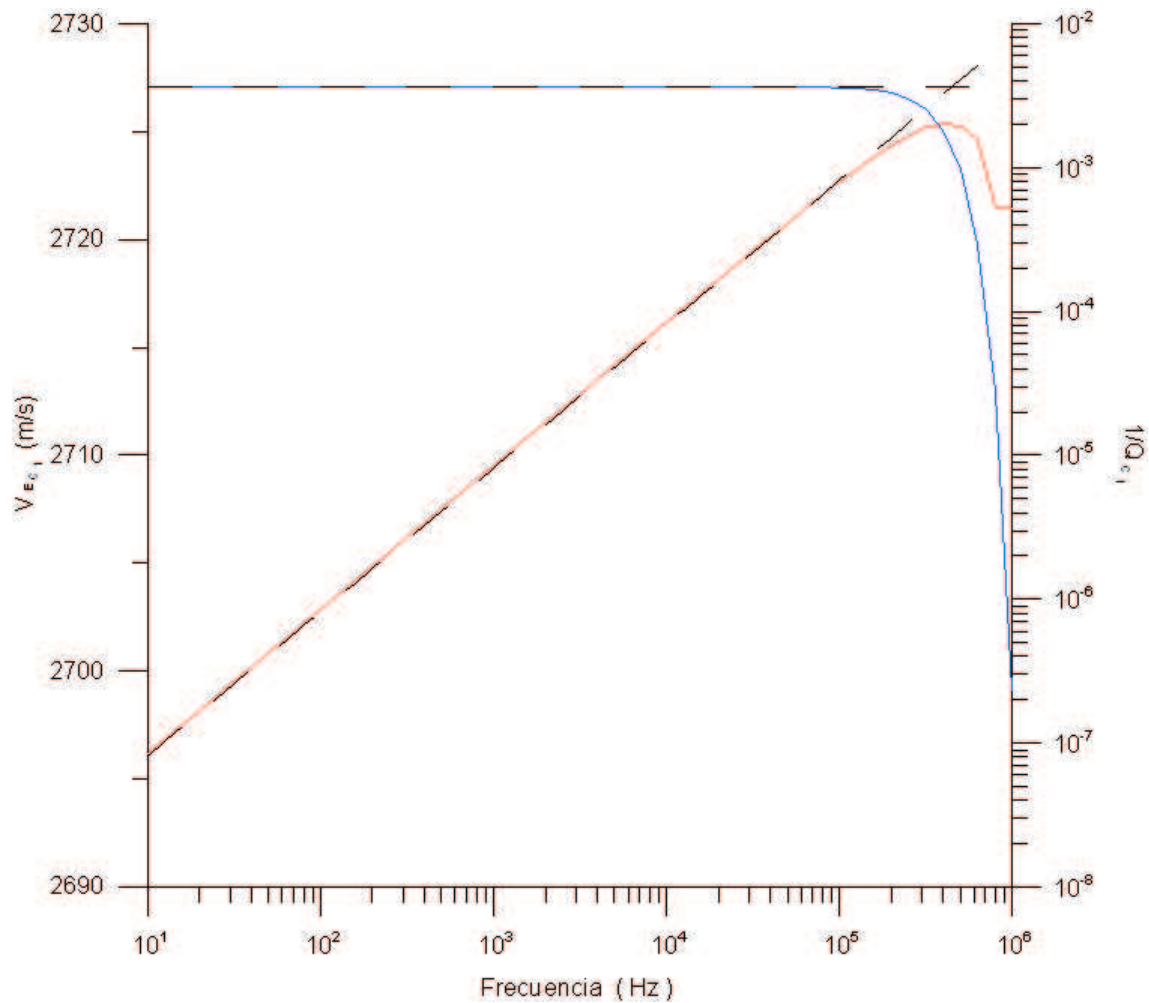


Figure 62. Comparación de los valores exactos para la velocidad de fase y la atenuación (ec 344) y los valores obtenidos mediante las fórmulas de aproximación de la velocidad de fase (ec 382) y la atenuación (ec 383) en la región por debajo de la frecuencia de frontera  $\Omega$ . La velocidad de fase y la atenuación exactas se representan por las curvas continuas azul y roja, respectivamente. Sobre las respectivas curvas exactas se superimponen en líneas punteadas negras los valores aproximados de la velocidad de fase y la atenuación.

where  $a$  is the radius of the cylinder,  $\omega$  is the angular frequency,  $P$ ,  $Q$  and  $R$  are the elastic constants in Biot's theory and,  $v_1^2$  and  $v_r^2$  are the fast-P and fast-S wave velocities squared, respectively, given by

$$v_1^2 = -\frac{3K^s K^c + 4\mu^0}{\rho_0^m}, \quad (385)$$

$$v_r^2 = \frac{\mu^0}{\rho_0^m}. \quad (386)$$

The  $c$  in the argument of  $\Theta$  function is given by

$$c = \frac{bH}{RP - Q^2}, \quad (387)$$

where  $H$  is a elastic constants in Biot's theory and  $b$  is related with material properties by

$$b = \frac{\eta_0^2 \mu^f}{K}. \quad (388)$$

The elastic constants in Biot's theory are related with solid and fluid constituents by

$$P = K^s (K^c - \eta_0) + \eta_0 M \left( \alpha - \eta_0 \frac{K^s}{K^f} \right) + \frac{4}{3} \mu^0, \quad (389)$$

$$Q = \eta_0 M (\eta_0 - \alpha), \quad (390)$$

$$R = -\eta_0^2 M, \quad (391)$$

$$H = K^s (K^c - \eta_0) - \eta_0 M \left[ \alpha - \eta_0 \left( 1 - \frac{K^s}{K^f} \right) \right] + \frac{4}{3} \mu^0. \quad (392)$$

The  $c$  constant appearing in the argument of the transcendental function  $\Theta$  in terms of material properties is

$$c = \frac{[3M \left( \alpha - \frac{K^0}{K^s} \right) - (3K^0 + 4\mu^0)]}{M(3K^0 + 4\mu^0)K}. \quad (393)$$

Substituting eqs (385), (386), (389), (390) and (391) in eq (384), Gardner's extensional complex velocity squared is rewritten as

$$V^2 = 9 \frac{-K^0 (3K^s K^c + 4\mu^0) \frac{K^f K^{s2}}{M} + 4\mu^0 K^f (K^0 - K^s)^2 [1 - \Theta(i^{3/2} a \sqrt{\omega c})]}{\rho_0^m (3K^0 + 4\mu^0) [(3K^s K^c + \mu^0) \frac{K^f K^{s2}}{M} - 9\mu^0 K^f (K^0 - K^s)^2 \Theta(i^{3/2} a \sqrt{\omega c})]}. \quad (394)$$

Utilizing the procedure described in section VI.7 to transform the transcendental function  $\Theta(i^{3/2} a \sqrt{\omega c})$  into an algebraic expression, in the region below the crossover frequency A, it simplifies as

$$\Theta(i^{3/2} a \sqrt{\omega c}) \approx 1 - i \frac{\omega a^2 c}{8}, \quad (395)$$

substituting eq (393) in eq (395), then using this result in eq (394), after some algebraic manipulation and retaining only the leading terms, eq (394) results in eqs (290) and (291).

In the region above the crossover frequency A the  $\Theta$  function simplifies as

$$\Theta(i^{3/2} a \sqrt{\omega c}) \approx \frac{(1 - i) \sqrt{2}}{a \sqrt{\omega c}}. \quad (396)$$

Substituting eq (393) in eq (396), then using this result in eq (394), after some algebraic manipulation and retaining only the leading terms, eq (394) results in eqs (297) and (298).

Hence, the results presented in this thesis in section VI.10.1 are in agreement with the well established Gardner's extensional formulas for the low-frequency regime, i.e. the regime below Biot critical frequency. Several authors basing their work on Gardner's extensional formulas are trying to understand the behavior of this mode of vibration and/or comparing their analytical results with those obtained in laboratory experi-

---

ments.

The works presented by Gardner (1962), Berryman (1983), White (1986), Dunn (1986) and Johnson et al (1995) on extensional waves in fully-saturated, isotropic and homogeneous porous circular cylinder subjected to open-pore stress-free boundary conditions are based on Biot theory. In chapter II an overview of Biot's theory was presented showing that this theory leads to a mathematical inconsistency since its foundations drop two degree of freedom when the fluid-strain rate term is ignored in its constitutive relations. Therefore, in this thesis the analysis of extensional vibrations is based on the modified Biot theory which incorporates in a natural way the fluid-strain rate term in its constitutive relations, so that there is no mathematical inconsistency.

Also instead of Gardner, Berryman, Dunn, White, Johnson, etc. ad hoc approximation of  $\Theta$  functions, which are transcendental functions in nature and give the transcendental form of the extensional dispersion relation becoming mathematically unmanageable, this thesis carries out in a systematic manner a simplification of the transcendental functions to an algebraic expression based upon clear physical arguments giving an algebraic extensional dispersion relation which roots represents the wave motions which are the study of this thesis.

This work provides a consistent and systematic mathematical development of the extensional oscillation theory, which presents in a transparent manner the phase velocity and attenuation linked with constituent properties.

## VI.16 Summary

The expressions for phase velocity and attenuation a poroelastic, circular cylinder in which dependence upon porous medium material properties are transparent were developed for the open-pore as well as closed-pore stress-free boundary value problem. The summary of these expressions in the different frequency regimes are presented below.

### Open-pore stress-free boundary value problem

#### Regime I ( $\omega < \Omega$ )

*Regime below A:*

Extensional phase velocity

$$V = \sqrt{\frac{E^0}{\rho_0^m}}. \quad (397)$$

Extensional Attenuation

$$\frac{1}{Q} = \frac{a^2 \omega}{8} \left( \frac{\mu^f}{K} \right) \left( \frac{\alpha}{3K^0} \right)^2 E^0. \quad (398)$$

where

$$E^0 = 9 \frac{K^0 \mu^0}{\mu^0 + 3K^0}. \quad (399)$$

*Regime above A and below B:*

Extensional phase velocity

$$V = \sqrt{\frac{E^c}{\rho^m}}. \quad (400)$$

Extensional Attenuation

$$\frac{1}{Q} = \frac{\sqrt{2}}{a\sqrt{\omega}} \left(\frac{\alpha M}{3K^c}\right)^2 E^c \sqrt{\left(\frac{K}{\mu^f}\right) \frac{3K^c + 4\mu^0}{M(3K^0 + 4\mu^0)}}. \quad (401)$$

where

$$E^c = 9 \frac{K^c \mu^0}{\mu^0 + 3K^c}, \quad (402)$$

$$K = K^0 + \alpha M. \quad (403)$$

*Regime above B and below  $\Omega$ :*

Extensional Attenuation

$$\frac{1}{Q} = \left(\frac{\omega}{\Omega}\right) \frac{\Im h_1^{\text{II}}}{\Re h_1^{\text{II}}}. \quad (404)$$

**Regime II** ( $\Omega < \omega$ ):

Extensional phase velocity

$$V = \sqrt{\left(\frac{1 - \delta_1^{\text{II}2} \gamma^{\text{II}2}}{1 - \gamma^{\text{II}}}\right) \Re h_1^{\text{II}}}. \quad (405)$$

Extensional Attenuation

$$\frac{1}{Q} = \left(\frac{\Omega}{\omega}\right) \frac{\Im h_1^{\text{II}}}{\Re h_1^{\text{II}}}. \quad (406)$$

where

$$\Re h_1^{\text{II}} = Tr(\mathbf{C}_\beta) \frac{[3\Re(\alpha_1^2) - 4Tr(\mathbf{C}_\beta)]}{\Re(\alpha_1^2) - Tr(\mathbf{C}_\beta)}, \quad (407)$$

$$\Im h_1^{\text{II}} = \frac{3\Re(\alpha_1^2)^2 \Im(\beta_1^2) + 4\Re(\beta_1^2)^2 \Im(\beta_1^2) - 8\Re(\alpha_1^2)\Re(\beta_1^2)\Im(\beta_1^2)}{[\Re(\alpha_1^2) - Tr(\mathbf{C}_\beta)]^2}, \quad (408)$$

$$\delta_1^{\text{II}} = 4 \frac{Tr(\mathbf{C}_\alpha)^2 - Det(\mathbf{C}_\alpha) - Tr(\mathbf{C}_\alpha)Tr(\mathbf{C}_\beta)}{3Tr(\mathbf{C}_\alpha)^2 - 3Det(\mathbf{C}_\alpha) - 4Tr(\mathbf{C}_\alpha)Tr(\mathbf{C}_\beta)}, \quad (409)$$

$$\gamma^{\text{II}} = -\frac{C_\alpha^{\text{mi}} C_\alpha^{\text{im}}}{(C_\alpha^{\text{mm}})^2}. \quad (410)$$

### Closed-pore stress-free boundary value problem

*Regime below  $\Omega$ :*

Extensional phase velocity

$$V = \sqrt{\frac{E^c}{\rho^m}}. \quad (411)$$

Extensional attenuation

$$\frac{1}{Q} = -\frac{1}{8} \left( \frac{\omega}{\Omega} \right) \frac{\alpha r_0^2}{(3MK^c)^2 \rho_0^m \mu^0} E^c \frac{\left[ \mu^0 (\rho_0^s)^2 (K^s + K^0) + 6K^s K^0 (\rho_0^s)^2 + 9\mu^0 (\rho_0^f)^2 (K^s - K^0) \right]}{\rho_0^i \rho_0^m K^s K^f}. \quad (412)$$

Based upon the above expressions there is a firm basis to design extensional oscillation experiments to determine solid-frame bulk modulus, solid-mineral bulk modulus, fluid bulk storage coefficient and fluid bulk modulus.

# Chapter VII

## Conclusions

In the framework of the modified Biot theory of poroelasticity the complete analysis of the torsional and extensional oscillations in a fully-saturated, porous, circular cylinder are carried out.

In the torsional case, it is shown that an underdamped harmonic oscillation (i.e. a propagating-wave process or fast process) and an overdamped harmonic oscillation (i.e. a diffusive process) constitute the eigenprocesses of the governing  $2 \times 2$  matrix wave equation. It is the former process which is observed in a torsional-resonance experiment.

In order to get insight into the nature of the eigenvectors and eigenvalues of this problem, an eigenvalue perturbation analysis is carried out. The set of two similarity transformations that allowed the construction of nearly exact eigenvalues have been vital to this analysis. It led to expressions of torsional resonance and temporal attenuation frequencies in which the link to the constituent properties are transparent. It showed that entire material-parameters space can be split into two regimes, namely, inertia dominated and viscosity dominated. The domain of two regimes is found to be defined by the parameter  $\Upsilon$  (eq 97). The domain  $\Upsilon < 1$  corresponds to former and the domain  $\Upsilon > 1$  is associated with later.



---

For sandstones or limestones saturated with light fluids such as air or light hydrocarbon we found  $\Upsilon \ll 1$ , therefore, the expressions for torsional resonance (eq 113) and temporal attenuation (eq 114) frequencies pertaining to inertia dominated regime are applicable here. For heavy hydrocarbons such as crude oil and tar  $\Upsilon > 1$  holds true suggesting the expressions for the torsional resonance (eq 128) and temporal attenuation (eqs 130 or 132) frequencies corresponding to the viscosity dominated regime are pertinent here.

In the extensional case, the solution of open-pore as well as closed-pore stress-free boundary value problem based on a consistent and clear mathematical development are shown. The problems under considerations involve transcendental functions, which complicate the analytical solution of the problems, however under consistent physical arguments those transcendental functions were transformed into an algebraic polynomial, simplifying the transcendental extensional dispersion relation to a fourth order polynomial for the open-pore problem and a third order polynomial for the closed-pore problem which roots are easy to find. One of this roots renders a propagating-wave process, which is considered the extensional wave for the problem under consideration. The remaining roots represents diffusive processes. Berryman (1983) affirms the inexistence of diffusive processes in the open-pore case, however one of these diffusive roots is in agreement with Gardner's equation (3.11, p.39) for the diffusive process associated with this mode of vibration.

Working out the general solution of the problems and based on physical arguments the expressions of phase velocity and temporal attenuation, for the open-pore as well as closed-pore problems, in which link to the cylinder properties are transparent have been developed. For the open-pore stress-free boundary value problem the phase veloc-

---

ity expression renders that the low frequency limit, i.e. frequencies below the crossover frequency (301), could be interpreted as a poroelastic Young's modulus related to dry-frame, eq (397). In this limit the attenuation expression shows its dependence on radius of the cylinder, solid-frame bulk modulus, Biot's coefficient  $\alpha$ , fluid viscosity and permeability, eq (398). The saturated (Gassmann) frequency range, i.e. regime between the crossover frequencies (eq 301) and (315), is governed by the saturated (Gassmann) Young's modulus, eq (400). The attenuation expression shows its dependence on fluid bulk storage coefficient, saturated (Gassmann) bulk modulus, fluid viscosity and permeability, eq (401). For the closed-pore stress-free boundary value problem the phase velocity expression renders that the frequency regime below the crossover frequencies  $\Omega$  is governed by the saturated (Gassmann) Young's modulus, eq (411). The attenuation expression shows its dependence on fluid bulk storage coefficient, saturated (Gassmann) bulk modulus, solid-mineral bulk modulus, eq (412).

The development carried out in this thesis enable us to work-out proper methodologies for deducing poro-elastic constants, for example frame shear modulus, permeability, fluid storage coefficient and tortuosity, by torsional and extensional resonance experiment. For low permeability rock where it is not always feasible to carry out a drain experiment to ascertain permeability, this may prove to be very valuable.

Future works in this field possibly should be oriented to the area of wave propagation in inhomogeneous porous cylinders.

# Bibliography

Bancroft, D., 1941. The velocity of longitudinal waves in cylindrical bars, *Phys. Rev.*, **59**: 588-593.

Berryman, J. M., 1983. Dispersion of extensional waves in fluid-saturated porous cylinders at ultrasonic frequencies, *J. Ac. Soc. Am.*, **74**: 1805-1812.

Biot, M. A., 1956, Theory of propagation of elastic waves in a fluid-saturated porous solid. I. low-frequency range, *J. Ac. Soc. Am.*, **28** (2): 168-178.

Biot, M. A., 1962, Mechanics of deformation and acoustic propagation in porous media, *J. Appl. Phys.*, **33** (4): 1482-1492.

Bourbie, T., Coussy, O. and Zinszner, B., 1987, Acoustic of porous media, Gulf Publishing Company. pp. 145-173.

Chree, C., 1889. The equations of an isotropic elastic solid in polar and cylindrical coordinates, their solution and application, *Trans. Camb. Philos. Soc.*, **14**: 250-369.

Davis, R.M., 1948. A critical study of the hopkinson pressure bar, *Philos. Trans. R. Soc. London Ser. A*, **240**: 375-457.

de la Cruz V. and Spanos T.J.T., 1985, Seismic wave propagation in a porous medium, *Geophysics*, **50** (10): 1556-1565.

de la Cruz V. and Spanos T.J.T., 1989, Thermomechanical coupling during seismic wave propagation in a porous medium, *J. Geop. Res.*, **94 B**: 637-642.

de la Cruz, V., Sahay, P.N., Spanos, T.J.T., 1993, Thermodynamic of porous media, *Proc. R. Soc. Lond.*, **A433**: 247-255.

Dunn, K.J., 1986, Acoustic attenuation in fluid-saturated porous cylinders at low frequencies, *J. Ac. Soc. Am.*, **79** (6): 1709-1721.

Dunn, K.J., 1986, Sample boundary effect in acoustic attenuation of fluid-saturated porous cylinders, *J. Ac. Soc. Am.*, **81** (5): 1259-1266.

- 
- Gardner, G.H.F., 1962. Extensional waves in fluid-saturated porous cylinders, *J. Ac. Soc. Am.*, **34** (1): 36-40.
- Golub, G. and Van Loan C. F., 1996, Matrix computations, The John Hopkins University Press. Section 7.4.6
- Hickey, C.J., Spanos, T.J.T. and de la Cruz, V., 1995, Deformation parameters of permeable media, *Geo. J. Int.*, **121**: 359-370.
- Johnson, D.L. and Kostek, S., 1995. A limitation of the Biot-Gardner theory of extensional waves in fluid-saturated porous cylinders, *J. Ac. Soc. Am.*, **97** (2): 741-744.
- Mörig, R. and Burkhardt, H., 1989. Experimental evidence for the Biot-Gardner theory, *Geophysics*, **54** (4): 524-527.
- Morse, P.M. and Feshbach, H., 1953, Methods of theoretical physics, Vol. II, McGraw-Hill. P. 1018
- O'Hara, S.G., 1985, Influence of pressure, temperature, and pore fluid on the frequency-dependent attenuation of elastic waves in Berea sandstone, *Phys. Rev. A*, **32** (1): 472-488.
- Pochhammer, L., 1876. Ueber die fortpflanzungsgeschwindigkeiten kleiner schwingungen in einem unbegrenzten isotropen kreiscylinder, *J. Reine Agnew, Math.*, **81**: 324-336.
- Sahay, P. N., 1996, Elastodynamics of deformable Porous Media, *Proc. R. Soc. Lond.*, **452**: 1517-1529.
- Sahay, P. N., Spanos T. J .T. and de la Cruz V. 2001, Seismic wave propagation in inhomogeneous and anisotropic porous media, *Geo. J. Int.*, **145**: 209-222.
- Sahay, P. N. 2001, Biot theory, BISQ model and porosity perturbation during deformation, 75th. Ann. Internat. Mtg., Soc. Expl. Geophys., Expanded Abstracts: 1752-1755.
- Selby, S. M. 1971, CRC standard mathematical tables, 19th ed., The Chemical Rubber Co. P. 454 and 518
- Sothcott, J., McCann, C. and O'Hara, S.G., 2000, The influence of two differ-

ent pore fluids on the acoustic properties of reservoir sandstones at sonic and ultrasonic frequencies, 74th Ann. Internat. Mtg., Soc. Expl. Geophys., Expanded Abstracts: 1883-1886.

White, J. E., 1986, Biot-Gardner theory of extensional waves in porous rods, *Geophysics*, **51**: 742-745.

# Appendix A

## Notation

The expressions for the matrix coefficients  $\mathbf{C}_\alpha$ ,  $\mathbf{C}_\beta$ ,  $\mathbf{N}_\alpha$  and  $\mathbf{N}_\beta$  are obtained in terms of the constituents material properties in a straightforward manner from the appendix of Sahay (1996). We have

$$\begin{aligned}
 \mathbf{C}_\alpha &= \begin{pmatrix} C_\alpha^{mm} & C_\alpha^{mi} \\ C_\alpha^{im} & C_\alpha^{ii} \end{pmatrix} \\
 &= \left\{ \begin{pmatrix} 1 & m^f \\ d^f & d^f m^f \end{pmatrix} \left( \phi_0 - \eta_0 (\alpha - \eta_0) \frac{M}{K^f} \right) + \begin{pmatrix} 1 & -m^s \\ d^f & -d^f m^s \end{pmatrix} \eta_0 (\alpha - \eta_0) \frac{M}{K^s} \right\} \frac{K^s}{\rho_0^m} \\
 &+ \left\{ \begin{pmatrix} 1 & -m^s \\ -d^s & d^s m^s \end{pmatrix} \left( \eta_0 - \eta_0 (\alpha - \eta_0) \frac{M}{K^s} \right) + \begin{pmatrix} 1 & m^f \\ -d^s & -d^s m^f \end{pmatrix} \eta_0 (\alpha - \eta_0) \frac{M}{K^f} \right\} \frac{K^f}{\rho_0^m} \\
 &+ \frac{4}{3} \begin{pmatrix} 1 & m^f \\ d^f & d^f m^f \end{pmatrix} m^s \beta_0^2 \tag{413}
 \end{aligned}$$

$$\begin{aligned}
 \mathbf{N}_\alpha &= \begin{pmatrix} N_\alpha^{mm} & N_\alpha^{mi} \\ N_\alpha^{im} & N_\alpha^{ii} \end{pmatrix} \\
 &= \left\{ \begin{pmatrix} 1 & -m^s \\ -d^s & d^s m^s \end{pmatrix} \left( \eta_0 - \eta_0 (\alpha - \eta_0) \frac{M}{K^s} \right) + \begin{pmatrix} 1 & m^f \\ -d^s & -d^s m^f \end{pmatrix} \eta_0 (\alpha - \eta_0) \frac{M}{K^f} \right\} \frac{\xi^f}{\rho_0^m}
 \end{aligned}$$

$$+ \frac{4}{3} \left\{ \left( \begin{array}{cc} 1 & -m^s \\ -d^s & d^s m^s \end{array} \right) + \left( \begin{array}{cc} 1 & m^f \\ -d^s & -d^s m^f \end{array} \right) \frac{(\beta - \eta_0)}{\eta_0} \right\} m^f \nu^f \quad (414)$$

$$\begin{aligned} \mathbf{C}_\beta &= \begin{pmatrix} C_\beta^{mm} & C_\beta^{mi} \\ C_\beta^{im} & C_\beta^{ii} \end{pmatrix} \\ &= \begin{pmatrix} 1 & m^f \\ d^f & d^f m^f \end{pmatrix} m^s \beta_0^2 \end{aligned} \quad (415)$$

$$\begin{aligned} \mathbf{N}_\beta &= \begin{pmatrix} N_\beta^{mm} & N_\beta^{mi} \\ N_\beta^{im} & N_\beta^{ii} \end{pmatrix} \\ &= \left\{ \left( \begin{array}{cc} 1 & -m^s \\ -d^s & d^s m^s \end{array} \right) + \left( \begin{array}{cc} 1 & m^f \\ -d^s & -d^s m^f \end{array} \right) \frac{(\beta - \eta_0)}{\eta_0} \right\} m^f \nu^f \end{aligned} \quad (416)$$

# Appendix B

## Data

The following data are used in the numerical computation

solid density:	$\rho_0^s = 2.65 \times 10^{+03} \left( \frac{kg}{m^3} \right),$
solid-mineral shear modulus:	$\mu^s = 2.30 \times 10^{+10} (Pa),$
fluid density:	$\rho_0^f = 1.00 \times 10^{+03} \left( \frac{kg}{m^3} \right),$
fluid shear viscosity:	$\mu^f = 1.00 \times 10^{-03} \left( \frac{kg}{m^3} \right),$
fluid bulk viscosity:	$\xi^f = 2.8 \times 10^{-03} \left( \frac{kg}{m^3} \right),$
solid-frame shear modulus:	$\mu^0 = 6.70 \times 10^{+09} (Pa),$
solid-frame bulk modulus:	$K^0 = 5.20 \times 10^{+09} (Pa),$
solid-mineral bulk modulus:	$K^s = 35 \times 10^{+09} (Pa),$
fluid bulk modulus:	$K^f = 2.2 \times 10^{+09} (Pa),$
permeability:	$K = 1.00 \times 10^{-14} (m^2),$
porosity:	$\eta_0 = 0.25,$
tortuosity factor:	$S = \frac{4}{3},$
radius of the cylindrical core:	$a = 1.9 \times 10^{-2} (m),$
length of the cylindrical core:	$L = 40 \times 10^{-2} (m).$



# Appendix C

## Dry-frame frequency

In the case for a porous frame devoid of fluid the governed equation of motion of the torsional resonance frequency (68) simplifies as

$$(1 - \eta_0) \rho_0^s \partial_t^2 \bar{u}_\theta^s = \mu^0 \left[ \frac{1}{r} \partial_r (r \partial_r) + \partial_z^2 - \frac{1}{r^2} \right] \bar{u}_\theta^s. \quad (417)$$

Its solution, subjected to the stress-free boundary conditions on the radial surface ( $r = a$ ), as well as on the top ( $z = L$ ) and bottom ( $z = 0$ ) end-caps, is

$$u_\theta^s = \sum_{p=1}^{\infty} \sum_{l=1}^{\infty} B(q_p, k_l) q_p J_1(q_p r) \cos(k_l z) \cos[\omega_0(q_p, k_l) t], \quad (418)$$

where  $B(q_p, k_l)$  is a constant to be determined by the initial conditions and the radial,  $q_p$ , and the axial,  $k_l$ , wavenumbers are defined as

$$q_p = \frac{N_p}{a}, \quad (419)$$

$$k_l = \frac{l\pi}{L}, \quad (420)$$

where  $N_p$  is the  $p^{\text{th}}$  root of the Bessel function of second-order and  $l$  is an integer.

Substituting eq (418) into eq (417) the dispersion relation for the dry-frame torsional

---

resonance frequency squared,  $\omega_0^2$ , is

$$\omega_0^2(p, l) = (q_p^2 + k_l^2) \frac{\mu^0}{(1 - \eta_0) \rho_0^s} = (q_p^2 + k_l^2) \beta_0^2. \quad (421)$$

# Appendix D

## Eigenvalue Perturbation Computations

To compute the perturbation of the zero<sup>th</sup>-order eigenfrequencies due to the perturbed operator  $\mathbf{Q}^I$  for the inertia dominated regime, the eigenvalue perturbation problem that was cast in section IV.2.1 as a  $2 \times 2$  system of 2<sup>nd</sup>-order ODEs is rewritten as a system of 1st-order ODEs.

The unperturbed and perturbed operators pertaining to the regime I can be expressed as  $3 \times 3$  matrix operators as follows

$$\mathcal{L}^{(0,I)} = \begin{pmatrix} 0 & i & 0 \\ -i(W^{mm} + W^{ii}) & -i\frac{m^f d^f}{1+m^f d^f}\Omega & 0 \\ 0 & 0 & -i\frac{1}{1+m^f d^f}\Omega \end{pmatrix} \quad (422)$$

$$\mathbf{Q}^I = \begin{pmatrix} 0 & 0 & 0 \\ 0 & 0 & -i\frac{m^f}{1+m^f d^f}\Omega \\ 0 & -i\frac{d^f}{1+m^f d^f}\Omega & 0 \end{pmatrix} \quad (423)$$

The unperturbed problem, with eigenvalues  $\omega_n^{(0,I)}$  and eigenvectors  $\mathbf{V}_n^{(0,I)}$ , is given by

$$\mathcal{L}^{(0,I)}\mathbf{V}_n^{(0,I)} = \omega_n^{(0,I)}\mathbf{V}_n^{(0,I)}. \quad (424)$$

The subindex  $n$  ( $n = 1, 2, 3$ ) labels the modes.

$\omega_n^{(0,I)}$  and  $\mathbf{V}_n^{(0,I)}$  are regarded as the zero<sup>th</sup>-order eigenvalues and eigenvectors, respectively, of the operator  $\mathcal{L}^{(0,I)} + \mathbf{Q}^I$ .

For the regime I, the eigenvalues associated with the unperturbed problem are given in eqs (110) and (115) and their corresponding eigenvectors computed using eq (424) are

$$\mathbf{V}_1^{(0,I)} = \begin{pmatrix} 1 \\ -i(\omega_1^{(0,I)})^* \\ 0 \end{pmatrix}, \quad \mathbf{V}_2^{(0,I)} = \begin{pmatrix} 1 \\ -i(\omega_2^{(0,I)})^* \\ 0 \end{pmatrix}, \quad \mathbf{V}_3^{(0,I)} = \begin{pmatrix} 0 \\ 0 \\ 1 \end{pmatrix}, \quad (425)$$

where \* stands for complex conjugate of the quantity inside the braces.

The perturbative correction to the zero<sup>th</sup>-order eigenvalues and eigenvectors due to the operator  $\mathbf{Q}^I$  is developed following Morse and Feshbach (1953; section 9.1, p. 1018). The perturbative first-order correction to the zero<sup>th</sup>-order eigenvalues and eigenvectors due to the operator  $\mathbf{Q}^I$  is given by

$$\omega_n^{(1,I)} = \omega_n^{(0,I)} + (\bar{\mathbf{V}}_n^{(0,I)} \cdot \mathbf{Q}^I \mathbf{V}_n^{(0,I)}) \quad (426)$$

where  $\bar{\mathbf{V}}_n^{(0,I)}$  is worked out as the solution of the adjoint of the operator  $\mathcal{L}^{(0,I)}$

$$\mathcal{L}^{(0,I)\dagger} \bar{\mathbf{V}}_n^{(0,I)} = \omega_n^{(0,I)} \bar{\mathbf{V}}_n^{(0,I)}. \quad (427)$$

in such a manner that

$$\bar{\mathbf{V}}_m^{(0)} \cdot \mathbf{V}_n^{(0)} = \delta_{mn}. \quad (428)$$

The operator  $\mathcal{L}^{(0,I)}$ , cast as system of 1st-order ODEs, is not symmetric, hence  $\mathbf{V}_n^{(0)}$  and  $\bar{\mathbf{V}}_n^{(0)}$  form its bi-orthogonal basis vectors. In addition,

$$P_{mn} = \bar{\mathbf{V}}_m^{(0,I)} \cdot \mathbf{Q}^I \mathbf{V}_n^{(0,I)}, \quad (429)$$

is the projection of the perturbation operator  $\mathbf{Q}^I$  on the basis vector space.

For the region under consideration, the eigenvectors associated to the adjoint operator  $\mathcal{L}^{(0,I)\dagger}$  (eq 427) are

$$\bar{\mathbf{V}}_1^{(0,I)} = \begin{pmatrix} 1 - \frac{(\omega_1^{(0,I)})^*}{\omega_1^{(0,I)} - \omega_2^{(0,I)}} \\ -i \frac{1}{\omega_1^{(0,I)} - \omega_2^{(0,I)}} \\ 0 \end{pmatrix}, \quad \bar{\mathbf{V}}_2^{(0,I)} = \begin{pmatrix} \frac{(\omega_1^{(0,I)})^*}{\omega_1^{(0,I)} - \omega_2^{(0,I)}} \\ i \frac{1}{\omega_1^{(0,I)} - \omega_2^{(0,I)}} \\ 0 \end{pmatrix}, \quad \bar{\mathbf{V}}_3^{(0,I)} = \begin{pmatrix} 0 \\ 0 \\ 1 \end{pmatrix}. \quad (430)$$

Hence, substituting eqs (423), (425) and (430) into eq (426) the first order eigenvalues are given by

$$\omega_1^{(1,I)} = \omega_1^{(0,I)} + (\bar{\mathbf{V}}_1^{(0,I)} \cdot \mathbf{Q}^I \mathbf{V}_1^{(0,I)}) = \omega_1^{(0,I)}, \quad (431)$$

$$\omega_2^{(1,I)} = \omega_2^{(0,I)} + (\bar{\mathbf{V}}_2^{(0,I)} \cdot \mathbf{Q}^I \mathbf{V}_2^{(0,I)}) = \omega_2^{(0,I)}, \quad (432)$$

$$\omega_3^{(1,I)} = \omega_3^{(0,I)} + (\bar{\mathbf{V}}_3^{(0,I)} \cdot \mathbf{Q}^I \mathbf{V}_3^{(0,I)}) = \omega_3^{(0,I)}. \quad (433)$$

Therefore, the perturbative correction of the first-order is zero.

Computation of the second-order eigenvalues correction is given by

$$\omega_n^{(2,I)} = \omega_n^{(0,I)} + (\bar{\mathbf{V}}_n^{(0,I)} \cdot \mathbf{Q}^I \mathbf{V}_n^{(1,I)}), \quad (434)$$

where the perturbative correction of the first-order eigenvectors  $\mathbf{V}_n^{(1,I)}$  associated to the operator  $\mathcal{L}^{(0,I)}$  are given by

$$\begin{aligned}
\mathbf{V}_1^{(1,I)} &= \mathbf{V}_1^{(0,I)} - \frac{\bar{\mathbf{V}}_2^{(0,I)} \cdot \mathbf{Q}^I \mathbf{V}_1^{(0,I)}}{\omega_2^{(0,I)} - \omega_1^{(0,I)}} \mathbf{V}_2^{(0,I)} - \frac{\bar{\mathbf{V}}_3^{(0,I)} \cdot \mathbf{Q}^I \mathbf{V}_1^{(0,I)}}{\omega_3^{(0,I)} - \omega_1^{(0,I)}} \mathbf{V}_3^{(0,I)} \\
&= \begin{pmatrix} 1 \\ -i\omega_1^{(0,I)} \\ \frac{d^f}{1+m^f d^f} \Omega \frac{(\omega_1^{(0,I)})^*}{\omega_3^{(0,I)} - \omega_1^{(0,I)}} \end{pmatrix}, \\
\mathbf{V}_2^{(1,I)} &= \mathbf{V}_2^{(0,I)} - \frac{\bar{\mathbf{V}}_1^{(0,I)} \cdot \mathbf{Q}^I \mathbf{V}_2^{(0,I)}}{\omega_1^{(0,I)} - \omega_2^{(0,I)}} \mathbf{V}_1^{(0,I)} - \frac{\bar{\mathbf{V}}_3^{(0,I)} \cdot \mathbf{Q}^I \mathbf{V}_2^{(0,I)}}{\omega_3^{(0,I)} - \omega_2^{(0,I)}} \mathbf{V}_3^{(0,I)} \\
&= \begin{pmatrix} 1 \\ -i\omega_2^{(0,I)} \\ \frac{d^f}{1+m^f d^f} \Omega \frac{(\omega_2^{(0,I)})^*}{\omega_3^{(0,I)} - \omega_2^{(0,I)}} \end{pmatrix}, \\
\mathbf{V}_3^{(1,I)} &= \mathbf{V}_3^{(0,I)} - \frac{\bar{\mathbf{V}}_1^{(0,I)} \cdot \mathbf{Q}^I \mathbf{V}_3^{(0,I)}}{\omega_1^{(0,I)} - \omega_3^{(0,I)}} \mathbf{V}_1^{(0,I)} - \frac{\bar{\mathbf{V}}_2^{(0,I)} \cdot \mathbf{Q}^I \mathbf{V}_3^{(0,I)}}{\omega_2^{(0,I)} - \omega_3^{(0,I)}} \mathbf{V}_2^{(0,I)} \\
&= \begin{pmatrix} -\frac{m^f}{1+m^f d^f} \Omega \left[ \frac{1}{(\omega_1^{(0,I)} - \omega_2^{(0,I)})(\omega_1^{(0,I)} - \omega_3^{(0,I)})} + \frac{1}{(\omega_1^{(0,I)} - \omega_2^{(0,I)})(\omega_2^{(0,I)} - \omega_3^{(0,I)})} \right] \\ i \frac{m^f}{1+m^f d^f} \Omega \left[ \frac{\omega_1^{(0,I)}}{(\omega_1^{(0,I)} - \omega_2^{(0,I)})(\omega_1^{(0,I)} - \omega_3^{(0,I)})} + \frac{\omega_2^{(0,I)}}{(\omega_1^{(0,I)} - \omega_2^{(0,I)})(\omega_2^{(0,I)} - \omega_3^{(0,I)})} \right] \\ 1 \end{pmatrix}.
\end{aligned} \tag{435}$$

Hence, substituting the eqs (423), (430) and (435) into eq (434) the eigenvalues corrected up to second-order are

$$\begin{aligned}
\omega_1^{(2,I)} &= \omega_1^{(0,I)} + \left( \bar{\mathbf{V}}_1^{(0,I)} \cdot \mathbf{Q}^I \mathbf{V}_1^{(1,I)} \right) \\
&= \omega_1^{(0,I)} + m^f d^f \left( \frac{\Omega}{1+m^f d^f} \right)^2 \frac{\omega_1^{(0,I)}}{(\omega_1^{(0,I)} - \omega_2^{(0,I)})(\omega_3^{(0,I)} - \omega_1^{(0,I)})^*}, \\
\omega_2^{(2,I)} &= \omega_2^{(0,I)} + \left( \bar{\mathbf{V}}_2^{(0,I)} \cdot \mathbf{Q}^I \mathbf{V}_2^{(1,I)} \right)
\end{aligned} \tag{436}$$

$$= \omega_2^{(0,I)} - \text{m}^f \text{d}^f \left( \frac{\Omega}{1 + \text{m}^f \text{d}^f} \right)^2 \frac{\omega_2^{(0,I)}}{(\omega_1^{(0,I)} - \omega_2^{(0,I)}) (\omega_3^{(0,I)} - \omega_2^{(0,I)})^*}, \quad (437)$$

$$\begin{aligned} \omega_3^{(2,I)} &= \omega_3^{(0,I)} + (\bar{\mathbf{V}}_3^{(0,I)} \cdot \mathbf{Q}^I \mathbf{V}_3^{(1,I)}) \\ &= \omega_3^{(0,I)} - \text{m}^f \text{d}^f \left( \frac{\Omega}{1 + \text{m}^f \text{d}^f} \right)^2 \frac{(\omega_1^{(0,I)})^* (\omega_2^{(0,I)} - \omega_3^{(0,I)})^* + (\omega_2^{(0,I)})^* (\omega_1^{(0,I)} - \omega_3^{(0,I)})^*}{(\omega_1^{(0,I)} - \omega_2^{(0,I)})^* (\omega_1^{(0,I)} - \omega_3^{(0,I)})^* (\omega_2^{(0,I)} - \omega_3^{(0,I)})^*}. \end{aligned} \quad (438)$$

The general form of the iterative expressions of  $k^{\text{th}}$ -order eigenvalues and eigenvectors are

$$\omega_n^{(k)} = \omega_n^{(0)} + (\bar{\mathbf{V}}_n^{(0)} \cdot \mathbf{Q} \mathbf{V}_n^{(k-1)}), \quad (439)$$

$$\begin{aligned} \mathbf{V}_n^{(k)} &= \mathbf{V}_n^{(0)} - \sum_{m_1 \neq n}^N \frac{P_{m_1 n}}{\omega_{m_1}^{(0)} - \omega_n^{(k)}} \mathbf{V}_{m_1}^{(0)} + \sum_{m_1 \neq n}^N \sum_{m_2 \neq n}^N \frac{P_{m_1 m_2} P_{m_2 n}}{(\omega_{m_1}^{(0)} - \omega_n^{(k)}) (\omega_{m_2}^{(0)} - \omega_n^{(k)})} \mathbf{V}_{m_1}^{(0)} \\ &+ \dots \\ &+ (-1)^k \sum_{m_1 \neq n}^N \dots \sum_{m_k \neq n}^N \frac{P_{m_1 m_2} P_{m_2 m_3} \dots P_{m_k n}}{(\omega_{m_1}^{(0)} - \omega_n^{(k)}) (\omega_{m_2}^{(0)} - \omega_n^{(k)}) \dots (\omega_{m_k}^{(0)} - \omega_n^{(k)})} \mathbf{V}_{m_1}^{(0)}, \end{aligned} \quad (440)$$

where the subindex  $n$  ( $n = 1, N$ ) labels the modes. The superindex labelling the regime is suppressed for the generalization of the methodology.

# Appendix E

## Complex Fast- and Slow- P Wave Velocities

The system of diffusive wave equation for compressional motion is, eq (170),

$$\boldsymbol{\alpha}\nabla^2\Phi + \omega^2\Phi = 0.$$

The explicit expression of  $\boldsymbol{\alpha}$  matrix is given in eq (164). The eigenvalues of  $\boldsymbol{\alpha}$  are

$$\alpha_{\text{I}}^2, \alpha_{\text{II}}^2 = \frac{\text{Tr}(\boldsymbol{\alpha}) \pm \sqrt{\text{Tr}(\boldsymbol{\alpha})^2 - 4\text{Det}(\boldsymbol{\alpha})}}{2} = \frac{\text{Tr}(\boldsymbol{\alpha})}{2} \left\{ 1 \pm \sqrt{1 - \frac{4\text{Det}(\boldsymbol{\alpha})}{\text{Tr}(\boldsymbol{\alpha})^2}} \right\},$$

where  $\alpha_{\text{I}}^2$  and  $\alpha_{\text{II}}^2$  represent the fast and slow P-wave velocities.

Because the norm of  $\frac{4\text{Det}(\boldsymbol{\alpha})}{\text{Tr}(\boldsymbol{\alpha})^2} \ll 1$ , that is  $\left\| \frac{4\text{Det}(\boldsymbol{\alpha})}{\text{Tr}(\boldsymbol{\alpha})^2} \right\| \ll 1$ , using the binomial expansion (Selby, S. M. 1971, CRC standard mathematical tables, p. 454), the  $\alpha_{\text{I}}^2$  and  $\alpha_{\text{II}}^2$  are approximated by

$$\alpha_{\text{I}}^2, \alpha_{\text{II}}^2 \approx \frac{\text{Tr}(\boldsymbol{\alpha})}{2} \left[ 1 \pm \left\{ 1 - \frac{2\text{Det}(\boldsymbol{\alpha})}{\text{Tr}(\boldsymbol{\alpha})^2} - \left( \frac{2\text{Det}(\boldsymbol{\alpha})}{\text{Tr}(\boldsymbol{\alpha})^2} \right)^2 \right\} \right].$$



## E.1 Region below Biot critical frequency, $\omega \ll \Omega$

In the regime below Biot critical frequency the following approximate expressions are valid

$$\begin{aligned}\alpha^{\text{mm}} &\approx C_{\alpha}^{\text{mm}}, \\ \alpha^{\text{mi}} &\approx C_{\alpha}^{\text{mi}}, \\ \alpha^{\text{im}} &\approx \left[ \left( \frac{\omega}{\Omega} \right)^2 - i \left( \frac{\omega}{\Omega} \right) \right] C_{\alpha}^{\text{im}}, \\ \alpha^{\text{ii}} &\approx \left[ \left( \frac{\omega}{\Omega} \right)^2 - i \left( \frac{\omega}{\Omega} \right) \right] C_{\alpha}^{\text{ii}}.\end{aligned}$$

Hence, in the region under consideration the complex square fast- and slow- P velocities, respectively, are given by

$$\alpha_{\text{I}}^2 \approx C_{\alpha}^{\text{mm}} - i \left( \frac{\omega}{\Omega} \right) \frac{C_{\alpha}^{\text{mi}} C_{\alpha}^{\text{im}}}{C_{\alpha}^{\text{mm}}}, \quad (441)$$

$$\alpha_{\text{II}}^2 \approx \left( \frac{\omega}{\Omega} \right)^2 \frac{\text{Det}(\mathbf{C}_{\alpha})}{C_{\alpha}^{\text{mm}}} \left( 1 + \frac{C_{\alpha}^{\text{ii}}}{C_{\alpha}^{\text{mm}}} \right) - i \left( \frac{\omega}{\Omega} \right) \frac{\text{Det}(\mathbf{C}_{\alpha})}{C_{\alpha}^{\text{mm}}}. \quad (442)$$

The complex fast-P velocity in terms of real,  $\Re\alpha_{\text{I}}^2$ , and imaginary,  $\Im\alpha_{\text{I}}^2$ , parts is obtained by

$$\alpha_{\text{I}} = \sqrt{\frac{1}{2} \left[ \sqrt{(\Re\alpha_{\text{I}}^2)^2 + (\Im\alpha_{\text{I}}^2)^2} + \Re\alpha_{\text{I}}^2 \right]} + i \sqrt{\frac{1}{2} \left[ \sqrt{(\Re\alpha_{\text{I}}^2)^2 + (\Im\alpha_{\text{I}}^2)^2} - \Re\alpha_{\text{I}}^2 \right]},$$

and can be rewritten as

$$\alpha_{\text{I}} = \sqrt{\frac{1}{2} \left[ \Re\alpha_{\text{I}}^2 \sqrt{1 + \left( \frac{\Im\alpha_{\text{I}}^2}{\Re\alpha_{\text{I}}^2} \right)^2} + \Re\alpha_{\text{I}}^2 \right]} + i \sqrt{\frac{1}{2} \left[ \Re\alpha_{\text{I}}^2 \sqrt{1 + \left( \frac{\Im\alpha_{\text{I}}^2}{\Re\alpha_{\text{I}}^2} \right)^2} - \Re\alpha_{\text{I}}^2 \right]}.$$

Because  $\left\| \frac{\Im \alpha_I^2}{\Re \alpha_I^2} \right\| \ll 1$ , using the binomial expansion (CRC standard mathematical tables, p. 518), the complex fast-P velocity is approximated by

$$\alpha_I = \sqrt{\Re \alpha_I^2} + i \frac{1}{2} \frac{\Im \alpha_I^2}{\sqrt{\Re \alpha_I^2}}.$$

Hence, the complex fast-P velocity in the region below Biot critical frequency is approximated as

$$\alpha_I \approx \sqrt{C_\alpha^{\text{mm}}} - i \frac{1}{2} \left( \frac{\omega}{\Omega} \right) \frac{C_\alpha^{\text{mi}} C_\alpha^{\text{im}}}{C_\alpha^{\text{mm}} \sqrt{C_\alpha^{\text{mm}}}}. \quad (443)$$

The complex slow-P velocity in the region under consideration is obtained by

$$\alpha_{\text{II}} = \sqrt{\frac{1}{2} \left[ \sqrt{(\Re \alpha_{\text{II}}^2)^2 + (\Im \alpha_{\text{II}}^2)^2} + \Re \alpha_{\text{II}}^2 \right]} - i \sqrt{\frac{1}{2} \left[ \sqrt{(\Re \alpha_{\text{II}}^2)^2 + (\Im \alpha_{\text{II}}^2)^2} - \Re \alpha_{\text{II}}^2 \right]},$$

and can be rewritten as

$$\alpha_{\text{II}} = \sqrt{\frac{1}{2} \left[ \Im \alpha_{\text{II}}^2 \sqrt{1 + \left( \frac{\Re \alpha_{\text{II}}^2}{\Im \alpha_{\text{II}}^2} \right)^2} + \Re \alpha_{\text{II}}^2 \right]} - i \sqrt{\frac{1}{2} \left[ \Im \alpha_{\text{II}}^2 \sqrt{1 + \left( \frac{\Re \alpha_{\text{II}}^2}{\Im \alpha_{\text{II}}^2} \right)^2} - \Re \alpha_{\text{II}}^2 \right]}.$$

Using that  $\frac{\Re \alpha_{\text{II}}^2}{\Im \alpha_{\text{II}}^2} \ll 1$ , the above equation simplifies as

$$\alpha_{\text{II}} \approx \sqrt{\frac{1}{2} \left[ \Im \alpha_{\text{II}}^2 \left( 1 + \frac{1}{2} \left( \frac{\Re \alpha_{\text{II}}^2}{\Im \alpha_{\text{II}}^2} \right)^2 \right) + \Re \alpha_{\text{II}}^2 \right]} - i \sqrt{\frac{1}{2} \left[ \Im \alpha_{\text{II}}^2 \left( 1 + \frac{1}{2} \left( \frac{\Re \alpha_{\text{II}}^2}{\Im \alpha_{\text{II}}^2} \right)^2 \right) - \Re \alpha_{\text{II}}^2 \right]}.$$

Because  $\left\| \frac{\Re \alpha_{\text{II}}^2}{\Im \alpha_{\text{II}}^2} \right\| \ll 1$ , using the binomial expansion, the complex slow-P velocity is approximated by

$$\alpha_{\text{II}} \approx \sqrt{\frac{1}{2} \left[ \Im \alpha_{\text{II}}^2 + \frac{1}{2} \Im \alpha_{\text{II}}^2 \left( \frac{\Re \alpha_{\text{II}}^2}{\Im \alpha_{\text{II}}^2} \right)^2 + \Re \alpha_{\text{II}}^2 \right]} - i \sqrt{\frac{1}{2} \left[ \Im \alpha_{\text{II}}^2 + \frac{1}{2} \Im \alpha_{\text{II}}^2 \left( \frac{\Re \alpha_{\text{II}}^2}{\Im \alpha_{\text{II}}^2} \right)^2 - \Re \alpha_{\text{II}}^2 \right]}.$$

Using that  $\Re \alpha_{\text{II}}^2 \ll \Im \alpha_{\text{II}}^2$ , the above equation simplifies as

$$\alpha_{\text{II}} \approx \left( \frac{1-i}{\sqrt{2}} \right) \sqrt{\text{Im} \{ \alpha_{\text{II}}^2 \}} = i^{-1/2} \sqrt{\text{Im} \{ \alpha_{\text{II}}^2 \}}.$$

The complex slow-P velocity in terms of  $\mathbf{C}_\alpha$  matrix elements is rewritten as

$$\alpha_{\text{II}} \approx i^{-1/2} \sqrt{\left( \frac{\omega}{\Omega} \right) \frac{\text{Det}(\mathbf{C}_\alpha)}{C_\alpha^{\text{mm}}}}. \quad (444)$$

## E.2 Region above Biot critical frequency, $\Omega \ll \omega$

In the regime below Biot critical frequency the following approximations are valid

$$\begin{aligned} \alpha^{\text{mm}} &\approx C_\alpha^{\text{mm}}, \\ \alpha^{\text{mi}} &\approx C_\alpha^{\text{mi}}, \\ \alpha^{\text{im}} &\approx \left( 1 - i \frac{\Omega}{\omega} \right) C_\alpha^{\text{im}}, \\ \alpha^{\text{ii}} &\approx \left( 1 - i \frac{\Omega}{\omega} \right) C_\alpha^{\text{ii}}. \end{aligned}$$

Hence, in the region under consideration the complex square fast- and slow- P velocities, respectively, are given by

$$\alpha_{\text{I}}^2 \approx \text{Tr}(\mathbf{C}_\alpha) - \frac{\text{Det}(\mathbf{C}_\alpha)}{\text{Tr}(\mathbf{C}_\alpha)} - i \left( \frac{\Omega}{\omega} \right) \left[ C_\alpha^{\text{ii}} - \left( \text{Tr}(\mathbf{C}_\alpha) + C_\alpha^{\text{ii}} \right) \frac{\text{Det}(\mathbf{C}_\alpha)}{\{\text{Tr}(\mathbf{C}_\alpha)\}^2} \right], \quad (445)$$

$$\alpha_{\text{II}}^2 \approx \frac{\text{Det}(\mathbf{C}_\alpha)}{\text{Tr}(\mathbf{C}_\alpha)} - i \left( \frac{\Omega}{\omega} \right) \left( \text{Tr}(\mathbf{C}_\alpha) + C_\alpha^{\text{ii}} \right) \frac{\text{Det}(\mathbf{C}_\alpha)}{\{\text{Tr}(\mathbf{C}_\alpha)\}^2}. \quad (446)$$

Analogously to the above procedure to obtain the fast- and slow- P velocities below Biot critical frequency, the complex fast- and slow- P velocities above Biot critical frequency are obtained, which respectively are

$$\alpha_{\text{I}} \approx \sqrt{\text{Tr}(\mathbf{C}_\alpha) - \frac{\text{Det}(\mathbf{C}_\alpha)}{\text{Tr}(\mathbf{C}_\alpha)}} - i \frac{1}{2} \left( \frac{\Omega}{\omega} \right) \frac{\left[ \text{Tr}(\mathbf{C}_\alpha) + C_\alpha^{\text{ii}} \right] \frac{\text{Det}(\mathbf{C}_\alpha)}{\{\text{Tr}(\mathbf{C}_\alpha)\}^2} - C_\alpha^{\text{ii}}}{\sqrt{\text{Tr}(\mathbf{C}_\alpha) - \frac{\text{Det}(\mathbf{C}_\alpha)}{\text{Tr}(\mathbf{C}_\alpha)}}}, \quad (447)$$

$$\alpha_{\text{II}} \approx \sqrt{\frac{\text{Det}(\mathbf{C}_\alpha)}{\text{Tr}(\mathbf{C}_\alpha)}}. \quad (448)$$

# Appendix F

## Complex Fast- and Slow- S Wave Velocities

The system of diffusive wave equation for shear motion is, eq (171),

$$\boldsymbol{\beta}\nabla^2\boldsymbol{\Xi} + \omega^2\boldsymbol{\Xi} = 0.$$

The explicit expression of  $\boldsymbol{\beta}$  matrix is given in eq (165). The eigenvalues of  $\boldsymbol{\beta}$  are

$$\beta_{\text{I}}^2, \beta_{\text{II}}^2 = \frac{\text{Tr}(\boldsymbol{\beta}) \pm \sqrt{\text{Tr}(\boldsymbol{\beta})^2 - 4\text{Det}(\boldsymbol{\beta})}}{2} = \frac{\text{Tr}(\boldsymbol{\beta})}{2} \left\{ 1 \pm \sqrt{1 - \frac{4\text{Det}(\boldsymbol{\beta})}{\text{Tr}(\boldsymbol{\beta})^2}} \right\},$$

where  $\beta_{\text{I}}^2$  and  $\beta_{\text{II}}^2$  represent the complex fast and slow-S wave velocities.

Because the norm of  $\frac{4\text{Det}(\boldsymbol{\beta})}{\text{Tr}(\boldsymbol{\beta})^2} \ll 1$ , that is  $\left\| \frac{4\text{Det}(\boldsymbol{\beta})}{\text{Tr}(\boldsymbol{\beta})^2} \right\| \ll 1$ , using the binomial expansion (Selby, S. M. 1971, CRC standard mathematical tables, p. 454),  $\beta_{\text{I}}^2$  and  $\beta_{\text{II}}^2$  are approximated by

$$\beta_{\text{I}}^2, \beta_{\text{II}}^2 \approx \frac{\text{Tr}(\boldsymbol{\beta})}{2} \left[ 1 \pm \left\{ 1 - \frac{2\text{Det}(\boldsymbol{\beta})}{\text{Tr}(\boldsymbol{\beta})^2} - \left( \frac{2\text{Det}(\boldsymbol{\beta})}{\text{Tr}(\boldsymbol{\beta})^2} \right)^2 \right\} \right].$$

## F.1 Region below Biot critical frequency, $\omega \ll \Omega$

In the regime below Biot critical frequency the following approximations are valid

$$\begin{aligned}\beta^{\text{mm}} &= \mathbf{C}_\beta^{\text{mm}} - i\omega\mathbf{N}_\beta^{\text{mm}}, \\ \beta^{\text{mi}} &= \mathbf{C}_\beta^{\text{mi}} - i\omega\mathbf{N}_\beta^{\text{mi}}, \\ \beta^{\text{im}} &\approx \left[ \left( \frac{\omega}{\Omega} \right)^2 - i \left( \frac{\omega}{\Omega} \right) \right] (\mathbf{C}_\beta^{\text{im}} - i\omega\mathbf{N}_\beta^{\text{im}}), \\ \beta^{\text{ii}} &\approx \left[ \left( \frac{\omega}{\Omega} \right)^2 - i \left( \frac{\omega}{\Omega} \right) \right] (\mathbf{C}_\beta^{\text{ii}} - i\omega\mathbf{N}_\beta^{\text{ii}}).\end{aligned}$$

Hence, in the region under consideration the complex square fast- and slow- S velocities, respectively, are given by

$$\beta_{\text{I}}^2 \approx \mathbf{C}_\beta^{\text{mm}} - i \left( \frac{\omega}{\Omega} \right) \mathbf{C}_\beta^{\text{ii}}, \quad (449)$$

$$\beta_{\text{II}}^2 \approx -\omega \left( \frac{\omega}{\Omega} \right) \frac{[\text{Tr}(\mathbf{C}_\beta) \text{Tr}(\mathbf{N}_\beta) - \text{Tr}(\mathbf{C}_\beta \mathbf{N}_\beta)]}{\mathbf{C}_\beta^{\text{mm}}} \left[ 1 + i \left( \frac{\omega}{\Omega} \right) \frac{\text{Tr}(\mathbf{C}_\beta)}{\mathbf{C}_\beta^{\text{mm}}} \right]. \quad (450)$$

Analogously to the procedure developed for the complex fast- and slow- P velocities (appendix E), the complex fast- and slow- S velocities are obtained, below Biot critical frequency, which respectively are

$$\beta_{\text{I}} \approx \sqrt{\mathbf{C}_\beta^{\text{mm}}} - i \frac{1}{2} \left( \frac{\omega}{\Omega} \right) \frac{\mathbf{C}_\beta^{\text{ii}}}{\sqrt{\mathbf{C}_\beta^{\text{mm}}}}, \quad (451)$$

$$\beta_{\text{II}} \approx -i \sqrt{\omega \left( \frac{\omega}{\Omega} \right) \frac{[\text{Tr}(\mathbf{C}_\beta) \text{Tr}(\mathbf{N}_\beta) - \text{Tr}(\mathbf{C}_\beta \mathbf{N}_\beta)]}{\mathbf{C}_\beta^{\text{mm}}}}. \quad (452)$$

## F.2 Region above Biot critical frequency, $\Omega \ll \omega$

In the regime above Biot critical frequency the following approximations are valid

$$\begin{aligned}\beta^{\text{mm}} &= \mathbf{C}_\beta^{\text{mm}} - i\omega\mathbf{N}_\beta^{\text{mm}}, \\ \beta^{\text{mi}} &= \mathbf{C}_\beta^{\text{mi}} - i\omega\mathbf{N}_\beta^{\text{mi}}, \\ \beta^{\text{im}} &\approx \left(1 - i\frac{\Omega}{\omega}\right) (\mathbf{C}_\beta^{\text{im}} - i\omega\mathbf{N}_\beta^{\text{im}}), \\ \beta^{\text{ii}} &\approx \left(1 - i\frac{\Omega}{\omega}\right) (\mathbf{C}_\beta^{\text{ii}} - i\omega\mathbf{N}_\beta^{\text{ii}}).\end{aligned}$$

Hence, in the region under consideration the complex square fast- and slow- S velocities, respectively, are given by

$$\beta_{\text{I}}^2 \approx \text{Tr}(\mathbf{C}_\beta) - i\left(\frac{\Omega}{\omega}\right) \mathbf{C}_\beta^{\text{ii}}, \quad (453)$$

$$\beta_{\text{II}}^2 \approx -i\omega \left(1 - i\frac{\Omega}{\omega}\right) \frac{\text{Tr}(\mathbf{C}_\beta)\text{Tr}(\mathbf{N}_\beta) - \text{Tr}(\mathbf{C}_\beta\mathbf{N}_\beta)}{\text{Tr}(\mathbf{C}_\beta)}. \quad (454)$$

Analogously to the procedure developed for the complex fast- and slow- P velocities (Appendix E), the complex fast- and slow- S velocities are obtained, above Biot critical frequency, which respectively are

$$\beta_{\text{I}} \approx \sqrt{\text{Tr}(\mathbf{C}_\beta)} - i\frac{1}{2}\left(\frac{\Omega}{\omega}\right) \frac{\mathbf{C}_\beta^{\text{ii}}}{\sqrt{\text{Tr}(\mathbf{C}_\beta)}}, \quad (455)$$

$$\beta_{\text{II}} \approx i^{3/2} \sqrt{\omega \frac{\text{Tr}(\mathbf{C}_\beta)\text{Tr}(\mathbf{N}_\beta) - \text{Tr}(\mathbf{C}_\beta\mathbf{N}_\beta)}{\text{Tr}(\mathbf{C}_\beta)}}. \quad (456)$$